Molecular Characterisation of *Shigella flexneri* IcsA and the Role of Lipopolysaccharide O-Antigen in Actin-based Motility

Kerrie Leanne May B.Sc. (Honours)

Submitted for the degree of Doctor of Philosophy

Discipline of Microbiology and Immunology

The School of Molecular and Biomedical Science

The University of Adelaide

— February 2007 —

Abstract

Shigella spp. cause bacillary dysentery through invasion of the colonic epithelium. *Shigella flexneri* IcsA (VirG) is a polarly localised, outer membrane (OM) protein that is essential for virulence. IcsA activates the host actin regulatory protein, neural Wiskott-Aldrich syndrome protein (N-WASP), which in-turn recruits the Arp2/3 complex that polymerises host actin. The resultant F-actin comet tails initiate bacterial actin-based motility (ABM) and intercellular spread. The N-terminal surface-exposed region of IcsA, referred to as the passenger domain (aa 53-758), is responsible for IcsA activity in ABM. A glycine-rich region (aa 140-307) within this passenger domain is involved in mediating N-WASP binding.

This thesis sought to conduct a comprehensive study of IcsA structure-function. Linker-insertion mutagenesis was undertaken to randomly introduce in-frame insertions of 5 aa within the IcsA passenger domain. Forty-seven linker-insertion mutants ($IcsA_i$) mutants were isolated and expressed in *S. flexneri* Δ*icsA*. The resultant strains were characterised for IcsA protein production, cell surface-expression and localisation, as well as intercellular spreading, F-actin comet tail formation, and the recruitment of N-WASP. Linker-insertions between aa 595-716 of IcsA affected production and lie in a region homologous to the putative auto-chaperone domain of *Bordetella pertussis* BrkA. Two mutant proteins ($IcsA_{i532}$ and $IcsA_{i563}$) exhibited disrupted polar targeting, enabling refinement of the polar targeting region to aa 532-563. Twenty-two of the *S. flexneri* strains expressing $IcsA_i$ mutants were unable to spread from cell-to-cell; further characterisation revealed that nineteen strains were unable to form either F-actin comet tails or recruit N-WASP.

Since lipopolysaccharide O-antigen (LPS-Oag) on the bacterial surface has been shown to mask IcsA function, $IcsA_i$ mutants were expressed in rough LPS (R-LPS) strains (that lack the Oag component) to investigate the effect of LPS-Oag on IcsA:N-WASP

interactions. Mutants were identified that were unable to recruit N-WASP and induce F-actin comet tails when expressed in smooth LPS (S-LPS) *S. flexneri* strains but able to recruit N-WASP and form F-actin comet tails in a R-LPS background. These studies enabled identification of two novel functional regions (aa 330-381 and aa 508-730) involved in N-WASP interaction.

For the first time, a structural model of the IcsA passenger domain was created using the Robetta protein prediction server and IcsA was predicted to form a β-helical structure. However, not all $IcsA_i$ mutant phenotypes could not be clearly correlated to the model.

As LPS-Oag had been shown to mask IcsA function, LPS profiles at the bacterial pole (where IcsA is predominantly located) were investigated. A comparison of the LPS profiles of purified minicells (derived from the bacterial cell pole) and purified whole cells, indicated that LPS populations are uniformly distributed on the polar and lateral regions of the bacterium.

IcsA is a member of the autotransporter (AT) family of proteins. Another AT protein, IgA protease of *Neisseria gonorrhoea* forms oligomeric structures in the OM. *In situ* chemical cross-linking revealed that IcsA is able to form high molecular weight complexes. Moreover, $IcsA_i$ mutants were shown to exert a negative dominant effect on WT IcsA, providing evidence for IcsA:IcsA interactions in the OM.

In conclusion, studies conducted in this thesis revealed that multiple regions of IcsA interact with N-WASP, suggesting that IcsA has evolved to activate N-WASP in the presence of LPS-Oag and host actin regulatory proteins.

This work contains no material which has been accepted for the award of any other degree or diploma in any university or other tertiary institution, and, to the best of my knowledge and belief, contains no material previously published or written by another person, except where due reference has been made in the text.

I give consent to this copy of my thesis, when deposited in the University Library, being available for loan and photocopying.

Kerrie May

Acknowledgements

I would firstly and foremost like to thank my supervisor and mentor, Dr Renato Morona. I doubt that I will ever be able to convey my appreciation fully, for giving me such a nifty project, as well as for your continuous support, guidance and contagious enthusiasm. Thank you for the many thought-provoking discussions, not just about my own work but on all aspects of microbiology, biochemistry and cell biology. I've learnt more in the last 4 yrs than I ever thought possible. Through your tutelage I've gained the confidence and know-how to tackle whatever comes my way next.

I am deeply indebted to Luisa Van Den Bosch, for sharing with me her extensive knowledge and expertise on IcsA, *Shigella*, microscopy, tissue culture techniques and trouble-shooting experiments – this work would not have been possible without your guidance and support. To Dr Gerald Murray, my "go-to" guy in the lab, thank you for enduring my many questions, for your guidance with my work and career. Thank you to Dr Stephen Attridge for the fine example you set for me in the beginning; your attention to detail, integrity and commitment to your work are truly inspiring – I thank you for your support and encouragement over the last 5 years.

Thank you to Assoc Prof Hiroaki Miki for the kind gift of N-WASP anti-sera, and the HIS-tagged and GST-tagged N-WASP constructs. Thank you to Prof Michael Way for the N-WASP-GFP constructs, and Prof Chihiro Sasakawa for *virG* deletion constructs.

A BIG thank you to all the members of the Morona and Paton Laboratories, past and present, for your support, friendship, and for making it such a great place to work. You've all helped me out at some stage, either trouble-shooting experiments or helping to cheer me up when things haven't gone exactly to plan – cheers to Liz who was always there with a Twix when I needed it.

A special thank you must go to Leanne for proof-reading my thesis introduction. I really appreciate all the support you've given me, particularly in the last few months – you've been a fantastic friend. Cheers to Dr Uwe Stroeher, Dr Tony Foccareta, Dr Rebecca Pinyon, and Sally McCloud for the interest you've taken in my work over the years, for your helpful discussions, and advice. Thank you to Damien Chong for helping me with all things photoshop and image formatting; and to Alistair, Rikki and Kim for the many beers and laughs along the way. You've all been fabulous friends.

Thank you to my family and friends for being so supportive throughout my many years of study, and for helping me to keep things in perspective. In particular, my Mum who truly is an amazing person, whose belief in me and encouragement has meant so much to me.

And finally, but most importantly, to Marcin: firstly thank you for your extensive proof-reading of this thesis and for helping to bring out the best in me. If only you could help me now to find the words to thank you enough for everything you've done for me both personally & professionally. I thank you for making some of the most difficult years of my life also my happiest. I'm truly grateful to you for your motivation, encouragement and for loving me, even at my worst. Everything is so much more wonderful now that I have you to share it with. Dziękuję, kocham cie – Mwa!

Abbreviations

Abbreviations acceptable to the American Society from Microbiology are used without definition in this thesis. Additional and frequently used abbreviations are defined when first used in the text, and are listed below.

Å	angstroms
A_{600}	absorbance at 600 nm
aa	amino acid
ABM	actin-based motility
Ap	ampicillin
Ap^R	ampicillin resistance
Arp	actin-related protein
AT	autotransporter
ATP	adenosine triphosphate
bp	base pairs
β-ME	β-mercaptoethanol
cfu	colony forming units
Cm	chloramphenicol
DAPI	4',6-diamidino-2-phenylindole, dihydrochloride
DNA	deoxyribonucleic acid
DMEM	Dulbecco's modified Eagle medium
DMF	dimethyl formamide
dNTP	deoxynucleoside triphosphate
dsDNA	double stranded deoxyribonucleic acid
DSP	Dithio-bis(succinimidylpropionate)
F-actin	filamentous actin
FCS	foetal calf serum
g	gravitational units

G-actin	globular actin
GFP	green fluorescent protein
GRR	glycine rich repeat
h	hour(s)
HMW	high molecular weight
$IcsA_i$	IcsA linker-insertion mutant
$IcsA_\Delta$	IcsA deletion mutant
IF	immunofluorescence
IL	interleukin
IM	inner membrane
IPTG	isopropyl-β-D-thiogalactopyranoside
Kb	kilobases
kDa	kilodaltons
Km	kanamycin
Km^R	kanamycin resistance gene or phenotype
L	litre
LB	Luria Bertani medium
LPS	lipopolysaccharide
M	molar
m	metre
M cells	membranous epithelial cells
min	minutes
MOPS	3-(N-morpholino) propane sulfonic acid
mRNA	messenger ribonucleic acid
NA	nutrient agar
NEB	New England Biolabs
nt	nucleotide
N-WASP	neural Wiskott-Aldrich syndrome protein
Oag	O antigen (O polysaccharide)

OM	outer membrane
OMPs	outer membrane proteins
ON	overnight
ORF	open reading frame
PAGE	polyacrylamide electrophoresis
PBS	phosphate buffered saline
PCR	polymerase chain reaction
PMN	polymorphonuclear
R-LPS	rough lipopolysaccharide
rpm	revolutions per minute
RT	room temperature
RUs	(Oag) Repeat units
SAP	shrimp alkaline phosphatase
sec	second
SD	standard deviation
SDS	sodium dodecylsulphate
S-LPS	smooth lipopolysaccharide
Sm	streptomycin
ss	signal sequence
S-type	short Oag modal length
Tc	tetracycline
Tc^R	tetracycline resistance cassette or phenotype
TCA	trichloroacetic acid
TTSS	type III secretion system
VL-type	VL Oag modal length
WASP	Wiskott-Aldrich syndrome protein
WT	Wild-type
X-gal	5-bromo-4-chloro-3-indolyl-β-D-galactoside
Δ	Deletion mutation

Contents

Abstract i
Declaration iii
Acknowledgements iv
Abbreviations vi
Contents ix

Chapter One: Introduction 1
1.1 *Shigella* 1
1.1.1 Classification and epidemiology 1
1.1.2 Pathogenesis 2
1.2 IcsA protein 4
1.2.1 Identification 4
1.2.2 Regulation of *icsA* expression and IcsA production 6
1.2.3 IcsA structure and function 7
1.2.3.1 IcsA polarity 9
1.2.3.2 Cleavage of IcsA by IcsP and other serine proteases 10
1.2.3.3 Phosphorylation of IcsA by protein kinase A 12
1.2.3.4 IcsB, Atg5 and autophagy 13
1.3 Autotransporter family and IcsA 14
1.3.1 Translocation across the inner-membrane 14
1.3.2 Periplasmic transit 16
1.3.3 Translocation across the outer-membrane 17
1.3.4 Structure of autotransporter proteins 19
1.4 *Shigella* Actin-based motility: the role of IcsA and the host actin cytoskeleton 20
1.4.1 Requirement of N-WASP for IcsA-mediated actin-based motility 21
1.4.2 N-WASP regulation and activation 22
1.4.3 IcsA-mediated activation of N-WASP 23
1.4.3.1 Role of Cdc42 25
1.4.3.2 Role of PIP2 25
1.4.3.3 Role of WIP 25
1.4.3.4 Role of N-WASP proline-rich region ligands Nck, Grb2, Profilin & WISH 26

1.4.3.5 Role of phosphorylation of N-WASP and Abl kinases 27
1.4.4 IcsA-mediated vinculin activation 27
1.6 Intercellular spread 29
1.6.1 Host cell factors involved in intercellular spread 29
1.6.2 Bacterial factors involved in intercellular spread 30
1.6.2.1 VacJ 30
1.6.2.2 Role of the Type III secretion system 31
1.7 The role lipopolysaccharide in ABM and intercellular spread 32
1.7.1 Structure of lipopolysaccharide 32
1.7.2 Role of LPS Oag in ABM and intercellular spread 32
1.7.3 Role of VirK in ABM 34
1.8 Project aims 35

Chapter Two: Materials and Methods 36
2.1 Chemicals and reagents 36
2.1.1 Antibodies and antisera 36
2.2 Bacterial strains and plasmids 37
2.3 Bacterial growth media 37
2.3.1 Liquid growth media 37
2.3.2 Solid growth media 37
2.3.3 Antibiotics and Congo Red solution 38
2.4..Maintenance of bacterial strains 38
2.4.1 General 38
2.4.1 Creation and maintenance of IcsA linker-insertion libraries 38
2.5..DNA isolation 39
2.5.1..Isolation of chromosomal DNA 39
2.5.2..Isolation of plasmid DNA from *E. coli* for *in vitro* cloning 39
2.5.3..Isolation of plasmid DNA from *E. coli* for transfection experiments 40
2.5.4 .Crude preparation of bacterial DNA by boiling method 40
2.6..Analysis of DNA 40
2.6.1 DNA quantitation 40
2.6.2 Restriction endonuclease digestion of DNA 41
2.6.3 Agarose gel electrophoresis 41
2.6.4 Calculation of DNA fragment length 41
2.6.5 DNA sequencing 42

2.6.5. Sequencing using dye-labelled oligonucleotides 42
2.6.5.2 DNA sequence analysis 42
2.7 DNA amplification 42
2.7.1 Synthesis of oligodeoxynucleotides 42
2.7.2 Polymerase chain reaction (PCR) 43
2.8 DNA purification 43
2.8.1 DNA gel extraction 43
2.8.2 Purification of PCR products 44
2.9 Manipulation of DNA 44
2.9.1 Oligonucleotide annealing 44
2.9.2 Phosphorylation of oligos 44
2.9.3 Shrimp alkaline phosphatase (SAP) treatment 45
2.9.4 Ligation of DNA fragments into cloning vectors 45
2.10 Transformation procedures 45
2.10.1 Preparation of chemically competent *E. coli* 45
2.10.2 Transformation of chemically competent *E. coli* with plasmid DNA 46
2.10.3 Preparation of electrocompetent *S. flexneri* and *E. coli* 46
2.10.4 Electroporation of *S. flexneri* and *E. coli* 46
2.10.5 Conjugation 47
2.11 Construction of chromosomal mutations 47
2.11.1 Allelic-exchange mutagenesis using pCACTUS 47
2.11.2 Allelic-exchange mutagenesis using the λ Red phage mutagenesis system 48
2.11.3 Transduction using P1 phage 49
2.11.3.1 Preparation of P1 Phage stocks 49
2.11.3.2 P1 Phage transduction 50
2.12 Protein techniques 50
2.12.1 Preparation of whole-cell lysates 50
2.12.2 Trichloroacetic acid precipitation of culture supernatants 50
2.12.3 Limited proteolysis with trypsin 51
2.12.4 SDS-PAGE 51
2.12.5 Coomassie blue staining 52
2.12.6 Western transfer and detection 52
2.12.7 Indirect immunofluorescence of whole bacteria 53
2.13 Minicell purification 53
2.13.1 Crude preparation of minicells by differential centrifugation 53

2.13.2 Purification of minicells by sucrose gradients 54
2.13.2.1 Preparation of sucrose gradients 54
2.13.2.2 Purification of minicells 54
2.14 Lipopolysaccharide techniques 55
2.14.1 Preparation of LPS samples 55
2.14.2 Analysis of LPS by silver-stained SDS-PAGE 55
2.15 Chemical Cross-linking 56
2.15.1 Formaldehyde cross-linking 56
2.15.2 DSP cross-linking 57
2.16 Tissue Culture 57
2.16.1 Maintenance of cell lines 57
2.16.2 Plaque assays 57
2.16.3 Infection of tissue culture monolayers with *S. flexneri* and immunofluorescence microscopy 58
2.16.4 Transfection and infection of CV-1 cells 59
2.17 Microscopy 60
2.17.1 Mounting medium 60
2.17.2 Microscopy 60
2.18 Pull-down experiments with sheep brain extracts 61
2.18.1 Preparation of sheep brain extracts 61
2.18.2 Preparation of bacteria for pull-down experiments 61
2.18.3 Pull-down experiments 62

Chapter Three: Linker-insertion mutagenesis and general characterisation of IcsA$_i$ mutants 63
3.1 Introduction 63
3.2 Linker-insertion mutagenesis 64
3.3 Dectection of mutated IcsA$_i$ proteins by Western immunoblotting 65
3.4 IcsA surface expression and localisation 67
3.5 Intercellular spread 68
3.6 Trypsin sensitivity of IcsA$_i$ mutants 69
3.7 Summary 70

Chapter Four: Intracellular behaviour of IcsA$_i$ mutants 72

4.1 Introduction 72

4.2 F-actin comet tail formation by IcsA$_i$ mutants 72

4.3 Investigation of the relationship between vinculin recruitment by IcsA$_i$ mutants and defective intercellular spreading 74

4.3.1 Recruitment of endogenous vinculin by IcsA$_i$ mutants inside HeLa cells 75

4.3.2 Binding of vinculin by IcsA$_i$ mutants in *in vitro* pull-down assays with sheep brain extracts 75

4.4 N-WASP Recruitment by IcsA$_i$ mutants inside HeLa cells 76

4.5 Effect of Oag on F-actin comet tail formation and the recruitment of host factors by *S. flexneri* expressing IcsA$_i$ mutants 78

4.5.1 F-actin tail formation by *S. flexneri* Δ*icsA* Δ*rmlD* expressing IcsA$_i$ mutants 78

4.5.2 N-WASP recruitment by *S. flexneri* Δ*icsA* Δ*rmlD* expressing IcsA$_i$ mutants 79

4.5.3 F-actin tail formation and N-WASP recruitment by *S. flexneri* Δ*icsA* Δ*rmlD* expressing IcsA$_{\Delta 103\text{-}320}$, IcsA$_{\Delta 319\text{-}507}$, IcsA$_{\Delta 508\text{-}730}$ and IcsA$_{\Delta 103\text{-}507}$ 80

4.6 Summary 81

Chapter Five: *In silico* structural modelling of the IcsA passenger domain 83

5.1 Introduction 83

5.2 Secondary structure analysis 84

5.3 BetawrapPro analysis 84

5.4 PHYRE structure prediction 85

5.5 Robetta structure prediction 86

5.6 Summary: IcsA structure-function 88

Chapter Six: Investigation of IcsA oligomerisation 89

6.1 Introduction 89

6.2 *In situ* cross-linking 89

6.3 Negative dominance of IcsA$_i$ mutants 90

6.3.1 Effect on intercellular spread 91

6.3.2 Effect on F-actin comet tail formation 92

6.4 Effect of co-expression of epitope-tagged IcsAi87::FLAG with IcsA$_{i563}$ and IcsA$_{i677}$ mutants 92

6.4.1 Epitope tagging of $IcsA_{i87}$ 93
6.4.2 Co-expression of $IcsA_{i87::FLAG}$ with $IcsA_{i563}$ and $IcsA_{i677}$ mutants 93
6.4.3 Effect on Intercellular spread 94
6.4.4 Detection of $IcsA_{i87::FLAG}$ co-expressed with $IcsA_{i532}$ and $IcsA_{i677}$ mutants by Western immunoblotting 95
6.4.5 Detection of $IcsA_{i87::FLAG}$ when co-expressed with $IcsA_{i563}$ and $IcsA_{i677}$ on the surface of *S. flexneri* 95
6.5 Summary 96

Chapter Seven: Investigation of LPS distribution in *Escherichia coli* bacteria 98
7.1 Introduction 98
7.2 Construction of a minicell mutant 99
7.2.1 Construction of a suicide vector encoding a disrupted *minD* gene 99
7.2.2 Allelic-exchange mutagenesis with pCACTUS-*minD*::KmR 101
7.2.3 Allelic-exchange mutagenesis with λ Red phage recombinase 102
7.3 Phase-contrast microscopy of *E. coli* minicell mutants 102
7.4 Construction of smooth LPS minicell-producing mutant of *E. coli* K-12 expressing IcsA 102
7.5 Analysis of LPS of minicell-producing mutants of *E. coli* expressing IcsA 104
7.6 Summary 105

Chapter Eight: Discussion 106
8.1 Overview: IcsA structure and function 106
8.2 Production of $IcsA_i$ mutants and identification of an auto-chaperone region (aa 595-716) 107
8.3 Refinement of the IcsA polar targeting region 108
8.4 IcsA-mediated N- WASP activation and initiation of ABM 109
8.4.1 Effect of Oag on N-WASP:IcsA interaction 110
8.4.2 Role of the GRR region of IcsA in N-WASP interaction 111
8.4.3 Role of aa 330-381 of IcsA (within the IcsB binding region) in N-WASP interaction 112
8.4.4 Role of aa 508-730 of IcsA in N-WASP interaction 113

8.4.5 Multiple regions of IcsA (the GRR region, aa 330-381 and 508-730) are required to activate N-WASP via interactions with its WH1 and GBD/CRIB domains 115
8.4.6 Role of host accessory proteins 116
8.5 Intercellular spreading defect of $IcsA_i$ mutants with proficient F-actin comet tail formation and ABM 117
8.6 Oligomerisation of IcsA and AT proteins 117
8.6.1 IcsA oligomerisation and its role in IcsA biogenesis and function 118
8.6.2 Oligomerisation of other AT proteins.....120
8.7 *In silico* analysis predicts a β-helical IcsA passenger domain 121
8.7.1 Predicted structural features of the IcsA.....121
8.7.2 Interaction between the IcsA passenger domain and LPS-Oag.....122
8.8 Conclusions.....123

References..... 125

Corrigenda

Page 1, line 9 and elsewhere - "*Shigellae*" should be written "Shigellae".

Page 2, line 5 - "Genetic and DNA sequence analyses of *Shigella spp.* ..."

Page 3, line 3 - "During this process, the bacteria become localised within an endocytic vacuoles."

Figure legend 1.4, line 1 - "A schematic diagram of IcsA functional domains."

Page 10, line 10 - "...detected with anti-IcsA antisera throughout the length of F-actin tails formed by *Shigella*"

Page 14, line 17 - "...the most closely related to IcsA based on sequence identity (~29% and ~ 24%, respectively)."

Page 16, line 7 - "The status of ATs in the periplasm is not known."

Page 17, line 14 and elsewhere - "Oomen *et al.*, 2002" should read "Oomen *et al.*, 2004".

Page 34, line 23 - "...*virK*::*Tn10* mutant had WT levels of *icsA* mRNA..."

Figure legend 3.5 and elsewhere - "Pannel" should be written "panel".

Figure legend 4.2 - "Alex594 and FITC-phalloidin images were false colour merged..."

Page 74, line 25 - "A *S. flexneri rmlD* strain is..."

Page 74, lines 16-18 – "One population of F-actin tails displayed WT morphology (Figure 4.2) whilst the other population appeared thicker, and more heavily labeled with FITC-phalloidin (refer to Figure 4.4)."

Page 78, line 13 - "...were transformed into *S. flexneri* Δ*icsA* Δ*rmlD* strain..."

Page 79, lines 12-14 – "Additionally, it was necessary to verify that $IcsA_i$ proteins (identified in the previous section that were able to induce F-actin comet tail formation in a R-LPS background) were able to recruit N-WASP."

Page 80, line 12 - "...an altered proteolysis profile did not correlate with..."

Page 80, lines 21-22 - "...perhaps to an even greater extent..."

Figure 4.11, lines 9-10 - "...polar localisation region #2 (aa 507-620, orange); and a putative auto-chaperone region (aa 634-735, white)..."

Page 83, lines 18-21 - " In this chapter, various *in silico* analysis tools were employed to create a structural model for the IcsA passenger domain, and correlations were made between these structure predictions and data from linker-mutagenesis and function studies (Chapters Three and Four).

Page 86, lines 22-23 -"The first α-helix (aa 260-270) was predicted to lie within the GRR #5..."

Page 88, line 17 - "These loop regions could possibly..."

Page 97, line 4 - "$IcsA_{i677}$ possesses a linker-insertion..."

Page 98, line 17 - "...may be explained by two hypotheses."

Page 98, line 20 - "...IcsA is still detected more readily at the poles..."

Figure legend 7.2, line 2 - "The chromosomal mutation of *minD* was confirmed..."

Page 104, line 13 - "7.5 Analysis of LPS of minicell-producing mutants..."

Page 122, line 18 - "Based on X-ray crystallography data..."

Page 123, lines17-18 - "As well as identifying novel N-WASP interacting regions, LPS-Oag has been shown..."

Chapter One

Introduction

Chapter One: Introduction

1.1 *Shigella*

Shigella spp. are highly adapted human pathogens that cause bacillary dysentery typified by a bloody mucoid diarrhoea. Annually, there are approximately 164.7 million cases of shigellosis resulting in an estimated 1.1 million deaths (Kotloff *et al*., 1999). Most cases of shigellosis occur in developing countries where the disease is endemic, but 580,000 cases occur each year among travellers from industrialised countries. Shigellae are a significant cause of paediatric disease, and 61% of all deaths attributed to the bacterium occur in children under the age of 5 years (Kotloff *et al*., 1999).

This chapter provides an overview of *Shigella* pathogenesis, and then focuses on the IcsA (VirG) protein. IcsA is a key virulence factor of *Shigella*, and its role in the phenomenon of bacterial actin-based motility is the focus of the studies undertaken in this thesis.

1.1.1 Classification and epidemiology

Members of the genus *Shigella* are Gram-negative bacteria and belong to the family *Enterobacteriaceae*. They share extensive genetic similarity with the genus *Escherichia* such that they are now considered to be a subtype of *E. coli* (Wei *et al.*, 2003; Jin *et al*., 2002; Jennison and Verma, 2004). The genus *Shigella* is divided into four species: *Shigella flexneri, Shigella boydii, Shigella sonnei* and *Shigella dysenteriae,* and the species are further subdivided into serotypes according to differences in the composition of their lipopolysaccharide O-antigen (LPS-Oag) (Niyogi, 2005). The significance of the LPS-Oag in *Shigella* pathogenesis is discussed in Section 1.7. *S. flexneri*, which is responsible for more mortality than any of the other species, is divided into 13 serotypes (Jennison and Verma,

2004; Niyogi, 2005). Of these, *S. flexneri* 1b, 2a, 3a, 4a, and 6 are the predominantly occurring serotypes in developing countries whilst *S. flexneri* 2a is the most predominant in industrialised countries (Jennison and Verma, 2004; Niyogi, 2005). The complete genome sequence for *S. flexneri* 2a strain 2457T has been determined (Wei *et al.*, 2003) and studies in our laboratory focus on this strain. Genetic and DNA sequence analyses of *Shigella spp.* shows that they have evolved independently on many occasions from *E. coli* and their pathogenicity can be attributed to the deletion of specific chromosomal genes and the acquisition of a large virulence plasmid encoding factors enabling them to colonise the intestinal epithelium (Sansonetti *et al.*, 1982; Lan and Reeves, 2002).

1.1.2 Pathogenesis

Shigella infection occurs via the faecal-oral route (Figure 1.1 – [1]). When ingested bacteria reach the colon and rectum, Shigellae are able to cross the colonic epithelium by exploiting membranous epithelial cells (M cells) which function to sample antigens from the gut lumen and target them to underlying mucosa-associated lymph nodes (Sansonetti *et al*., 1999; Sansonetti and Phalipon, 1999) (Figure 1.1 – [2]). Shigellae pass through the epithelial barrier via M cells to reach the underlying lymphoid follicles, where they infect resident macrophages. Subsequent *Shigella*-induced macrophage killing results in release of pro-inflammatory cytokines, including interleukin-1β (IL-1β) (Zychlinsky *et al*., 1992; Zychlinsky *et al*., 1996; Sansonetti *et al*., 2000) (Figure 1.1 – [3]).

Shigellae can invade colonic epithelial cells via their basolateral surface through bacterial induced endocytosis (Mounier *et al.*, 1992) (Figure 1.1 – [4]). The invasion process is mediated by various virulence-plasmid encoded proteins, including IpaA, IpaB, IpaC, IpgB1, IpgD and VirA that are delivered into the target host cell via a Type III secretion system (TTSS) (Mxi/Spa) (Tran Van Nhieu *et al*., 2005; Hamiaux *et al*., 2006; Ogawa and

Figure 1.1. An overview of *Shigella* Pathogenesis.

[1] *Shigella* infection occurs via the faecal-oral route. **[2]** Shigellae exploit M (microfold/membranous) cells to cross the colonic epithelium. **[3]** *Shigella* induce macrophage apoptosis/necrosis that results in release of the bacteria and interleukin-1β (IL-1β). **[4]** Shigellae actively invade colonic epithelial cells using the proteins, IpaA, IpaB, IpaC, IpgB1, IpgD and VirA that are delivered into the target host cell via a Type III secretion system (Mxi/Spa), inducing endocyotosis of the bacteria. **[5]** Shigellae engage host actin regulatory proteins, via the *Shigella* IcsA protein, to polymerise host actin in a process known as actin-based motility (ABM). Motile bacteria form protrusions that are taken up by the adjacent cells. Shigellae become enclosed within a double membrane-bound vacuole which they are able to lyse to gain entry into the cytoplasm. **[6]** *Shigella* LPS and peptidoglycan activate host cell signalling pathways leading to NF-κB activation and IL-8 production. **[7]** Recruitment of polymorphonuclear (PMN) cells in response to IL-8 and IL-1β disrupts the integrity of the colonic epithelium, enabling transepithelial migration of bacteria. **[8]** Shigellae are able to directly manipulate the tight junction-associated proteins and translocate across the colonic epithelium. Adapted from a figure courtesy of G. Murray.

[1] Oral route of infection

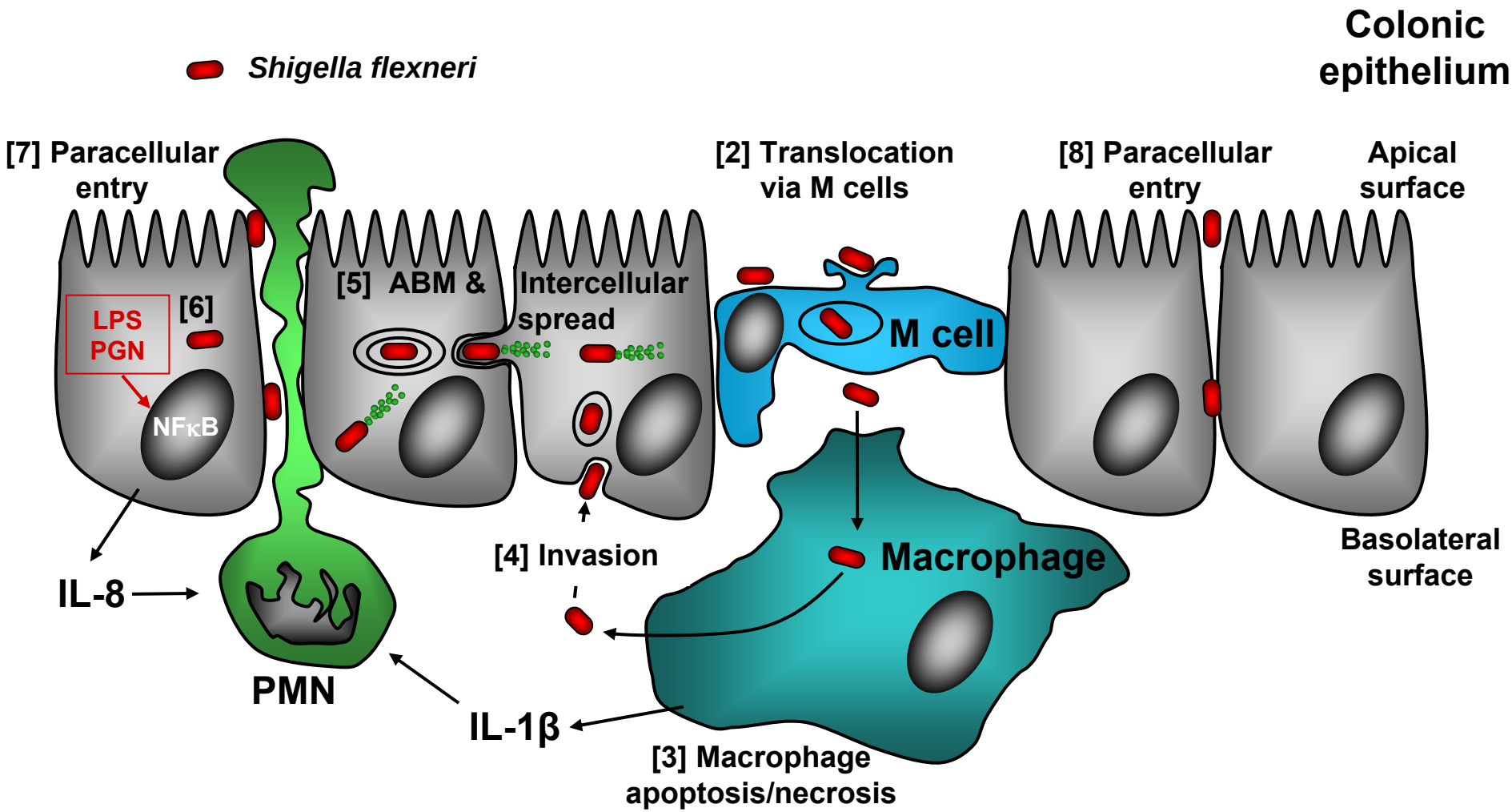

Sasakawa, 2006). These proteins are involved in manipulating the host cell architecture through localised reorganisation of the actin and microtubule cytoskeleton, triggering the uptake of the bacteria. During this process, the bacteria become localised within an endocytic vacuoles. *Shigella* produces the contact haemolysin, IpaB, to lyse this vacuole, thereby gaining entry into the host cell cytoplasm (Sansonetti *et al*., 1986; Blocker *et al*., 1999).

Within the cytoplasm of colonic epithelial cells, *Shigellae* are able to multiply and polymerise host actin by engaging host actin regulatory proteins (Suzuki *et al*., 1996; Suzuki *et al*., 1998; Suzuki *et al*., 2002) (Figure 1.1 – [5]). Actin polymerisation, at one pole of the bacterial cell, is initiated by the *Shigella* IcsA (VirG) protein, and produces a force that propels the bacterium throughout the cytoplasm in a process known as actin-based motility (ABM) (Pantaloni *et al.*, 2001; Goldberg, 2001). Motile bacteria push against the host cell membrane to form a protrusion (with the bacterium at its tip) that is taken up by the adjacent cell. The protrusion is then pinched off to form a double membrane-bound vacuole with the bacterium inside (Kadurugamuwa *et al.*, 1991; Prevost *et al.*, 1992). *Shigella* is able to lyse this vacuole releasing the bacteria into the cytoplasm of the adjacent cell (Schuch *et al*., 1999; Rathman *et al.*, 2000a; Suzuki and Sasakawa, 2001). This process enables the lateral spread of the focus of infection through the epithelium.

Whilst in the cytoplasm, Shigellae are recognised by the host cell's immune surveillance systems (Ogawa and Saskawa, 2006). For example, lipopolysaccharide (LPS) (a cell-surface polysaccharide displayed by *Shigella*) and bacterial peptidoglycan (a component of the bacterial cell wall) activate a signalling pathway mediated by nucleotide-binding oligomerisation domain protein 1 (NOD1)/caspase recruitment domain protein 4 (CARD4), which ultimately leads to activation of nuclear factor-κB (NF-κB), a transcriptional activator of, among others, the chemotactic factor IL-8 (Philpott *et al*., 2000; Girardin *et al*., 2001;

Ogawa and Saskawa, 2006) (Figure 1.1 –[6]). The production of IL-8 from epithelial cells and IL-1β from apoptotic/necrotic macrophages induces a potent inflammatory response and recruits polymorphonuclear (PMN) cells to the site of infection. Transmigration of PMN cells leads to disruption of the integrity of the colonic epithelium, enabling further transepithelial migration of bacteria (Perdomo *et al*., 1994) (Figure 1.1 – [7]). Additionally, another mechanism for paracellular translocation of Shigellae across the colonic epithelium has recently been described, in which Shigellae are able to directly manipulate tight junction-associated proteins (Sakaguchi *et* al., 2002) (Figure 1.1 – [8]).

ABM and the capacity for intercellular spread are important for *Shigella* virulence for two mains reasons. Firstly, it assists *Shigella* to evade the host immune response. Secondly, the extensive colonisation of the epithelium that occurs as a result of intercellular spread of the bacterium acts to amplify the inflammatory response, greatly contributing to the clinical manifestations of shigellosis. Indeed, *Shigella* mutants deficient in ABM are greatly attenuated in humans, as well as in mouse and monkey experimental models (Makino *et al*., 1986; Lett *et al*., 1989; Sansonetti *et al*., 1991; Kotloff *et al*., 1996; Kotloff *et al*., 2002). Development of an effective vaccine strategy for *Shigella* has proven difficult, since immunity is serotype-specific (Jennison and Verma, 2004), and with the increase in resistance of *Shigella* to antibiotics (Niyogi, 2005), inhibition of ABM maybe a novel therapeutic target.

1.2 IcsA protein

1.2.1 Identification

Shigella intracellular motility was first observed by phase-contrast microscopy by Ogawa *et al*. (1968). For reasons that were not understood at the time, it was observed that the bacterial movement exhibited polarity. It was not until the 1980s that the IcsA protein was recognised as the *Shigella* factor responsible for intracellular motility and cell-cell spread.

This began first with the identification of a large plasmid (140 megadaltons) in *S. flexneri*, subsequently named the virulence-plasmid as it was shown to be required for invasion of epithelial cells and essential for virulence (Sansonetti *et al*., 1982). A transposon mutagenesis study conducted by Makino *et al.* (1986) later showed that *Tn5* insertions within a 4 kb region of the virulence plasmid, referred to as *virG*, rendered *Shigella* defective in intercellular spread. A few years later the *virG* gene sequence was determined concurrently by Lett *et al.* (1989) and Bernardini *et al.* (1989), and the 1102 amino acid (aa) protein responsible for intracellular spread was independently named VirG and IcsA, respectively. Bernardini *et al.* (1989) also reported IcsA-dependent accumulation of host filamentous actin (F-actin) at one pole of motile bacteria, alluding to the mode of action of this protein. The morphology of the actin filaments induced by IcsA lead them to be coined “F-actin comet tails”.

IcsA (VirG) is an outer-membrane (OM) protein that, unusually for bacterial proteins, is polarly distributed on the surface of bacteria (Goldberg *et al.*, 1993) (Figure 1.2A). The finding that IcsA was polarly localised shed some light as to why *Shigella* movement exhibited polarity. IcsA is both essential and sufficient for *Shigella* motility (Makino *et al*., 1986; Lett *et al.*, 1989; Bernardini *et al.*, 1989; Goldberg and Theriot, 1995; Kocks *et al*., 1995). Heterologous expression of IcsA in *E. coli* K-12 *ompT* strains is sufficient to confer the ability to polymerise actin and movement by ABM (Goldberg and Theriot, 1995). ABM of *S. flexneri* and invasive strains of *E. coli* K-12 *ompT* expressing IcsA has been directly observed in a number of model systems. In infected tissue culture cells using time-lapse video microscopy, *Shigella* has been shown to move at rates of 5.4 to 26 μm/min (Goldberg, 2001). Additionally, F-actin comet tails have been observed in infected cells by either immunofluorescence (IF) microscopy, with F-actin detected by labelling with phalloidin conjugated to fluorescein isothiocyanate (FITC) (Figure 1.2B), or by electron microscopy (Gouin *et al*., 1999). IcsA-dependent ABM has also been studied *in vitro* using either cell

Figure 1.2.

A - Polar localisation of IcsA on the surface of *Shigella flexneri*.

Indirect-immunofluorescence microscopy of *S. flexneri* showing IcsA localisation on the surface of the bacteria. Arrows indicate polarly localised IcsA. Figure courtesy of L. Van Den Bosch.

B - *S. flexneri* F-actin comet tails visualised by immunofluorescence microscopy.

S. flexneri inside infected Hela cells were labelled with rabbit anti-LPS anti-sera and donkey anti-rabbit-Alexa594 (red), and F-actin tails formation were stained with phalloidin conjugated to fluorescein isothiocyanate (FITC) (green). Arrow indicates an F-actin comet tail. Figure courtesy of L. Van Den Bosch.

A

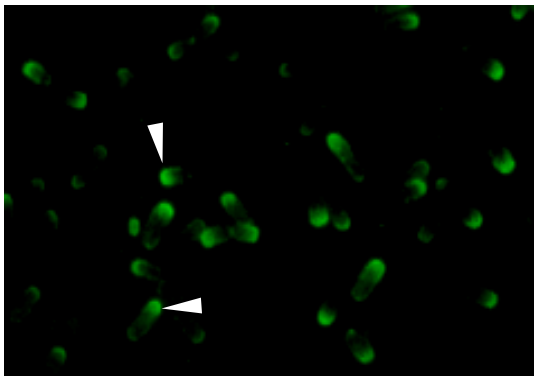

B

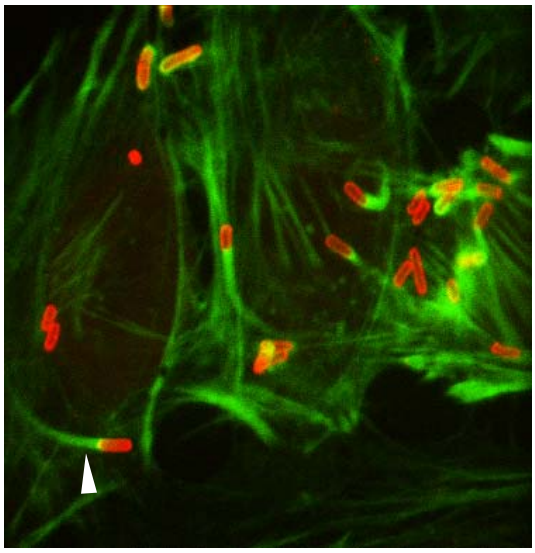

extracts (*Xenopus* eggs, platelets) (Goldberg and Theriot, 1995; Kocks *et al*., 1995; Egile *et al*., 1999) or purified proteins (Loisel *et al.*, 1999), which have been found to support bacterial motility. In these studies, *E. coli* K-12 *ompT* strains expressing plasmid-encoded IcsA were used as a substitute for wild type *S. flexneri* as the latter was not motile in these assays due to relatively poor IcsA expression under the experimental conditions (Magdalena and Goldberg, 2002). Additionally, plaque formation in tissue culture monolayers (plaque assay) and the development of keratoconjunctivitis in guinea pigs and mice in response to *S. flexneri* infection (Sereny assay) are used as an indicator of intercellular spread (Oaks *et al*., 1985; Sereny *et al*., 1957; Murayama *et al*., 1986). As these processes require efficient ABM, these assays can be used to indirectly assess the capacity for ABM.

1.2.2 Regulation of *icsA* expression and IcsA production

The expression of *icsA* and many other virulence-plasmid genes (including the *ipa* genes and the TTSS apparatus) is positively regulated by VirF, a temperature regulated transcription factor active at temperatures >32°C (Adler *et al.*, 1989; Dorman *et al*., 1998) (Figure 1.3). Optimal induction of VirF regulated gene expression occurs at 37°C and also requires a moderate level of osmotic stress and a physiological pH of 7.4 (Dorman *et al*., 1998). In this way, expression of these genes is strictly controlled such that it is appropriately coupled to infection of a host. Another gene regulator, VirB, is also positively activated by VirF (Dorman *et al*., 1998). Although not directly affecting IcsA expression, VirB activates expression of the IcsP protease, which results in increased IcsA cleavage on the bacterial surface (Wing *et al*., 2004). This is thought to help maintain IcsA polarity whilst it is expressed at high levels. The IcsP protease and cleavage of IcsA by IcsP are further discussed in Sections 1.2.3 and 1.2.3.2.

Figure 1.3 Regulation of IcsA expression

Model of the regulatory pathways that regulate IcsA expression in *Shigella*. VirF positively regulates transcription of *icsA* and *virB*. Increased IcsA expression leads to an increase in IcsA on the surface of bacteria, resulting in increased F-actin comet tail formation. VirB positively regulates transcription of *icsP*, leading to an increase in IcsP on the surface of bacteria and increased IcsA cleavage from the bacterial surface.

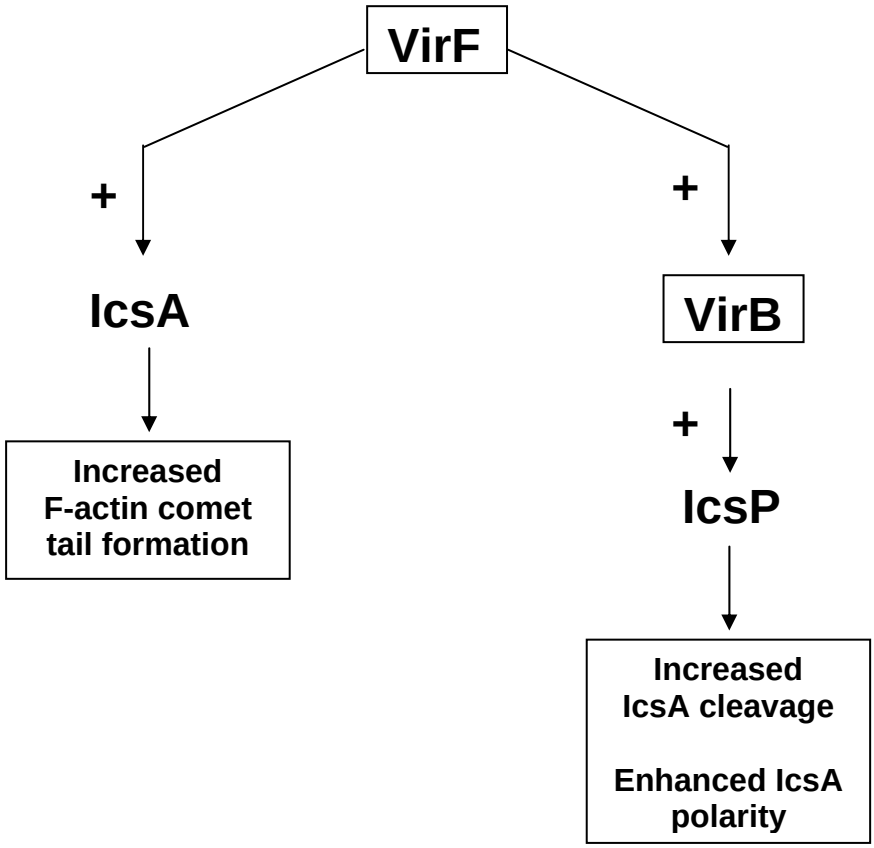
VirF
+
+
IcsA
VirB
+
IcsP
Increased
F-actin comet
tail formation
Increased
IcsA cleavage
Enhanced IcsA
polarity

It has been calculated that approximately 4000 molecules of IcsA on an individual bacterium are required for it to efficiently form F-actin tails in cell extracts and it was originally suggested that a similar number was required for F-actin tail formation inside cells, although this was not quantitated (Magdalena and Goldberg, 2002). The same study also reported that the level of IcsA protein was 3.2-fold higher for bacteria grown inside cells compared to those grown in Tryptic Soy broth. This study compared protein levels, as it was suggested that due to evidence for post-translational processing of IcsA by *Shigella* factors IcsP (Egile *et al.,* 1997; Shere *et al.,* 1997; discussed in Section 1.2.3.2) and VirK (Nakata *et al.,* 1992; discussed in Section 1.7.3), mRNA levels might not be a reliable indicator of IcsA expression. Indeed they reported preliminary reverse transcription-PCR to support such a view. A recent microarray analysis of *S. flexneri* infected HeLa cells (human epithelial derived cells) and U397 cells (human macrophage-like cells) has shown *icsA* gene expression to be significantly down-regulated intracellularly in both the cell lines, compared with *in vitro* growth in Luria broth (Lucchini *et al.,* 2005). This is in disagreement with the data of Magdalena and Goldberg (2002) and it would perhaps seem counter-intuitive for a gene to be down-regulated during the stage of infection where it is required. Lucchini *et al.* reconciled this by suggesting two hypotheses: (i) either that the level of *icsA* gene expression was sufficient to support ABM, or (ii) that two populations of intracellular bacteria exist, those that are dormant and those that are motile.

1.2.3 IcsA structure and function

IcsA is an autotransporter (AT) protein and like other members of this family, it consists of three major domains (Figure 1.4) (Henderson *et al*., 2004). A 52 aa N-terminal signal sequence (aa 1-52), to direct SecAB dependent transport of the protein across the inner-membrane; a 344 aa C-terminal (aa 759-1102) translocation domain that enables export of the remaining N-terminal region of IcsA, the passenger domain (aa 53-758), across the OM

Figure 1.4. IcsA functional domains

A schematic diagram of IcsA functional domains. The 3 major domains of IcsA: a signal sequence (aa 1-52), a passenger domain (aa 53-758) and the translocation domain (aa 759-1102). A glycine-rich repeat region (GRR; aa 140-307) that interacts with the host protein N-WASP. A region encompassing the GRR (aa 104-506) interacts with vinculin. Another region (aa 320-433) interacts with the *Shigella* protein, IcsB, and the host autophagy protein Atg5, and two regions responsible for polar localisation (region #1 aa 1-104; and region #2 aa 507-620) are also shown. The IcsP cleavage site is located between aa 758-759 and a region overlapping this (aa 756-762) encodes a phosphorylation consensus motif "SSRRASS". Numbering is based on the IcsA (VirG) sequence from Lett *et al*. (1989; GenBank accession # AAA26547)

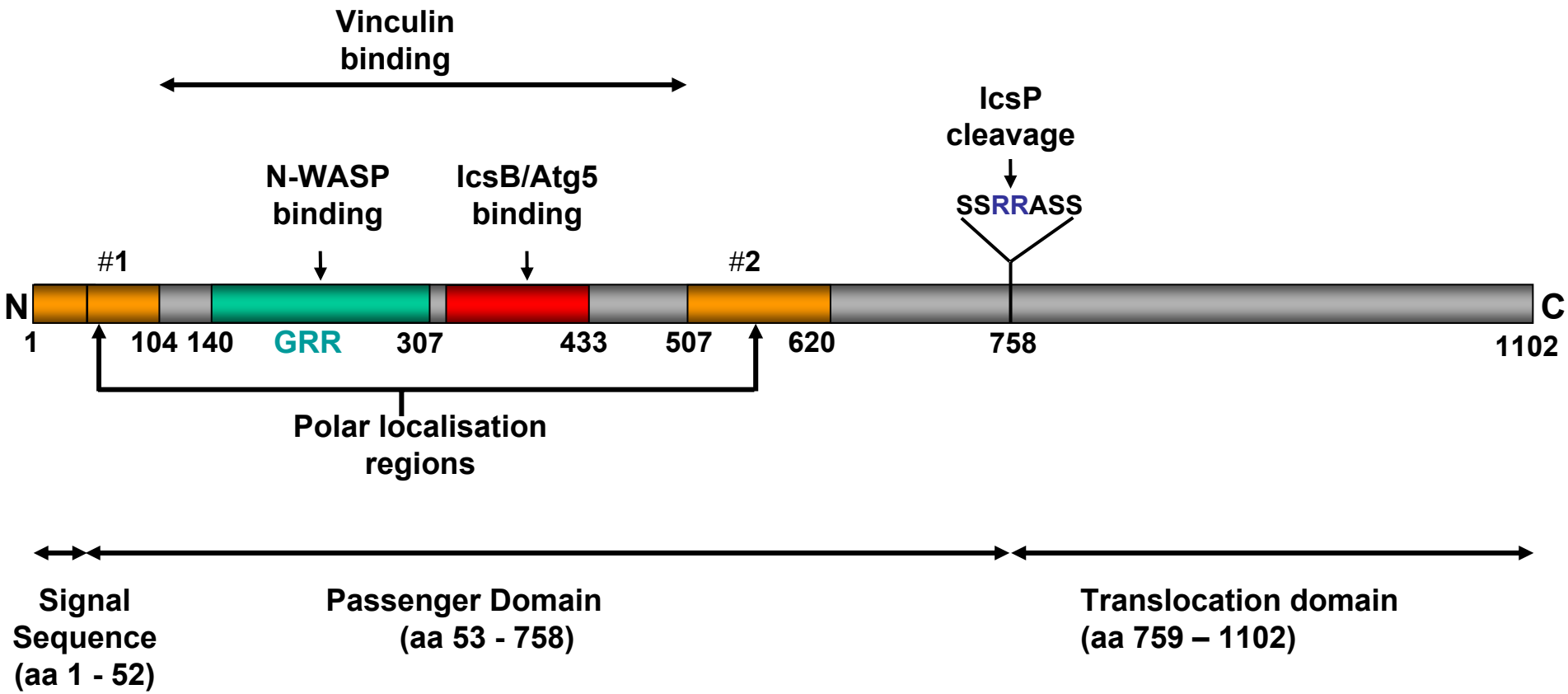
Vinculin
binding
IcsP
cleavage
N-WASP
binding
IcsB/Atg5
binding
SSRRASS
#1
#2
N
C
1
104 140
GRR
307
433
507
620
758
1102
Polar localisation
regions
Signal
Sequence
(aa 1 - 52)
Passenger Domain
(aa 53 - 758)
Translocation domain
(aa 759 – 1102)

(Suzuki *et al*., 1995; Brandon and Goldberg, 2001; Brandon *et al*., 2003). The current models for IcsA and AT protein export are discussed in Section 1.3. Ultimately, the passenger domain of IcsA becomes exposed on the outer surface, anchored by the translocation domain. Various IcsA structure and function studies have been undertaken and these have involved either systematic deletion of IcsA regions, amino acid substitutions and sub-clones of IcsA regions. Functional regions that have been identified to date are shown in Figure 1.4.

A glycine rich repeat (GRR) region exists within the IcsA passenger domain (aa 140-307) (Goldberg *et al.*, 1993) (Figure 1.5A) and has been identified as the region responsible for IcsA interaction with the host neural Wiskott-Aldrich syndrome protein (N-WASP), leading to F-actin tail formation (Suzuki *et al*., 1998; Snapper *et al*., 2001; Suzuki *et al*., 2002). Another similar GRR exists just upstream of this (aa 117-139) (Figure 1.5B) and recent work in our laboratory has shown that its deletion results in reduced N-WASP recruitment, shorter F-actin comet tails and reduced plaque size formation (Russell, 2005). Furthermore, deletion of part of this region (aa 104-226) has been reported to abolish F-actin tail formation (Suzuki *et al*., 1996). A region encompassing the GRR (aa 104-506) has also been shown to interact with the host protein vinculin (Suzuki *et al*., 1996). The roles of IcsA, N-WASP and vinculin in regulating F-actin comet tail formation and *Shigella* ABM are discussed in detail in Section 1.4. Two regions of the passenger domain (aa 1-104 and aa 507-620) have been attributed to polar localisation of IcsA (Suzuki *et al*., 1996; Charles *et al*., 2001). An IcsP cleavage site exists between aa R_{758}-R_{759} and an overlapping region (aa 756-762) encodes a phosphorylation consensus motif “SSRRASS” (d'Hauteville and Sansonetti, 1992). Another region (aa 320-433) interacts with the *Shigella* IcsB protein and a host autophagy protein, Atg5 (Ogawa *et al*., 2003; Ogawa *et al*., 2005). The significance of each of these functional regions is discussed below (Section 1.2.3.1-4). Additionally, IcsA has been reported to bind and hydrolyse ATP (Goldberg *et al.*, 1993). How this contributes to IcsA

Figure 1.5. The glycine rich repeat-region of the IcsA passenger domain.

A - The glycine rich repeat (GRR) region within the IcsA passenger domain (aa 140-307) identified by Goldberg *et al.* (1993), which was later identified as the region responsible for IcsA interaction with the host Neural Wiskott-Aldrich syndrome protein (N-WASP). Shown is an alignment of the GRRs. Identical residues are shaded and glycine residues are shown in bold.

B - A refinement of the GRR region to include an additional GRR (aa 117-139) identified by Russell (Russell, 2005) that is required for efficient N-WASP recruitment and F-actin comet tail formation.

A

```
140 GSDLSIINQGMIIGGSGGSGA----DHNGDGGE-AVT 171
172 GDNLFIINGEIISGGHGGDSYS---DSDGGNGGDAVT 205
206 GVNLPIINGKTISGGNGGNNYG---EGDGGNGGDAIT 239
240 GSSLSVINKGTFAGGNGGAAYGYGYDGYGGN---AIT 273
274 GDNLSVINNGAILGGNGGHWGD---AINGSNMTIANS 307
```

B

```
117 GHGGAGDNNDGNSCGGNGGDSIT-------------- 139
140 G-SDLSIINQGMIIGGSGGSGA----DHNGDGGE-AVT 171
172 G-DNLFIINGEIISGGHGGDSYS---DSDGGNGGDAVT 205
206 G-VNLPIINGKTISGGNGGNNYG---EGDGGNGGDAIT 239
240 G-SSLSVINKGTFAGGNGGAAYGYGYDGYGGN---AIT 273
274 G-DNLSVINNGAILGGNGGHWGD---AINGSNMTIANS 307
```

function is not known but it has been suggested it may provide energy to assist in F-actin comet tail formation (Goldberg *et al.*, 1993).

1.2.3.1 IcsA polarity

As mentioned previously, IcsA is asymmetrically distributed on the surface of both extracellular and intracellular bacteria, and is found predominantly expressed at the old pole, which is the pole not arising from the previous septation. (Goldberg *et al.* 1993). Interestingly, IcsA is not the only AT to exhibit polarity. It has recently been discovered that ATs from a variety of bacteria are polarly targeted, although the mechanisms are not yet understood (Jain *et al*., 2006).

For IcsA, two regions of its passenger domain, polar localisation region #1 (aa 1-104) and polar localisation region #2 (aa 507-620), are independently responsible for targeting IcsA export to the old cell pole (Suzuki *et al*., 1996; Charles *et al*., 2001). The unipolar localisation is reinforced at bacterial division such that the old pole retains high levels of IcsA and the new pole created from the septation zone is effectively devoid of IcsA (Goldberg *et al*., 1994). It has been observed that 85% of intracellular bacteria expressing IcsA on the surface are actively dividing (Goldberg *et al*., 1994) suggesting that perhaps polar localisation and export may be linked to cell division. The prokaryotic actin homologue, MreB, determines the shape for rod shaped bacteria (Figge, *et al*., 2004; Esue *et al*., 2005) and has recently been implicated in polar targeting of IcsA. Inactivation of *mreB* lead to disruption of IcsA polarisation and the formation of ectopic sites containing IcsA (Nilsen *et al*., 2005). However, a direct interaction between IcsA and MreB has not been demonstrated. Also, apyrase, a periplasmic enzyme that hydrolyses deoxynucleoside triphosphate (dNTP) and deoxynucleoside diphosphate molecules, has been shown to be required for efficient intercellular spreading (Santapaola *et al*., 2006). More specifically, inactivation of the apyrase

gene (*apy*) was shown to disrupt IcsA polarity and this effect was shown to be independent of the dNTP-hydrolysing activity of apyrase. Just as for MreB, a direct interaction between IcsA and apyrase has not been shown.

Two other factors have been shown to influence IcsA polarity: the cell surface LPS molecules (discussed in sections 1.7.2 and 1.7.3), and the OM protease IcsP.

1.2.3.2 Cleavage of IcsA by IcsP and other serine proteases

Cleavage of IcsA was suggested after the observation was made that IcsA could be detected with anti-IcsA antisera throughout the length of F-actin tails formed by *Shigella* in infected HeLa cells (Goldberg *et al*. 1993). Also, IcsA was secreted into the culture supernatant *in vitro* (Goldberg *et al*. 1993). It has since been confirmed that in *S. flexneri*, IcsA is cleaved by the virulence plasmid-encoded, OM, serine protease IcsP (SopA) between residues R_{758}-R_{759} to release a 95 kDa fragment (Fukuda *et al.*, 1995; d'Hauteville *et al*., 1996; Egile *et al.*, 1997; Shere *et al.*, 1997; Steinhauer *et al.*, 1999). However, d'Hauteville *et al*. (1996) demonstrated that the IcsA polyclonal sera used by Goldberg *et al*. (1993) cross-reacts with a 70kDa host protein bringing into question whether IcsA is actually localised throughout F-actin tails as originally reported by Goldberg *et al.* (1993). Indeed, IcsA was unable to be detected in F-actin comet tails in studies conducted by our laboratory using independently prepared antisera (Morona *et al*., 2003).

IcsP cleavage of IcsA occurs over the entire bacterial surface, but at a low efficiency, such that during exponential growth of the bacteria 80% of the IcsA molecules remain uncleaved and anchored to the OM (Shere *et al*., 1997; Steinhauer *et al.*, 1999). IcsP is a member of the Omptin family of serine proteases and *E. coli* OmpT, which is 60% identical to IcsP is also able to cleave IcsA (Nakata *et al.,* 1993; Egile *et al.*, 1997; Shere *et al.*, 1997).

However, in contrast to IcsP, OmpT cleaves IcsA at high efficiency so that IcsA can no longer be detected on the surface of bacteria (Goldberg *et al.,* 1993; Nakata *et al.,* 1993). Consequently, *E. coli* K-12 *ompT*$^{+}$ strains expressing IcsA are deficient in ABM (Nakata *et al.,* 1993). In fact, *Shigella* strains lack the *ompT* gene and expression of OmpT in these strains renders them avirulent (Nakata *et al.,* 1993). Studies investigating the role of IcsP have taken one of two different approaches: (i) inactivation of the *icsP* gene, or (ii) mutation of IcsA to prevent its cleavage by IcsP.

S. flexneri 2a wild-type (WT) strain YSH6200 expressing a single chromosomally-integrated copy of a non-cleavable mutant, $IcsA_{R758D}$, exhibited WT F-actin tail formation and plaque formation on MK2 cell (monkey-derived kidney cells) monolayers, and gave Sereny positive reactions earlier than the WT (Fukuda *et al*., 1995). Results of this initial study suggested that IcsA cleavage is not required for efficient ABM and intercellular spread.

Conversely, d'Hauteville *et al*. (1996) later reported that *S. flexneri* serotype 5 WT strain M90T expressing non-cleavable forms of the IcsA protein ($IcsA_{R758D}$ and $IcsA_{R758D, R759D}$) encoded on multi-copy plasmids, demonstrated non-polar localisation of F-actin on the surface of intracellular bacteria and thicker F-actin tails perpendicular to the longitudinal axis of the bacteria. However, neither plaque formation nor Sereny tests were performed in that study, and the same mutants had been reported earlier by these authors to have an increased capacity for intercellular spread (d'Hauteville and Sansonetti, 1992) (see Section 1.2.3.3). Therefore, whether the observed phenotype actually correlates to an affect on virulence remains questionable.

Two studies have investigated the effect of inactivation of *icsP* (*sopA*). In the first of these, disruption of *sopA* (*icsP*) in *S. flexneri* M90T resulted in altered IcsA localisation, with

IcsA distributed over the entire surface of the bacteria with some polar reinforcement (Egile *et al*., 1997). This mutant exhibited shorter protrusions in HeLa cells and formed smaller plaques on Caco-2 cells (polarised human colonic carcinoma derived cells).

The second study (Shere *et al.* 1997) found that disruption of *icsP* in *S. flexneri* serotype 2a leads to a marked reduction in IcsA cleavage, increased amounts of IcsA associated with the bacterium, and altered localisation similar to that reported by Egile *et al.* (1997). This *icsP* mutant demonstrated increased mean speed and an increased frequency of ABM, despite the formation of plaques on monolayers of Caco-2 cells, HeLa cells and L2 cells (rat fibroblast cells), being comparable to the WT. The discrepancy between the results of these two studies is unclear, but may reflect a strain or serotype-specific phenomenon. Nonetheless, a common finding by both these studies was that cleavage of IcsA by IcsP acts to reinforce polar localisation of IcsA.

In summary, it would appear that IcsA cleavage by IcsP is not essential for efficient ABM and intercellular spread. The necessity of IcsP for *S. flexneri* virulence remains uncertain but this may reflect limitations of the model systems used to study virulence.

1.2.3.3 Phosphorylation of IcsA by protein kinase A

In addition to being a target for protease cleavage, residues 756-762 of IcsA encode a phosphorylation consensus motif "SSRRASS" that is a substrate for phosphorylation by host cell cyclic-dependent protein kinases (d'Hauteville and Sansonetti, 1992). Site-directed mutagenesis ($R_{759}D$) almost completely abolished phosphorylation of IcsA by protein kinase A *in vitro*. Such mutants demonstrated an increased capacity for intercellular spread in HeLa cell monolayers. The authors of this study attributed the phenotype of this mutant to a lack of phosphorylation of IcsA by protein kinases. However, as discussed above, subsequent studies

have demonstrated that the “SSRRASS” motif is also a target site for cleavage by the IcsP protease and mutation of this site prevents IcsA cleavage by IcsP (Fukada *et al.*, 1995; d'Hauteville *et al*., 1996). Subsequently, it was suggested that the phenotype of this mutant could be attributed to a lack of IcsA cleavage. Moreover, despite several attempts (d'Hauteville and Sansonetti, 1992; Frischknecht *et al.*, 1999), the phosphorylation of IcsA inside host cells has not been demonstrated.

1.2.3.4 IcsB, Atg5 and autophagy

An early study of the virulence-plasmid encoded IcsB protein mistakenly identified it as a factor required for lysis of bacteria-containing protrusions endocytosed by neighbouring cells (Allaoui *et al.*, 1992). In that study *icsB* mutants were shown to invade eukaryotic cells and form protrusions into neighbouring cells, but formed abnormally small plaques on eukaryotic cell monolayers, and were unable to induce keratoconjunctivitis in guinea-pigs. The observation that bacteria became trapped in double membrane vacuoles lead to the suggestion that IcsB must be required for lysis of the vacuole enabling intercellular spread. The *icsB* mutation used in that study was subsequently shown to be a polar mutation potentially affecting downstream gene expression, including the *ipa* genes (Rathman *et al*., 2000a). In a follow-up study using a non-polar *icsB* mutant, no affect on plaque formation was observed (Rathman *et al.*, 2000a).

However, in more recent investigations (Ogawa *et al.*, 2003; Ogawa *et al.*, 2005) using an independently constructed non-polar *icsB* mutant, a similar phenotype was observed to that first described by Allaoui *et al.* (1992). The reason for the discrepancy between these studies and the study by Rathman *et al.* (2000a) is unclear although it may have been cell-line-dependent (Ogawa *et al.*, 2003). In subsequent studies, Ogawa *et al.* went on to show that IcsB was delivered by the type III secretion system into the host cell cytosol (Ogawa *et al.*

2003). In the cytosol, competitive binding of IcsB to IcsA (region aa 320-433) prevented binding of the host Atg5 autophagy protein and initiation of degradation of the bacteria via the autophagy pathway (Ogawa *et al.*, 2005). These results indicated that IcsB functions to protect *Shigella* from an innate host defence mechanism.

1.3 Autotransporter family and IcsA

The AT family of proteins (Type V secretory proteins) is the largest family of Gram-negative bacterial extracellular proteins with more than 700 members (Pallen *et al*., 2003). As previously mentioned (Section 1.2.3), AT proteins share common domains: an N-terminal signal sequence (ss), an internal passenger domain that exerts the effector function, and a C-terminal translocation domain (Henderson *et al.*, 2004). There is limited sequence identity between the passenger domains of AT proteins, corresponding with a diverse range of effector functions (Henderson and Nataro, 2001; Henderson *et al.*, 2004). These range from serum resistance, adherence, invasion, proteolysis and cytotoxicity, and in the case of IcsA, intracellular motility. Of all the functionally characterised ATs AIDA-I, an adherence factor associated with some diarrheagenic *E. coli* strains, and MisL, from *Salmonella enterica*, are the most closely related to IcsA based on sequence identity (~29% and ~ 24%, respectively) (Henderson *et al.*, 2004). The AT export pathway was first described by Pohlner *et al*. (1987) for the *Neisseria* IgA1 protease. It was designated the “autotransporter” export pathway, as export across the OM did not require either ATP or a proton gradient (Pohlner *et al*., 1987; Henderson *et al.*, 2004). The current models for AT protein export are described below, with reference to studies performed with IcsA where possible.

1.3.1 Translocation across the inner-membrane

IcsA and other AT proteins possess an N-terminal ss that mediates targeting to, and translocation across, the inner-membrane (IM) via the Sec machinery (Henderson *et al.*,

2004). The Sec machinery consists of the IM proteins, SecY, SecE and SecG that form a pore in the IM. This complex interacts with the peripheral membrane protein SecA that possesses ATPase activity providing energy to catalyse translocation of proteins through the SecYEG pore. During the translocation process, the ss is cleaved (Brandon and Goldberg, 2001; Brandon *et al.*, 2003). In *E. coli*, at least three pathways exist to target proteins to the SecYEG complex: the SecB pathway, the signal recognition peptide (SRP) pathway and the DnaK pathway. The first of these involves post-translational targeting of proteins to SecA mediated by the cytoplasmic chaperone SecB (Henderson *et al.*, 2004). In the second pathway, SRP interacts with the ribosome to co-translationally target proteins to the SecYEG translocon via its receptor, FtsY (Henderson *et al.*, 2004). A DnaK pathway has also been described in which DnaK acts as a chaperone and binds selectively to outer membrane proteins (OMPs) in order to maintain them in an export competent state until a SecA molecule becomes available to direct them across the IM via the SecYEG translocon (Qi *et al.*, 2002). IcsA has been shown to utilise the Sec machinery for export by interacting with SecB but it does not appear to be targeted by the SRP pathway (Brandon *et* al., 2003). It is yet to be determined if the DnaK pathway is involved in IcsA translocation across the IM.

Polar distribution was shown to be independent of the ss since IcsA fusions to the green fluorescent protein (GFP) that lack the N-terminal ss are still polarly targeted (Charles *et al.*, 2001). Hence, polar targeting of IcsA occurs in the cytoplasm prior to translocation across the IM by the Sec machinery. The typical ss ranges from 18-26 amino acids long and consists of an N-terminal region of positively charged residues, a hydrophobic internal region and a C-terminal consensus signal peptidase recognition site (Desvaux *et al.*, 2004; Fekkes *et al.*, 1999). IcsA and some other ATs possess an atypical ss that is much longer (approximately 50 aa) with two unique conserved sequence motifs. An N-terminal "MNKIYSLKY(S/C/H)" motif followed by a second motif of aromatic and hydrophobic

residues (Henderson *et al*., 1998; Desvaux *et al.*, 2004). The purpose of this N-terminal extension is unclear, but it has recently been proposed that for the *E. coli* AT EspP, it functions as a transient inner-membrane anchor that precludes improper folding of the passenger domain in the periplasm (Szabady *et al.*, 2005; Peterson *et al.*, 2006).

1.3.2 Periplasmic transit

The status of ATs in the periplasm is not known. Whether they exist in an unfolded, partially folded or folded state remains under investigation (Henderson *et al.*, 2004). For IcsA at least, insertion of the translocation domain into the OM is thought to be a relatively rapid process and translocation of the passenger domain is the rate-limiting step (Brandon and Goldberg, 2001). It has also been shown that IcsA is folded in a proteinase K resistant conformation whilst in transit in the periplasm, prior to translocation across the OM (Brandon and Goldberg, 2001). Additionally, IgA1 protease and EspP have also been shown to form folded periplasmic intermediates (Skillman *et al.*, 2005; Veiga *et al*., 2004). IcsA contains three cysteines in the ss, three in the passenger domain and one in the translocation domain (Lett *et al*., 1989; Brandon and Goldberg, 2001). IcsA has been shown to form one disulphide bond in the periplasm that is thought to stabilise the protease resistant folded conformation (Brandon and Goldberg, 2001).

The periplasmic chaperone/serine protease DegP has been implicated in IcsA export. Inactivation of *degP* resulted in a decreased percentage of bacteria with IcsA expressed on the surface, despite production of WT levels of the protein (Purdy *et al*., 2002). Although a direct interaction between DegP and IcsA has not been demonstrated, it has been proposed that DegP may facilitate efficient delivery of IcsA to the surface of bacteria. Another periplasmic chaperone, Skp has been implicated in the export of integral OM proteins via a pathway involving LPS-dependent insertion of OMPs into the lipid bilayer of the OM (Bulieris *et al*.,

2003; Desvaux *et al.*, 2004). However, the roles of Skp and other periplasmic chaperones in the export of IcsA have not yet been investigated.

1.3.3 Translocation across the outer-membrane

There are four models for the export of AT's across the OM (Figure 1.6). The classical model for AT export across the OM proposes translocation of the passenger domain through a β-barrel pore, formed by the C-terminal translocation domain (Pohlner *et al*., 1987). Indeed, analysis of the secondary structure of the IcsA translocation domain, based on amphipathic β-sheet predictions, suggested that it forms a β-barrel pore consisting of 14 amphipathic, anti-parallel, transmembrane β-strands adjoined with loop regions and hairpin turns (Suzuki *et al*., 1995). Subsequently, this model was supported by the crystal structure of the *in vitro*-folded NalP translocation domain in which the α helical linker region of the translocation domain (located between the passenger domain and the β-barrel pore) is positioned in the pore of the β-barrel formed by an individual translocation domain (Figure 1.7) (Oomen *et al.*, 2004).

Two variations on the classical model exist with respect to translocation of the passenger domain through the β-barrel pore. In the hairpin model, a helical domain adjoining the β-barrel pore and the passenger domain is first inserted into the pore to form a hairpin structure driving translocation of an unfolded passenger domain to the cell surface (Pohlner *et al*., 1987 and Jose *et al.*, 1995) (Figure 1.6A).

In keeping with the hairpin model, a putative intra-molecular chaperone region has been described in *Bordetella pertussis* AT protein BrkA (aa 601-692) (Oliver *et al*., 2003). It has been suggested that the hairpin formed could possibly include this auto-chaperone region (Desvaux, *et al.*, 2004; Jacob-Dubuisson; 2004). Deletion of this region in BrkA made the protein susceptible to degradation by OM proteases and trypsin (Oliver *et al*., 2003).

Figure 1.6. Four proposed models for autotransporters translocation across the OM

A - Hairpin model

A region of the translocation domain forms a β-barrel pore in the OM and a helical domain adjoining the β-barrel pore and the passenger domain is first inserted into the pore to form a hairpin structure driving translocation of an unfolded passenger domain. (Pohlner *et al*., 1987 and Jose *et al.*, 1995)

B - Threading model

Translocation proceeds with the N-terminal region of the passenger domain being threaded through the β-barrel pore in an unfolded conformation (Oomen *et al*., 2004)

C - Oligomeric model

Translocation domains of the AT protein forms and oligomeric structure in the OM and translocation of the passenger domain proceeds through a central pore formed by this oligomer (Veiga *et al*., 2002).

D - Omp85 model

The proposed model for export involves Omp85-mediated insertion of the AT translocation domain into the OM. Translocation of the passenger domain proceeds through a pore formed by the Omp85 complex, an OM hetero-oligomeric protein complex composed of at least four currently identified components in *E. coli*: Omp85/YaeT, YfgL, YfiO, and NlpB.

Figure courtesy of M. Grabowicz.

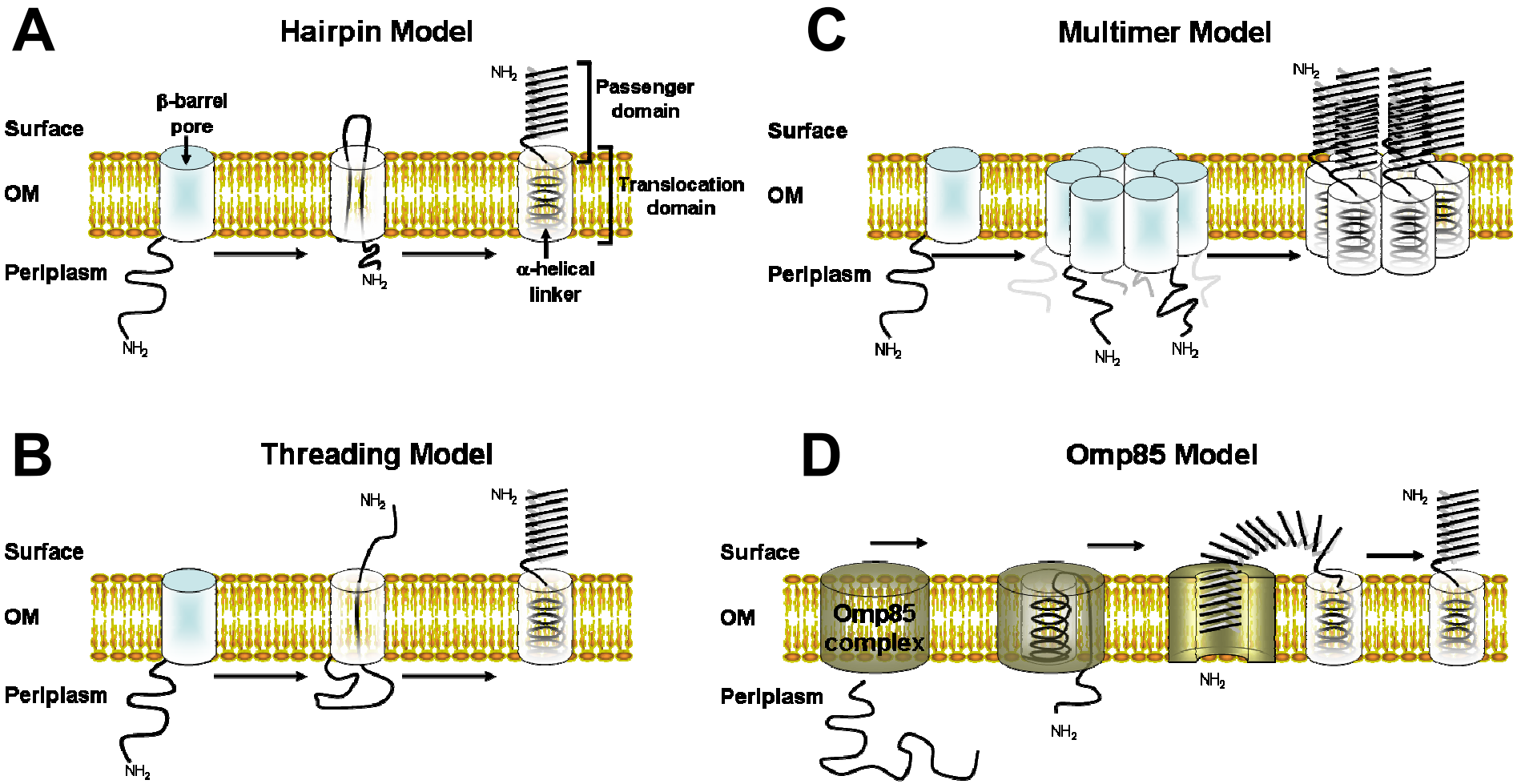
A
Hairpin Model
β-barrel pore
Surface
OM
Periplasm
NH2
Passenger domain
Translocation domain
α-helical linker
B
Threading Model
C
Multimer Model
D
Omp85 Model
Omp85 complex

Figure 1.7. β-barrel pore formation by an autotransporter protein translocation domain

The crystal structure of the *in vitro*-folded NalP AT protein of *N. meningitidis* (PDB #1UYN; Oomen *et al.*, 2004) is shown and was created using PyMOL (http://pymol.sourceforge.net, DeLano Scientific). β-strands are coloured yellow, loop regions are coloured white and an α-helice is coloured red. **A -** side view and **B -** top view**.**

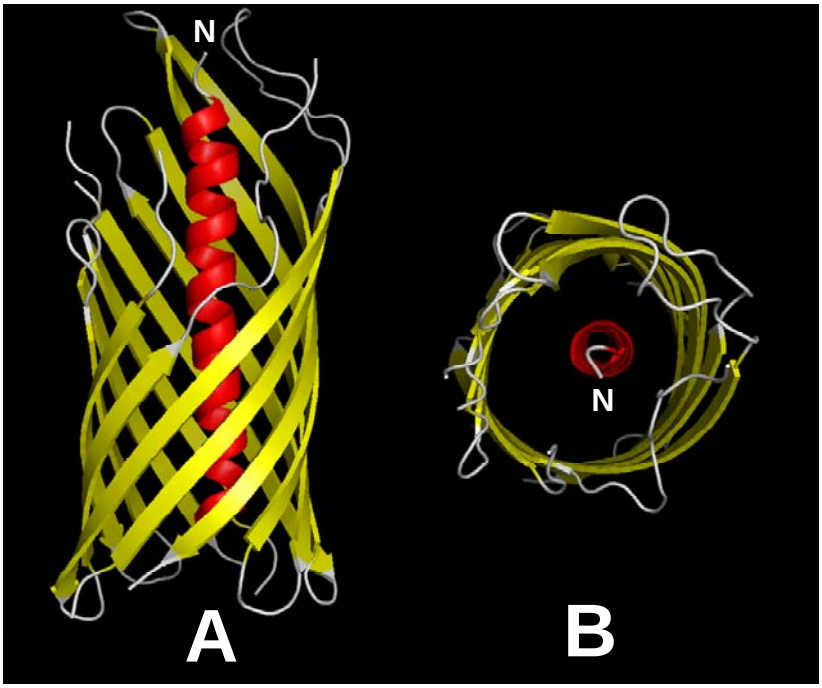
N
N
A
B

Similarly, this has been shown for homologous regions within AT proteins SSP of *Serratia marcescens* and Pet of enteroaggregative *E. coli* (Ohnishi *et al*., 1994; Dutta *et al*., 2003). Moreover, this region is also found in many other AT proteins, including IcsA (aa 634-735), (Figure 1.8) (Oliver *et al*., 2003; Henderson *et al*., 2004). A similar function for this region in IcsA has yet to be shown, although it should be noted that deletion of almost this entire region (aa 509-729) was reported to have no effect on the level of IcsA production (Suzuki *et al*., 1996).

A threading model has been proposed for AT export in which translocation proceeds with the N-terminal region of the passenger domain being threaded through the β-barrel pore in an unfolded conformation (Oomen *et al*., 2004) (Figure 1.6B). This model seems unlikely, as it would require targeting via the N-terminal region of the passenger domain, and neither N-terminal deletions nor the fusion of artificial passengers to the translocation domains of ATs, appear to affect their export (Oliver *et al*., 2003; Jose *et al*., 1996; Maurer *et al*., 1997; Henderson *et al*., 2004).

Alternatively, the observation that the translocation domain of the IgA1 protease AT protein forms oligomeric structures in the OM lead to a model whereby translocation of the passenger domain proceeds through a central pore formed by an oligomer of translocation domains (Veiga *et al*., 2002) (Figure 1.6C). However, attempts to show similar oligomerisation of *Neisseria meningitidis* NalP, *E. coli* AIDA-I and EspP have been unsuccessful (Oomen *et al*., 2004; Muller *et al*., 2005; Skillman *et al*., 2005). IcsA has not been investigated in this regard.

The final export model involves the highly conserved Omp85 family of proteins, identified as essential for assembly of integral OMPs (Voulhoux *et al*., 2003). Depletion of

Figure 1.8 A region in *S. flexneri* IcsA that shares similarity to the putative auto-chaperone region of *B. pertussis* BrkA.

An alignment of the *B. pertussis* BrkA putative auto-chaperone region (Oliver *et al*., 2003), aa 601-692 (Fernandez and Weiss, 1994; GenBank accession # AAA51646), and a similar region in *S. flexneri* IcsA, aa 634-735 (Lett *et al*., 1989; GenBank accession # AAA26547), generated using the CLUSTAL W algorithm (http://www.ebi.ac.uk/clustalw; Higgins *et al*., 1994). Regions of >80% identity (*****), >40% identity (**.**), and >60% similarity (**:**) are shown. Identical residues are shaded grey.

```
IcsA aa 634-735 --TY--VQKGNWHGKGGILSLGAVLGNDNSKTDRLEIAGHASGITYVAVTNEGGSGDKTLEGVQIISTDSSDKNAFIQKGRIVAGSYDYRLK-QGTVSGLNTNKWYL-
BrkA aa 601-692 EASYKTLTLQTLDGNG-VFVLNTNVAAG--QNDQLRVTGRADGQHRVLVRNAGGEADSRGARLGLVHTQ---------G---QGNATFRLANVGKAVDLGTWRYSLA
                  :*  :   . .*:* :: *.: :. .  :.*:*.::*:*.*   * * * **..*.    : :: *:      ::  * :: *.  :**   *.. .*.* :: *
```

either Omp85 in *N. meningitidis*, or its orthologue YaeT in *Escherichia coli*, results in transient accumulation of OMPs in the periplasm as soluble intermediates, suggesting Omp85 and YaeT are involved in their insertion in the OM. The observation that IgA1 protease AT in *N. meningitidis* was also affected by the depletion has lead researchers to suggest that other AT proteins may also use the Omp85 pathway (Voulhoux *et al.*, 2003; Oomen *et al.*, 2004). The proposed model for export involves Omp85-mediated insertion of the AT translocation domain into the OM, and translocation of the passenger domain through a pore formed by the Omp85 complex (Figure 1.6D). In this model, AT proteins are not true "autotransporters" but use a generic helper protein system. Whether the Omp85 family of proteins is generally utilised by ATs is unknown.

1.3.4 Structure of autotransporter proteins

The passenger domains of two ATs, *B. pertussis* P.69 Pertactin and *E. coli* Haemoglobin protease have been crystallised and both have been found to form right-handed parallel β-helices (Emsley *et al*., 1996; Otto *et al*., 2005) (Figure 1.9). Subsequent *in silico* analysis of ATs with modelling programs BetaWrap and BetaWrapPro, which can identify β-helix folds without relying on sequence homology to proteins of known structure, have predicted that the vast majority of AT passenger domains have this structure (Bradley *et al*., 2001; Junker *et al*., 2006). The β-helical proteins whose structures have been determined have been found to be elongated proteins. Notably, the function of many of these (e.g. *Erwinia chrysanthemi* pectate lyases, *B. pertussis* P.69 pertactin, P22 phage and Sf6 phage tails spike proteins) involves recognition or interaction with either polysaccharides or lipopolysaccharides (Steinbacher *et al*., 1996 Jenkins and Pickersgill, 2001; Freiberg *et al*., 2003; Henderson *et al*., 2004).

Figure 1.9 Crystal structures of auto-transporter protein passenger domains.

A - *B. pertussis* P.69 pertactin

A ribbon diagram was created using PyMOL (http://pymol.sourceforge.net, DeLano Scientific) showing the overall structure of the P.69 pertactin passenger domain (PDB ID: 1dab; Emsley *et al*., 1996). The X-ray crystal structure was determined to 2.5 Å. The protein fold consists of a 16-stranded parallel β helix and towards the C-terminus forms two rungs of a two-stranded β-roll.

B – ***E. coli*** **Haemoglobin protease**

A ribbon was created using PyMOL (http://pymol.sourceforge.net, DeLano Scientific) showing the overall structure of the Haemoglobin protease passenger domain (PDB ID: 1wxr; Otto *et al*., 2005). The X-ray crystal structure was determined to 2.2 Å. The protein fold consists of a 24-stranded parallel β helix.

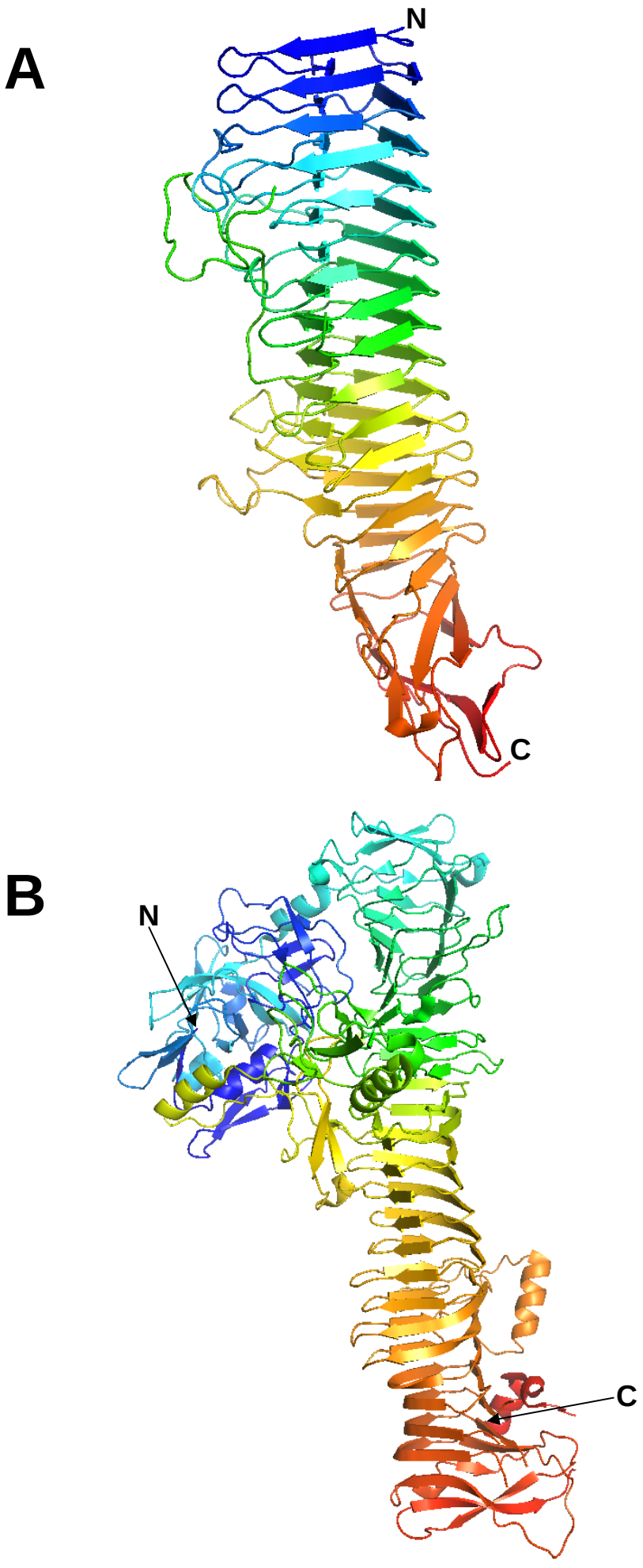
A
N
C
B
N
C

1.4 *Shigella* actin-based motility: the role of IcsA and the host actin cytoskeleton

The ability of mammalian cells to move and alter their shape is fundamental to many biological processes. Cell shape and motility is largely controlled by the actin cytoskeleton, which is robust, dynamic and able to respond to external stimuli via signalling pathways relayed through the cell membrane. Regulation of the actin cytoskeleton is a complex process controlled by numerous regulatory proteins that possess adapter, globular actin (G-actin) cross-linking, G-actin monomer binding, and filamentous-actin (F-actin) bundling, binding or severing functions (Goldberg, 2001; Winder, 2003; Miki and Takenawa, 2003). *Shigella* is able to subvert the host actin regulatory proteins and initiate formation of F-actin filaments. Polymerisation of G-actin to F-actin on the surface of a bacterium creates a force that propels it through the host cytoplasm (Carlier *et al*., 2003a). *Shigella* produces uniformly short actin filaments of around 0.1 μm in length that appear to be randomly oriented (Gouin *et al*., 1999). These individual filaments are bundled into a branched network producing F-actin comet tails approximately 7 μm in length and 0.7 μm in width (Gouin *et al*., 1999). The filaments are present at a high density near the end of the bacterium but the density decreases throughout the length of the tail, forming what has been described as a fan effect (Tilney and Portnoy, 1989; Gouin *et al*., 1999). Various actin regulatory proteins have been found associated with *Shigella* and their F-actin comet tails (Table 1.1). However, the presence of these proteins does not strictly imply their necessity in *Shigella* ABM, and there has been much investigation into identifying the factors essential for *Shigella* ABM. In particular, N-WASP, which is recruited to the bacterial pole but absent from the F-actin comet tail itself, has been identified as a critical host factor for intracellular *Shigella* motility (Suzuki *et al*., 1998; Snapper *et al*., 2001; Goldberg, 2001).

Table 1.1 – Host proteins associated with intracellular *Shigella* and/or F-actin comet tails

Host protein	Function	Reference(s)
N-WASP	Regulation/nucleation of actin polymerisation	Loisel *et al.* (1999)
Arp2/3 complex	Actin polymerisation	Loisel *et al.* (1999)
Cdc42	N-WASP activation	Loisel *et al.* (1999)
Grb2	N-WASP activation	Carlier *etal*. (2000)
α-actinin	F-actin cross-linking	Gouin *et al*. (1999)
Profilin	Actin turnover	Loisel *et al*. (1999)
ADF/cofilin	Actin turnover	Loisel *et al.* (1999)
Plastin	F-actin cross-linking	Prévost *et al*. (1992)
Filamin	F-actin cross-linking	Prévost *et al*. (1992)
Nck	N-WASP activator	Moreau *et al*. (2000)
WIP	N-WASP regulator	Moreau *et al*. (2000)
CapZ	F-actin capping	Gouin *et al*. (1999)
Ezrin	Plasma membrane - actin cytoskeleton linker	Gouin *et al*. (1999) Skoudy *et al*. (1999)
Zyxin	Focal adhesion protein involved in actin-remodelling	Frischknecht *et al*. (1999)
Vinculin	Adapter protein	Kadurugamuwa *et al*. (1991) Suzuki *et al*. (1996)
VASP	Regulation/nucleation of actin polymerisation	Chakraborty *et al.* (1995)

1.4.1 Requirement of N-WASP for IcsA-mediated actin-based motility

The Wiskott-Aldrich syndrome protein (WASP) family of proteins function as a link between signalling pathways and *de novo* actin polymerisation, initiating actin polymerisation-driven host cell motility and morphological changes (Yarar *et al*., 1999; Miki and Takenawa, 2003). The WASP protein was named so because mutations in this protein were identified as the cause of Wiskott-Aldrich syndrome, a disease characterised by thrombocytopenia, eczema and immunodeficiency (Miki and Takenawa, 2003). There have been four other WASP-related proteins identified, including WAVE/Scar (WASP-family verprolin-homologous protein/suppressor of cAMP receptor) 1, 2 and 3, and N-WASP (neural Wiskott-Aldrich syndrome protein) (Miki and Takenawa, 2003). N-WASP was first isolated from the bovine brain by Miki *et al.* (1996). Subsequently rat and human homologues were identified, which share >95% homology with each other and 50% homology to WASP (Fukuoka *et al*., 1997).

The absolute requirement for N-WASP in *Shigella* actin-based motility has been demonstrated in a number of model systems. Firstly, *in vitro* studies demonstrated that immunodepletion of N-WASP from cell extracts lead to a significant reduction in F-actin tail formation by *E. coli* expressing IcsA, which could be restored by the addition of purified N-WASP (Suzuki *et al*., 1998). Similarly, *E. coli* expressing IcsA were only able to form F-actin tails in platelet extracts, which naturally lack N-WASP, after pre-incubation of *Shigella* with N-WASP (Egile *et al*., 1999). Additionally, in N-WASP deficient cells, *Shigella* was able to invade and multiply but was unable to form either F-actin comet tails, protrusions, or spread from cell-to-cell (Snapper *et al*., 2001). F-actin comet tail formation could be restored by expression of N-WASP in *trans* from an integrated retroviral vector, indicating that this phenotype arose exclusively due a lack of N-WASP (Snapper *et al*., 2001). Interestingly, despite the initial view that N-WASP was expressed ubiquitously, haematopoietic cells

including macrophages and PMNs were found not to support *Shigella* F-actin tail formation and ABM (Miki *et al.*, 1996; Suzuki *et al.*, 2002). It was subsequently shown that N-WASP expression was significantly reduced in these cells and WASP expression predominated (Suzuki *et al.*, 2002). Furthermore, ectopic expression of N-WASP restored *Shigella* motility. The regulation of N-WASP activity during physiological processes is complex and there is much that is poorly understood, but the current models for its activation are described below.

1.4.2 N-WASP regulation and activation

Human N-WASP is a 505 aa multi-domain protein with various distinct domains: an N-terminal WASP-homology domain 1 (WH1; aa 34-138); a highly basic region (B; aa 184-200); a Cdc42/Rac interactive binding domain (CRIB; aa 203-222), also known as the GTPase-binding domain (GBD); a proline-rich domain (aa 277-389); and a C-terminal VCA domain (V, verprolin-homology domain; C, cofilin-homology domain; A, acidic region; aa 389-505) (Figure 1.10) (Fukuoka *et al.*, 1997; Martinez-Quiles *et al.*, 2001). The WH1 domain overlaps a pleckstrin homology domain (PH; aa 1-98) and a calmodulin binding IQ motif (IQ; aa 128-147). The VCA domain includes a verprolin-homology region 1 (V1; aa 405-421), verprolin-homology region 2 (V2; aa 433-449), cofilin-homology domain (C; aa 470-489) and an acidic region (A; aa 486-505).

The original model of N-WASP activation and regulation was delineated predominantly using *in vitro* systems utilising purified proteins and cytoplasmic extracts (Ma *et al.*, 1998a; Ma *et al.*, 1998b; Rohatgi *et al.*, 1999). It was shown that N-WASP activity is regulated by an intramolecular interaction between the VCA and GBD/CRIB regions of the protein (Kim *et al.*, 2000). In this auto-inhibited conformation the actin-related protein (Arp)2/3 complex, a seven protein complex capable of *de novo* actin filament formation by the polymerisation of G-actin monomers is unable to bind the VCA region and be activated

Figure 1.10. Functional domains of Human N-WASP

A schematic diagram of the functional domains of human N-WASP (aa 505) (Fukuoka *et al*., 1997; Martinez-Quiles, 2001). WASP-homology domain 1 (WH1; aa WH1 34-138), which overlaps a pleckstrin homology domain (PH; aa 1-98) and a calmodulin binding IQ motif (IQ; aa 128-147); a basic region (B; aa 184-200) a Cdc42/Rac interactive binding domain (CRIB; aa 203-222), also called the GTPase-binding domain (GBD); a proline-rich domain (aa 277-389); and the VCA domain (aa 389-505), which is comprised of verprolin-homology region 1 (V1; aa 405-421), verprolin-homology region 2 (V2; aa 433-449), a cofilin-homology domain (C; aa 470-489) and an acidic region (A; aa 486-505). A tyrosine residue is located at aa 256. Refer to the text for a detailed description of binding interactions (Section 1.4.2)

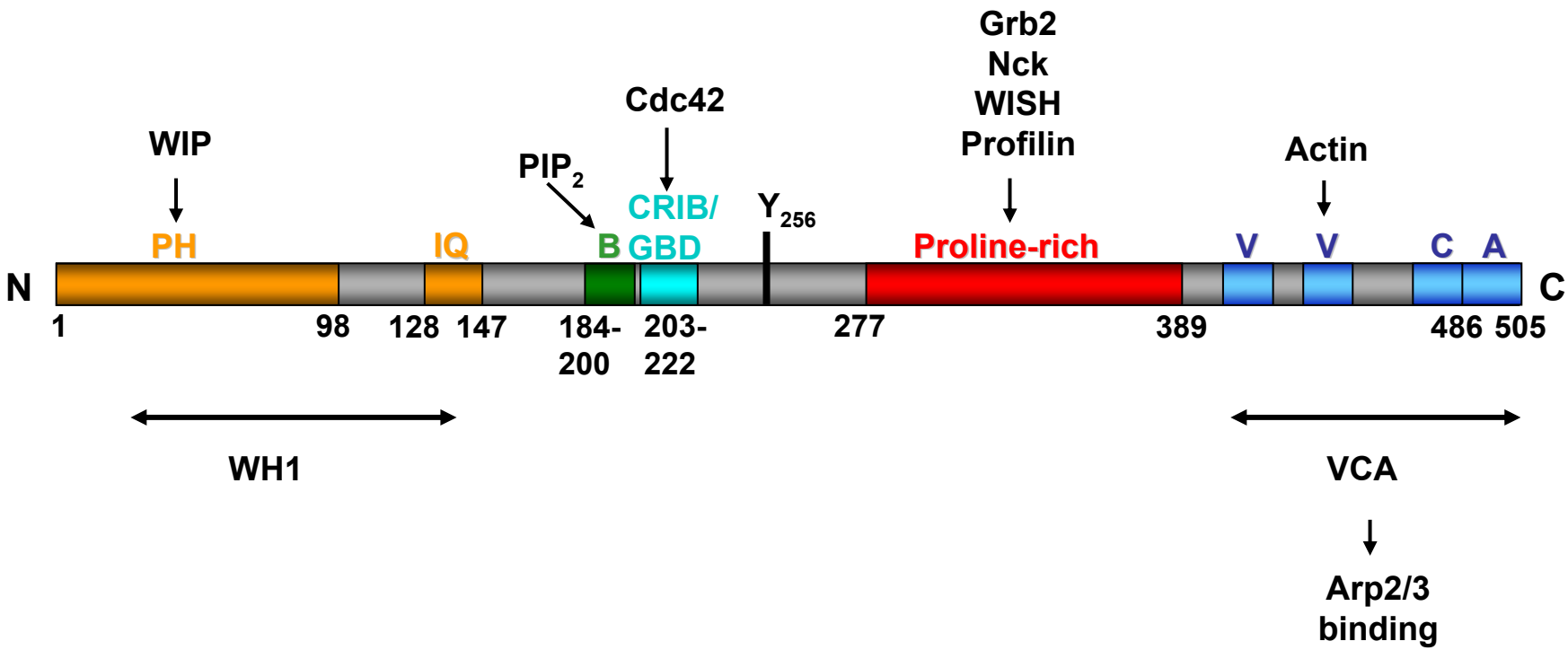
Grb2
Nck
WISH
Profilin
Cdc42
WIP
PIP2
Actin
CRIB/
Y256
PH
IQ
B
GBD
Proline-rich
V
V
C
A
N
C
1
98
128
147
184-
200
203-
222
277
389
486
505
WH1
VCA
Arp2/3
binding

(Figure 1.11). The binding of the GTP-bound form of the Rho-GTPase, Cdc42 to the CRIB domain and phosphatidylinositol 4,5-bisphosphate (PIP_2) to the basic region was shown to activate N-WASP synergistically (Ma *et al*., 1998a; Ma *et al*., 1998b; Rohatgi *et al.*, 1999). Upon activation, the VCA region of N-WASP becomes exposed, and can bind and activate the Arp2/3 complex (Kim *et al*., 2000). In addition to Cdc42 and PIP_2, N-WASP can be activated by the binding of the proteins Nck, Grb2, WISH, and other Src homology domain 3 (SH3)-adaptors to the proline-rich domain (Miki and Takenawa, 2003). Furthermore, the Src family and Abl family of kinases can enhance N-WASP activation by phosphorylating a tyrosine residue (Y_{256}) near the CRIB/GBD domain. (Miki and Takenawa, 2003). It is not yet well understood which activators are important during various physiological processes.

Recent work has lead to revision of the original model. In *Xenopus* cell extracts the majority of N-WASP was found complexed with either the WASP-interacting protein (WIP) or the related CR16 protein that bind to the N-terminal WH1 region of N-WASP (Ho *et al*., 2001; Ho *et al.*, 2004). WIP has been shown to suppress N-WASP activation in the absence of activators and it has been proposed that WIP stabilises the auto-inhibited conformation of N-WASP (Ho *et al*., 2004). Furthermore, an additional protein, transducer of Cdc42-dependent actin assembly (Toca-1) has been identified as essential for activation of the WIP-N-WASP complex and Cdc42 (Ho *et al*., 2004).

How IcsA is able to activate N-WASP is not well understood, however the current model for IcsA-mediated N-WASP activation and the extent of knowledge about the roles of various other host factors in this process is discussed herein.

1.4.3 IcsA-mediated activation of N-WASP

Figure 1.11. N-WASP regulation activation.

N-WASP is thought to exist in an auto-inhibited conformation due to an intra-molecular interaction between the VCA and GBD/CRIB regions (Kim *et al*., 2000). Binding of PIP_2 to the basic domain and Cdc42 to the GBD/CRIB region is thought to act synergistically to disrupt this intramolecular interaction thereby inducing a conformational change in N-WASP from its inactive state to the active state, enabling the Arp2/3 complex to be recruited to the C-terminal VCA domain of N-WASP. WIP binds to the WH1 region of N-WASP and in the absence of activators and WIP stabilises the auto-inhibited conformation and suppresses N-WASP activation (Ho *et al*., 2004). Toca-1 is essential for activation of the WIP-N-WASP complex and Cdc42 (Ho *et al*., 2004).

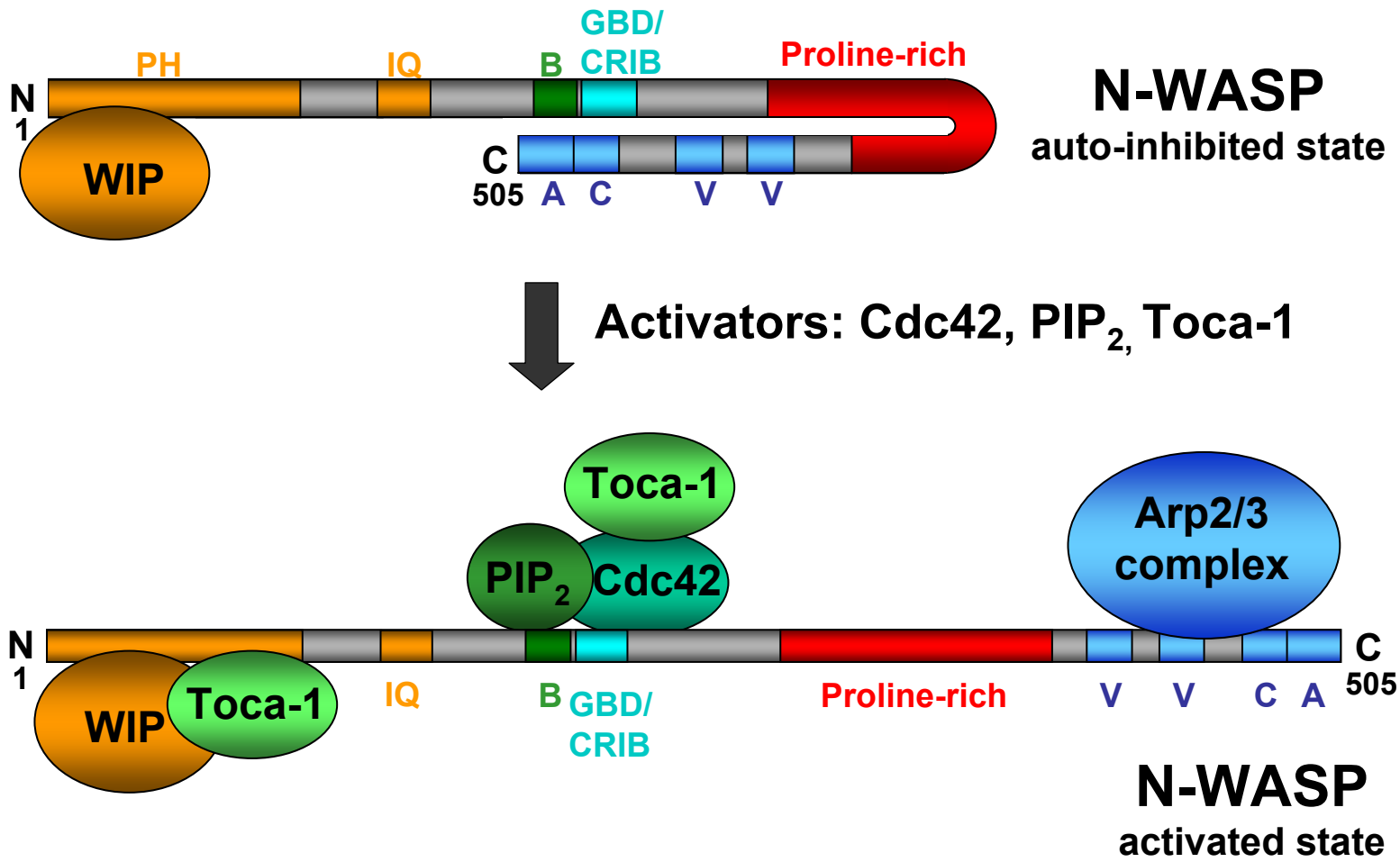
GBD/
CRIB
PH
IQ
B
Proline-rich
N
1
WIP
C
505
A
C
V
V
N-WASP
auto-inhibited state
Activators: Cdc42, PIP2, Toca-1
Toca-1
Arp2/3
complex
PIP2
Cdc42
N
1
WIP
Toca-1
IQ
B
GBD/
CRIB
Proline-rich
V
V
C
A
C
505
N-WASP
activated state

Direct binding of IcsA to N-WASP is thought to result in a disruption of the intra-molecular interaction between the VCA region and GBD/CRIB regions of N-WASP. The latter induces a conformational change in N-WASP from the auto-inhibited state to the active state, thereby enabling Arp2/3 complex recruitment via the C-terminal VCA domain (Suzuki *et al*., 1998; Suzuki *et al*., 2002; Egile *et al*., 1999; Goldberg, 2001) (Figure 1.12). The IcsA passenger domain, N-WASP and Arp2/3 have been shown to interact to form a ternary complex that polymerises actin (Egile *et al.*, 1999).

Despite an initial report that IcsA binds to the VCA region of N-WASP (Suzuki *et al.*, 1998), it has since been convincingly shown that IcsA interacts with the GBD and the WH1 regions of N-WASP (Egile *et al.*, 1999; Suzuki *et al.*, 2002; Moreau *et al*., 2000). Amino acids 103-433 of IcsA, which contains series of glycine-rich repeats (Section 1.2.3), are sufficient for N-WASP binding, as shown by *in vitro* pull-down assays with purified proteins (Suzuki *et al.*, 1998). IcsA amino acids 53 to 508 are sufficient to induce actin polymerisation using *in vitro* assays (Goldberg, 2001). Therefore, it has been suggested that the residues involved in N-WASP activation are within this region (Suzuki *et al.*,1996; Suzuki and Sasakawa, 2001; Goldberg, 2001) Similarly, a *Shigella* strain expressing IcsA lacking aa 509-729, was reported to recruit N-WASP inside cells (Suzuki *et al.*, 1998 - unpublished data cited therein). However, this mutant had previously been shown to have a defect in F-actin tail formation (Suzuki *et al*., 1996), and although this was attributed to altered IcsA localisation, whether aa 53 to 508 of IcsA are actually sufficient for F-actin comet tail formation inside cells awaits clear verification.

Currently, it is not clear to what extent IcsA is able to directly activate N-WASP inside host cells or whether additional host activators are essential for this process. What is

Figure 1.12. Model of IcsA-mediated activation of N-WASP.

Binding of IcsA to N-WASP disrupts the intra-molecular interaction between the VCA region and GBD/CRIB regions of N-WASP. This induces a conformational change in N-WASP from its inactive state to the active state, enabling the Arp2/3 complex to be recruited to the C-terminal VCA domain of N-WASP. The IcsA passenger domain, N-WASP and Arp2/3 interact to form a ternary complex that polymerises actin. IcsA has been shown to interact with both the WH1 and GBD/CRIB regions of N-WASP and this interaction is thought to be mediated by the GRR region of IcsA. Several host factors are likely to play a role in N-WASP activation. (refer to text for details).

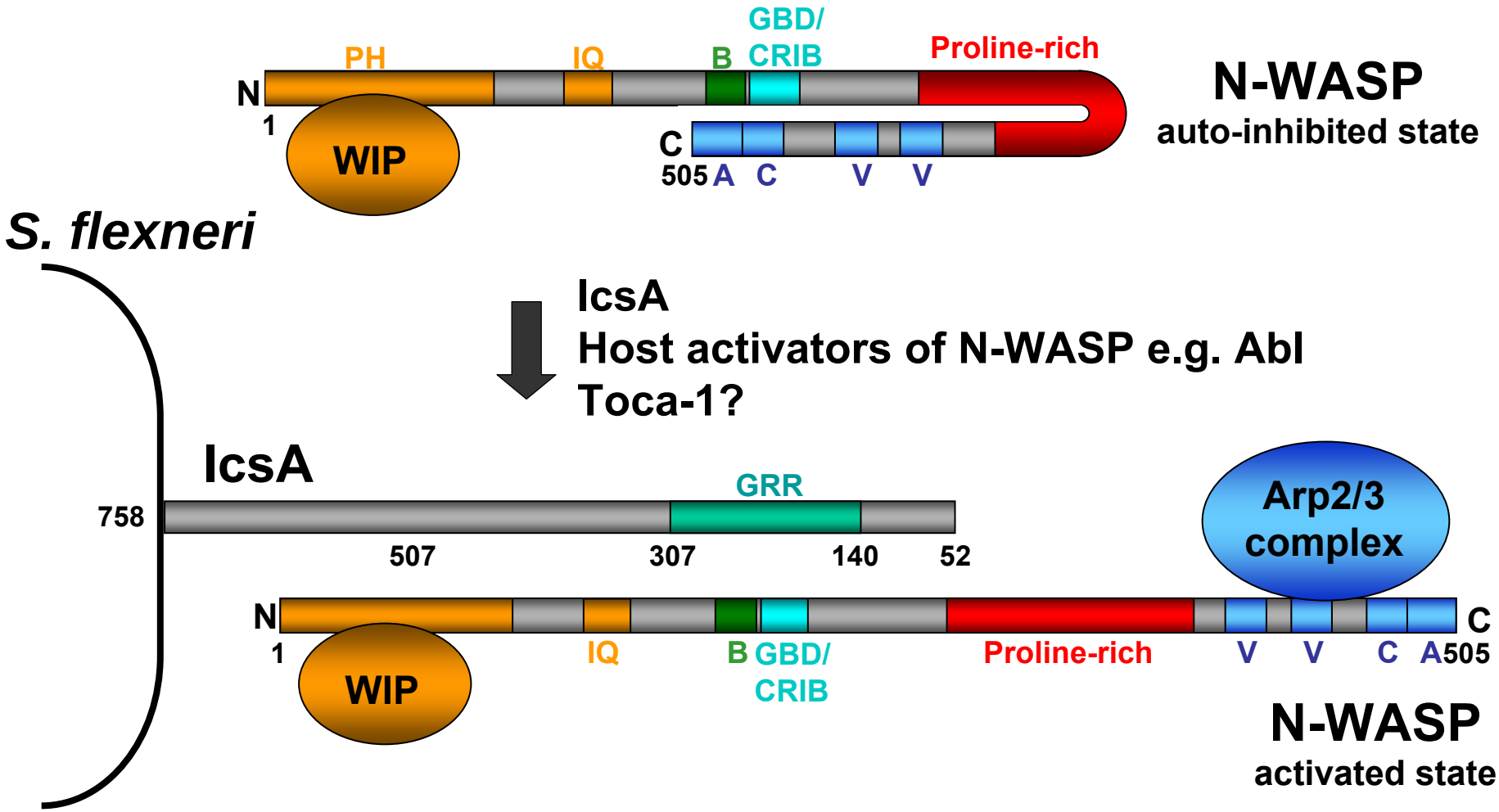
PH
IQ
B
GBD/
CRIB
Proline-rich
N
1
WIP
C
505
A
C
V
V
N-WASP
auto-inhibited state
S. flexneri
IcsA
Host activators of N-WASP e.g. Abl
Toca-1?
IcsA
758
GRR
507
307
140
52
Arp2/3
complex
N
1
WIP
IQ
B
GBD/
CRIB
Proline-rich
V
V
C
A
505
C
N-WASP
activated state

understood of the role of several of the known activators of N-WASP in IcsA-mediated ABM is discussed below.

1.4.3.1 Role of Cdc42

Cdc42 is a Rho family GTPase that activates N-WASP by binding to its CRIB domain (Miki and Takenawa, 2003). Although its was reported that Cdc42 was essential for IcsA-mediated activation of N-WASP (Suzuki *et al*., 2000), other reports claiming IcsA activation of N-WASP occurs independently of Cdc42 (Egile *et al*., 1999; Loisel *et al*., 1999; Mounier *et al*., 1999) have been validated by work with Cdc42-deficient cells, with *Shigella* able to form F-actin comet tails and exhibiting efficient ABM in these cells (Shibata *et al*., 2002).

1.4.3.2 Role of PIP_2

Phosphatidylinositol 4,5-bisphosphate ($PI(4,5)P_2$), also called PIP_2, has been shown to either directly activate N-WASP via binding to the basic region or to act upstream by activating Cdc42 (Rohatgi *et al*., 2000). The recent discovery of Toca-1 (Ho *et al*., 2004) and its role in Cdc42-dependent actin nucleation through activation of both Cdc42 and the N-WASP-WIP complex suggests an upstream position for PIP_2 in the signalling pathway (Ho *et al*., 2004; Insall and Machesky, 2004). Furthermore, it has also been suggested that the interaction between PIP_2 and N-WASP might only occur under non-physiological conditions and is perhaps biologically irrelevant (Ho *et al*., 2004).

1.4.3.3 Role of WIP

Recruitment of WIP to *Shigella* and their F-actin comet tails has been observed inside infected cells (Moreau *et al*., 2000; Zetti and Way, 2002). However, WIP is not required for *Shigella* ABM *in vitro* and expression of a negative dominant form of WIP does not affect *Shigella* motility inside cells (Loisel *et al*., 1999, Moreau *et al*., 2000; Zettl and Way, 2002).

It is thought that WIP is recruited to intracellular *Shigella* via its interaction with the WH1 domain of N-WASP. Indeed, mutation of the WH1 binding motif abolished WIP recruitment to *Shigella* (Zettl and Way, 2002). However, recruitment of WIP in *Shigella* infected N-WASP deficient cells has not been investigated.

1.4.3.4 Role of N-WASP proline-rich region ligands Nck, Grb2, profilin and WISH

Over-expression of an N-WASP mutant lacking the proline-rich domain inside infected cells inhibits F-actin tail formation, suggesting a role for this region of N-WASP in *Shigella* ABM (Mimuro *et al.*, 2000).

Profilin, an actin monomer-binding protein, that functions to recruit G-actin to sites of actin polymerisation, can interact with the proline-rich region of N-WASP (Yang *et al*., 2000). Although apparently not essential for IcsA-mediated ABM, profilin has been shown to increase motility rates of *E. coli* expressing IcsA in either *Xenopus* cytoplasmic extracts or reconstituted systems with purified cytoskeletal proteins (Loisel *et al*., 1999; Mimuro *et al.*, 2000; Goldberg, 2001). However, enhancement of *Shigella* motility by profilin has been demonstrated to be independent of its binding to the N-WASP proline-rich sequences (Yang *et al*., 2000).

Nck, a known activator of N-WASP (Miki and Takenawa, 2003) is recruited to *Shigella* and their F-actin tails but appears to have no direct function in this process (Loisel *et al*., 1999; Moreau *et al.*, 2000). This is evident by the fact that Nck is not required for *Shigella* ABM *in vitro* and that over-expression of a dominant negative form of Nck (Nck lacking its SH2 domain) has no effect on *Shigella* motility inside cells (Loisel *et al*., 1999; Moreau *et al.*, 2000).

Grb2 acts as an SH2-SH3 domain adaptor that interacts with the proline-rich region of N-WASP via a C-terminal SH3 domain (Miki and Takenawa, 2003). Although Grb2 is not essential for IcsA-mediated ABM, *in vitro* studies involving reconstituted proteins and *E. coli* expressing IcsA, show that the addition of Grb2 increased the efficiency of ABM by decreasing the delay prior to F-actin comet formation and bacterial movement (Carlier *et al.*, 2000).

The role of WISH, a potent activator of N-WASP (Miki and Takenawa, 2003), in *Shigella* ABM has not been investigated.

1.4.3.5 Role of phosphorylation of N-WASP and Abl kinases

Despite the report that phosphotyrosine proteins could not be detected associated with either *Shigella* or their F-actin comet tails (Frischknecht *et al.*, 1999), a more recent study has suggested that phosphorylation of N-WASP may be required for efficient formation of *Shigella* F-actin comet tails (Burton *et al*., 2005). N-WASP has been shown to be a substrate for phosphorylation by Abl kinases; in Abl-deficient cells, *Shigella* form shorter F-actin tails and exhibit reduced plaque formation (Burton *et al*., 2005). Moreover, the expression of an activated form of N-WASP in Abl-deficient cells restores *Shigella* F-actin tail formation supporting its role in N-WASP activation.

1.4.4 IcsA-mediated vinculin activation

Apart from N-WASP, vinculin is the only other host actin-regulatory protein known to interact directly with IcsA. Inside cells, vinculin is recruited to the poles of bacteria, throughout F-actin comet tails and within protrusions (Kadurugamuwa, *et al*., 1991; Suzuki *et al.*, 1996; Frischknecht *et al.*, 1999; Laine *et al*., 1997; Goldberg, 2001). However, the precise role of vinculin in *Shigella* ABM and intercellular spread remains controversial.

Vinculin consists of a 95-kDa "head" domain at the N-terminus, a 30-kDa "tail" domain at the C-terminus and a central proline-rich region. Similarly to N-WASP, in its auto-inhibited conformation, vinculin is folded such that an intramolecular interaction between the head and tail domains blocks binding of the tail domain to F-actin (Johnson and Craig, 1994; Johnson and Craig, 1995).

It has been shown that it is the head domain of vinculin that is recruited to *Shigella* inside cells (Suzuki *et al.*, 1996; Laine *et al*., 1997). Upon infection of cells with *Shigella*, a small amount of vinculin is cleaved to produce a fragment containing the head domain with the proline-rich region at its C-terminus (Laine *et al*., 1997). However, other researchers have not been able to detect vinculin cleavage in infected cells (Suzuki *et al*., 1998). Nonetheless, microinjection of the purified head domain of vinculin has been shown to accelerate *Shigella* ABM, which lead to the proposal that *Shigella* cleaves vinculin and the released head domain binds IcsA and acts as linker between IcsA and the vasodilator-stimulated phosphoprotein (VASP) (Laine *et al*., 1997). VASP, which is found associated with *Shigella* F-actin comet tails, can bind F-actin and profilin and is implicated in regulation of the actin cytoskeleton (Gertler *et al.*, 1996; Goldberg, 2001; Galler *et al*., 2005). However, the involvement of vinculin is unlikely to be for VASP recruitment since *Shigella* ABM and protrusion formation was found to be normal in ena/VASP-deficient cells (Ally *et al*., 2004).

The role of vinculin was brought into question when *Shigella* ABM and protrusion formation was found to be normal in vinculin-deficient cells (F9 5.51 cells), and vinculin was not required for IcsA-mediated ABM using purified cytoskeletal proteins (Goldberg, 1997; Loisel *et al*., 1999). However, it was later reported that F9 5.51 cells contain low levels of truncated vinculin and it was suggested that this may be sufficient to support *Shigella* ABM (Southwick *et al*., 2000).

Interestingly, the identified vinculin binding region for IcsA (aa 104-506) overlaps the N-WASP binding region and, as the latter has been shown to be essential for *Shigella* ABM, it is of interest to determine if and how vinculin binding might affect IcsA mediated activation of N-WASP. Indeed, Suzuki *et al*. reported unpublished data in which purified VCA fragment of N-WASP competed with binding of purified vinculin to purified IcsA (Suzuki *et al*., 1998). However, this data is hard to interpret since the researchers had mistakenly identified the VCA regions as mediating an N-WASP-IcsA interaction, and it is now known that IcsA instead interacts with the WH1 and CRIB/GBD domains (Suzuki *et al.*, 1998; Egile *et al.*, 1999; Suzuki *et al.*, 2002; Moreau *et al*., 2000).

1.6 Intercellular spread

ABM is not sufficient for intercellular spread of *Shigella* (Sansonetti *et al.*, 1994). One area of *Shigella* pathogenesis that remains poorly understood is the mechanism for the formation of bacteria-containing protrusions and their uptake into neighbouring cells leading to intercellular spread. What is known about the host and bacterial factors involved in this process is summarised below.

1.6.1 Host cell factors involved in intercellular spread

The formation of bacterial-containing protrusions and intercellular spread of *Shigella* occurs primarily in the region of the eukaryotic cell's adherens junctions (Sansonetti *et al.*, 1994), protein complexes involved in cell-cell adhesion, and tissue development and function (Gumbiner, 1996). Intercellular spread of *Shigella* is inhibited by either pharmacological reagents or host cell mutations that completely disrupt the junctional complex (Rathman *et al.*, 2000b). Cadherin, a component of adherens junctions important in cell-cell adhesion, has been shown to be associated with bacteria-containing protrusions and to be required for cell-to-cell spread (Sansonetti *et al.*, 1994). Additionally, other components such as vinculin, α-

catenin, β-catenin and α-actinin have also been reported to be associated with *Shigella*-containing protrusions, although their involvement in intercellular spread of *Shigella* has not been directly examined (Kadurugamuwa *et al*., 1991; Sansonetti *et al.*, 1994; Goldberg 2001).

Shigella-induced opening of host-cell connexin channels promotes the release of ATP into the extracellular milieu, calcium signalling events that enhance invasion, and intercellular spread of *Shigella* (Tran Van Nhieu *et al*., 2003). Although the mechanisms are still being elucidated, transient increases in intracellular calcium concentration appear dependent on a functional type-III secretory apparatus, suggesting secreted effector proteins are involved in mediating these processes (Tran Van Nhieu *et al*., 2003).

Myosins, a protein superfamily of actin-dependent molecular motors, have been indirectly implicated in the process of intercellular spreading (Rathman *et al.*, 2000b). Inhibitors of the myosin light chain kinase (MLCK) have been shown to significantly reduce intercellular spreading by *S. flexneri* despite efficient bacterial invasion, growth and ABM within the host cell. This has lead to the suggestion that the phosphorylation of myosin by MLCK, and its subsequent activation, is required for the formation of the bacteria-containing protrusions, and may possibly play a role in the endocytosis of protrusions by the neighbouring cells. Further investigation is required in order to understand how myosins contribute to this process.

1.6.2 Bacterial factors involved in intercellular spread

1.6.2.1 VacJ

In addition to virulence-plasmid encoded factors a chromosomal gene, *vacJ*, has been identified as being potentially required for intercellular spread. A *vacJ* mutant exhibited ABM and formed protrusions, but demonstrated a reduced ability to escape into the cytoplasm of

neighbouring cells (Suzuki *et al*., 1994). VacJ was shown to be a 28 kDa protein exposed on the bacterial surface, and possessing a motif characteristic of lipoproteins. The exact function of this protein has not yet been identified and the results of this study warrant further investigation of this protein. However, the *vacJ* mutant used in this study was made using a polar mutation and effects of this mutation on downstream genes cannot be ruled out.

1.6.2.2 Role of the type III secretion system

Researchers have identified post-invasion contributions of the TTSS and its effectors (Schuch *et al.*, 1999; Rathman *et al.*, 2000a). Intracellular repression of the TTSS apparatus (MxiM and Spa33) and the secreted effectors, IpaB, IpaC and IpaD affected the ability of *Shigella* to spread from cell-cell (Schuch *et al.*, 1999). Electron microscopy demonstrated that secretion of the Ipa proteins via Mxi-Spa TTSS was required for *Shigella* to escape from protrusion-derived, double-membrane-bound vacuoles (Schuch *et al.*, 1999). Rathman *et al.* (2000a) confirmed this result using a fluorescence activated cell sorter (FACS)-based study to identify factors required for intercellular spread.

Additionally, the *S. flexneri* VirA protein, which is secreted into the host cell via the TTSS, has also been shown to be important for intracellular and intercellular spread as *virA* mutants failed to move within host cells cytoplasm and into adjacent cells (Uchiya *et al*., 1995; Yoshida *et al*., 2002; Yoshida *et al*., 2006). VirA has cysteine protease–like activity that is specific for α-tubulin, a component of host cell microtubules (Yoshida *et al*., 2006). In the absence of VirA, movement of *S. flexneri* within the host cytoplasm is inhibited drastically by microtubules (Yoshida *et al*., 2002; Yoshida *et al*., 2006). Destabilisation of host cell microtubules by VirA enables *S. flexneri* to move freely within the cytoplasm via ABM and spread to adjacent cells (Yoshida *et al*., 2002; Yoshida *et al*., 2006).

Interestingly in the study of Rathman *et al.* (2000a), seeking to discover genes involved in intercellular spread, most of the mutants identified possessed mutations that affected their LPS structure.

1.7 The role lipopolysaccharide in ABM and intercellular spread

1.7.1 Structure of lipopolysaccharide

Lipopolysaccharide (LPS) is a major constituent of the OM of Gram-negative bacteria. LPS consists of three major parts: (1) the lipid A, (2) the core polysaccharide, and (3) the O antigen (Oag) polysaccharide chain (Figure 1.13). An LPS molecule lacking Oag is referred to as rough LPS (R-LPS) whereas LPS with Oag chains is referred to as smooth LPS (S-LPS). The number of Oag sub-units in a LPS molecule, display a characteristic modal length that is dependent on Wzz protein activity (Morona *et al*., 1995). *S. flexneri* 2a has S-LPS with two modal chain lengths (Figure 1.14). A short (S) type (12-17 repeat units), that is dependent on the chromosomally encoded Wzz_{SF} and a very long (VL) type (>90 repeat units) determined by a plasmid encoded Wzz_{pHS-2} (Morona *et al*., 1995; Hong and Payne, 1997). The combination of these modal lengths contributes to virulence with VL-type LPS conferring serum resistance and S-type LPS permitting IcsA function (Hong and Payne, 1997; Morona *et al*., 2003).

1.7.2 Role of LPS Oag in ABM and intercellular spread

Through mutagenesis of genes known to be involved in LPS biosynthesis (*galU, wecA* [*rfe*], *wzy* [*rfc*], *rfb, rmlD*), it has been well established that S-LPS is required for efficient ABM and intercellular spread of *S. flexneri* (Okada *et al*., 1991; Sandlin *et al*., 1995; Sandlin *et al*., 1996; Hong and Payne, 1997; Van Den Bosch and Morona, 2003).

Figure 1.13. The structure of lipopolysaccharide.

A representation of the three domains of smooth lipopolysaccharide (LPS) embedded in the outer-membrane (OM); the lipid A, the core polysaccharide and the O antigen (Oag) polysaccharide chain. A rough LPS molecule that lacks the Oag polysaccharide chain is also shown. Adapted from G.M. Murray, PhD thesis (2004).

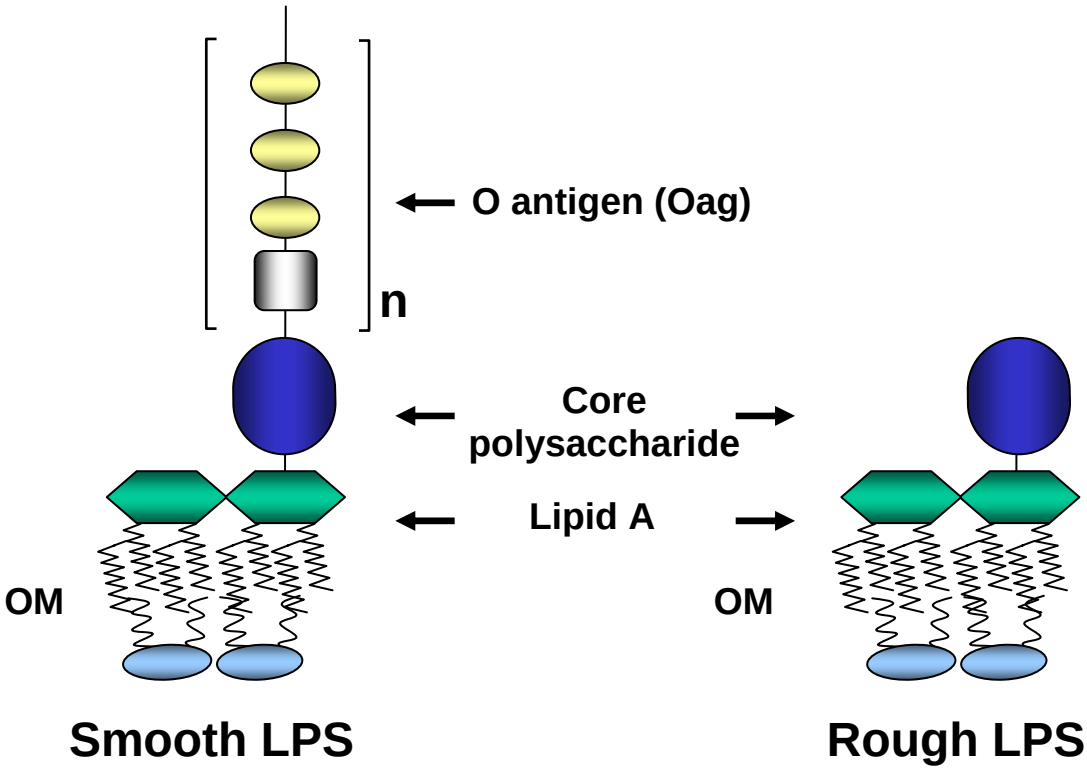
O antigen (Oag)
n
Core
polysaccharide
Lipid A
OM
OM
Smooth LPS
Rough LPS

Figure 1.14. Silver-stained SDS-PAGE anaysis of *S. flexneri* LPS.

LPS from 10^8 bacteria of *S. flexneri* 2a strain 2457T (lane 1) and *S. flexneri* 2a 2457T Δ*rmlD* (lane 2) was electrophoresed on a 15% polyacrylamide gel and silver-stained. The very long-type LPS (VL-type) modal length conferred by Wzz_{pHS-2} and the Short-type LPS (S-type) modal length conferred by Wzz_{SF} are shown. Rough LPS (R-LPS) and smooth LPS (S-LPS) populations of LPS are also indicated. n = number of O-antigen repeat units. Figure courtesy of L. Van den Bosch.

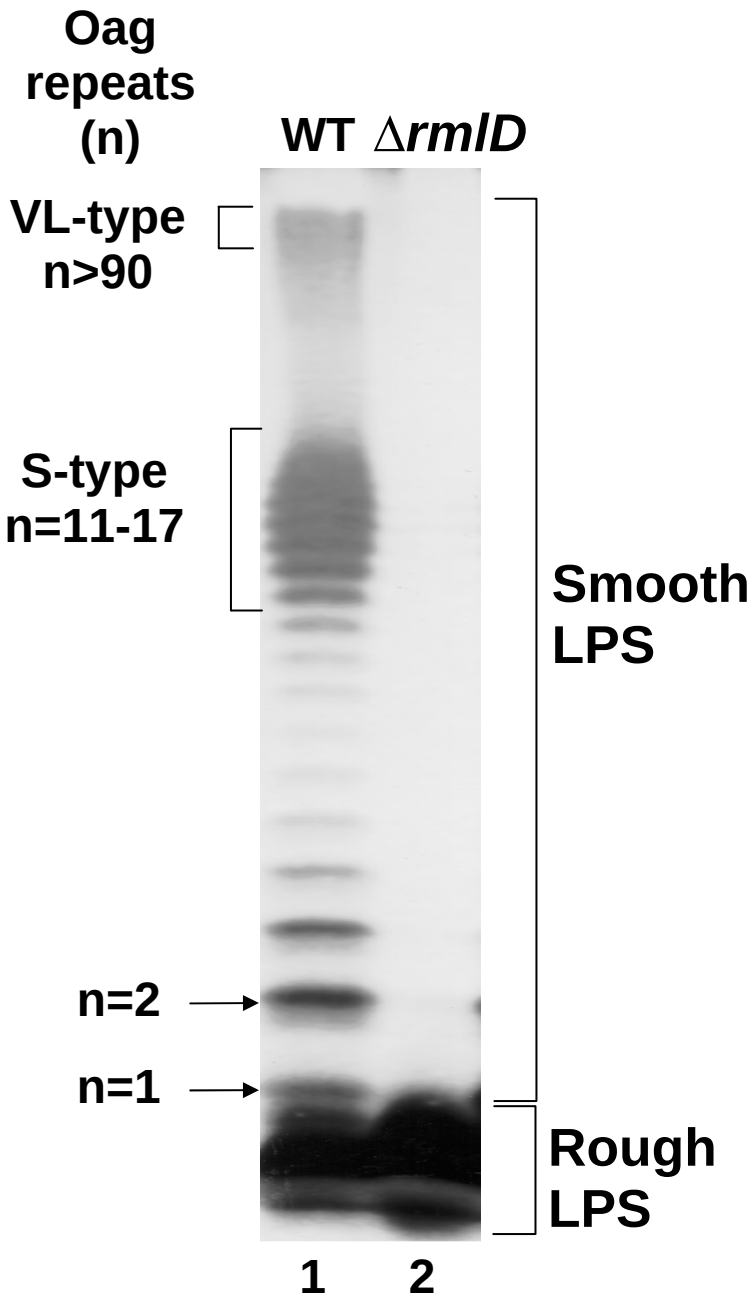
Oag repeats (n)
WT
ΔrmlD
VL-type n>90
S-type n=11-17
Smooth LPS
n=2
n=1
Rough LPS
1
2

Deep rough mutants of *Shigella* (e.g. *galU*) that lack Oag and have an incomplete core, exhibit diffuse circumferential distribution of IcsA, and although some accumulation of F-actin is observed in infected cells, these mutants are unable to form either F-actin comet tails or protrusions, and spread from cell-to-cell (Okada *et al*., 1991; Sandlin *et al*., 1995). Rough mutants have an intermediate phenotype with IcsA detected all over the entire surface of bacteria but with some polar reinforcement (Okada *et al*., 1991; Sandlin *et al*., 1995). Also, rough mutants generate F-actin comet tails with an altered morphology and demonstrate a marked reduction in their ability to form plaques in tissue culture monolayers, with either tiny plaques or no plaques being observed (Okada *et al*., 1991; Sandlin *et al*., 1995; Sandlin *et al*., 1996; Van Den Bosch and Morona 2003).

While the sugar composition of Oag doesn't appear to affect ABM, the length of the chains is important (Sandlin *et al*., 1996; Van Den Bosch *et al*., 1997; West *et al*., 2005). LPS Oag chains with 2 to <90 repeat units are required for efficient actin based motility but Oag with 2 to <20 repeat units is required in the presence of VL-type LPS Oag (Van Den Bosch *et al*., 1997). One model for the role of LPS Oag in ABM is that it is responsible for maintaining unipolar IcsA localisation to ensure efficient ABM and intercellular spread (Sandlin *et al.*, 1995; Robbins *et al*., 2001). Since rough strains display altered IcsA localisation, with IcsA detected on the lateral regions as well as the poles, it has been suggested that LPS Oag reinforces IcsA polarisation by reduction of membrane fluidity, thereby preventing diffusion of IcsA away from the pole towards lateral regions of the bacterium (Sandlin *et al.*, 1995; Robbins *et al*., 2001). In addition to this possibility, studies from our laboratory suggest that there is also an indirect effect of LPS Oag on IcsA localisation, as L-type and VL-type Oag have been shown to mask IcsA detection on the bacterial surface (Morona *et al*., 2003; Morona and Van Den Bosch, 2003b). A recent study involving S-LPS *Shigella* strains showed that newly synthesised IcsA is indeed found on lateral regions as well as the old pole but Oag

chains mask detection of IcsA with antibodies on lateral regions (Morona and Van Den Bosch, 2003b). The higher IcsA concentration gradient at the pole would explain why polar IcsA is readily detectable, compared to laterally located protein. In agreement with this idea is the finding that on immunogold labelled R-LPS *E. coli* mutants, where Oag is not present to mask IcsA, IcsA is still detected more readily at the poles than the lateral regions (Van Den Bosch *et al*., 1997).

Regardless of the effect of LPS-Oag on IcsA localisation, studies have shown that the defect in intercellular spread of rough *Shigella* strains is perhaps not due to non-polar IcsA localisation (Van Den Bosch and Morona, 2003). Smooth *Shigella* strains expressing high levels of non-cleavable IcsA have comparable IcsA localisation to rough-LPS *Shigella* strains and are competent in ABM and intercellular spread (as discussed earlier in Section 1.2.3.2), suggesting an alternative function of LPS-Oag in ABM and intercellular spread (Van Den Bosch and Morona, 2003; Fukuda *et al*., 1995). Consequently, although there is a correlation between protrusion formation and uni-directional movement, (Monack and Theriot, 2001), there is however no correlation between IcsA localisation and intercellular spread (Van Den Bosch and Morona, 2003).

1.7.3 Role of VirK in ABM

A role for *virK* in intercellular spreading and ABM was identified during a *Tn10* insertion mutagenesis study in which a *virK* mutant exhibited reduced intracellular spread and was unable to form plaques on epithelial cell monolayers (Nakata *et al.*, 1992). This *S. flexneri virK*::*Tn10* mutant had WT levels of *icsA* mRNA, but reduced levels of IcsA protein in cell lysates and lead to the suggestion that *virK* post-transcriptionally regulates IcsA expression. A more recent study has shown that inactivation of *virK* results in increased IcsP levels, which in-turn results in increased IcsA cleavage and secretion into the supernatant

(Wing *et al.*, 2005). The *virK* gene is located on the virulence plasmid between the genes *rfbU* and *msbB2* that are involved in the modification of LPS and therefore it has been speculated that *virK* may have a similar function.

1.8 Project aims

IcsA is a critical virulence factor in *S. flexneri* pathogenesis. Little is known about its structure, and only general details are known about its interaction with host proteins. The overall aim of this thesis is to conduct a comprehensive study of IcsA structure and function in the process of ABM. More specifically the aims were to:

(1) Create a range of IcsA mutants by random linker-insertion mutagenesis and characterise the relationship between IcsA structure and its function in ABM.

(2) Investigate the relationship between Oag chains and IcsA-dependent ABM, specifically looking at the effect Oag chains have on the interaction of IcsA with host factors.

(3) To create a 3D-structural model of IcsA using *in silico* analysis tools.

(4) Investigate the oligomeric state of IcsA, as it may relate to its function and biogenesis.

(5) Examine the distribution of different LPS populations on the surface of *Shigella flexneri* and determine if the LPS profile at the poles of bacteria is distinct to the overall LPS profile. The latter will enable a better understanding of how LPS-OAg contributes to IcsA detection and function.

Chapter Two

Materials and Methods

Chapter Two: Materials and Methods

2.1 Chemicals and reagents

Unless otherwise stated, chemicals and reagents were sourced from the following suppliers: Ajax (Analytical grade), Amresco, BDH Chemicals (AnalaR® grade), Difco, Gibco BRL, New England Biolabs, Roche and Sigma-Aldrich.

2.1.1 Antibodies and antisera

Affinity purified rabbit poly-clonal anti-IcsA antisera was made by Luisa Van Den Bosch from our laboratory as described by Van Den Bosch *et al*. (1997). The anti-IcsA antibody was used at 1:500-1:4000 for Western immunoblotting and 1:50-1:100 for immunofluorescence microscopy. The polyclonal rabbit anti-N-WASP antibody was initially a generous gift from Assoc. Prof. Hiroaki Miki. Subsequent stocks of comparable polyclonal rabbit anti N-WASP antibodies were made by Luisa Van Den Bosch in our laboratory according to the method described by Fukuoka *et al*. (1997). The vector encoding a GST tagged carboxyl-terminal region of N-WASP (VCA region; amino acids 388–501), used to produce purified protein for the production of antiserum, was kindly provided by Assoc. Prof. Hiroaki Miki. The anti-N-WASP antibody was used at 1:100 for immunofluorescence microscopy. The polyclonal anti-*Shigella* LPS (3,4) was from Denka Seiken Co. (Japan) and was used at 1:100 for immunofluorescence microscopy. The anti-FLAG M2 (#F3165) and monoclonal anti-human vinculin (V-9131) antibodies were from Sigma. The anti-FLAG M2 antibody was used at 1:1000-1:2000 for Western immunoblotting and 1:50-1:100 for immunofluorescence microscopy and the anti-vinculin antibody was used at 1:500 for Western immunoblotting and 1:100 for immunofluorescence microscopy.

2.2 Bacterial strains and plasmids

The *Escherichia coli* and *Shigella flexneri* strains used in this study are included in Table 2.1 and strains created in this thesis are included in Table 2.2. The plasmids used and constructed in this study are listed in Table 2.3.

2.3 Bacterial growth media

2.3.1 Liquid growth media

All *E. coli* and *S. flexneri* strains were grown at 37°C or 30ºC (for temperature sensitive strains) in LB-broth or LB-agar plates with the appropriate antibiotics unless stated otherwise. The following liquid media were used for cultivation of bacteria: Luria Bertani broth (LB, 10 g/L tryptone [Becton Dickinson], 5 g/L yeast extract [BD], 5 g/L NaCl); Tryptic soy broth (TSB, 30 g/L TSB [BD] 30 g/L); and SOC (20 g/L tryptone [BD], 5 g/L yeast extract, 20 mM glucose, 8.6 mM NaCl, 2.5 mM KCl, 20 mM $MgSO_4$). All were prepared in distilled water and sterilised by autoclaving.

2.3.2 Solid growth media

Solid growth media used were: Luria Bertani agar (15 g/L Bacto-agar [BD] in LB); Tryptic soy agar (TSA, 15 g/L Bacto-agar in TSB); R-TOP agar (10 g/L tryptone, 8 g/L NaCl, 1 g/L yeast extract, 8 g/L agar, autoclaved and supplemented with 2 mM $CaCl_2$, 0.1% [w/v] glucose); R-agar plates (R-TOP agar with 12 g/L of agar). In order to confirm virulence-plasmid expression in *Shigella*, strains were streaked out on to TSA supplemented with 0.01% (v/v) Congo Red solution (Section 2.3.3) and incubated at 37°C, a permissive temperature for virulence-plasmid expression. Virulence-plasmid positive colonies appeared red, whilst virulence-plasmid negative colonies appeared white. When blue/white colony screening was required, plates were supplemented with 80 µg/ml 5-bromo-4-chloro-3-indolyl-β-D-galactoside (X-Gal; Progen) and 0.5 mM isopropyl-β-D-thiogalactopyranoside (IPTG;

Table 2.1 - Bacterial strains

Strain	Relevant characteristics	Reference/source
Escherichia coli K-12		
DH5α	cloning host	Gibco-BRL
UT5600	protease-deficient strain; Δ*ompT* Δ*ompP*; Sm^R	Laboratory stock/P.Manning
S-17	conjugative strain	Laboratory stock/P.Manning
RMA156	S-17 [pJRD215]	Morona *et al.*, (1994)
RMA160	S-17 [pRMA154]	Morona *et al.*, (1994)
Shigella flexneri		
2457T	*S. flexneri* 2a wild-type	LaBrec *et al.*, (1964) (ATCC 700930)
RMA2041	2457T Δ*icsA*::Tc^R	Van Den Bosch and Morona (2003)
RMA2090	RMA2041 [pIcsA]	Van Den Bosch and Morona (2003)
RMA2043	RMA2041 Δ*rmlD*::Km^R	Van Den Bosch and Morona (2003)
RMA2107	RMA2043 [pIcsA]	Van Den Bosch and Morona (2003)
AB1133 (P109)	P1 phage propagation strain	Laboratory stock

Table 2.2 - Bacterial strains created in this thesis

Strain	Relevant characteristics	Reference/source
Escherichia coli K-12		
KMRM1	DH5α [pKMRM1]	Section 3.2
KMRM2	DH5α [pKMRM2]	Section 3.2
KMRM3	DH5α [pKMRM3]	Section 3.2
KMRM4	DH5α [pKMRM4]	Section 3.2
KMRM5	DH5α [pKMRM5]	Section 3.2
KMRM6	DH5α [pKMRM6]	Section 3.2
KMRM7	DH5α [pKMRM7]	Section 3.2
KMRM8	DH5α [pKMRM8]	Section 3.2
KMRM9	DH5α [pKMRM9]	Section 3.2
KMRM10	DH5α [pKMRM10]	Section 3.2
KMRM11	DH5α [pKMRM11]	Section 3.2
KMRM12	DH5α [pKMRM12]	Section 3.2
KMRM13	DH5α [pKMRM13]	Section 3.2
KMRM14	DH5α [pKMRM14]	Section 3.2
KMRM15	DH5α [pKMRM15]	Section 3.2
KMRM16	DH5α [pKMRM16]	Section 3.2
KMRM17	DH5α [pKMRM17]	Section 3.2
KMRM18	DH5α [pKMRM18]	Section 3.2
KMRM19	DH5α [pKMRM19]	Section 3.2
KMRM20	DH5α [pKMRM20]	Section 3.2
KMRM21	DH5α [pKMRM21]	Section 3.2
KMRM22	DH5α [pKMRM22]	Section 3.2
KMRM23	DH5α [pKMRM23]	Section 3.2
KMRM24	DH5α [pKMRM24]	Section 3.2
KMRM25	DH5α [pKMRM25]	Section 3.2
KMRM26	DH5α [pKMRM26]	Section 3.2
KMRM27	DH5α [pKMRM27]	Section 3.2
KMRM28	DH5α [pKMRM28]	Section 3.2
KMRM29	DH5α [pKMRM29]	Section 3.2
KMRM30	DH5α [pKMRM30]	Section 3.2
KMRM31	DH5α [pKMRM31]	Section 3.2
KMRM32	DH5α[pKMRM32]	Section 3.2
KMRM33	DH5α [pKMRM33]	Section 3.2
KMRM34	DH5α [pKMRM34]	Section 3.2
KMRM35	DH5α [pKMRM35]	Section 3.2
KMRM36	DH5α [pKMRM36]	Section 3.2
KMRM37	DH5α [pKMRM37]	Section 3.2
KMRM38	DH5α [pKMRM38]	Section 3.2
KMRM39	DH5α [pKMRM39]	Section 3.2
KMRM40	DH5α [pKMRM40]	Section 3.2
KMRM41	DH5α [pKMRM41]	Section 3.2
KMRM42	DH5α [pKMRM42]	Section 3.2
KMRM43	DH5α [pKMRM43]	Section 3.2
KMRM44	DH5α [pKMRM44]	Section 3.2
KMRM47	DH5α [pKMRM47]	Section 3.2
KMRM51	DH5α [pKMRM51]	Section 3.2

(Table continued over page)

Table 2.2 - Bacterial strains created in this thesis (continued)

Strain	Relevant characteristics	Reference/source
Escherichia coli K-12		
KMRM62	DH5α [pKMRM62]	Section 3.2
KMRM67	DH5α [pKMRM67]	Section 3.2
KMRM78	UT5600 [pKD46]	Section 7.2.3
KMRM87	UT5600 [pIcsA]	Section 3.6; Section 7.4
KMRM96	DH5α [pGEMT-*minCDE*]	Section 7.2.1
KMRM99	DH5α [pGEMT-Km^R_{PacI}]	Section 7.2.1
KMRM161	DH5α [pGEMT-*minCDE*::Km^R]	Section 7.2.1
KMRM180a	DH5α [pCACTUS-*minCDE*::Km^R]	Section 7.2.1
KMRM183	UT5600 *minD*::Km^R	Section 7.2.3
KMRM186	UT5600 *minD*::85nt	Section 7.2.3
KMRM187	UT5600 *minD*::85nt [pIcsA]	Section 7.4
KMRM189	UT5600 *minD*::85nt [pIcsA] [pJRD215]	Section 7.4
KMRM191	UT5600 *minD*::85nt [pIcsA] [pRMA154]	Section 7.4
KMRM204	UT5600 [pKMRM4]	Section 3.6
KMRM209	UT5600 [pKMRM9]	Section 3.6
KMRM211	UT5600 [pKMRM11]	Section 3.6
KMRM212	UT5600 [pKMRM12]	Section 3.6
KMRM213	UT5600 [pKMRM13]	Section 3.6
KMRM214	UT5600 [pKMRM14]	Section 3.6
KMRM215	UT5600 [pKMRM15]	Section 3.6
KMRM216	UT5600 [pKMRM16]	Section 3.6
KMRM217	UT5600 [pKMRM17]	Section 3.6
KMRM219	UT5600 [pKMRM19]	Section 3.6
KMRM222	UT5600 [pKMRM22]	Section 3.6
KMRM225	UT5600 [pKMRM25]	Section 3.6
KMRM227	UT5600 [pKMRM27]	Section 3.6
KMRM228	UT5600 [pKMRM28]	Section 3.6
KMRM229	UT5600 [pKMRM29]	Section 3.6
KMRM231	UT5600 [pKMRM31]	Section 3.6
KMRM232	UT5600 [pKMRM32]	Section 3.6
KMRM234	UT5600 [pKMRM34]	Section 3.6
KMRM237	UT5600 [pKMRM37]	Section 3.6
KMRM239	UT5600 [pKMRM39]	Section 3.6
KMRM240	UT5600 [pKMRM40]	Section 3.6
KMRM247	UT5600 [pKMRM47]	Section 3.6
KMRM250	DH5α [pKMRM1::FLAG]	Section 6.4.1
KMRM252	DH5α [pBBRMCS2- *icsA*]	Section 6.3
KMRM270	DH5α [pBBRMCS2 - pKMRM1::FLAG]	Section 6.4.1
Shigella flexneri		
KMRM79	2457T [pKD46]	Section 7.2.3
KMRM101	RMA2041 [pKMRM1]	Section 3.2
KMRM102	RMA2041 [pKMRM2]	Section 3.2
KMRM103	RMA2041 [pKMRM3]	Section 3.2
KMRM104	RMA2041 [pKMRM4]	Section 3.2
KMRM105	RMA2041 [pKMRM5]	Section 3.2
KMRM106	RMA2041 [pKMRM6]	Section 3.2
KMRM107	RMA2041 [pKMRM7]	Section 3.2
KMRM108	RMA2041 [pKMRM8]	Section 3.2
KMRM109	RMA2041 [pKMRM9]	Section 3.2

(Table continued over page)

Table 2.2 - Bacterial strains created in this thesis (continued)

Strain	Relevant characteristics	Reference/source
Shigella flexneri		
KMRM110	RMA2041 [pKMRM10]	Section 3.2
KMRM111	RMA2041 [pKMRM11]	Section 3.2
KMRM112	RMA2041 [pKMRM12]	Section 3.2
KMRM113	RMA2041 [pKMRM13]	Section 3.2
KMRM114	RMA2041 [pKMRM14]	Section 3.2
KMRM115	RMA2041 [pKMRM15]	Section 3.2
KMRM116	RMA2041 [pKMRM16]	Section 3.2
KMRM117	RMA2041 [pKMRM17]	Section 3.2
KMRM118	RMA2041 [pKMRM18]	Section 3.2
KMRM119	RMA2041 [pKMRM19]	Section 3.2
KMRM120	RMA2041 [pKMRM20]	Section 3.2
KMRM121	RMA2041 [pKMRM21]	Section 3.2
KMRM122	RMA2041 [pKMRM22]	Section 3.2
KMRM123	RMA2041 [pKMRM23]	Section 3.2
KMRM124	RMA2041 [pKMRM24]	Section 3.2
KMRM125	RMA2041 [pKMRM25]	Section 3.2
KMRM126	RMA2041 [pKMRM26]	Section 3.2
KMRM127	RMA2041 [pKMRM27]	Section 3.2
KMRM128	RMA2041 [pKMRM28]	Section 3.2
KMRM129	RMA2041 [pKMRM29]	Section 3.2
KMRM130	RMA2041 [pKMRM30]	Section 3.2
KMRM131	RMA2041 [pKMRM31]	Section 3.2
KMRM132	RMA2041 [pKMRM32]	Section 3.2
KMRM133	RMA2041 [pKMRM33]	Section 3.2
KMRM134	RMA2041 [pKMRM34]	Section 3.2
KMRM135	RMA2041 [pKMRM35]	Section 3.2
KMRM136	RMA2041 [pKMRM36]	Section 3.2
KMRM137	RMA2041 [pKMRM37]	Section 3.2
KMRM138	RMA2041 [pKMRM38]	Section 3.2
KMRM139	RMA2041 [pKMRM39]	Section 3.2
KMRM140	RMA2041 [pKMRM40]	Section 3.2
KMRM141	RMA2041 [pKMRM41]	Section 3.2
KMRM142	RMA2041 [pKMRM42]	Section 3.2
KMRM143	RMA2041 [pKMRM43]	Section 3.2
KMRM144	RMA2041 [pKMRM44]	Section 3.2
KMRM145	RMA2043 [pKMRM17]	Section 4.5
KMRM146	RMA2043 [pKMRM22]	Section 4.5
KMRM147	RMA2041 [pKMRM47]	Section 3.2
KMRM148	RMA2043 [pKMRM32]	Section 4.5
KMRM149	RMA2043 [pKMRM40]	Section 4.5
KMRM151	RMA2041 [pKMRM51]	Section 3.2
KMRM152	RMA2043 [pKMRM12]	Section 4.5
KMRM153	RMA2043 [pKMRM19]	Section 4.5
KMRM156	RMA2043 [pKMRM27]	Section 4.5
KMRM157	RMA2043 [pKMRM16]	Section 4.5
KMRM158	RMA2043 [pKMRM29]	Section 4.5
KMRM160	RMA2043 [pKMRM37]	Section 4.5
KMRM162	RMA2041 [pKMRM62]	Section 3.2
KMRM167	RMA2041 [pKMRM67]	Section 3.2
KMRM195	RMA2043[pD10-*virG*1]	Section 4.5.3

(Table continued over page)

Table 2.2 - Bacterial strains created in this thesis (continued)

Strain	Relevant characteristics	Reference/source
Shigella flexneri		
KMRM197	RMA2043[pD10-*virG*3]	Section 4.5.3
KMRM198	RMA2043[pD10-*virG*4]	Section 4.5.3
KMRM254	RMA2041 [pKMRM252]	Section 6.3
KMRM255	RMA2090 [pKMRM252]	Section 6.3
KMRM256	KMRM111 [pKMRM252]	Section 6.3
KMRM257	KMRM116 [pKMRM252]	Section 6.3
KMRM258	KMRM134 [pKMRM252]	Section 6.3
KMRM259	KMRM119 [pKMRM252]	Section 6.3
KMRM260	KMRM132 [pKMRM252]	Section 6.3
KMRM261	KMRM143 [pKMRM252]	Section 6.3
KMRM263	KMRM123 [pKMRM252]	Section 6.3
KMRM264	KMRM135 [pKMRM252]	Section 6.3
KMRM273	RMA2041 [pKMRM270]	Section 6.4.1
KMRM275	RMA2090 [pKMRM270]	Section 6.4.2
KMRM276	KMRM111 [pKMRM270]	Section 6.4.2
KMRM277	KMRM134 [pKMRM270]	Section 6.4.2
KMRM278	RMA2043 [pKMRM13]	Section 4.5
KMRM279	RMA2043 [pKMRM31]	Section 4.5
KMRM280	RMA2043 [pKMRM11]	Section 4.5
KMRM281	RMA2043 [pKMRM15]	Section 4.5
KMRM282	RMA2043 [pKMRM25]	Section 4.5
KMRM283	RMA2043 [pKMRM28]	Section 4.5

Table 2.3 - Plasmids

Plasmid	Relevant characteristics	Reference/source
pIcsA	*icsA* gene cloned into pBR322; Ap^R ; medium copy no.; ColE1 *ori*	Morona and Van Den Bosch (2003a)
pIcsA*	noncleavable *icsA* gene cloned into pBR322; Ap^R; medium copy no.; ColE1 *ori*;	Morona and Van Den Bosch (2003a)
pBBRMCS2	broad-host-range vector; Km^R; medium copy no.; *ori* compatible with ColE1 plasmids	Kovach *et al.*, (1995)
pKD4	plasmid encoding Tn5 neomycin phosphotransferase (Km^R) flanked by natural FRT sites; temperature-sensitive origin of replication (ori_{ts}); Ap^R	Datsenko and Wanner (2000)
pKD46	Red recombinase helper plasmid; Ap^R; ori_{ts}	Datsenko and Wanner (2000)
pCP20	Ap^R; ori_{ts} ; thermal induction of FLP recombinase synthesis	Datsenko and Wanner (2000)
pGEMT-EASY	TA cloning vector Ap^R; *lacZ* (blue/white selection);	Promega
pJRD215	broad-host-range cosmid cloning vector; Km^R and Sm^R; *mob*, plasmid mobilisation functions;	Davison *et al.*, (1987)
pRMA154	$pJRD215_{ClaI\ -\ KpnI}$ -$pPM2213_{ClaI\ –\ KpnI}$ Km^R; Sm^R; encodes *galF*, *rfb* locus, *rfc* and *gnd*, Oag biosynthesis genes from *S. flexneri*	Morona *et al.*, (1994)
pCACTUS	suicide vector; ori_{ts}; *sacB*; Cm^R	Morona *et al.*, (1995)
pD10	plasmid encoding $IcsA_{WT}$; Tp^R	Suzuki *et al.*, (1996)
pD10-*virG*1	plasmid encoding $IcsA_{\Delta 103\text{-}320}$; Tp^R	Suzuki *et al.*, (1996)
pD10-*virG*3	plasmid encoding $IcsA_{\Delta 508\text{-}730}$; Tp^R	Suzuki *et al.*, (1996)
pD10-*virG*4	plasmid encoding $IcsA_{\Delta 103\text{-}507}$; Tp^R	Suzuki *et al.*, (1996)
pKMRM250	pKMRM1::FLAG; Ap^R ; medium copy no.; ColE1 *ori* ; encodes FLAG-tagged $IcsA_{i87}$	Section 6.4.1
pKMRM252	pBBRMCS2- *icsA*; Ap^R ; Km^R medium copy no.; *ori* compatible with ColE1 plasmids	Section 6.3
pKMRM270	$pBBRMCS2_{EcoRI\text{-}\ SalI}$ - $pKMRM1::FLAG_{EcoRI\text{-}\ SalI}$; Km^R medium copy no.; *ori* compatible with ColE1 plasmids; encodes FLAG-tagged $IcsA_{i87}$	Section 6.4.1
pKMRM96	pGEMT-*minCDE*; Ap^R	Section 7.2.1
pKMRM99	pGEMT-Km^R_{PacI}; Ap^R; Km^R	Section 7.2.1
pKMRM161	pGEMT-*minCDE*::Km^R; Ap^R; Km^R	Section 7.2.1
pKMRM180a	pCACTUS-*minCDE*::Km^R; ori_{ts}; *sacB*; Cm^R; Km^R	Section 7.2.1

(Table continued over page)

Table 2.3 - Plasmids (continued)

Plasmid	Relevant characteristics				Reference/source
	Description	Inserted epitope	Insertion site (aa number)	Reading frame	
pKMRM1	pIcsA derivative created by the MGS™ (Finnzymes)	TGC GGC CGC AAT GGA	87	1	Section 3.2
pKMRM2	pIcsA derivative created by the MGS™ (Finnzymes)	ATT GCG GCC GCA TCT	138	3	Section 3.2
pKMRM3	pIcsA derivative created by the MGS™ (Finnzymes)	TGC GGC CGC AAC TCT	137	1	Section 3.2
pKMRM4	pIcsA derivative created by the MGS™ (Finnzymes)	TGC GGC CGC AAT TGG	292	1	Section 3.2
pKMRM5	pIcsA derivative created by the MGS™ (Finnzymes)	TGC GGC CGC ACA GGT	386	1	Section 3.2
pKMRM6	pIcsA derivative created by the MGS™ (Finnzymes)	TGC GGC CGC ACT ATC	456	1	Section 3.2
pKMRM7	pIcsA derivative created by the MGS™ (Finnzymes)	ACT GCG GCC GCA CCA	369	3	Section 3.2
pKMRM8	pIcsA derivative created by the MGS™ (Finnzymes)	ATT GCG GCC GCA CTA	595	3	Section 3.2
pKMRM9	pIcsA derivative created by the MGS™ (Finnzymes)	ACT GCG GCC GCA CAG	633	3	Section 3.2
pKMRM10	pIcsA derivative created by the MGS™ (Finnzymes)	TGC GGC CGC AGT AAA	314	1	Section 3.2
pKMRM11	pIcsA derivative created by the MGS™ (Finnzymes)	CGT GCG GCC GCA ACA	563	3	Section 3.2
pKMRM12	pIcsA derivative created by the MGS™ (Finnzymes)	TGC GGC CGC ACT ATA	297	1	Section 3.2
pKMRM13	pIcsA derivative created by the MGS™ (Finnzymes)	ACT GCG GCC GCA ATC	330	3	Section 3.2
pKMRM14	pIcsA derivative created by the MGS™ (Finnzymes)	TGC GGC CGC AAT GGA	643	1	Section 3.2
pKMRM15	pIcsA derivative created by the MGS™ (Finnzymes)	GTT GCG GCC GCA TCT	342	3	Section 3.2
pKMRM16	pIcsA derivative created by the MGS™ (Finnzymes)	TGC GGC CGC AGG GAG	532	1	Section 3.2
pKMRM17	pIcsA derivative created by the MGS™ (Finnzymes)	TGC GGC CGC AAT TAT	226	1	Section 3.2
pKMRM18	pIcsA derivative created by the MGS™ (Finnzymes)	TGC GGC CGC ACC GGA	140	1	Section 3.2
pKMRM19	pIcsA derivative created by the MGS™ (Finnzymes)	GGT GCG GCC GCA AAG	248	3	Section 3.2
pKMRM20	pIcsA derivative created by the MGS™ (Finnzymes)	TGC GGC CGC ATG AGC	748	1	Section 3.2
pKMRM21	pIcsA derivative created by the MGS™ (Finnzymes)	TGC GGC CGC ACA GGT	324	1	Section 3.2
pKMRM22	pIcsA derivative created by the MGS™ (Finnzymes)	GTG CGG CCG CAC TCT	244	2	Section 3.2
pKMRM23	pIcsA derivative created by the MGS™ (Finnzymes)	TGC GGC CGC AGC GGT	288	1	Section 3.2
pKMRM24	pIcsA derivative created by the MGS™ (Finnzymes)	TGC GGC CGC ACT GGT	122	1	Section 3.2
pKMRM25	pIcsA derivative created by the MGS™ (Finnzymes)	TGC GGC CGC ACC GGT	219	1	Section 3.2
pKMRM27	pIcsA derivative created by the MGS™ (Finnzymes)	TGC GGC CGC AAT GCT	271	1	Section 3.2

Table 2.3 - Plasmids (continued)

Plasmid	Relevant characteristics				Reference/source
	Description	Inserted epitope	Insertion site (aa number)	Reading frame	
pKMRM28	pIcsA derivative created by the MGS™ (Finnzymes)	GGT GCG GCC GCA ACT	330	3	Section 3.2
pKMRM29	pIcsA derivative created by the MGS™ (Finnzymes)	GTT GCG GCC GCA ACT	381	3	Section 3.2
pKMRM30	pIcsA derivative created by the MGS™ (Finnzymes)	GGT GCG GCC GCA GGC	132	3	Section 3.2
pKMRM31	pIcsA derivative created by the MGS™ (Finnzymes)	TGC GGC CGC AAC GGT	268	1	Section 3.2
pKMRM32	pIcsA derivative created by the MGS™ (Finnzymes)	TGC GGC CGC AGT GAG	228	1	Section 3.2
pKMRM33	pIcsA derivative created by the MGS™ (Finnzymes)	GTG CGG CCG CAT TCG	56	2	Section 3.2
pKMRM34	pIcsA derivative created by the MGS™ (Finnzymes)	TGC GGC CGC ATT GCA	677	1	Section 3.2
pKMRM35	pIcsA derivative created by the MGS™ (Finnzymes)	GAT GCG GCC GCA GCT	502	3	Section 3.2
pKMRM36	pIcsA derivative created by the MGS™ (Finnzymes)	TGC GGC CGC AGT GGT	120	1	Section 3.2
pKMRM37	pIcsA derivative created by the MGS™ (Finnzymes)	GAT GCG GCC GCA GGT	346	3	Section 3.2
pKMRM38	pIcsA derivative created by the MGS™ (Finnzymes)	GTG CGG CCG CAT TCA	312	2	Section 3.2
pKMRM39	pIcsA derivative created by the MGS™ (Finnzymes)	TGC GGC CGC AGT GAT	230	1	Section 3.2
pKMRM40	pIcsA derivative created by the MGS™ (Finnzymes)	TGC GGC CGC ACA GGT	185	1	Section 3.2
pKMRM41	pIcsA derivative created by the MGS™ (Finnzymes)	ATT GCG GCC GCA GCT	326	3	Section 3.2
pKMRM42	pIcsA derivative created by the MGS™ (Finnzymes)	GTG CGG CCG CAC TTG	81	2	Section 3.2
pKMRM43	pIcsA derivative created by the MGS™ (Finnzymes)	TGC GGC CGC AAT AGT	193	1	Section 3.2
pKMRM44	pIcsA derivative created by the MGS™ (Finnzymes)	TGC GGC CGC AAT CAA	148	1	Section 3.2
pKMRM47	pIcsA derivative created by the MGS™ (Finnzymes)	TGC GGC CGC AGT TAT	716	1	Section 3.2
pKMRM51	pIcsA derivative created by the MGS™ (Finnzymes)	GCT GCG GCC GCA GTA	322	3	Section 3.2
pKMRM62	pIcsA derivative created by the MGS™ (Finnzymes)	AAT GCG GCC GCA GGT	128	3	Section 3.2
pKMRM67	pIcsA derivative created by the MGS™ (Finnzymes)	TGC GGC CGC AAT AAT	598	1	Section 3.2

Biovectra). Blue/white selection allows identification of recombinant plasmid molecules in *E. coli* via disruption of the LacZα peptide in cloning plasmids such as pGEMT-Easy (Promega; Table 2.2) and pBBRMCS2 (Kovach *et al*., 1995; Table 2.2)

2.3.3 Antibiotics and Congo Red solution

Antibiotics were added to broths and solid media at the following concentrations: ampicillin (Ap), 100 µg/ml; kanamycin sulphate (Km), 50 µg/ml; tetracycline (Tc) 50 µg/ml, streptomycin (Sm) 100 µg/ml. Stocks of Congo Red solutions were made with 1% (w/v) Congo Red (Sigma) in Milli Q water (MQ, 18.2MΩcm^{-1}; Millipore).

2.4 Maintenance of bacterial strains

2.4.1 General

Bacterial strains were maintained in a suspension of 30% (v/v) glycerol and 1% (w/v) peptone (Difco) in glass vials (Wheaton) for long-term storage at -70ºC. Cultivation from glycerol stocks was achieved by streaking a loop-full of the frozen suspension onto LB-agar plates or TSA plates supplemented with Congo Red, with appropriate antibiotics.

2.4.1 Creation and maintenance of IcsA linker-insertion libraries

Libraries of linker-insertion mutants were made by pooling colonies from individual transformation plates. This involved the addition of 1-3 ml of LB to a transformation plate, emulsification of the colonies with a sterile spreader, followed by aspiration and transfer of the bacterial suspensions into a reaction tube. Bacteria were pelleted by centrifugation (13000 rpm, 5 min, RT; Eppendorf 5417R), resuspended in 30% (v/v) glycerol and 1% (w/v) peptone (Difco), and transfered into glass vials (Wheaton) for long-term storage at -70ºC.

2.5 DNA isolation

2.5.1 Isolation of chromosomal DNA

Overnight (ON; 16 h) cultures were centrifuged (4500 rpm; 10 min; Sigma 3K15) and resuspended in 3 ml of 0.85% (w/v) saline prior to the addition of 3 ml of phenol (Tris-equilibrated, pH 7.5). The mixture was then vortexed intermittently (3 x 30 sec pulses over a period of 2 min), and then centrifuged as before. The aqueous phase was collected and added to 3 ml of ice-cold 100% isopropanol in a 10 ml McCartney bottle. The chromosomal DNA was then precipitated by vigorous agitation of the bottle and incubation at -20°C for 15-20 min. The precipitated DNA was then spooled using a Pasteur pipette fashioned into a hook, and washed in 70% (v/v) ethanol in a 1.5 ml reaction tube. Washed DNA was transferred to a new reaction tube and resuspended in 1 ml MQ water. The integrity of the isolated chromosomal DNA was assessed by agarose gel electrophoresis (Section 2.6.3).

2.5.2 Isolation of plasmid DNA from *E. coli* for *in vitro* cloning

10 ml of 16 h bacterial culture was pelleted by centrifugation (4500 rpm, 10min, 4ºC, Sigma 3K15) and the supernatant discarded. Bacterial pellets were resuspended in 300 µl of solution P1 (50 mM Tris-HCI, 10 mM EDTA, 100 µg/ml RNase, pH 8.0, 4ºC), and transferred to a 1.5 ml reaction tube. 300 µl of solution P2 (0.2 M NaOH, 1% [w/v] SDS, room temperature [RT]) was added and mixed by inversion. After incubation at RT of no more than 5 min, 300 µl of solution P3 (3 M potassium acetate, pH 5.5, 4ºC) was added and mixed by inversion and then incubated on ice for 10 min. Chromosomal DNA and cell debris were pelleted by centrifugation (13000 rpm, 10 min; Biofuge 13, Sepatech Heraeus) and the supernatant containing the plasmid DNA was transferred to a fresh tube. Plasmid DNA was separated from protein by the addition of 500 µl chloroform, vortexing (10 sec) centrifugation (13000 rpm, 5 min; Biofuge 13, Sepatech Heraeus) and removal of the upper aqueous layer to a fresh tube. DNA was precipitated with 600 µl of isopropanol and incubated at -20°C for 30-

60 min and then centrifuged (14000 rpm, 5 min, 4ºC; Eppendorf 5417R). The pellet was washed in 500 µl 70% (v/v) ethanol, centrifuged (14000 rpm, 5 min, 4ºC; Eppendorf 5417R), dried at 65ºC (Thermoline dry block heater) and resuspended in 20-100 µl MQ water and stored at 4ºC. A 5 µl sample of extracted plasmid DNA was analysed on a 1% (w/v) agarose gel (Section 2.6.3) to check the integrity.

2.5.3 Isolation of plasmid DNA from *E. coli* for transfection experiments

Plasmid DNA was extracted from 20 ml of culture using a plasmid mini-prep kit (Qiagen) according to manufacturer's instructions, except for elution of the DNA, which was performed in MQ at ½ the recommended volume in order to obtain a more concentrated sample of DNA.

2.5.4 Crude preparation of bacterial DNA by boiling method

The boiling method of DNA preparation was used to prepare DNA for large-scale PCR screening. Bacterial colonies were resuspended in 50 µl of MQ using a pipette. Samples were boiled (100°C, 5-10 min) and then centrifuged (14000 rpm, 5 min, room temperature; Eppendorf 5417R) and the supernatant was collected. One microlitre of supernatant was used as a template for PCR.

2.6 Analysis of DNA

2.6.1 DNA quantitation

DNA concentration was determined by the measurement of absorption at 260 nm with the assumption that an optical density of 1.0 is equal to 50 µg/ml of double stranded DNA.

2.6.2 Restriction endonuclease digestion of DNA

Restriction digests of plasmid DNA and PCR amplicons for either analytical purposes or in preparation for *in vitro* cloning (Section 2.9) were performed with 1-2 µg of DNA with the appropriate enzyme(s) (2 units of each) in the commercial buffers provided by New England Biolabs (NEB; Buffers 1-4) as per the manufacturer's instructions. Restriction enzyme digests of plasmid vectors, for gel extraction (Section 2.8.1), were performed on a larger scale with 4-8 µg of DNA in an 80 µl reaction volume. Five µl samples of digested DNA were analysed by agarose gel electrophoresis (Section 2.6.3). Wherever possible, restriction enzymes were heat inactivated according to the manufacturer's instructions, prior to further manipulation.

2.6.3 Agarose gel electrophoresis

DNA samples for electrophoresis were added to one-tenth the volume of tracking dye (1 mg/ml bromophenol blue, 20% [v/v] glycerol, 0.1 mg/ml RNase; boiled for 30 min) and loaded on to 1% (w/v) agarose gels in 1 x TBE buffer (67 mM Tris, 22 mM boric acid, 1 mM EDTA). The DNA samples were electrophoresed at 80-120 V for 45-60 min in 1 x TBE. Gels were stained for 5 min in distilled water containing 2 µg/ml ethidium bromide and de-stained in distilled water for 15-30 min. DNA bands were visualized using an UV trans-illuminator and photographed using a Mitsubishi video imaging system (Tracktel).

2.6.4 Calculation of DNA fragment length

The sizes of DNA fragments were determined according to their relative mobilities along an agarose gel relative to the DNA fragments of *Eco*RI digested bacteriophage SPP1 DNA standards. The SPP1 sizes (kb) were 8.51, 7.35, 6.11, 4.84, 3.59, 2.81, 1.95, 1.86, 1.51 1.39, 1.16, 0.98, 0.72, 0.48, 0.36 and 0.09. SPP1-*Eco*Rl digested molecular weight standards were prepared as described by Ratcliffe *et al.* (1979).

2.6.5 DNA sequencing

2.6.5.1 Sequencing using dye-labelled oligonucleotides

DNA sequencing was performed on extracted plasmid DNA (Section 2.5.2), using the ABI Prism Dye Terminator Cycle Sequencing Ready Reaction Kit ™. Reactions totaled 12 µl and consisted of 100 ng of template, 50 pmoles of primer, 4 µl of BIG DYE reaction mix (Version 3.1). The sequencing reaction consisted of 25 cycles (95ºC for 30 sec, 50ºC for 15 sec, 60ºC for 4 min) followed by a hold 4ºC in an Eppendorf Mastercycler. The 12 µl reaction mix was adjusted to a volume of 20 µl by the addition of 8 µl of MQ. Then the reaction mix was purified to using a Sodium acetate/ethanol precipitation method. 20 µl samples were added to 80 µl of a precipitation solution (3.0 µl of 3M sodium acetate, 62.5 µl of non-denatured 95% (v/v) ethanol, 14.5 µl MQ) and incubated for 1 h at RT. The DNA was pelleted by centrifugation (14000 rpm, 20 min, 4ºC; Eppendorf 5415R) and washed in 250 µl of 70% (v/v) ethanol and centrifuged for 5 min as before. The supernatant was discarded and the pellet dried for 1 h at RT. Sequencing reactions were analysed at the Australian Genomic Research Facility (AGRF), Gehrmann laboratories, Research, Road, University of Queensland.

2.6.5.2 DNA sequence analysis

Raw DNA sequence data obtained from the AGRF was aligned with native DNA sequences and analysed using the web based NCBI Basic Loval Alignment Search Tool (BLAST 2.0) (Tatusova and Madden, 1999).

2.7 DNA amplification

2.7.1 Synthesis of oligodeoxynucleotides

Oligodeoxynucleotides (primers) used in this study were purchased from Geneworks (Adelaide) and are listed in Table 2.4. Primers were supplied in lyophilized form and

Table 2.4 - Oligonucleotides

Oligonuceotide	Sequence (5' - 3')[a]	Annealing site / application	Nucleotide positions
2156 IcsAF	AACGGAATCTTTTCAGGGG	used to amplify the *icsA* gene	525-543[b]
2170 IcsAR	CCCATGTGATTTGCCTCG	used to amplify the *icsA* gene	4427-4444[b]
IcsA549F	TTCAGGTGGACATGGTGG	primer to amplify the *icsA* gene starting from nt 549	1122-1139[b]
IcsA2381R	GTGTTCATTGCTATCAGG	reverse primer to amplify the *icsA* gene from nt 2381	2937-2957[b]
*Not*I mini	TGCGGCCGCA		N/A
minF	GACTTGCCTCAATATAATCC		1210181-1210200[c]
minR	TCTGTGCGTGGGAACAGC		1208137-1208154[c]
P1_*Pac*I	CCTTAATTAAGTGTAGGCTGGAGCTGCTTC	Used to amplify the Km^R cartridge and flanking FRT sites of pKD4	N/A
P2_*Pac*I	CCTTAATTAACATATGAATATCCTCCTTAG	used to amplify the Km^R cartridge and flanking FRT sites of pKD4	N/A
minF_ *BamH*I	CGGGATCCGACTTGCCTCAATATAATCC	used to amplify the *min* locus	1210181-1210200[c]
minR_ *BamH*I	CGGGATCCTCTGTGCGTGGGAACAGC	used to amplify the *min* locus	1208137-1208154[c]
IcsA_FLAG_F1	**GGCC**GCGACTACAAGGACGATGACGACAAG	top strand of FLAG epitope to be annealed and ligated into the *Not*I site of $IcsA_i$ linker-insertions in reading frame 1	N/A
IcsA_FLAG_R1	**GGCCC**TTGTCGTCTACGTCCTTGTAGTCGC	bottom strand of FLAG epitope to be annealed and ligated into the *Not*I site of $IcsA_i$ linker-insertions in reading frame 1	N/A

[a] Underlined nucleotides comprise restriction enzyme recognition site; bold nucleotides comprise the *Not*I overhang of the annealed FLAG epitope.
[b] Nucleotide positions based on the *icsA* coding sequence from Lett *et al.*, (1989) - GenBank accession # M22802.
[c] Nucleotide positions based on the sequence of the *S. flexneri* 2a strain 2457T chromosome from Wei *et al.* (2003) - GenBank accession # AE014073.

resuspended in MQ water at a concentration of 100 pmoles/µl and stored at -20°C. Working stocks of primers were made by further diluting in MQ water to 50 pmoles/µl.

2.7.2 Polymerase chain reaction (PCR)

PCR from either vector or genomic template was performed in a 20 µl reaction volume containing PCR buffer (NEB), 1-2 units of Taq DNA polymerase (NEB), 20 pmoles of each primer, at least 100 ng DNA template, 200 µM of dNTPs (Roche; Sigma). PCR reactions were performed in an Eppendorf Mastercycler and subjected to 25 amplification cycles with conditions adjusted according to the specific DNA being amplified. A standard cycle involved denaturation of the template at 95ºC for 30 sec, annealing of primers to the DNA was at a temperature 1ºC below the primer melting temperature (T_m), estimated from the calculation T_m= 2ºC (A+T) + 4ºC (G+C) followed by extension at 72ºC. The extension time was calculated according to a replication rate of 1 kb of DNA per minute.

2.8 DNA purification

2.8.1 DNA gel extraction

80 µl restriction enzyme digested DNA samples were added to 8 µl of tracking dye (Section 2.6.3) and were electrophoresed in 1% (w/v) low melting point agarose (Progen) in TBE. 80 µl was used for gel extraction and loaded into a central well; 4 µl samples were loaded into flanking wells. The flanking lanes were cut from the rest of the gel and stained with ethidium bromide. The position of the desired DNA fragment was visualized by UV trans-illumination and marked with a scalpel. These marked flanking lanes were aligned with the unstained central lanes enabling the corresponding DNA fragment (required for ligation) to be excised from the gel, and transferred to a 1.5 ml reaction tube. The DNA was extracted from the gel slice and purified using a QIAquick Gel Extraction Kit (Qiagen) following the

manufacturer's protocol for fragments between 500 bp and 4 kb. Purified DNA was resuspended in 40 µl of MQ water and stored at 4ºC.

2.8.2 Purification of PCR products

PCR products were purified with a QIAquick PCR Purification Kit (Qiagen) as per the manufacturer's instructions. The DNA was eluted in 50 µl of MQ water and stored at 4ºC and analysed by agarose gel electrophoresis (Section 2.6.3).

2.9 Manipulation of DNA

2.9.1 Oligonucleotide annealing

Oligonucleotides encoding the FLAG epitope (Table 2.4) were annealed in preparation for insertion into plasmid vectors according to the method of Enninga *et al*. (2005). 1 µl each oligonucleotide (corresponding to 1 nmole of each) was added to 48 µl of annealing buffer (100 mM potassium acetate, 30 mM Hepes pH 7.4, 2 mM magnesium acetate in MQ). Annealing reactions were incubated in a Perkin Elmer Thermal Cycler at 95°C for 4 min, 70°C for 10 min. The thermal cycler was then switched off and allowed to equilibrate to RT. The annealing reaction was then cooled to 4°C in the Perkin Elmer Thermal Cycler by incubation at 15°C for 5 min, 10°C for 5 min and then 4°C for 5 min.

2.9.2 Phosphorylation of oligos

Annealed oligos (Section 2.9.1) were phosphorylated in order to enable their ligation into Shrimp Alkaline Phosphatase (SAP; Roche) treated vectors (Section 2.9.3). 2 µl of annealed oligos were mixed with 1 µl of T4 polynucleotide kinase (NEB) and 1 µl of T4 polynucleotide kinase buffer (NEB) in a 10 µl reaction in MQ. Reactions were incubated at 37°C for 30 min, followed by deactivation of the enzyme at 70°C for 10 min. 2 µl of this reaction was subsequently used in a 10 µl ligation reaction (Section 2.9.4).

2.9.3 Shrimp alkaline phosphatase (SAP) treatment

SAP treatment was used in order to prevent re-ligation of plasmid vectors digested with a single restriction enzyme (Section 2.6.2). 5 µl of digested plasmid was mixed with 1 µl of SAP (Roche) and 1 µl of SAP buffer (Roche) in a 10 µl reaction in MQ. Reactions were incubated at 37°C for 20 min, followed by deactivation of the enzyme at 65°C for 15 min. 1 µl of SAP treated plasmid was used in a 10 µl ligation reaction (Section 2.9.4).

2.9.4 Ligation of DNA fragments into cloning vectors

PCR products and plasmids for ligation were first purified (Section 2.8.2 and Section 2.5.2), restriction enzyme digested (Section 2.6.2) and mixed in a ratio of 3:1 (insert:vector). The ligation reactions were typically performed in a total volume of 20 µl with 2 units of T4 DNA ligase (NEB) and 2 µl T4 DNA ligase buffer (NEB) and incubated at 16°C (Perkin Elmer Thermal cycler) for 16 h or alternatively incubated at RT for 1 h. For large-scale ligations, 4x the amount of each component was used in a total volume of 80 µl. Ligation of PCR products into pGEMT-Easy was performed as instructed by the manufacturer (Promega). Ligation products were transformed directly into chemically competent *E. coli* (Section 2.10.1 & 2.10.2) or desalted by drop dialysis and electroporated into electrocompetent *E. coli* (Section 2.10.3 & 2.10.4).

2.10 Transformation procedures

2.10.1 Preparation of chemically competent *E. coli*

A 10 ml overnight (16 h) culture of *E. coli* DH5α in LB broth was sub-cultured 1:20 into a fresh 10 ml broth and incubated with aeration for 2 h, followed by centrifugation (4500 rpm, 5 min, 4ºC; Sigma 3K15 centrifuge). The bacterial pellet was resuspended in 10 ml ice-cold Solution α (30 mM KAc, 100 mM KCl, 10 mM $CaCl_2$, 50 mM $MnCl_2$, 15% [v/v] glycerol) and centrifuged (5000 rpm, 20 min, 4ºC). The pellet was then resuspended in 1 ml

ice-cold Solution β (10 mM MOPS, 75 mM $CaCl_2$, 10 mM KCl, 15% [v/v] glycerol) and stored on ice (2 h). 100 µl aliquots were transferred to sterile 1.5 ml reaction tubes and stored at –70ºC until required.

2.10.2 Transformation of chemically competent *E. coli* with plasmid DNA

Competent cells were thawed on ice before the addition of 1 µg of plasmid DNA. The mix was left on ice for 10 min before heat shock (37ºC water-bath, 5 min) and further incubation on ice for 10 min. 900 µl LB was added and the mix was incubated at 30ºC or 37ºC for 30-90 min with aeration to allow expression of antibiotic resistance genes on the plasmid(s). 100 µl aliquots of ten-fold dilutions were plated on LB-agar plates containing the appropriate antibiotic selection, and incubated overnight. All transformation procedures were accompanied by appropriate positive and negative controls.

2.10.3 Preparation of electrocompetent *S. flexneri* and *E. coli*

A 10 ml overnight culture (16 h) of the *S. flexneri* strain in LB was sub-cultured 1:20 in LB broth and grown for 2 h before centrifugation (4500 rpm, 10 min, 4ºC; Sigma 3K15 centrifuge). Bacterial pellets were washed twice by resuspension in 10 ml of ice-cold MQ and centrifuged as before. Then bacteria were washed twice by resuspension in 10 ml of ice-cold 10% (v/v) glycerol and centrifuged as before. Washed pellets were resuspended in 100 µl of 10% (v/v) glycerol. 100 µl aliquots of the suspension were stored at –70ºC until required.

2.10.4 Electroporation of *S. flexneri* and *E. coli*

A 100 µl aliquot of electrocompetent cells was thawed on ice and the electroporation cuvette (1 mm electrode gap; Bio-Rad) was chilled. The cells and 5-10 µl of plasmid preparation (Section 2.5.2) were electroporated (Bio-Rad Gene Pulser, 1.8 kV, 25 µF, Capacitance extender 960 µF, Pulse Controller 200 Ω) in the cold cuvette, with time

constraints of 4.4-5.0 msec. The cells were added to 900 µl of LB in a 20 ml McCartney bottle and incubated with aeration for 30-90 min at either 37ºC or 30ºC for temperature sensitive strains. 100 µl of neat and 1/10 (diluted in LB) electroporated cultures were plated on LB-agar with appropriate antibiotics and incubated for 16-24 h at either 37ºC or 30ºC, as required.

2.10.5 Conjugation

Donor and recipient strains were grown 16 h at 37ºC in 10 ml of LB with the appropriate antibiotics. Cultures were pelleted by centrifugation (4500 rpm, 10 min, 4ºC; Sigma 3K15 centrifuge), the supernatant containing antibiotics was discarded and the bacterial pellets were resuspended in 10 ml of LB without antibiotics. 100 µl of the donor strain was mixed with 900 µl of the recipient strain and plated onto sterile 0.45 µm HA gridded membrane filters (Millipore) on LB plates. Following incubation overnight at 37ºC filters were transferred to 10 ml of LB, vortexed to resuspend the bacteria, and diluted 10^{-3} and 10^{-4} in LB. 100 µl of each dilution was plated on LB-agar containing antibiotics specific for the plasmid and the recipient strain, and incubated 16 h at 37ºC.

2.11 Construction of chromosomal mutations

2.11.1 Allelic-exchange mutagenesis using pCACTUS

Chromosomal mutations were constructed with the suicide vector pCACTUS (Table 2.2), possessing a temperature sensitive origin of replication (ori_{ts}), chloramphenicol resistance marker (Cm^R) and the *sacB* gene. The target gene was disrupted by an antibiotic resistance marker, e.g. Km^R, as detailed in the results (Section 6.2.1), and sub-cloned into pCACTUS. Strains containing mutagenesis constructs were grown 16 h in LB broth at 30ºC with aeration and antibiotic selection. Broths were plated onto LB plates containing Km and incubated at 42ºC. After 16 h incubation, colonies were inoculated into broth and grown for

16 h at 37ºC. Broths were plated onto selective medium (LB agar, without NaCl, 6% [w/v] sucrose) either with or without Km, and incubated 16 h at 30ºC to resolve co-integrates. The resultant isolates were patched onto plates containing Cm to confirm loss of the plasmid construct. Isolates from selective medium without Km were also patched onto plates containing Km to confirm Km^R indicative of allelic exchange.

2.11.2 Allelic-exchange mutagenesis using the λ Red phage mutagenesis system

Mutagenesis using the λ Red mutagenesis system was performed as described by Datsenko and Wanner (2000). Briefly, pKD46 was electroporated (Section 2.10.4) into the recipient strain. An Ap^R transformant was selected and, after growth of this strain at 30°C in 10 ml of LB in the presence of 0.2% (v/v) arabinose, the bacteria were made electrocompetent (Section 2.10.3) and the concentrated (100x). PCR products were purified according to Section 2.8.2 and resuspended in MQ, concentrating the DNA 10-fold in the process. 5 µl of this purified PCR product was mixed with 50 µl of electrocompetent bacteria. After electroporation (Section 2.10.4) bacteria were resuspended in SOC medium (Section 2.3.1) and incubated at 37ºC for 1 h prior to selection on LB plates containing Km. The absence of the temperature sensitive plasmids pKD46 and PCR template plasmids was confirmed by plating on LB containing the appropriate antibiotics. Strains that retained one of the plasmids were subjected to growth at 42ºC for 16 h to ensure plasmid loss. To enable removal of the antibiotic resistance marker, the antibiotic resistance marker used in this method flanked by FRT (FLP recognition target) sites allowing FLP-mediated excision. Accordingly, the mutated strain was transformed with the temperature sensitive FLP expression plasmid (pCP20; Table 2.3; Section 2.10.3-4). Ap^R transformants were selected and incubated overnight at 37°C in LB broth with aeration. ON (16 h) cultures were incubated at 42°C degrees 2 h (statically) and diluted to 10^{-3} and 10^{-4} in LB, and plated onto LB agar plus the

appropriate antibiotics and incubated 16 h at 37°C. Colonies were selected on the basis of sensitivity to the antibiotic to which the antibiotic resistance marker conferred resistance.

2.11.3 Transduction using P1 phage

Transduction with P1 phage was performed using a modification of the method described by Miller, J.H. (1972).

2.11.3.1 Preparation of P1 phage stocks

In order to prepare phage stocks, the P1 phage propagation strain AB1133 (P109) (Table 2.1) or a particular donor strain (e.g. UT5600 *minD*::Km^R) was grown overnight (16 h) at 37ºC with aeration in 10 ml of LB broth. The bacteria were pelleted by centrifugation (4500 rpm, 5 min, RT; Sigma 3K15 centrifuge) and resuspended in 1 ml of MC salts (0.1 M $MgSO_4$, 5 mM $CaCl_2$ in MQ). Bacteria were then incubated at 37ºC for 15 min with aeration. A P1 phage stock was diluted to 10^{-2}, 10^{-4} and 10^{-6} in LB and 100 µl of neat and diluted phage stocks were incubated with 100 µl of bacteria and incubated at 37ºC for 20 min with aeration. The mixture of bacteria and phage was added to 3 ml of pre-warmed (45ºC) R-TOP agar (Section 2.3.2) and poured onto pre-warmed (42ºC) R-agar plates (Section 2.3.2). Plates were incubated face up at 37ºC for 7-9 h. Plates exhibiting >50% lysis were used to prepare a phage stock. Overlays from these plates were scraped off using a tissue culture cell scraper and transferred to 10 ml of LB. 200 µl of chloroform was added and the broths incubated at 37ºC for 30 min with aeration at to kill any bacteria. The broth was centrifuged (4500rpm, 10 min, 4ºC; Sigma 3K15 centrifuge) to pellet the agar, and the supernatant (containing the phage stock) was collected and stored at 4ºC.

2.11.3.2 P1 Phage transduction

Strains to be mutated were grown overnight (16 h) at 37ºC with aeration in 10 ml of LB. The bacteria were pelleted by centrifugation (4500 rpm, 5 min, RT; Sigma 3K15 centrifuge) and resuspended in 1 ml of MC salts (Section 2.11.3.1). Bacteria were incubated at 37ºC for 15 min with aeration. P1 phage stocks prepared on UT5600 *minD*::Km^R were diluted 10^{-2}, 10^{-4} and 10^{-6} in LB. 100 µl of neat and diluted phage stocks were incubated with 100 µl of bacteria and incubated at 37ºC for 1 h and 20 min with aeration. The mixture of bacteria and phage was either directly plated, or added to 200 µl of 1 M sodium citrate and then plated on LB agar with Km and incubated 24 h at 37ºC.

2.12 Protein techniques

2.12.1 Preparation of whole-cell lysates

ON (16 h) cultures of bacterial strains were sub-cultured 1:50 in LB (10 ml) with antibiotics and incubated with aeration for 2 h at 37°C. The bacterial cell concentration was calculated on the basis that an Absorbance at 600nm (A_{600}) of 1.0 was equivalent to $5x10^8$ cells. The equivalent of $5x10^8$ bacteria were pelleted by centrifugation (6000 rpm, 6 min, 4ºC; Eppendorf 5417R) and resuspended in 100 µl of 2x sample buffer (0.125 M Tris-HCl, pH 6.8, 4% [w/v] SDS, 20% [v/v] glycerol, 10% [v/v] β-mercaptoethanol, 0.04% [w/v] Bromophenol blue).

2.12.2 Trichloroacetic acid precipitation of culture supernatants

ON (16 h) cultures of bacterial strains were sub-cultured 1:50 in LB (10 ml) with antibiotics and incubated with aeration for 2 h at 37°C. The equivalent of $5x10^9$ bacteria were pelleted by centrifugation (4500 rpm, 10 min, 4ºC; Sigma 3K15 centrifuge). The supernatants were collected, supplemented with 5% (v/v) ice-cold trichloroacetic acid (TCA) and incubated on ice for 1 h. The TCA precipitate was pelleted by centrifugation (18 000 rpm, 30

min, 4ºC; JA20 rotor, Beckman J2-21M centrifuge). The supernatant was removed and the pellet centrifuged again for 5 min as before, to remove the remaining supernatant. The brown protein pellet was washed with ice-cold acetone, centrifuged for another 5 min and the acetone carefully removed. The pellet was air-dried and then resuspended in 100 µl of 1x Sample buffer (Section 2.12.1).

2.12.3 Limited proteolysis with trypsin

Limited proteolysis was performed as described by Oliver *et al*. (2003) with modifications. ON (16 h) cultures of bacterial strains were sub-cultured 1:50 in LB (10 ml) with antibiotics and incubated with aeration for 2 h at 37°C. The equivalent of $5x10^9$ bacteria were pelleted by centrifugation (4500 rpm, 10 min, 4ºC; Sigma 3K15 centrifuge), the supernatant was discarded and the pellet resuspended in 150 µl of phosphate-buffered saline (PBS). Bacterial suspensions were supplemented with 0.1 µg/ml of Trypsin from bovine pancreas (Roche #109819) in MQ and incubated at RT to allow proteolysis. Aliquots were taken at several timepoints (0 min, 5 min, and 10 min) and supplemented with phenylmethylsulphonylfluoride (PMSF; Sigma), from a 10 mM stock in isopropanol, at a final concentration of 1 mM, to inhibit Trypsin and further proteolysis. An equal volume of 2x Sample buffer (Section 2.12.1) was added to each sample, which were then heated at 100°C for 5 min prior to storage at -20°C.

2.12.4 SDS-PAGE

Samples for SDS-PAGE analysis were heated at 100°C for 5 min prior to loading, unless otherwise stated. The SDS-PAGE gel apparatus used were the either the Bio-Rad Mini-Protean System III or a Sigma vertical gel electrophoresis unit (gel dimensions: 16.5 cm width x 14.5 cm height). SDS-PAGE was performed by electrophoresing samples through 7.5% or 12% (w/v) acrylamide gels in PAGE running buffer (0.025 M Tris-HCl, 0.2 M

glycine, 0.1% [w/v] SDS) at 200V for 1-4 h as required. Proteins were visualised by either staining with Coomassie blue (Section 2.12.5) or by Western immunoblot analysis (Section 2.11.6). Benchmark™ pre-stained standard (Invitrogen; 190 kDa, 120 kDa, 85 kDa, 60 kDa, 50 kDa, 40 kDa, 25 kDa, 20 kDa, 15 kDa, 10 kDa); HiMark™ pre-stained standard (Invitrogen; 460 kDa, 268 kDa, 238 kDa, 171 kDa, 117 kDa, 71 kDa, 55 kDa, 41 kDa, 31 kDa); and protein Low molecular weight standards (Pharmacia; 95 kDa [phosphorylase B], 67 kDa [bovine serum albumin], 43 kDa [ovalbumin], 30 kDa [carbonice anhydrase], 20 kDa [soybean trypsin inhibitor], 14.4 kDa [α-lactalbumin]) were included to allow estimation of protein molecular weights.

2.12.5 Coomassie blue staining

Proteins separated by SDS-PAGE (Section 2.11.4) were incubated in Coomassie blue staining solution (5% [v/v] perchloric acid, 0.09% [w/v] Coomassie blue G250) overnight (16 h), then destained in 5% (v/v) acetic acid until the background colour was removed.

2.12.6 Western transfer and detection

Proteins separated by SDS-PAGE (Section 2.11.4) were transferred to a membrane (Protran nitrocellulose membrane BA85 [Schleicher and Schuell] or Nitrobind 0.45 micron pure nitrocellulose [GE Water and Process Technologies]) for 1-2 h at 200 mA in transfer buffer (0.025 M Tris, 0.2 M glycine, 5% [v/v] methanol). The membrane was then blocked for 1 h in TTBS (0.016 M Tris, 0.12 M NaCl, 0.05% [v/v] Tween 20 [Sigma]) with 5% (w/v) skim milk and incubated with the desired primary antibody (Section 2.1.1) in the same buffer for 16 h. After three 10 min washes in TTBS the membrane was incubated with horseradish peroxidase (HRP)-conjugated goat anti-rabbit or a HRP-conjugated goat anti-mouse secondary antibodies (Biomediq DPC) for 2 h, washed three times in TTBS, then three times in TBS (0.016 M Tris-HCl, 0.12 M NaCl). The membrane was incubated with

Chemiluminescence Blotting Substrate (Roche) for 1 min. Chemiluminescence was detected by exposure of the membrane to X-ray film (AGFA), starting with 2-5 min exposures, and increasing if necessary. The film was developed using a Curix 60 automatic X-ray film processor (AGFA).

2.12.7 Indirect immunofluorescence of whole bacteria

ON (16 h) cultures were sub-cultured 1:50 and grown to log-phase in LB broth (10 ml) at 37°C. Bacteria were pelleted by centrifugation (4500 rpm, 10 min, 4ºC; Sigma 3K15 centrifuge), the supernatant discarded. Bacteria were fixed in formalin (3.7% [w/v] paraformaldehyde in 0.85% [w/v] saline) for 15 min at RT. Sterile coverslips were placed into 24-well trays (Falcon) and incubated with 10% (v/v) poly-L-lysine (Sigma) in PBS for 1 min. The poly-L-lysine was aspirated and formalin fixed bacteria were centrifuged (2500 rpm, 5 min, 25°C; Labofuge 400R Sepatech Heraeus) onto the coverslips. Bacteria were incubated with the desired primary antibody (Section 2.1.1) diluted 1:100 in PBS with 10% (v/v) foetal calf serum (FCS). Bacteria were washed three times in PBS and incubated with either Alexa 488-conjugated donkey anti-rabbit or Alex 488-conjugated donkey anti-mouse secondary antibodies (Molecular Probes); diluted 1:100 in PBS with 10% (v/v) FCS. The coverslips were mounted on glass microscope slides with mounting medium (Section 2.17.1) and analysed by immunofluorescence microscopy as described in Section 2.17.2.

2.13 Minicell purification

2.13.1 Crude prepartion of minicells by differential centrifugation

A crude purification of *E. coli* minicells was performed using a method adapted from Lai *et al.* (2004). Overnight (16 h) cultures of bacterial strains were sub-cultured 1:50 in LB (10 ml) with antibiotics and incubated with aeration for 3 h at 37°C. Two 1 ml aliquots were taken for each strain. For one of the aliquots, whole cells and minicells were pelleted by

centrifugation (13 000 rpm, 15 min, RT; Eppendorf 5417R), the supernatant was discarded, and the pellet resuspended in formalin (Section 2.11.7). For the other aliquot, whole cells were pelleted by centrifugation (6000 rpm, 5 min, RT; Eppendorf 5417R) and resuspended in formalin. Meanwhile the supernatant was collected and transferred to a new 1.5 ml reaction tube and centrifuged (14 000 rpm, 15 min, RT; Eppendorf 5417R) to pellet minicells. The minicell pellet was also resuspended in formalin. After washing in PBS, all three samples were (Section 2.11.7) analysed by indirect immunofluorescence and phase contrast microscopy as described in Section 2.17.

2.13.2 Purification of minicells by sucrose gradients

Minicells were purified according to the method of Achtman *et al.* (1979) as described in Sections 2.13.2.1-2.

2.13.2.1 Preparation of sucrose gradients

Sucrose gradients were prepared by placing 32 ml of 20% (w/v) sucrose in buffered saline gelatin (BSG; 0.85% [w/v] NaCl, 0.03% [w/v] KH_2PO_4, 0.06% [w/v] Na_2HPO_4, 100 μg/ml Gelatin) into Ultra-Clear™ tubes (25 x 89 mm; Beckman), freezing at -20°C and allowing to thaw overnight (16 h) at 4°C.

2.13.2.2 Purification of minicells

ON (16 h) cultures of minicell strains were sub-cultured 1:25 in 250 ml of LB with antibiotics and incubated with aeration overnight at 37°C to produce stationary phase cultures. Log-phase cultures of minicells strains were also prepared by sub-culturing ON cultures 1:20 in 1 L of LB with antibiotics and incubated with aeration for 2 h at 37°C. Bacteria and minicells from both log-phase and stationary-phase cultures were pelleted by centrifugation (7000 rpm, 20 min, 0ºC; Beckman J2-M1) and resuspended in 10 ml of BSG

(Section 2.12.2.1). Cells were pelleted again by centrifugation (13 000 rpm, 8 min, 0ºC; Beckman J2-M1) and resuspended in 2 ml of BSG. Cells were layered onto sucrose gradients and centrifuged (5500 rpm, 30 min, 0ºC, acceleration 1, deceleration 1; Sigma 3K15 centrifuge with NR11133 swing-out rotor). The minicell fraction in the middle of the tube was extracted using a syringe. A sample of the whole cell fraction at the bottom of the tube was also collected and diluted in 50 mM Tris pH7.5. The minicells were centrifuged (13 000 rpm, 8 min, 0ºC; Beckman J2-M1), resuspended in 1 ml of BSG and purified once more on a sucrose gradient as described above. The minicells were then centrifuged (13 000 rpm, 8 min, 0ºC; Beckman J2-M1) and resuspended in 2 ml of 50 mM Tris pH7.5. The cell concentrations were calculated on the basis that an A_{600} = 1.0 represents 5 x 10^8 whole cells and 2 x 10^9 minicells.

2.14 Lipopolysaccharide techniques

2.14.1 Preparation of LPS samples

LPS samples were prepared according to the method of Hitchcock and Brown (1983). Overnight (16 h) cultures of bacterial strains were sub-cultured 1:20 in LB (10 ml) with antibiotics and incubated with aeration for 3-4 h at 37°C. The equivalent of 10^9 bacteria were pelleted by centrifugation (6000 rpm, 6 min, 4ºC; Eppendorf 5417R) and resuspended in 50 µl of Lysing buffer (0.66 M Tris pH 7.6., 2% [w/v] SDS, 10% [v/v] glycerol, 4% [v/v] β-mercaptoethanol, 0.1% [w/v] Bromophenol blue). Samples were heated at 100°C for 5-10 min, and allowed to cool before the addition of 10 µl of 2.5 mg/ml Proteinase K (Invitrogen) in Lysing Buffer. Samples were treated with Proteinase K for 4-18 h at 56°C.

2.14.2 Analysis of LPS by silver-stained SDS-PAGE

The SDS-PAGE gel apparatus used for LPS gels were the either the Bio-Rad Mini-Protean System III or a Sigma vertical gel electrophoresis unit (gel dimensions: 16.5 cm

width x 22 cm height). LPS samples prepared in Section 2.14.1 were heated at 100°C for 5 min prior to loading 5-10 µl on 15% SDS (w/v) polyacrylamide gels (Macpherson *et al*., 1991). For mini-Protean gels (Biorad) samples were diluted 1/4 in Lysing Buffer (Section 2.14.1) and 5-10 µl of the diluted sample was used. Samples were electrophoresed at 15 mA for 14.5 h. Silver-staining was performed as described by Tsai and Frasch (1982). Developing was achieved with developing solution warmed to 56ºC, and stopped by the addition of stopping solution. Briefly, the gel was fixed for 2 h in fixing solution (40% [v/v] ethanol, 5% [v/v] glacial acetic acid in MQ) with gentle agitation and then oxidised for 5 min in oxidising solution (40% [v/v] ethanol, 5% [v/v] glacial acetic acid, 0.7% [w/v] periodic acid in MQ). After 1 h of washing in MQ water (changed at 10 min intervals), the gel was stained for 10 min in staining solution (0.08% [w/v] NaOH, 1.33% [v/v] ammonium hydroxide, 0.66% [w/v] silver nitrate) and washed again as above. Developing was achieved with developing solution (0.05 mg/ml citric acid, warmed to 56ºC, with 500 µl of formaldehyde solution (UNIVAR; 37% [w/w] added just prior to developing) and stopped by the addition of stopping solution (4% [v/v] acetic acid).

2.15 Chemical cross-linking

2.15.1 Formaldehyde cross-linking

Overnight (16 h) cultures of bacterial strains were sub-cultured 1:50 in Luria Bertani (LB; 10 ml) with antibiotics and incubated with aeration for 2 h at 37°C. The equivalent of $5x10^8$ bacteria were pelleted by centrifugation (6000 rpm, 6 min, 4ºC; Eppendorf 5417R) and washed once in ice-cold 10 mM K_2PO_4/KH_2PO_4 buffer and resuspended in 1 ml of the same buffer. For each sample 13.5 µl of formaldehyde solution (UNIVAR; 37% [w/w]) was added and incubated for 1 h at RT. Samples were then washed once again as above and resuspended in 80 µl of 1x Sample buffer (Section 2.12.1). Aliquots of each sample were heated at either 60°C for 10 min or 100°C for 20 min, prior to SDS-PAGE.

2.15.2 DSP cross-linking

Overnight (16 h) cultures of bacterial strains were sub-cultured 1:50 in Luria Bertani (LB; 10 ml) with antibiotics and incubated with aeration for 2 h at 37°C. The equivalent of 10^9 bacteria were pelleted by centrifugation (6000 rpm, 6 min, RT; Eppendorf 5417R) and washed once in 1 ml of buffer (120 mM NaCl, 20 mM Na_2HPO_4/NaH_2PO_4 buffer pH 7.2, in distilled H_2O) and resuspended in 1 ml of the same buffer. Dithio-bis(succinimidylpropionate) (DSP; Pierce) from a 50 mM stock in dimethyl sulphoxide (DMSO; Sigma) was added to each sample at a final concentration of 0.2 mM and samples were incubated for 30 min at 37°C. Excess DSP was quenched with 20 mM Tris pH 7.5 and samples were then washed once again and resuspended in 100 µl of 1x Sample buffer (Section 2.12.1) without β-mercaptoethanol. Duplicates of each sample were prepared and one of which was resuspended in 100 µl of 1x Sample buffer (Section 2.12.1) with β-mercaptoethanol, as a control.

2.16 Tissue culture

2.16.1 Maintenance of cell lines

HeLa cells (Human, cervical, epithelial cells ATCC #CCL-2) and CV-1 cells (African green monkey, kidney, fibroblast cells ATCC #CCL-70) were maintained in Modified Eagle's medium (MEM, Gibco BRL) with 4 mM L-glutamine adjusted to contain 1.5 g/L sodium bicarbonate and 4.5 g/L glucose, 10% (v/v) FCS and 100 U/ml penicillin and 100 U/ml streptomycin. Cells were grown and maintained in a humidified atmosphere at 37°C, 5% CO_2.

2.16.2 Plaque assays

Plaque assays were performed with HeLa cells using a modification of the method described by Oaks *et al*. (1985). HeLa cells were seeded to 60 mm diameter, 6-well trays (Falcon) at 1 x 10^6 in MEM, 10% (v/v) FCS with penicillin and streptomycin. Cells were

grown to confluence overnight and washed twice with Dulbecco's PBS (D-PBS; 0.1% [w/v] $CaCl_2$, 0.1% [w/v] $MgCl_2$ in PBS) and once in Dulbecco's MEM (DMEM, Gibco BRL) prior to inoculation. Overnight (16 h) cultures of *S. flexneri* strains were sub-cultured 1:50 in LB (10 ml) with antibiotics and incubated with aeration for 2 h at 37°C. Bacteria were diluted to 1:100 and 1:300 in DMEM, and 0.2 ml was added to each well. Trays were incubated at 37°C in humidified CO_2 (5%) incubator and the trays were rocked gently every 15 min to ensure that the inoculum was spread evenly across the monolayer. At 90 min post-infection the inoculum was carefully aspirated and 4 ml of the first overlay (DMEM, 5% [v/v] FCS, 20 μg/ml of gentamicin, 0.5% [w/v] agarose [Seakem ME]) was added to each well. The second overlay (DMEM, 5% [v/v] FCS, 20 μg/ml of gentamicin, 0.5% [w/v] agarose, 0.1% [v/v] Neutral Red solution [Gibco BRL]) was added at either 24 h or 48 h post-infection and plaque formation observed 6-8 h later. Plaques were in general visible without staining at 48 h.

2.16.3 Infection of tissue culture monolayers with *S. flexneri* and immunofluorescence microscopy

Infection of tissue culture cells and immunofluorescence staining were performed as recently described (Morona, *et al*., 2003). In brief, overnight (16 h) cultures of *S. flexneri* strains were sub-cultured 1:50 in LB (10 ml) with antibiotics and incubated with aeration for 2 h at 37°C. Approximately $5x10^8$ bacteria were pelleted by centrifugation (6000 rpm, 6 min, RT; Eppendorf 5417R) and resuspended at approximately 10^9 bacteria/ml in D-PBS 100 μl of bacterial suspension was then centrifuged (2500 rpm, 7 min, 25°C; Labofuge 400R Sepatech Heraeus) onto HeLa or transfected CV-1 cells grown to semiconfluence on sterile glass coverslips. After 1 h incubation at 37°C in a humidified CO_2 incubator (5% CO_2), the infected cells were washed three times with D-PBS and incubated with 0.5 ml MEM containing 40 μg/ml of gentamicin for a further 1.5 h at 37°C in a CO_2 incubator. Infected cells were washed a further 3 times in D-PBS then fixed for 15 min in 3.7% (w/v) paraformaldehyde in

0.85% (w/v) saline, incubated with 50 mM NH_4Cl in D-PBS for 10 min and then permeabilised with 0.1% (w/v) Triton X-100 in MQ for 5 min. After blocking in 10% (v/v) FCS in PBS, the infected cells were incubated at 37°C for 30 min with the desired primary antibody (Section 2.1.1). After washing in PBS, coverslips were incubated with either Alexa 594-conjugated donkey anti-rabbit or Alexa 594-conjugated donkey anti-mouse secondary antibodies (Molecular probes) (1:100), as required. F-actin was visualised by staining with FITC-phalloidin (0.1 μg/ml, Sigma), and DAPI (0.1 μg/ml, Sigma) was used to counterstain bacteria and cellular nuclei as required. The coverslips were mounted onto glass slides with mounting medium (Section 2.17.1) and were examined by immunofluorescence microscopy, as described in Section 2.17.2

2.16.4 Transfection and infection of CV-1 cells

Transfection and infection of CV-1 cells was conducted by Luisa Van Den Bosch as described herein. CV-1 cells (Section 2.16.1) were used for these experiments as they are highly amenable to transfection, and *Shigella* are able to infect and spread intercellularly in this cell line (L. Van Den Bosch and R. Morona, unpublished data). Twenty-four hours prior to transfection, CV-1 cells were seeded to 60 mm diameter, 6-well trays (Falcon) and grown to 90% confluence. Cells were washed in D-PBS and then 0.2 ml of MEM (without serum or antibiotics) was added to each well immediately prior to transfection. DNA to be transfected was prepared as described in Section 2.5.3, and quantitated according to Section 2.6.1. For each well, 10 μl of lipofectamine 2000 (Invitrogen) was diluted in 50 μl of MEM (without serum or antibiotics) and incubated for 5 min at RT. This mixture was added to 4 μg of DNA diluted in 50 μl of MEM (without serum or antibiotics) and incubated at RT for an additional 20 min. The DNA/lipofectamine complex was added to each well (100 μl/well) and incubated for 1 h at 37°C in a humidified CO_2 incubator (5% CO_2). 5 ml of MEM supplemented with 10% (v/v) FCS was added to each well and the cells were incubated for 18-48 h at 37°C in a

humidified CO_2 incubator (5% CO_2). Transfected CV-1 cells were washed with PBS for 5 min, detached from the tray by incubation with trypsin (Gibco BRL) and seeded to 24-well trays in MEM maintenance medium (Section 2.16.4) with serum and antibiotics. Infection of CV-1 cells was performed according to Section 2.16.3.

2.17 Microscopy

2.17.1 Mounting medium

Mowiol 4-88 (Calbiochem), for mounting medium was prepared by mixing 0.4 g of Mowiol 4-88, 1 g of glycerin and 1 ml of MQ. This was incubated for 2 h at 56°C, before adding 2 ml of 0.2 M Tris-HCl pH 8.5 and heating at 50°C for at least 10 min, or until dissolved. Then, to remove any remaining solids, this mixture was centrifuged at 5000 × g for 15 min, and the supernatant collected and stored at 4°C. A fresh stock of *p*-phenylenediamine (PPD; Sigma) was prepared each time at 25 mg/ml in ethanol. The stock was vortexed and centrifuged (13 000 rpm, 1 min, RT; Eppendorf 5417R) to remove undissolved PPD. The PPD solution was added to Mowiol 4-88 (prepared as described above) at a ratio of 1:5 (PPD:Mowiol). This mounting medium was vortexed and centrifuged (13 000 rpm, 1 min, RT; Eppendorf 5417R) to remove any air bubbles. Coverslips were mounted (cell-side down) onto glass slides using 3-4 µl of mounting medium and sealing the edge of the coverslip with nail polish.

2.17.2 Microscopy

Slides were examined with an Olympus IX-70 microscope with phase-contrast optics using a 100× oil immersion objective and on occasion using a 1.5× enlarger. The Omega optical filter set XF67-1 set was used with a filter wheel (Sutter) containing a narrow band excitation filter (X67, Pinkel Set [Omega]), and was controlled by Metamorph (Version 6.3r7,

Molecular devices). Fluorescence and phase-contrast images were false colour merged using Metamorph.

2.18 Pull-down experiments with sheep brain extracts

The methods below were based on those described by David *et al*. (1998) and the regeneration mix in Section 2.18.3 was described by Murray *et al.* (1991).

2.18.1 Preparation of sheep brain extracts

Sheep brain extracts were prepared by Luisa Van Den Bosch as described herein. A sheep brain was cut into small pieces and added to ice-cold extraction buffer (20 mM Hepes, pH 7.5, 100 mM potassium acetate, 1 mM magnesium acetate, 1 mM EGTA, 0.2 mM $CaCl_2$, 0.5 mM ATP, 1 mM dithiothreitol [DTT; Sigma], 10 μg/ml leupeptin, pepstatin-A and chymostatin, 1 mM PMSF) at 1 g/ml. The brain tissue was ground by 15 passages in a homogeniser. Nuclei were removed from the homogenate by centrifugation at 2 000 x *g*. Crude extracts were obtained from the supernatant by further centrifugation 10 000 x *g* and divided into 100 μl aliquots for storage at -70°C. Immediately prior to use, aliquots of the crude extract were thawed and mixed in 0.1% (v/v) Triton X-100, clarified by centrifugation (60 000 x *g*, 1 h, 4°C, Beckman Optima^{TM} TLX Ultracentrifuge) and supernatants used in pull-down experiments with whole bacteria.

2.18.2 Preparation of bacteria for pull-down experiments

Overnight (16 h) cultures of *S. flexneri* strains were sub-cultured 1:50 in LB (10 ml) with antibiotics and incubated with aeration for 2 h at 37°C. The equivalent of $7.5x10^8$ bacteria were pelleted by centrifugation (13 000 rpm, 3 min, RT; Biofuge 15), washed once in 1 ml of XB buffer (100 mM KCl_2, 1 mM $MgCl_2$, 0.1 mM $CaCl_2$, 10 mM Hepes pH 7.4, 50 mM sucrose), centrifuged as before, and finally resuspended in 80 μl of XB buffer.

2.18.3 Pull-down experiments

For pull-down experiments, 70 µl of sheep brain extract (Section 2.18.1), 10 µl of regeneration mix (150 mM creatine phosphate, 20 mM ATP pH 7.4, 2 mM EGTA, 20 mM, $MgCl_2$), 10 µl of energy mix (1 mM ATP, 30 mM creatine phosphate) and 10 µl of bacteria in XB buffer (Section 2.18.2) were mixed in an reaction tube and incubated for 30 min at 37°C. Bacteria were pelleted by centrifugation (13 000 rpm, 3 min, RT; Hereaus Sepatech Biofuge 15), and the supernatant was aspirated carefully without disturbing the pellet. The pellet was washed twice in ice-cold low salt buffer (10 mM Hepes pH 7.4, 40 mM KCl, 5 mM ATP), each time without disturbing the pellet, and centrifuging as before. For the second wash, 50 µl of the supernatant was left in the tube and 50 µl of 2x Sample buffer (Section 2.18.1) was added. The pellet was resuspended by gentle pipetting and samples stored at -20°C until required. 50 µl of each sample was subjected to SDS-PAGE and Western immunoblotting (Sections 2.12.4 and 2.12.6).

Chapter Three

Linker-insertion mutagenesis and general characterisation of IcsA$_i$ mutants

Chapter Three: Linker-insertion mutagenesis and general characterisation of IcsA$_i$ mutants

3.1 Introduction

Previous IcsA structure and function studies have identified several functional regions within the passenger domain (as discussed in Section 1.2.3). A glycine rich repeat (GRR) region exists within the IcsA passenger domain (aa 140-307) (Goldberg *et al.*, 1993) and has been identified as the region responsible for IcsA interaction with host N-WASP, leading to F-actin comet tail formation (Suzuki *et al*., 1998; Snapper *et al*., 2001; Suzuki *et al*., 2002). A region encompassing this GRR (aa 104-506) has been shown to interact with the host protein vinculin (Suzuki *et al*., 1996). Additionally, two regions (aa 1-104 and aa 507-620) have been attributed to determining polar localisation of IcsA (Charles *et al*., 2001), and another region (aa 320-433) interacts with the *Shigella* IcsB protein and the host autophagy protein, Atg5 (Ogawa *et al*., 2005).

These structure-function studies have relied almost exclusively on deletions of large regions of IcsA (Suzuki *et al.*, 1996; Charles *et al.*, 1999). Such approaches may have resulted in the removal of multiple functional domains, complicating the interpretation of structure-function relationships. Alternatively, the creation of smaller internal deletions within IcsA produced constructs that were unstable (Charles *et al.*, 1999), while alanine scanning mutagenesis (involving single amino acid substitutions) was likewise unrewarding, yielding a wild-type phenotype (Charles *et al.*, 1999). In order to more clearly define IcsA functional regions, pentapeptide linker-insertion mutagenesis was undertaken. Pentapeptide mutagenesis has been applied to a variety of proteins from a range of organisms (reviewed in Hallet and

Hayes, 2000). Previous studies have proven this approach to be a powerful tool for investigating structure-function relationships, revealing both essential and non-essential regions of target proteins and producing mutant proteins with novel properties (Hallet and Hayes, 2000). Therefore, the aim of this chapter was to apply this mutagenesis strategy to create IcsA mutants for structure-function studies.

3.2 Linker-insertion mutagenesis

In order to further characterise IcsA structure-function, pentapeptide linker-insertion mutagenesis of IcsA was undertaken. An outline of the method used is shown in Figure 3.1. Using the Mutation Generation System^{TM} (Finnzymes; http://www.finnzymes.fi), an *in vitro* transposition reaction was performed to randomly introduce an artificial entranceposon (M1-Cm^R) that encodes chloramphenicol resistance (Cm^R) into pIcsA (Morona and Van Den Bosch, 2003; Table 2.3), a plasmid encoding wild-type IcsA ($IcsA_{WT}$) and that confers ampicillin resistance (Ap^R). Entranceposon mutated plasmids were then transformed into *E. coli* DH5α by electroporation (Section 2.10.4) and transformants selected on the basis of resistance to chloramphenicol and ampicillin.

Transformants were pooled to create 6 independent libraries (KMRM52-56, KMRM71) (Section 2.4.1). After sub-culturing in LB overnight, plasmid DNA was prepared from each of the libraries (Section 2.5.2). The entranceposon was then removed from these plasmids by large-scale restriction digests (Section 2.6.2) with the *Not*I restriction enzyme, and the digested plasmids were then re-ligated (Section 2.9.4) to leave an in-frame insertion of 15 bp encoding 5 aa within the plasmid. These were then electroporated back into *E. coli* DH5α (Section 2.10.4), and Ap^R transformants were pooled to create 11 sub-libraries (KMRM72 - 77, LC1-5) (Section 2.4.1). Bacteria from these libraries were plated for single colonies and screened for sensitivity to chloramphenicol (Cm^S) (by replica plating onto LB-agar with chloramphenicol) to ensure removal of the entranceposon.

Figure 3.1 Linker-insertion mutagenesis of IcsA using the Mutation Generation System™.

[1] Using the Mutation Generation System™ (Finnzymes), an *in vitro* transposition reaction was performed to randomly introduce and artificial entranceposon that encodes Chloramphenicol resistance (Cm^R), into pIcsA (Morona and Van Den Bosch, 2003; Table 2.3), a plasmid encoding wild-type (WT) *icsA* and resistance to ampicillin (Ap^R).

[2] Entranceposon mutated plasmids were then transformed into *E. coli* DH5α by electroporation (Section 2.10.4), and transformants selected on the basis of resistance to Cm and Ap.

[3] Pooled preparations of plasmid DNA were prepared from each of libraries (Section 2.5.2).

[4] - The entranceposon was then removed by *Not*I restriction digestion (Section 2.6.2)

[5] - Digested plasmids were then re-ligated (Section 2.9.4).

[6] - Plasmids were transformed back into *E. coli* DH5α (Section 2.10.4) with selection for Ap^R.

[7] - Plasmid DNA was prepared from Ap^R Cm^S transformants.

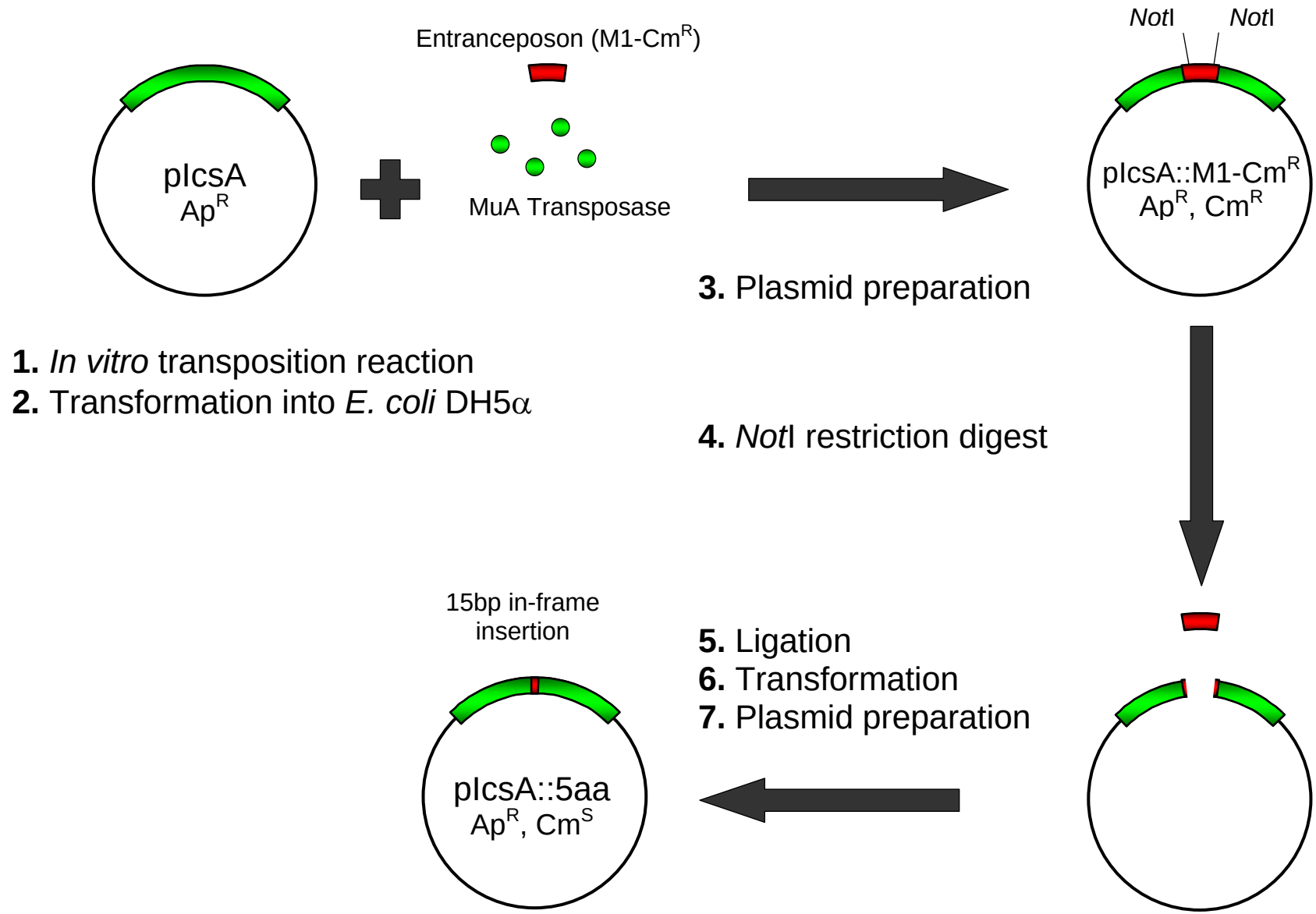
Entranceposon (M1-Cm^R)
pIcsA
Ap^R
MuA Transposase
*Not*I
*Not*I
pIcsA::M1-Cm^R
Ap^R, Cm^R
3. Plasmid preparation
1. *In vitro* transposition reaction
2. Transformation into *E. coli* DH5α
4. *Not*I restriction digest
15bp in-frame
insertion
5. Ligation
6. Transformation
7. Plasmid preparation
pIcsA::5aa
Ap^R, Cm^S

PCR screens were performed on crude DNA prepared from pools of Ap^R Cm^S colonies (Section 2.5.4) using the *Not*I mini primer (Finnzymes, Table 2.4), a primer complementary to 10 bp of the insertion, and the primer 2156 IcsAF (Table 2.4), complementary to a region 100 bp upstream of the *icsA* gene in pIcsA. From this screening, 969 colonies (from the 11 sub-libraries) were identified as potentially harbouring insertions within IcsA (data not shown). Plasmid DNA was prepared from each of these colonies (Section 2.5.2) and the PCR screen used above was repeated to re-screen 969 mutated plasmids individually. False positives from the initial screen and plasmids with insertions outside of the IcsA passenger domain (based on the size of the PCR product) were excluded from further analysis.

For the remaining 77 mutated plasmids, the location of the insertion and the encoded amino acids for each of these plasmids was determined by DNA sequencing (Section 2.6.5) using primers 2156 IcsAF, IcsA549F, IcsA2381R, 2170IcsAR (Table 2.4). Of these, 47 were identified as harbouring unique insertions within the IcsA passenger domain. A summary of the 47 $IcsA_i$ mutants, and the location and sequences of their 5 aa linker-insertions is shown in Table 3.1. Additionally, a schematic diagram of the insertion sites is presented in Figure 3.2. For each insertion, the 5 aa acid sequence that was introduced differed according to the reading frame and the native amino acid sequence into which the entranceposon had inserted. However, there was a consensus for each reading frame: CGRXX for frame #1, VRPHX for frame #2 and XAAAX for frame #3 (Table 3.1). The plasmid pIcsA, encoding $IcsA_{WT}$, and plasmids encoding IcsA linker-insertion mutants ($IcsA_i$) were electroporated into a *Shigella flexneri* Δ*icsA* strain (RMA2041; Table 2.1) for characterisation of production and function.

3.3 Detection of mutated IcsA proteins by Western immunoblotting

In order to investigate potential deleterious effects on protein production arising from the linker-insertion in each $IcsA_i$ mutant, SDS-PAGE and Western immunoblotting with anti-

Table 3.1 – IcsA linker-insertion mutants.

KMRM Collection Number[a]	$IcsA_i$ mutant	Insertion site[b]	Reading frame[c]	Inserted DNA sequence	Inserted amino acid sequence
33	$IcsA_{i56}$	56	2	GTG CGG CCG CAT TCG	VRPHS
42	$IcsA_{i81}$	81	2	GTG CGG CCG CAC TTG	VRPHL
1	$IcsA_{i87}$	87	1	TGC GGC CGC AAT GGA	CGRNG
36	$IcsA_{i120}$	120	1	TGC GGC CGC AGT GGT	CGRSG
24	$IcsA_{i122}$	122	1	TGC GGC CGC ACT GGT	CGRTG
62	$IcsA_{i128}$	128	3	AAT GCG GCC GCA GGT	NAAAG
30	$IcsA_{i132}$	132	3	GGT GCG GCC GCA GGC	GAAAG
3	$IcsA_{i137}$	137	1	TGC GGC CGC AAC TCT	CGRNS
2	$IcsA_{i138}$	138	3	ATT GCG GCC GCA TCT	IAAAS
18	$IcsA_{i140}$	140	1	TGC GGC CGC ACC GGA	CGRTG
44	$IcsA_{i148}$	148	1	TGC GGC CGC AAT CAA	CGRNQ
40	$IcsA_{i185}$	185	1	TGC GGC CGC ACA GGT	CGRTG
43	$IcsA_{i193}$	193	1	TGC GGC CGC AAT AGT	CGRNS
25	$IcsA_{i219}$	219	1	TGC GGC CGC ACC GGT	CGRTG
17	$IcsA_{i226}$	226	1	TGC GGC CGC AAT TAT	CGRNY
32	$IcsA_{i228}$	228	1	TGC GGC CGC AGT GAG	CGRSE
39	$IcsA_{i230}$	230	1	TGC GGC CGC AGT GAT	CGRSD
22	$IcsA_{i244}$	244	2	GTG CGG CCG CAC TCT	VRPHS
19	$IcsA_{i248}$	248	3	GGT GCG GCC GCA AAG	GAAAK
31	$IcsA_{i268}$	268	1	TGC GGC CGC AAC GGT	CGRNG
27	$IcsA_{271}$	271	1	TGC GGC CGC AAT GCT	CGRNA
23	$IcsA_{i288}$	288	1	TGC GGC CGC AGC GGT	CGRSG
4	$IcsA_{i292}$	292	1	TGC GGC CGC AAT TGG	CGRNW
12	$IcsA_{i297}$	297	1	TGC GGC CGC ACT ATA	CGRTI

(Table continued over page)

Table 3.1 (continued) - IcsA linker-insertion mutants.

KMRM Collection Number[a]	$IcsA_i$ mutant	Insertion site[b]	Reading frame[c]	Inserted DNA sequence	Inserted amino acid sequence
38	$IcsA_{i312}$	312	2	GTG CGG CCG CAT TCA	VRPHS
10	$IcsA_{i314}$	314	1	TGC GGC CGC AGT AAA	CGRSK
51	$IcsA_{i322}$	322	3	GCT GCG GCC GCA GTA	AAAAV
21	$IcsA_{i324}$	324	1	TGC GGC CGC ACA GGT	CGRTG
41	$IcsA_{i326}$	326	3	ATT GCG GCC GCA GCT	IAAAA
13	$IcsA_{i330a}$	330	3	ACT GCG GCC GCA ATC	TAAAI
28	$IcsA_{i330b}$	330	3	GGT GCG GCC GCA ACT	GAAAT
15	$IcsA_{i342}$	342	3	GTT GCG GCC GCA TCT	VAAAS
37	$IcsA_{i346}$	346	3	GAT GCG GCC GCA GGT	DAAAG
07	$IcsA_{i369}$	369	3	ACT GCG GCC GCA CCA	TAAAP
29	$IcsA_{i381}$	381	3	GTT GCG GCC GCA ACT	VAAAT
05	$IcsA_{i386}$	386	1	TGC GGC CGC ACA GGT	CGRTG
06	$IcsA_{i456}$	456	1	TGC GGC CGC ACT ATC	CGRTI
35	$IcsA_{i502}$	502	3	GAT GCG GCC GCA GCT	DAAAA
16	$IcsA_{i532}$	532	1	TGC GGC CGC AGG GAG	CGRRE
11	$IcsA_{i563}$	563	3	CGT GCG GCC GCA ACA	RAAAT
08	$IcsA_{i595}$	595	3	ATT GCG GCC GCA CTA	IAAAL
67	$IcsA_{i598}$	598	1	TGC GGC CGC AAT AAT	CGRNN
09	$IcsA_{i633}$	633	3	ACT GCG GCC GCA CAG	TAAAQ
14	$IcsA_{i643}$	643	1	TGC GGC CGC AAT GGA	CGRNG
34	$IcsA_{i677}$	677	1	TGC GGC CGC ATT GCA	CGRIA
47	$IcsA_{i716}$	716	1	TGC GGC CGC AGT TAT	CGRSY
20	$IcsA_{i748}$	748	1	TGC GGC CGC ATG AGC	CGRMS

[a] *E. coli* DH5α strain harbouring the corresponding $IcsA_i$ mutant on a multi-copy number plasmid.
[b] amino acid number preceeding the linker-insertion.
[c] Sequence used was that of Lett *et al*. (1989), GenBank accession # Q7BCK4

Figure 3.2 Schematic locations of the 5 amino acid insertions in 47 mutant IcsA proteins.

The location of the linker-insertion for each of the 47 $IcsA_i$ mutants is indicated with a vertical line. Three mutants ($IcsA_{i56}$, $IcsA_{i81}$, $IcsA_{i87}$,) have linker-insertions in polar localisation region #1 (aa 1-104, orange); 15 mutants ($IcsA_{i140}$, $IcsA_{i148}$, $IcsA_{i185}$, $IcsA_{i193}$, $IcsA_{i219}$, $IcsA_{i226}$, $IcsA_{i228}$, $IcsA_{i230}$, $IcsA_{i244}$, $IcsA_{i248}$, $IcsA_{i268}$, $IcsA_{i271}$, $IcsA_{i288}$, $IcsA_{i292}$, $IcsA_{i297}$) have linker-insertions in the GGR region (aa 140-307, green); 10 mutants ($IcsA_{i322}$, $IcsA_{i324}$, $IcsA_{i326}$, $IcsA_{i330a}$, $IcsA_{i330b}$, $IcsA_{i342}$, $IcsA_{i346}$, $IcsA_{i369}$, $IcsA_{i381}$, $IcsA_{i386}$) have linker-insertions in the IcsB/Atg5 binding region (aa 320-433, red); 4 mutants ($IcsA_{i532}$, $IcsA_{i563}$, $IcsA_{i595}$, $IcsA_{i598}$) have linker-insertions in polar localisation region #2 (aa 507-620, orange); and 3 mutants ($IcsA_{i643}$, $IcsA_{i677}$, $IcsA_{i716}$) have linker-insertions in a putative auto-chaperone region (aa 634-735, white). The remaining 12 mutants ($IcsA_{i120}$, $IcsA_{i122}$, $IcsA_{i128}$, $IcsA_{i132}$, $IcsA_{i137}$, $IcsA_{i138}$, $IcsA_{i312}$, $IcsA_{i314}$, $IcsA_{i456}$, $IcsA_{i502}$, $IcsA_{i633}$ and $IcsA_{i748}$) have linker-insertions in undefined regions.

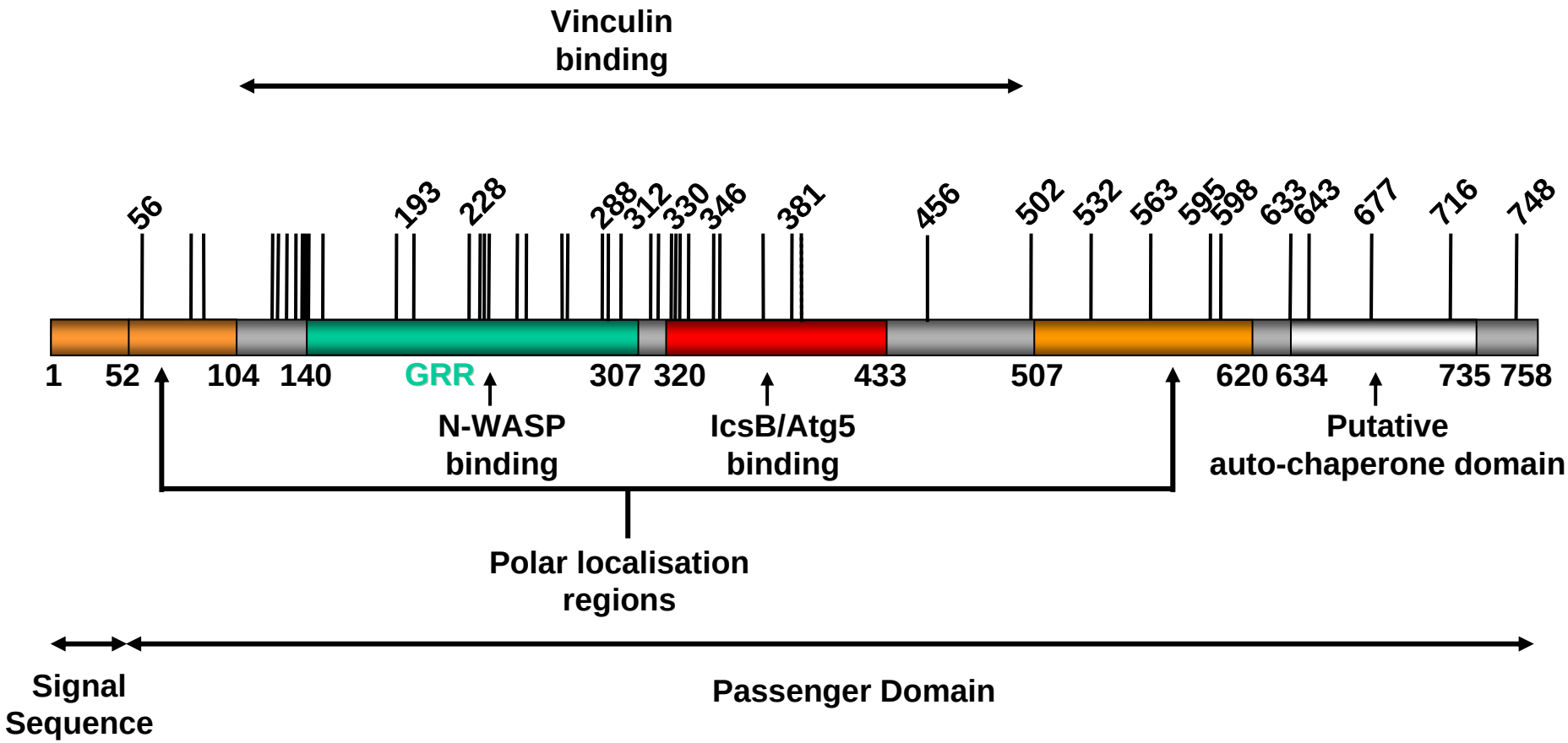
Vinculin
binding
56
193
228
288
312
330
346
381
456
502
532
563
595
598
633
643
677
716
748
1
52
104
140
GRR
307
320
433
507
620
634
735
758
N-WASP
binding
IcsB/Atg5
binding
Putative
auto-chaperone domain
Polar localisation
regions
Signal
Sequence
Passenger Domain

IcsA antibody was performed on whole cell lysates of log-phase cultures (A_{600} = 0.7-1.0) of *Shigella flexneri* Δ*icsA* expressing the various $IcsA_i$ mutant proteins (Sections 2.12.1, 2.12.4, 2.12.6). In 41 of 47 mutants, IcsA levels were comparable to WT (Table 3.2). There was no correlation observed between the inserted aa sequence and the stability of the mutant $IcsA_i$ proteins (Table 3.2). Strains with plasmids encoding $IcsA_{i595}$, $IcsA_{i598}$, $IcsA_{i633}$, $IcsA_{i643}$, $IcsA_{i677}$ or $IcsA_{i716}$ demonstrated aberrant production of the mutant proteins, with $IcsA_{i595}$ and $IcsA_{i598}$ produced at very low levels compared to $IcsA_{WT}$; whilst $IcsA_{i633}$, $IcsA_{i643}$, $IcsA_{i677}$ and $IcsA_{i716}$ could only be detected with high concentrations of anti-IcsA antibody (Figure 3.3A and Figure 3.4). For $IcsA_{WT}$ it was possible to detect not only the full-length IcsA (116 kDa) in whole cell lysates, but also low levels of the IcsP cleaved form IcsA' (95 kDa), which remains associated with bacterial cells (Figure 3.3A). Whilst IcsA' could be detected faintly for $IcsA_{i598}$ (Figure 3.3A, Lane 3), cleaved forms of $IcsA_{i595}$, $IcsA_{i633}$, $IcsA_{i643}$, $IcsA_{i677}$ or $IcsA_{i716}$ could not be detected in whole cell lysates (Figure 3.3A, Lanes 2, 4-7). For these mutants, the amount of protein in the culture supernatant was evaluated in order to determine if reduction of the full-length, membrane-anchored form of IcsA was due to increased IcsA cleavage and secretion into the supernatant. Proteins in the culture supernatants of these strains were precipitated with trichloroacetic acid (TCA) according to Section 2.12.2, and analysed by SDS-PAGE and Western immunoblotting with anti-IcsA antibody. Cleaved $IcsA_{i595}$ and $IcsA_{i598}$ were observed in the supernatant, albeit at slightly lower levels compared to $IcsA_{WT}$, and the cleaved forms of $IcsA_{i633}$, $IcsA_{i643}$, $IcsA_{i677}$ and $IcsA_{i716}$ could not be detected in this fraction (Figure 3.3B).

Notably, all these mutants possessed insertions immediately upstream of, or within, a region of IcsA (aa 634-735) that shares similarity to the putative auto-chaperone domain (aa 601-692) of *Bordetella pertussis* BrkA (refer to Figure 1.9; Section 1.3.4) (Oliver *et al.*, 2003). Deletion of this region in BrkA made the protein susceptible to degradation by outer membrane (OM) proteases and trypsin (Oliver *et al.*, 2003). Therefore, it was of interest to

Table 3.2 – Production of IcsA$_i$ mutants in *S. flexneri* Δ*icsA* (RMA2041).

KMRM Collection Number[a]	IcsA$_i$ mutant	Insertion site[b]	Inserted amino acid sequence	IcsA production[c]
133	IcsA$_{i56}$	56	VRPHS	+++
142	IcsA$_{i81}$	81	VRPHL	+++
101	IcsA$_{i87}$	87	CGRNG	+++
136	IcsA$_{i120}$	120	CGRSG	+++
124	IcsA$_{i122}$	122	CGRTG	+++
162	IcsA$_{i128}$	128	NAAAG	+++
130	IcsA$_{i132}$	132	GAAAG	+++
103	IcsA$_{i137}$	137	CGRNS	+++
102	IcsA$_{i138}$	138	IAAAS	+++
118	IcsA$_{i140}$	140	CGRTG	+++
144	IcsA$_{i148}$	148	CGRNQ	+++
140	IcsA$_{i185}$	185	CGRTG	+++
143	IcsA$_{i193}$	193	CGRNS	+++
125	IcsA$_{i219}$	219	CGRTG	+++
117	IcsA$_{i226}$	226	CGRNY	+++
132	IcsA$_{i228}$	228	CGRSE	+++
139	IcsA$_{i230}$	230	CGRSD	+++
122	IcsA$_{i244}$	244	VRPHS	+++
119	IcsA$_{i248}$	248	GAAAK	+++
131	IcsA$_{i268}$	268	CGRNG	+++
127	IcsA$_{i271}$	271	CGRNA	+++
123	IcsA$_{i288}$	288	CGRSG	+++
104	IcsA$_{i292}$	292	CGRNW	+++
112	IcsA$_{i297}$	297	CGRTI	+++

[a] *S. flexneri* Δ*icsA* (RMA2041) strain harbouring the corresponding IcsA$_i$ mutant on a multi-copy number plasmid.
[b] amino acid number preceding the linker-insertion.
[c] as determined by Western immunoblotting of whole-cell lysates.

(Table continued over page)

Table 3.2 (cont'd) – Production of IcsA$_i$ mutants in *S. flexneri* Δ*icsA* (RMA2041).

KMRM Collection Number[a]	IcsA$_i$ mutant	Insertion site[b]	Inserted amino acid sequence	IcsA production[c]
138	IcsA$_{i312}$	312	VRPHS	+++
110	IcsA$_{i314}$	314	CGRSK	+++
151	IcsA$_{i322}$	322	AAAAV	+++
121	IcsA$_{i324}$	324	CGRTG	+++
141	IcsA$_{i326}$	326	IAAAA	+++
113	IcsA$_{i330a}$	330	TAAAI	+++
128	IcsA$_{i330b}$	330	GAAAT	+++
115	IcsA$_{i342}$	342	VAAAS	+++
137	IcsA$_{i346}$	346	DAAAG	+++
107	IcsA$_{i369}$	369	TAAAP	+++
129	IcsA$_{i381}$	381	VAAAT	+++
105	IcsA$_{i386}$	386	CGRTG	+++
106	IcsA$_{i456}$	456	CGRTI	+++
135	IcsA$_{i502}$	502	DAAAA	+++
116	IcsA$_{i532}$	532	CGRRE	+++
111	IcsA$_{i563}$	563	RAAAT	+++
108	IcsA$_{i595}$	595	IAAAL	+
167	IcsA$_{i598}$	598	CGRNN	++
109	IcsA$_{i633}$	633	TAAAQ	+/-
114	IcsA$_{i643}$	643	CGRNG	+/-
134	IcsA$_{i677}$	677	CGRIA	+/-
147	IcsA$_{i716}$	716	CGRSY	+/-
120	IcsA$_{i748}$	748	CGRMS	+++

[a] *S. flexneri* Δ*icsA* (RMA2041) strain harbouring the corresponding IcsA$_i$ mutant on a multi-copy number plasmid.
[b] amino acid number preceeding the linker-insertion.
[c] +++, ++, + , +/- = relative band intensity upon Western immunoblotting of whole-cell lysates.

Figure 3.3 Western blot analyses of $IcsA_i$ mutant production and secretion.

A,B - Production and secretion of $IcsA_i$ mutants by *S. flexneri.*

S. flexneri strains to be examined were grown to log-phase in LB at 37°C. Lysates were prepared from whole cells (**A**) or tricholoroacetic acid precipitated culture supernatants (**B**) and electrophoresed on a 7.5% SDS-PAGE gel prior to Western blot analysis with rabbit anti-IcsA polyclonal antibodies. The 116 kDa band corresponds to full-length IcsA and the 95 kDa band corresponds to the cleaved form ($IcsA^{'}$). Samples represent 1 x 10^8 cells (**A**) or the culture supernatant equivalent of 1 x 10^8 cells (**B**).

Lane 1: *S. flexneri* Δ*icsA* $IcsA_{WT}$ (RMA2090)
Lane 2: *S. flexneri* Δ*icsA* $IcsA_{i595}$ (KMRM108)
Lane 3: *S. flexneri* Δ*icsA* $IcsA_{i598}$ (KMRM167)
Lane 4: *S. flexneri* Δ*icsA* $IcsA_{i633}$ (KMRM109)
Lane 5: *S. flexneri* Δ*icsA* $IcsA_{i643}$ (KMRM114)
Lane 6: *S. flexneri* Δ*icsA* $IcsA_{i677}$ (KMRM134)
Lane 7: *S. flexneri* Δ*icsA* $IcsA_{i716}$ (KMRM147)
Lane 8: *S. flexneri* Δ*icsA* (RMA2041)

C - Production of $IcsA_i$ mutants by *E. coli* UT5600.

E. coli strains to be examined were grown to log-phase in LB at 37°C. Whole cell lysates were prepared and electrophoresed on a 7.5% SDS-PAGE gel prior to Western blot analysis with rabbit anti-IcsA polyclonal antibodies. The 116 kDa band corresponds to full-length IcsA. Samples represent the equivalent of 1 x 10^8 cells.

Lane 1: *E. coli* UT5600 $IcsA_{WT}$ (KMRM87)
Lane 2: *E. coli* UT5600 $IcsA_{i595}$ (KMRM208)
Lane 3: *E. coli* UT5600 $IcsA_{i598}$ (KMRM267)
Lane 4: *E. coli* UT5600 $IcsA_{i633}$ (KMRM209)
Lane 5: *E. coli* UT5600 $IcsA_{i643}$ (KMRM214)
Lane 6: *E. coli* UT5600 $IcsA_{i677}$ (KMRM234)
Lane 7: *E. coli* UT5600 $IcsA_{i716}$ (KMRM247)
Lane 8: *E. coli* UT5600

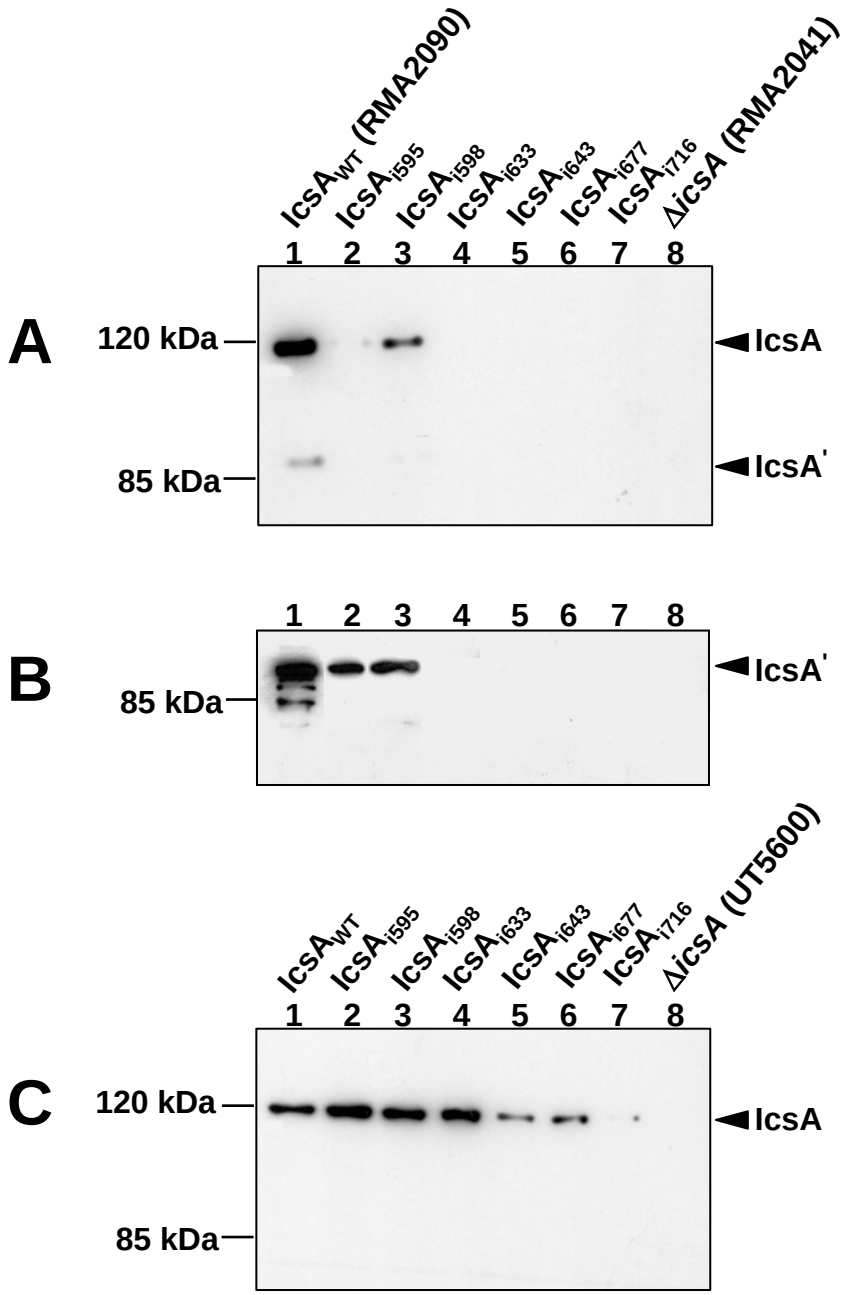
IcsA$_{WT}$ (RMA2090)
IcsA$_{i595}$
IcsA$_{i598}$
IcsA$_{i633}$
IcsA$_{i643}$
IcsA$_{i677}$
IcsA$_{i716}$
Δ*icsA* (RMA2041)
1 2 3 4 5 6 7 8
A
120 kDa
85 kDa
IcsA
IcsA'
1 2 3 4 5 6 7 8
B
85 kDa
IcsA'
IcsA$_{WT}$
IcsA$_{i595}$
IcsA$_{i598}$
IcsA$_{i633}$
IcsA$_{i643}$
IcsA$_{i677}$
IcsA$_{i716}$
Δ*icsA* (UT5600)
1 2 3 4 5 6 7 8
C
120 kDa
85 kDa
IcsA

Figure 3.4 Production of $IcsA_i$ mutants by *S. flexneri* detected using an increased concentration of antibodies.

S. flexneri strains to be examined were grown to log-phase in LB at 37°C. Whole cell lysates were prepared and electrophoresed on a 12% SDS-PAGE gel prior to Western immunoblotting with a rabbit anti-IcsA antibody (Section 2.1.1). The antibody concentration used was 50x more than that used in Figure 3.3. The 116 kDa band corresponds to full-length IcsA and the 95 kDa band corresponds to the cleaved form ($IcsA^{'}$). Samples represent the equivalent of 1 x 10^8 cells.

Lane 1: *S. flexneri* Δ*icsA* $IcsA_{i633}$ (KMRM109)

Lane 2: *S. flexneri* Δ*icsA* $IcsA_{i643}$ (KMRM114)

Lane 3: *S. flexneri* Δ*icsA* $IcsA_{i677}$ (KMRM134)

Lane 4: *S. flexneri* Δ*icsA* $IcsA_{i716}$ (KMRM147)

Lane 5: *S. flexneri* Δ*icsA* $IcsA_{WT}$ (RMA2090)

Lane 6: *S. flexneri* Δ*icsA* (RMA2041)

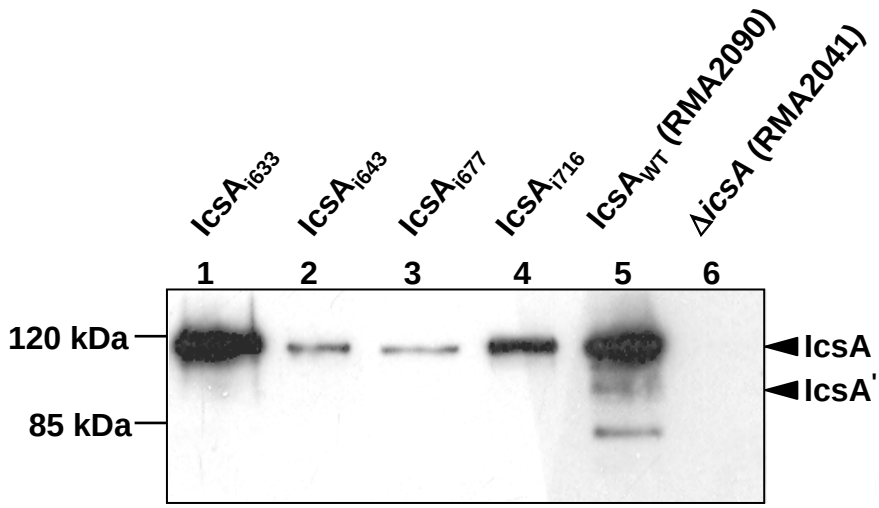
IcsA1633
IcsA1643
IcsA1677
IcsA1716
IcsAWT (RMA2090)
ΔicsA (RMA2041)
1
2
3
4
5
6
120 kDa
85 kDa
IcsA
IcsA'

examine whether production of mutants $IcsA_{i595}$, $IcsA_{i598,}$ $IcsA_{i633}$, $IcsA_{i643}$, $IcsA_{i677}$, and $IcsA_{i716}$ could be restored to WT levels when expressed in a strain deficient in OM proteases. Subsequently, $IcsA_{i595}$, $IcsA_{i598,}$ $IcsA_{i633}$, $IcsA_{i643}$, $IcsA_{i677}$ and $IcsA_{i716}$ were expressed in *E. coli* UT5600 (Table 2.1), which is deficient in the OM proteases *ompT* and *ompP*. Whole cell lysates where prepared from these strains and analysed by SDS-PAGE and Western immunoblotting with anti-IcsA antibody. Mutants $IcsA_{i595}$, $IcsA_{i598,}$ $IcsA_{i633}$ that were produced in low amounts in *S. flexneri* Δ*icsA* (RMA2041), were produced at levels comparable to $IcsA_{WT}$ in the OM protease deficient *E. coli* strain (UT5600) (Figure 3.3C), suggesting a susceptibility of these proteins to degradation by outer-membrane proteases in *S. flexneri* (e.g. IcsP). However, production of $IcsA_{i643}$, $IcsA_{i677}$ and $IcsA_{i716}$ was still greatly reduced in *E. coli* UT5600 (Figure 3.3C), suggesting that perhaps these latter mutants are more sensitive to digestion by periplasmic and/or other OM proteases.

3.4 IcsA surface expression and localisation

To examine the distribution of mutant forms of IcsA on the surface of bacteria, log-phase cultures (A_{600} = 0.7-1.0) of *S. flexneri* Δ*icsA* (RMA2041) expressing $IcsA_i$ mutants were formalin-fixed and analysed by immunofluorescence (IF) microscopy with anti-IcsA antibody (Section 2.12.7).

IcsA mutants $IcsA_{i633}$, $IcsA_{i643}$, $IcsA_{i677}$, and $IcsA_{i716}$ could not be detected on the surface of bacteria (data not shown; Table 3.3). $IcsA_{i595}$ and $IcsA_{i598,}$ which demonstrated reduced production (Section 3.3) could be detected, albeit faintly (Figure 3.5; Table 3.3). The 41 remaining $IcsA_i$ mutants could all be readily detected on the surface of *S. flexneri* (data not shown; Table 3.3).

IF microscopy revealed that 41 of the mutants exhibited a surface distribution that was comparable $IcsA_{WT}$, with IcsA predominantly localised to the pole(s), with very limited

Table 3.3 - Surface expression and distribution of $IcsA_i$ mutants in *S. flexneri* Δ*icsA* (RMA2041).

$IcsA_i$ mutant	IcsA production[a]	IcsA surface expression[b]	IcsA surface distribution[c]
$IcsA_{WT}$	+++	+++	polar
$IcsA_{i56}$	+++	+++	polar
$IcsA_{i81}$	+++	+++	polar
$IcsA_{i87}$	+++	+++	polar
$IcsA_{i120}$	+++	+++	polar
$IcsA_{i122}$	+++	+++	polar
$IcsA_{i128}$	+++	+++	polar
$IcsA_{i132}$	+++	+++	polar
$IcsA_{i137}$	+++	+++	polar
$IcsA_{i138}$	+++	+++	polar
$IcsA_{i140}$	+++	+++	polar
$IcsA_{i148}$	+++	+++	polar
$IcsA_{i185}$	+++	+++	polar
$IcsA_{i193}$	+++	+++	polar
$IcsA_{i219}$	+++	+++	polar
$IcsA_{i226}$	+++	+++	polar
$IcsA_{i228}$	+++	+++	polar
$IcsA_{i230}$	+++	+++	polar
$IcsA_{i244}$	+++	+++	polar
$IcsA_{i248}$	+++	+++	polar
$IcsA_{i268}$	+++	+++	polar
$IcsA_{i271}$	+++	+++	polar
$IcsA_{i288}$	+++	+++	polar
$IcsA_{i292}$	+++	+++	polar

(Table continued over page)

Table 3.3 (cont'd) – Surface expression and distribution of IcsA$_i$ mutants *S. flexneri* Δ*icsA* (RMA2041).

IcsA$_i$ mutant	IcsA production[a]	IcsA surface expression[b]	IcsA surface distribution[c]
IcsA$_{i297}$	+++	+++	polar
IcsA$_{i312}$	+++	+++	polar
IcsA$_{i314}$	+++	+++	polar
IcsA$_{i322}$	+++	+++	polar
IcsA$_{i324}$	+++	+++	polar
IcsA$_{i326}$	+++	+++	polar
IcsA$_{i330a}$	+++	+++	polar
IcsA$_{i330b}$	+++	+++	polar
IcsA$_{i342}$	+++	+++	polar
IcsA$_{i346}$	+++	+++	polar
IcsA$_{i369}$	+++	+++	polar
IcsA$_{i381}$	+++	+++	polar
IcsA$_{i386}$	+++	+++	polar
IcsA$_{i456}$	+++	+++	polar
IcsA$_{i502}$	+++	+++	polar
IcsA$_{i532}$	+++	+++	non-polar
IcsA$_{i563}$	+++	+++	non-polar
IcsA$_{i595}$	+	+	polar
IcsA$_{i598}$	++	++	polar
IcsA$_{i633}$	-	-	N/A[d]
IcsA$_{i643}$	-	-	N/A[d]
IcsA$_{i677}$	-	-	N/A[d]
IcsA$_{i716}$	-	-	N/A[d]
IcsA$_{i748}$	+++	+++	polar

[a] +++, ++, + , +/- indicate relative band intensity upon Western immunoblotting of whole-cell lysates.
[b] +++, ++, + indicate relative fluorescence as determined by IF microscopy.
[c] as determined by IF microscopy of bacteria.
[d] NA = Not applicable. Mutant IcsA proteins not detected on the surface of the bacteria.

Figure 3.5 Expression of $IcsA_{i595}$ and $IcsA_{i598}$ mutants on the surface of *S. flexneri.*

S. flexneri strains to be examined were grown to log-phase in LB at 37°C. Bacteria were formalin fixed and centrifuged onto poly-L-lysine-coated coverslips. Bacteria were incubated with an affinity purified poly-clonal anti-IcsA antibodies and Alexa-488-conjugated donkey anti-rabbit secondary antibodies. The coverslips were mounted on glass microscope slides and examined with an Olympus IX-70 microscope with phase-contrast optics using a 100× oil immersion, objective with a 1.5x enlarger. Alexa-488 (**A, C, E**) and phase-contrast images were false colour merged (**B, D, F**) using Metamorph (Version 6.3r7, Molecular devices). Scale bars indicate 10 μm.

Panel A and B: *S. flexneri ΔicsA* $IcsA_{WT}$ (RMA2090)

Panel C and D: *S. flexneri ΔicsA* $IcsA_{i595}$ (KMRM108)

Panel E and F: *S. flexneri ΔicsA* $IcsA_{i598}$ (KMRM167)

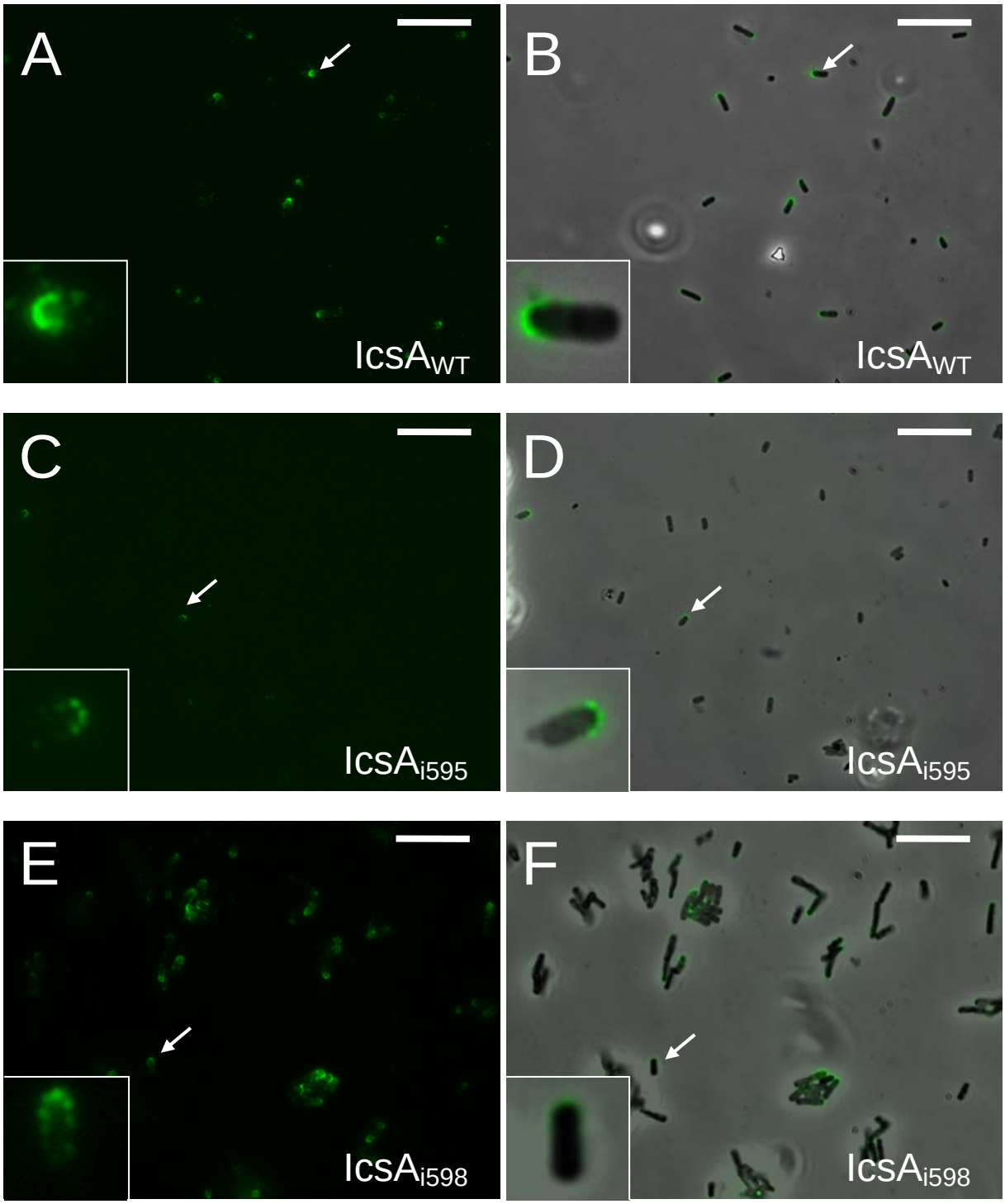
A
IcsA$_{WT}$
B
IcsA$_{WT}$
C
IcsA$_{i595}$
D
IcsA$_{i595}$
E
IcsA$_{i598}$
F
IcsA$_{i598}$

expression on the lateral regions of the bacteria. Only two mutants, IcsA$_{i532}$ and IcsA$_{i563}$, displayed altered IcsA localisation (Figure 3.6 A and B; Table 3.3). The IcsA$_{i532}$ mutant was distributed polarly on only 5% of the bacteria whilst for the majority of bacteria this protein was either distributed uniformly on the surface (47.5%) or distributed over the entire surface of the bacteria with some polar reinforcement (47.5%) (Figure 3.6 C and D; Table 3.4). Similarly, the IcsA$_{i563}$ mutant was distributed polarly on only 22.5% of the bacteria whilst for the majority of bacteria this protein was either distributed uniformly on the surface (35%) or distributed over the entire surface of the bacteria with some polar reinforcement (42.5%) (Figure 3.6 E and F; Table 3.4). Notably, other mutants IcsA$_{i56}$, IcsA$_{i81}$ and IcsA$_{i87}$ (Figure 3.7 A-F), which have linker-insertions in polar localisation region #1 (aa 1-104), and IcsA$_{i595}$ and IcsA$_{i598}$ (Figure 3.5 C-F), which have linker-insertion in polar region #2 (aa 507-620) were polarly distributed, with these IcsA$_i$ mutants being localised to the pole on at least 90% of the bacteria (Table 3.4). Mutant IcsA$_{i502}$ with an insertion adjacent polar localisation region #2 was also distributed in a polar fashion (data not shown, Table 3.3).

IcsA$_{i595}$ and IcsA$_{i598,}$ which have linker-insertion in polar region #2 appeared to be polarly distributed (Figure 3.5). However, due to the low level of expression of these proteins on the bacterial surface quantitation was not possible (Figure 3.5). In conclusion, none of the linker-insertions within polar localisation region # 1 (aa 1-104) affected polar localisation. Two mutants IcsA$_{i532}$ and IcsA$_{i563}$ have been identified with altered localisation on the bacterial surface and both of these IcsA$_i$ mutants possessed linker-insertions within polar localisation region #2 (aa 507-620), enabling a refinement of the region involved in polar targeting to aa 532-563.

3.5 Intercellular spread

The function of IcsA is to facilitate actin polymerisation and hence promote ABM. Therefore the ability of the mutated IcsA proteins to support ABM was investigated by the

Figure 3.6 Non-polar distribution of $IcsA_{i532}$ and $IcsA_{i563}$ mutants on the surface of *S. flexneri.*

S. flexneri strains to be examined were grown to log-phase in LB at 37°C. Bacteria were formalin fixed and centrifuged onto poly-L-lysine-coated coverslips. Bacteria were incubated with an affinity purified poly-clonal anti-IcsA antiserum and incubated with Alexa-488-conjugated goat anti-rabbit secondary antibodies. The coverslips were mounted on to glass microscope slides and examined with an Olympus IX-70 microscope with phase-contrast optics using 100x oil immersion objective with a 1.5x enlarger. Alexa-488 (**A**, **C**, **E**), and phase-contrast images were false colour merged (**B**, **D**, **F**), using Metamorph (Version 6.3r7, Molecular devices). Scale bars indicate 10 μm.

Panel A and B: *S. flexneri* Δ*icsA* $IcsA_{WT}$ (RMA2090)

Panel C and D: *S. flexneri* Δ*icsA* $IcsA_{i532}$ (KMRM116)

Panel E and F: *S. flexneri* Δ*icsA* $IcsA_{i563}$ (KMRM111)

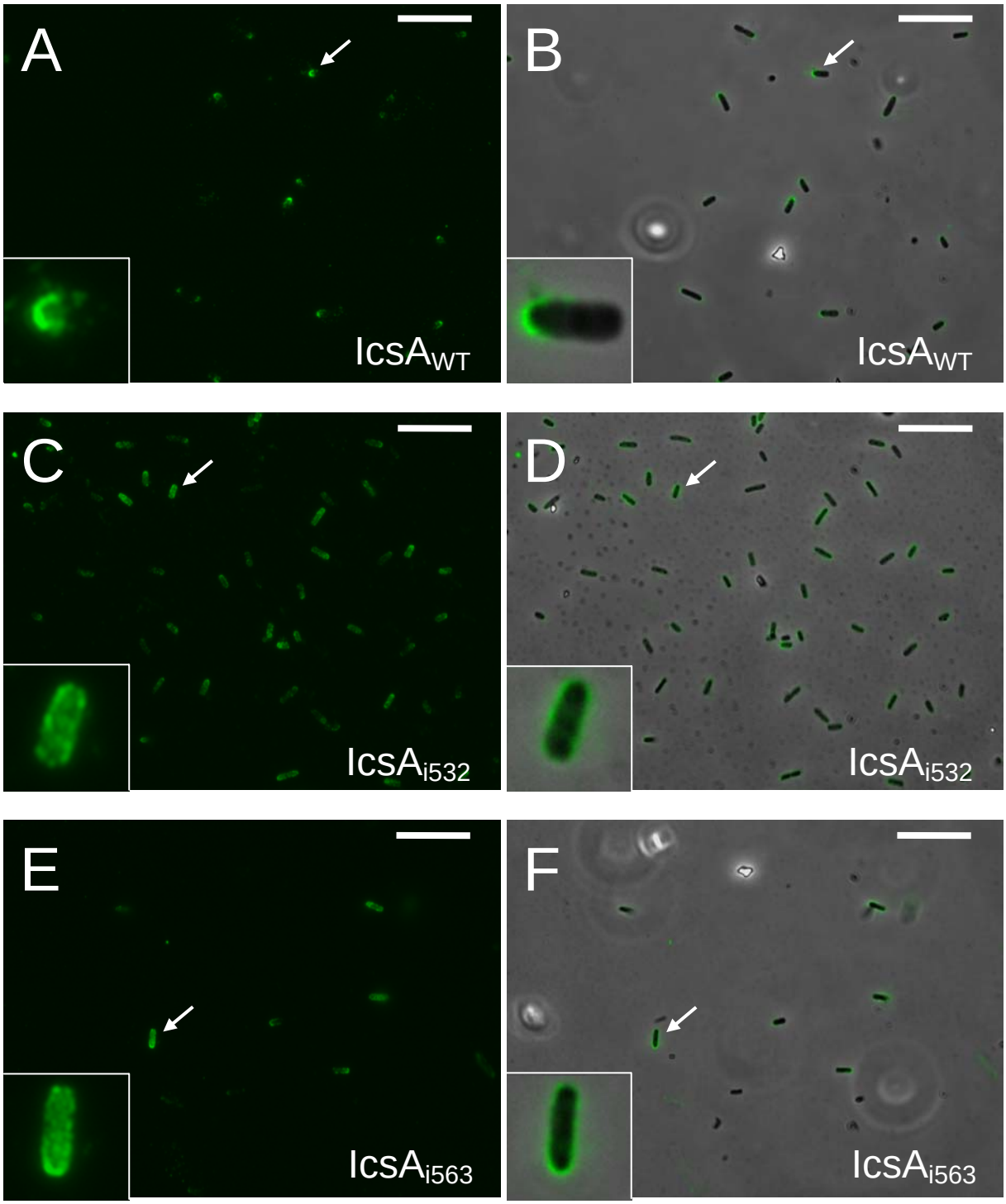
A
IcsA$_{WT}$
B
IcsA$_{WT}$
C
IcsA$_{i532}$
D
IcsA$_{i532}$
E
IcsA$_{i563}$
F
IcsA$_{i563}$

Table 3.4 – Cell surface distribution of $IcsA_i$ mutants with linker-insertion mutants in polar localisation regions #1 and #2.

$IcsA_i$ mutant	Polar localisation region [a]	% Bacteria with IcsA polarly localised [b]	% Bacteria with IcsA all over the surface with some polar reinforcement [b]	% Bacteria with IcsA all over the surface [b]	IcsA surface distribution
$IcsA_{iWT}$	N/A	100	0	0	polar
$IcsA_{i56}$	1	90	10	0	polar
$IcsA_{i81}$	1	95	5	0	polar
$IcsA_{i87}$	1	97.5	2.5	0	polar
$IcsA_{i532}$	2	5	47.5	47.5	non-polar
$IcsA_{i563}$	2	22.5	42.5	35	non-polar

[a] polar localisation region 1 (aa 1-104); polar localisation region 2 (aa 507-620).
[b] n = 40.

Figure 3.7 Polar distribution of $IcsA_{i56}$, $IcsA_{i81}$ and $IcsA_{i87}$ on the surface of *S. flexneri.*

S. flexneri strains to be examined were grown to log-phase in LB at 37°C. Bacteria were formalin fixed and centrifuged onto poly-L-lysine-coated coverslips. Bacteria were incubated with an affinity purified poly-clonal anti-IcsA antibodies and Alexa-488-conjugated donkey anti-rabbit secondary antibodies. The coverslips were mounted on glass microscope slides and examined with an Olympus IX-70 microscope with phase-contrast optics using a 100× oil immersion, objective with a 1.5x enlarger. Alexa-488 (**A, C, E**) and phase-contrast images were false colour merged (**B, D, F**) using Metamorph (Version 6.3r7, Molecular devices). Scale bars indicate 10 μm.

Panel A and B: *S. flexneri* Δ*icsA* $IcsA_{i56}$ (KMRM133)

Panel C and D: *S. flexneri* Δ*icsA* $IcsA_{i81}$ (KMRM142)

Panel E and F: *S. flexneri* Δ*icsA* $IcsA_{i87}$ (KMRM101)

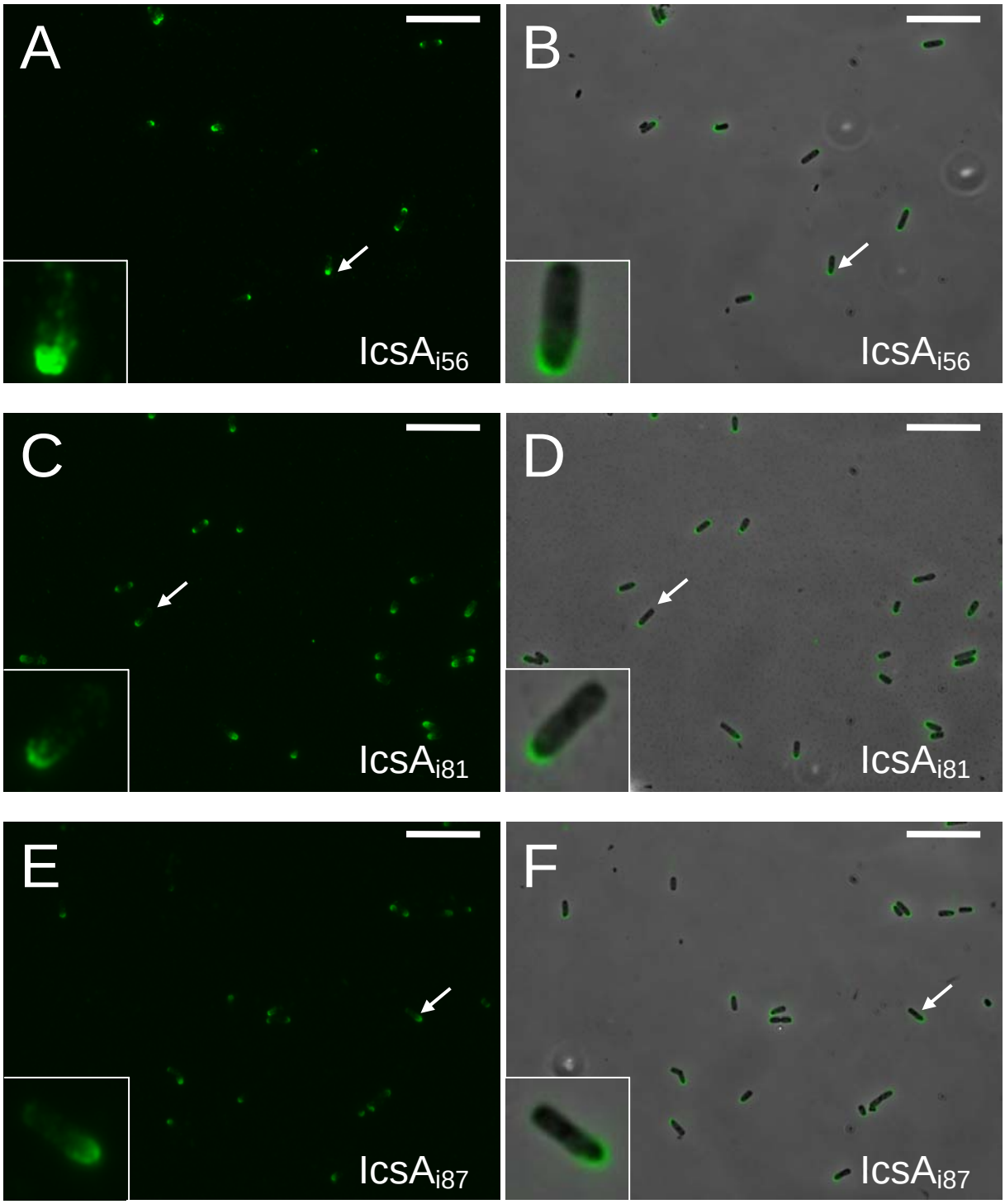
A
IcsA$_{i56}$
B
IcsA$_{i56}$
C
IcsA$_{i81}$
D
IcsA$_{i81}$
E
IcsA$_{i87}$
F
IcsA$_{i87}$

capacity of *S. flexneri* Δ*icsA* (RMA2041) strains expressing $IcsA_i$ mutants to form plaques on HeLa cell monolayers (Section 2.16.2). Plaque formation is an indication of intercellular spread, a process that requires IcsA-dependent ABM.

Eighteen *S. flexneri icsA* mutants formed WT plaques (Table 3.5) indicating that linker-insertions were located in permissive sites. Twenty-two of the *S. flexneri icsA* mutants were unable to form plaques in three independent experiments (Table 3.5). These IcsA mutants had linker-insertions either within the "GRR" region (aa 140-307) ($IcsA_{i185}$, $IcsA_{i219}$, $IcsA_{i226}$, $IcsA_{i228}$, $IcsA_{i230}$, $IcsA_{i244}$, $IcsA_{i248}$, $IcsA_{i268}$, $IcsA_{i271}$, $IcsA_{i292}$, $IcsA_{i297}$); the IcsB binding region (aa 320-433) ($IcsA_{i330a}$, $IcsA_{i330b}$, $IcsA_{i342}$, $IcsA_{i346}$, $IcsA_{i381}$); within polar localisation region #2 (aa 507-620) ($IcsA_{i532}$, $IcsA_{i563}$); or within or adjacent to the putative auto-chaperone domain (aa 634-735) ($IcsA_{i633}$, $IcsA_{i643}$, $IcsA_{i677}$, $IcsA_{i716}$). The remaining strains had intermediate phenotypes, exhibiting a WT frequency of plaque formation but forming plaques that varied in size compared to the control. Strains expressing mutants $IcsA_{i56}$, $IcsA_{i595}$ and $IcsA_{i598}$ formed plaques that were smaller than $IcsA_{WT}$ (Figure 3.8), albeit only slightly smaller in the case of $IcsA_{i56.}$ Additionally, whilst $IcsA_{i193}$, $IcsA_{i288}$, $IcsA_{i312}$ and $IcsA_{i502}$ were unable to form plaques, they did form small foci of dead HeLa cells that were not observed for *S. flexneri* Δ*icsA* (RMA2041) suggesting that mutants $IcsA_{i193}$, $IcsA_{i288}$, $IcsA_{i312}$ and $IcsA_{i502}$ still retained some capacity to promote intercellular spread. Further characterisation of the intracellular behaviour of *S. flexneri* Δ*icsA* expressing $IcsA_i$ mutants is described in Chapter Four.

3.6 Trypsin sensitivity of $IcsA_i$ mutants

Despite being small (5 aa), in-frame, linker-insertions in IcsA, these mutations could potentially disrupt native IcsA conformation, such that the failure of some strains expressing $IcsA_i$ mutants to form plaques may be due to major conformational changes in IcsA resultant

Table 3.5 - Plaque formation on HeLa cell monolayers by *S. flexneri* Δ*icsA* (RMA2041) expressing $IcsA_i$ mutants.

$IcsA_i$ mutant	Plaque formation[a]	$IcsA_i$ mutant	Plaque formation[a]
$IcsA_{WT}$	++++	$IcsA_{i297}$	-
$IcsA_{i56}$	+++	$IcsA_{i312}$	+
$IcsA_{i81}$	++++	$IcsA_{i314}$	++++
$IcsA_{i87}$	++++	$IcsA_{i322}$	++++
$IcsA_{i120}$	++++	$IcsA_{i324}$	++++
$IcsA_{i122}$	++++	$IcsA_{i326}$	++++
$IcsA_{i128}$	++++	$IcsA_{i330a}$	-
$IcsA_{i132}$	++++	$IcsA_{i330b}$	-
$IcsA_{i137}$	++++	$IcsA_{i342}$	-
$IcsA_{i138}$	++++	$IcsA_{i346}$	-
$IcsA_{i140}$	++++	$IcsA_{i369}$	++++
$IcsA_{i148}$	++++	$IcsA_{i381}$	-
$IcsA_{i185}$	-	$IcsA_{i386}$	++++
$IcsA_{i193}$	+	$IcsA_{i456}$	++++
$IcsA_{i219}$	-	$IcsA_{i502}$	+
$IcsA_{i226}$	-	$IcsA_{i532}$	-
$IcsA_{i228}$	-	$IcsA_{i563}$	-
$IcsA_{i230}$	-	$IcsA_{i595}$	++
$IcsA_{i244}$	-	$IcsA_{i598}$	++
$IcsA_{i248}$	-	$IcsA_{i633}$	-
$IcsA_{i268}$	-	$IcsA_{i643}$	-
$IcsA_{i271}$	-	$IcsA_{i677}$	-
$IcsA_{i288}$	+	$IcsA_{i716}$	-
$IcsA_{i292}$	-	$IcsA_{i748}$	++++

[a] ++++,+++,++,+,- indicate relative plaque sizes on HeLa cell monolayers. (++++) plaques size comparable to *S. flexneri* Δ*icsA* (RMA2041) expressing $IcsA_{WT}$ control strain; (+++) slightly reduced plaque size compared to control strain; (++) small plaque size; (+) foci (-) plaque formation not detected. All strains that formed plaques or foci did so at a WT frequency.

Data is based on observation of plaque formation for three independent experiments.

Figure 3.8 Plaque formation by *S. flexneri* Δ*icsA* expressing $IcsA_i$ mutants.

S. flexneri strains to be examined were grown to log-phase in LB at 37°C. Bacteria were diluted and added to confluent HeLa cell monolayers. At 90 min post-infection an overlay of medium containing gentamycin and 0.5% (w/v) agarose was added. A second overlay, additionally containing 0.1% (w/v) Neutral Red solution was added at 24 h post-infection and plaque formation observed 6-8 h later. Arrows indicate plaque formation.

Panel A: *S. flexneri*Δ*icsA* $IcsA_{WT}$ (RMA2090)

Panel B: *S. flexneri*Δ*icsA* $IcsA_{i56}$ (RMA2090)

Panel C: *S. flexneri*Δ*icsA* $IcsA_{i595}$ (RMA2090)

Panel D: *S. flexneri*Δ*icsA* $IcsA_{i598}$ (RMA2090)

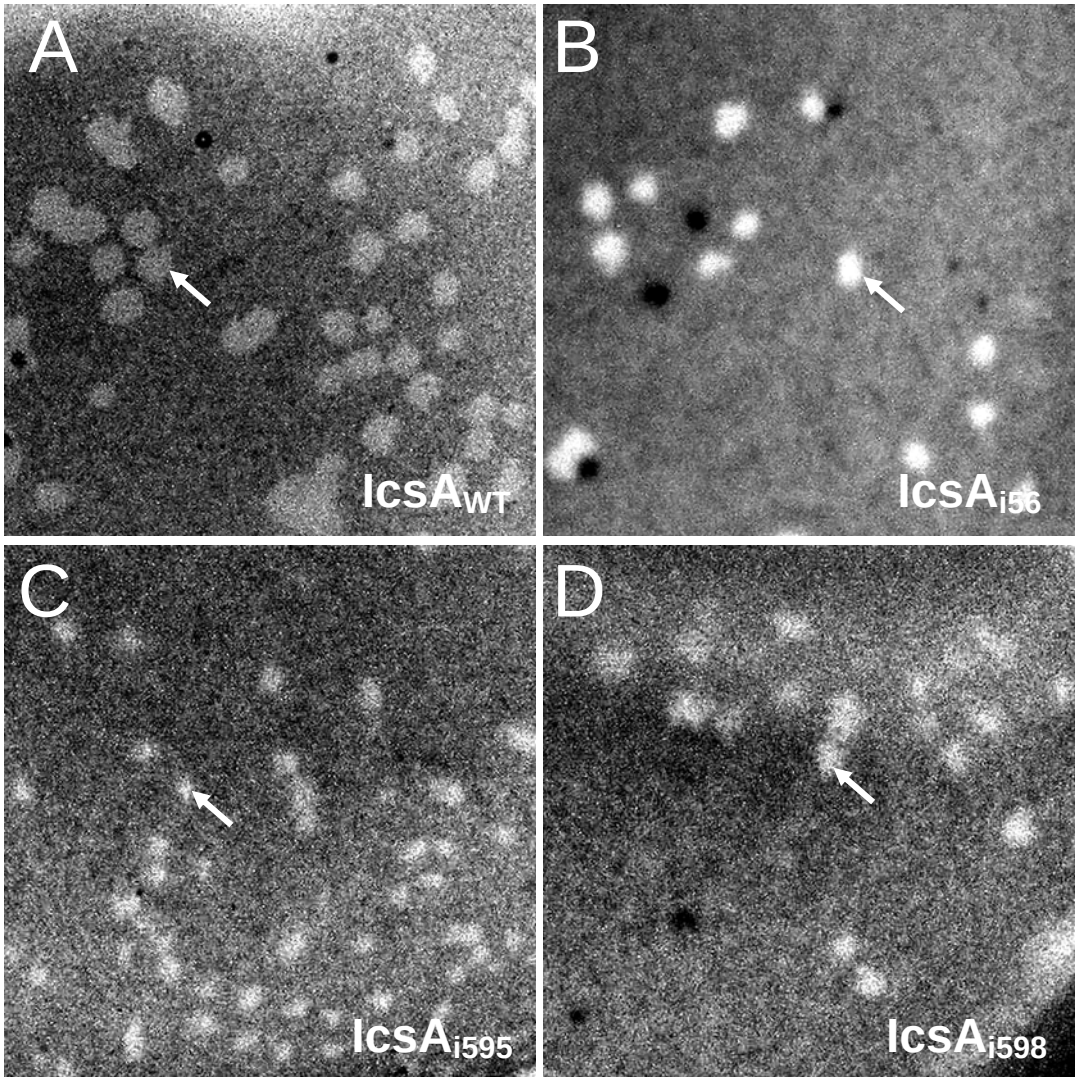
A
IcsA$_{WT}$
B
IcsA$_{i56}$
C
IcsA$_{i595}$
D
IcsA$_{i598}$

from the linker-insertion. In order to evaluate this possibility, *in situ* limited proteolysis with trypsin was performed (Section 2.12) on the twenty-two $IcsA_i$ mutants that were negative for plaque formation (Section 3.5). To avoid intrinsic protein degradation by endogenous proteases, these studies were performed in an *E. coli* OM protease deficient background (UT5600; Table 2.1). The protease digestion profiles of $IcsA_{WT}$ and twenty-two $IcsA_i$ mutants (Section 3.5) were compared after SDS-PAGE and Western immunoblotting with polyclonal anti-IcsA antibody (Sections 2.12.1, 2.12.4, 2.12.6). Three molecular weight bands of approximately 120 kDa, 100 kDa and 85 kDa were observed when the $IcsA_{WT}$ protein was subjected to *in situ* proteolysis with trypsin for either 5 or 10 minutes (Figure. 3.9).

Mutants $IcsA_{i185}$, $IcsA_{i219}$, $IcsA_{i228}$, $IcsA_{i244}$, $IcsA_{i271}$, $IcsA_{i292}$, $IcsA_{i297}$, $IcsA_{i330a}$, $IcsA_{i563}$, $IcsA_{i633}$, $IcsA_{i643}$, $IcsA_{i677}$ and $IcsA_{i716}$ had a different proteolysis profile to $IcsA_{WT}$, indicative of an altered sensitivity to trypsin, suggesting that these $IcsA_i$ mutant proteins may have altered folding (Figure. 3.9; Table 3.6). Mutants $IcsA_{i226}$, $IcsA_{i230}$, $IcsA_{i248}$, $IcsA_{i268}$, $IcsA_{i330b}$, $IcsA_{i342}$, $IcsA_{i346}$, $IcsA_{i381}$ and $IcsA_{i532}$ had proteolysis profile similar to $IcsA_{WT}$, signifying that they were likely to have a native conformation (Figure 3.9; Table 3.6). Hence, corresponding phenotypes exhibited by *S. flexneri* producing these proteins were unlikely to have resulted from major conformational changes in IcsA. Interestingly, mutants $IcsA_{i330a}$ and $IcsA_{i330b}$ had different proteolysis profiles despite harbouring linker-insertions in the same position. The only difference between these mutants is the encoded 5 aa insertion, with $IcsA_{i330a}$ harbouring the insertion “TAAAI” and $IcsA_{i330b}$ the insertion “GAAAT” (Table 3.1).

3.7 Summary

In this chapter, 47 IcsA mutants were created by pentapeptide linker-insertion mutagenesis in order to further characterise IcsA structure-function.

Figure 3.9 *In situ*, limited proteolysis with trypsin.

E. coli strains to be examined were grown to log-phase in LB at 37°C and bacterial suspensions were treated with 0.1 μg/ml of trypsin at 25°C to facilitate proteolysis. Aliquots were taken at 0 min (0'), 5 min (5‘) and 10 min (10'), and supplemented with 1 mM PMSF to inhibit further proteolysis. Whole cell lysates were electrophoresed on a 7.5% SDS-PAGE gel and subjected to Western blot analysis with a rabbit anti-IcsA antibody. Samples represent the equivalent of 1 x 10^9 cells. The region of IcsA that the linker-insertion is located within for each $IcsA_i$ protein is indicated. These are the glycine rich repeat (GRR) region (aa 140-307); the IcsB/Atg5 protein binding region(aa 320-433); the polar localisation region #2 (aa 507-620); and the putative auto-chaperone region (aa 634-735).

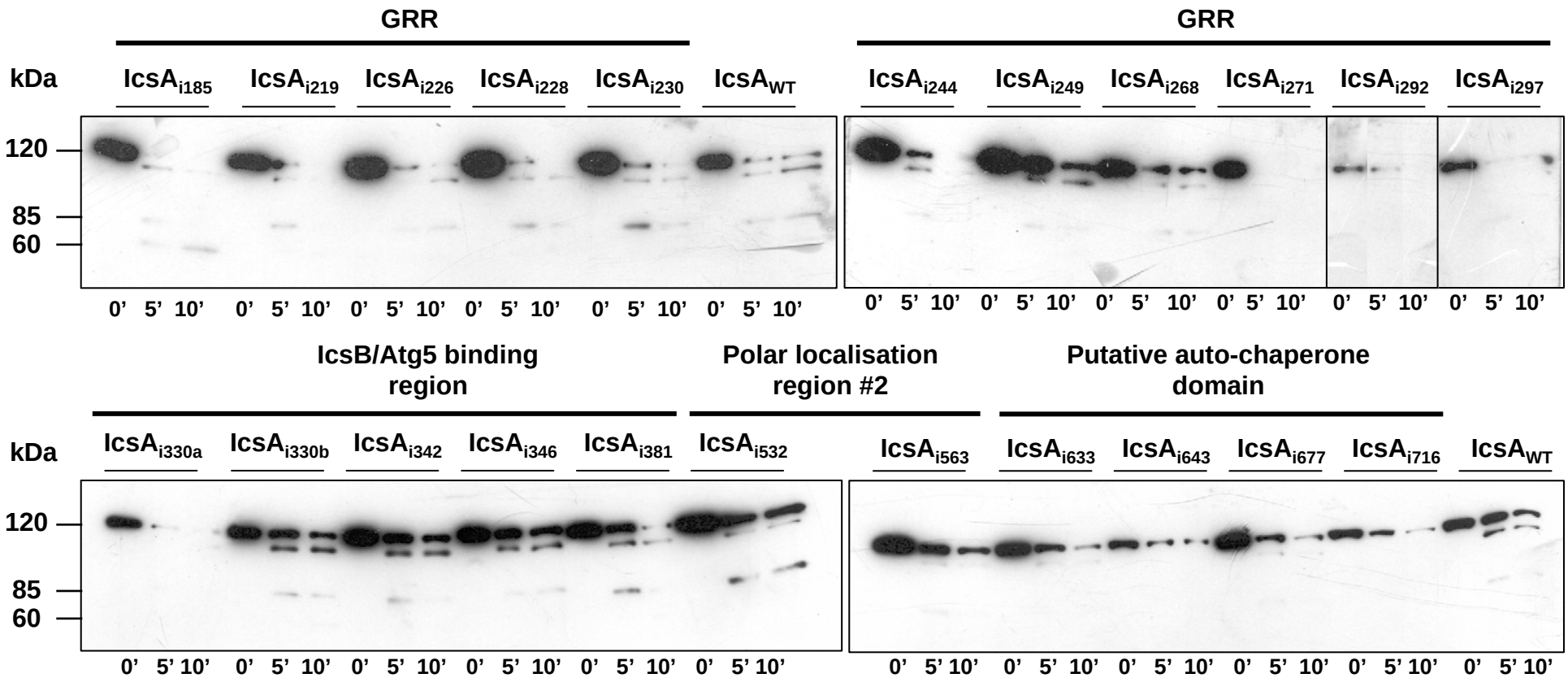
GRR
GRR
kDa
IcsA$_{i185}$
IcsA$_{i219}$
IcsA$_{i226}$
IcsA$_{i228}$
IcsA$_{i230}$
IcsA$_{WT}$
IcsA$_{i244}$
IcsA$_{i249}$
IcsA$_{i268}$
IcsA$_{i271}$
IcsA$_{i292}$
IcsA$_{i297}$
120
85
60
0’ 5’ 10’
IcsB/Atg5 binding region
Polar localisation region #2
Putative auto-chaperone domain
kDa
IcsA$_{i330a}$
IcsA$_{i330b}$
IcsA$_{i342}$
IcsA$_{i346}$
IcsA$_{i381}$
IcsA$_{i532}$
IcsA$_{i563}$
IcsA$_{i633}$
IcsA$_{i643}$
IcsA$_{i677}$
IcsA$_{i716}$
IcsA$_{WT}$
120
85
60
0’ 5’ 10’

Table 3.6 – *In situ,* trypsin proteolysis of $IcsA_i$ mutants in *E. coli* UT5600

$IcsA_i$ Mutant[a]	Trypsin proteolysis Profile[b]
$IcsA_{i185}$	-
$IcsA_{i219}$	-
$IcsA_{i226}$	+
$IcsA_{i228}$	-
$IcsA_{i230}$	+
$IcsA_{i244}$	-
$IcsA_{i248}$	+
$IcsA_{i268}$	+
$IcsA_{i271}$	-
$IcsA_{i292}$	-
$IcsA_{i297}$	-
$IcsA_{i330a}$	-
$IcsA_{i330b}$	+
$IcsA_{i342}$	+
$IcsA_{i346}$	+
$IcsA_{i381}$	+
$IcsA_{i532}$	+
$IcsA_{i563}$	-
$IcsA_{i633}$	-
$IcsA_{i643}$	-
$IcsA_{i677}$	-
$IcsA_{i716}$	-

[a] All $IcsA_i$ mutants when expressed in *S. flexneri* Δ*icsA* (RMA2041) were negative for plaque formation on HeLa cell monolayers.
[b] (+)WT proteolysis profile; (-)Altered proteolysis profile.

A putative auto-chaperone region of IcsA was identified from aa 595-716, as six mutants (IcsA$_{i595}$, IcsA$_{i598}$, IcsA$_{i633}$, IcsA$_{i643}$, IcsA$_{i677}$ and IcsA$_{i716}$) with linker-insertions in this region were produced at low levels by *S. flexneri* compared to IcsA$_{WT}$. The production of three of these mutants (IcsA$_{i595}$, IcsA$_{i598}$ and IcsA$_{i633}$) was restored when they were expressed in an *E. coli* strain deficient in OM proteases indicating a sensitivity of these mutants to degradation by these OM proteases present in WT *S. flexneri*.

Two mutants, IcsA$_{i532}$ and IcsA$_{i563}$, were identified with linker-insertions in polar localisation region #2 (aa 507-620) that demonstrated altered localisation on the bacterial surface, enabling a refinement of the region involved in polar targeting to aa 532-563.

Eighteen of the IcsA$_i$ mutants induced WT plaque formation when expressed in *S. flexneri.* In addition to identifying regions of IcsA not involved in IcsA function in intercellular spreading, this data has identified sites permissive for epitope insertion. The N-terminal region of IcsA appeared particularly permissive for epitope insertion with 10 IcsA$_i$ mutants with linker-insertions within aa 80-149 all displaying WT function.

Twenty-two of the *S. flexneri icsA* mutants were unable to form plaques and seven exhibited intermediate phenotypes. Notably, 10 of these IcsA$_i$ mutants (that were produced at WT levels) possessed linker-insertions outside of the GRR region (aa 140-307), which is considered to be the region responsible for IcsA interaction with host N-WASP (Suzuki *et al*., 1998; Suzuki *et al*., 2002).

Chapter Four

Intracellular behaviour of IcsA$_i$ mutants

Chapter Four: Intracellular behaviour of IcsA$_i$ mutants

4.1 Introduction

In the previous chapter, 47 IcsA mutants were created for structure-function studies using pentapeptide linker-insertion mutagenesis (Section 3.2), and plaque formation on HeLa cell monolayers was used to assess the ability of *S. flexneri* Δ*icsA* expressing IcsA$_i$ mutant proteins to spread from cell-cell (Section 3.5). Twenty-nine strains were identified as having aberrant intercellular spread (Section 3.5) and were chosen for further characterisation in this chapter. Specifically, the aim was to investigate the ability of these mutants to form F-actin comet tails and recruit the host-factor N-WASP, which is essential for IcsA-mediated ABM, and hence intercellular spread. The role of vinculin in *S. flexneri* ABM remains controversial (see Section 1.4.5), but a correlation between increased vinculin recruitment and intercellular spreading defects has been observed for certain *S. flexneri* mutants in our laboratory (Van Den Bosch and Morona, unpublished data) and hence vinculin recruitment was also investigated. Additionally, as evidence of masking of IcsA by LPS Oag has previously been reported by our laboratory (Morona and Van Den Bosch, 2003b), it was hypothesised that LPS Oag may interfere with recruitment of N-WASP by IcsA$_i$ mutants. Therefore an additional aim of this chapter was to investigate the role of LPS Oag in N-WASP recruitment.

4.2 F-actin comet tail formation by IcsA mutants

To further investigate the molecular basis for the defects in plaque formation exhibited by strains expressing IcsA$_i$ proteins (Section 3.5), IF microscopy was used to assess F-actin comet tail formation inside infected host cells, as it is associated with intercellular spreading. HeLa cells were infected with log-phase cultures of *S. flexneri* Δ*icsA* (RMA2041) expressing

different $IcsA_i$ proteins, and F-actin comet tail formation was visualised by staining with FITC-phalloidin as described in Section 2.16.3. A summary of the phenotypes for each mutant is shown in Table 4.1.

Nineteen out of the twenty-nine strains expressing $IcsA_i$ mutants were unable to form F-actin comet tails. All of these strains were negative for plaque formation (Section 3.5). This included strains expressing mutant proteins $IcsA_{i185}$, $IcsA_{i219}$, $IcsA_{i226}$, $IcsA_{i230}$, $IcsA_{i244}$, $IcsA_{i248}$, $IcsA_{i268}$, $IcsA_{i271}$ and $IcsA_{i297}$, with insertions within the GRR region, strains expressing $IcsA_{i330a}$, $IcsA_{330b}$, $IcsA_{i342}$, $IcsA_{i346}$ and $IcsA_{i381}$ with linker-insertions within the IcsB binding region, and strains expressing $IcsA_{i532}$, and $IcsA_{i563}$ with linker-insertions within polar localisation region #2 (Table 4.1). Although a strain producing $IcsA_{i346}$ was unable to form F-actin comet tails, capping of the bacterial pole with F-actin was observed (Figure 4.1 C). Despite an inability to form detectable plaques or foci (Section 3.5), F-actin tail formation was seen at a very low frequency for $IcsA_{i228}$, $IcsA_{i292}$ (which had insertions located in the GRR region), and $IcsA_{i633}$ (which had an insertion in the putative auto-chaperone region) (Figure. 4.1 A, B and D). Notably, the latter mutant protein was produced at very low levels in *S. flexneri* (Section 3.3). Strains producing $IcsA_{i595}$ and $IcsA_{i598}$ that also had reduced levels of protein (Section 3.3), were readily able to form F-actin comet tails (Figure 4.2 G and H).

Although *S. flexneri* strains expressing $IcsA_{i56}$, $IcsA_{i193}$, $IcsA_{i288}$, $IcsA_{i312}$, and $IcsA_{i502}$ formed reduced sized plaques; these mutants still displayed efficient F-actin comet tail formation (Figure 4.2 A-F). This result was unexpected as efficient F-actin tail formation and ABM are correlates for intercellular spread (Monack and Theriot, 2001). To reconcile this data, it was hypothesised that the frequency of tail formation of these strains might have been reduced, correlating to a decrease in intercellular spreading and plaque formation. In order to investigate this hypothesis, HeLa cells were infected with *S. flexneri* Δ*icsA* (RMA2041) expressing $IcsA_{i56}$, $IcsA_{i193}$, $IcsA_{i288}$, $IcsA_{i312}$, $IcsA_{i502}$ and also $IcsA_{i598}$ (which only had a

Table 4.1 – F-actin comet tail formation by *S. flexneri* Δ*icsA* (RMA2041) expressing $IcsA_i$ mutants.

$IcsA_i$ mutant	F-actin tail formation		$IcsA_i$ mutant	F-actin tail formation	
	Tails[a]	F-actin capping[b]		Tails[a]	F-actin capping[b]
$IcsA_{WT}$	++	++	$IcsA_{i312}$	++	++
$IcsA_{i56}$	++	++	$IcsA_{i330a}$	-	-
$IcsA_{i185}$	-	-	$IcsA_{i330b}$	-	-
$IcsA_{i193}$	++	++	$IcsA_{i342}$	-	-
$IcsA_{i219}$	-	-	$IcsA_{i346}$	-	+
$IcsA_{i226}$	-	-	$IcsA_{i381}$	-	-
$IcsA_{i228}$	+	+	$IcsA_{i502}$	++	++
$IcsA_{i230}$	-	-	$IcsA_{i532}$	-	-
$IcsA_{i244}$	-	-	$IcsA_{i563}$	-	-
$IcsA_{i248}$	-	-	$IcsA_{i595}$	++	++
$IcsA_{i268}$	-	-	$IcsA_{i598}$	++	++
$IcsA_{i271}$	-	-	$IcsA_{i633}$	+	+
$IcsA_{i288}$	++	++	$IcsA_{i643}$	-	-
$IcsA_{i292}$	+	+	$IcsA_{i677}$	-	-
$IcsA_{i297}$	-	-	$IcsA_{i716}$	-	-

[a] (++) frequent F-actin comet tail formation; (+) F-actin comet tail formation observed rarely; (-) not detected.

[b] (++) frequent capping of the bacterial pole F-actin; (+) Capping of the bacterial pole F-actin observed rarely; (-) Capping of the bacterial pole F-actin not detected.

N.B. This data is based on qualitative observation of *S. flexneri* Δ*icsA* (RMA2041) expressing $IcsA_i$ mutants in infected HeLa cells

Figure 4.1 F-actin capping of intracellular *S. flexneri* Δ*icsA* expressing IcsA$_i$ mutants

Log-phase cultures of bacteria were added to semi-confluent monolayers of HeLa cells grown on glass coverslips. After centrifugation monolayers were incubated for 60 min to allow invasion, then 90 min in medium containing 40 µg/mL gentamycin. Monolayers were washed and formalin fixed. Bacteria were labelled with DAPI (blue) and F-actin was labelled with FITC-phalloidin (green). The coverslips were mounted on glass microscope slides and examined with an Olympus IX-70 microscope with phase-contrast optics using 100x oil immersion objective with a 1.5x enlarger. DAPI and FITC-phalloidin images were false colour merged using Metamorph (Version 6.3r7, Molecular devices). Arrows indicate capping of the bacteria with F-actin. Strains were assessed in 3 independent experiments. Scale bars indicate 10 µm.

Panel A: *S. flexneri* Δ*icsA* IcsA$_{i228}$ (KMRM132)

Panel B: *S. flexneri* Δ*icsA* IcsA$_{i292}$ (KMRM104)

Panel C: *S. flexneri* Δ*icsA* IcsA$_{i346}$ (KMRM137)

Panel D: *S. flexneri* Δ*icsA* IcsA$_{i633}$ (KMRM109)

Panel E: *S. flexneri* Δ*icsA* IcsA$_{WT}$ (RMA2090)

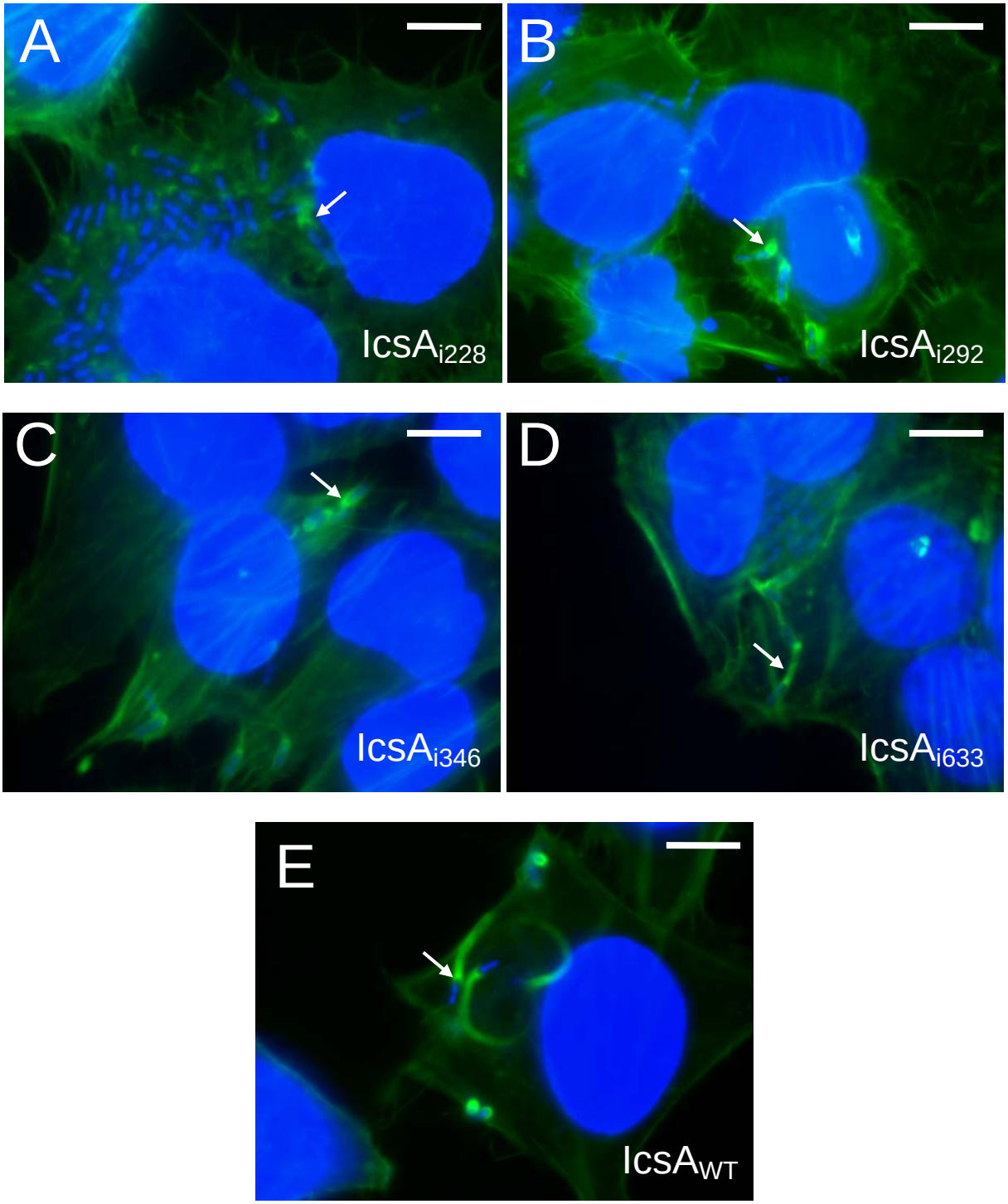
A
IcsA$_{i228}$
B
IcsA$_{i292}$
C
IcsA$_{i346}$
D
IcsA$_{i633}$
E
IcsA$_{WT}$

Figure 4.2 F-actin tail formation by intracellular *S. flexneri* Δ*icsA* expressing IcsA$_i$ mutants.

Log-phase cultures of bacteria were added to semi-confluent monolayers of HeLa cells grown on glass coverslips. After centrifugation monolayers were incubated for 60 min to allow invasion, then 90 min in medium containing 40 µg/mL gentamycin. Monolayers were washed, formalin fixed, permeabilised with 0.1% Triton X-100 in PBS, and blocked with 10% FCS in PBS. Bacteria were labelled with a polyclonal anti-LPS antibodies and Alexa 594-conjugated donkey anti-rabbit antibodies (red) and F-actin was labelled with FITC-phalloidin (green). The coverslips were mounted on glass microscope slides and examined with an Olympus IX-70 microscope with phase-contrast optics using 100x oil immersion objective with a 1.5x enlarger. Alex594 and FITC-phalloidin images were false colour merged using Metamorph (Version 6.3r7, Molecular devices). Arrows indicate F-actin tail formation. Strains were assessed in 3 independent experiments. Scale bars indicate 10 µm.

Panel A: *S. flexneri* Δ*icsA* IcsA$_{WT}$ (RMA2090)

Panel B: *S. flexneri* Δ*icsA* IcsA$_{i56}$ (KMRM133)

Panel C: *S. flexneri* Δ*icsA* IcsA$_{i193}$ (KMRM143)

Panel D: *S. flexneri* Δ*icsA* IcsA$_{i288}$ (KMRM123)

Panel E: *S. flexneri* Δ*icsA* IcsA$_{i312}$ (KMRM138)

Panel F: *S. flexneri* Δ*icsA* IcsA$_{i502}$ (KMRM135)

Panel G: *S. flexneri* Δ*icsA* IcsA$_{i595}$ (KMRM108)

Panel H: *S. flexneri* Δ*icsA* IcsA$_{i598}$ (KMRM167)

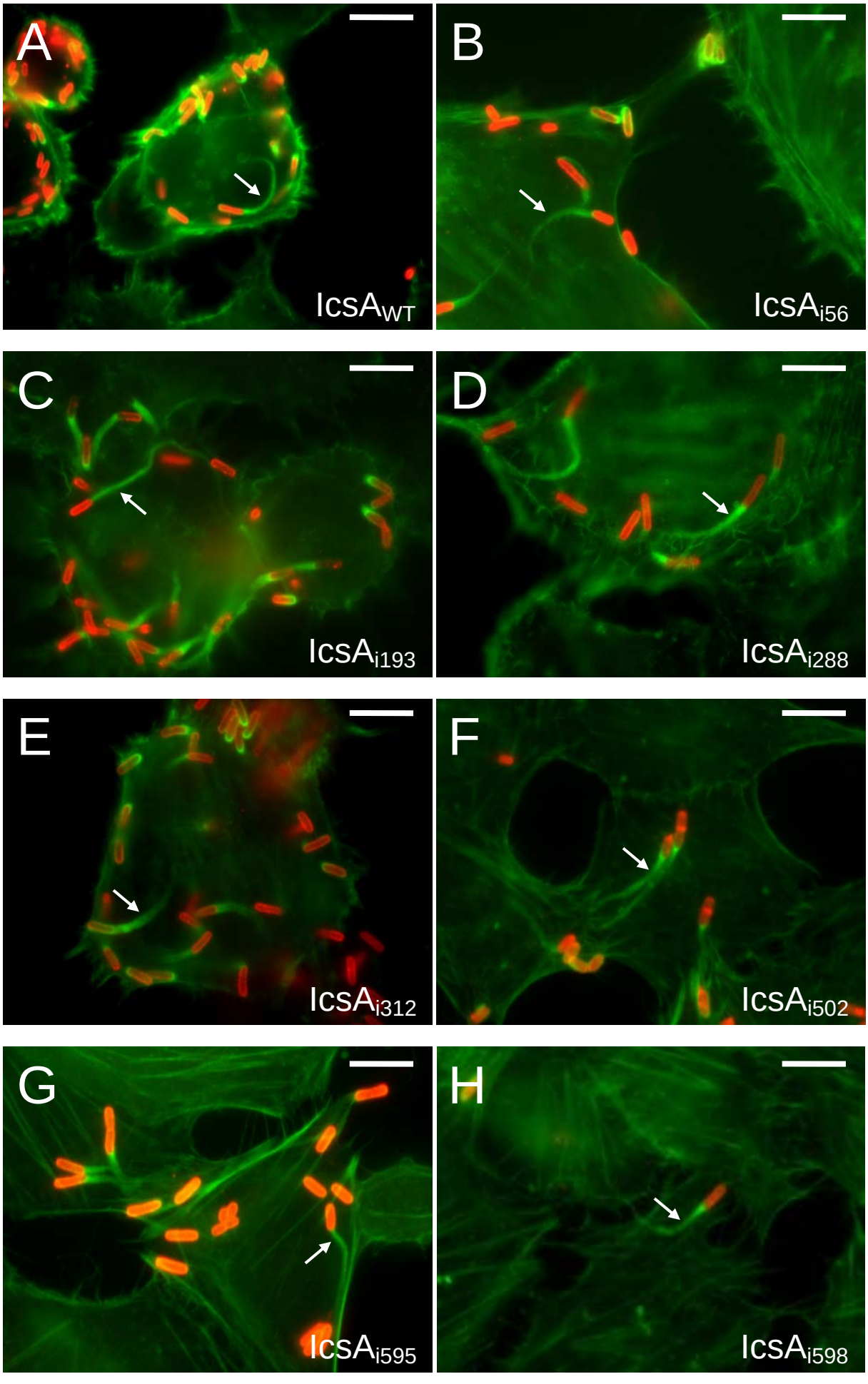
A
IcsA$_{WT}$
B
IcsA$_{i56}$
C
IcsA$_{i193}$
D
IcsA$_{i288}$
E
IcsA$_{i312}$
F
IcsA$_{i502}$
G
IcsA$_{i595}$
H
IcsA$_{i598}$

slight production defect) and F-actin comet tail formation was quantified. $IcsA_{i595}$ was not included in these studies as the low level production of this mutant would complicate interpretation of its phenotype. Quantification of F-actin comet tails is made difficult by the fact that their numbers naturally vary greatly between cells. Therefore the quantification method used by Frischknecht *et al*. (1999) was adopted in which the presence of a single actin tail within an infected cell was scored as positive. Interestingly, for all strains tested F-actin comet tail formation was found to occur at a frequency that was not statistically different to $IcsA_{WT}$, except for strains expressing $IcsA_{i288}$ (P <0.001) and $IcsA_{i502}$ (P <0.05) (Figure. 4.3).

The molecular basis for the severe intercellular spread defect of *S. flexneri ΔicsA* strains expressing $IcsA_{i193}$, $IcsA_{i288}$, $IcsA_{i312}$, or $IcsA_{i502}$; and the mild intercellular spread defect of $IcsA_{i56}$ and $IcsA_{i598}$ was unclear as these strains exhibited efficient F-actin comet tail formation and N-WASP recruitment (Sections 4.2 and 4.3). Whether the 10% reduction in the frequency of F-actin comet tail formation was enough to cause such a dramatic effect on cell-cell spread was unclear. However, for two of these strains, *S. flexneri* Δ*icsA* $IcsA_{i193}$ and *S. flexneri* Δ*icsA* $IcsA_{i288}$, two populations of F-actin comet tails were observed. One population of F-actin tails displayed WT morphology (Figure 4.2) whilst the other population appeared thicker, and more heavily labeled with FITC-phalloidin (refer to Figure 4.4). This phenotype has also been observed for R-LPS strains in our laboratory (Van Den Bosch *et al*., 1997; Van Den Bosch and Morona, unpublished data). Hence, the phenotypes of *S. flexneri* Δ*icsA* $IcsA_{i193}$ and *S. flexneri* Δ*icsA* $IcsA_{i288}$ were examined further in Section 4.3.

4.3 Investigation of the relationship between vinculin recruitment by $IcsA_i$ mutants and defective intercellular spreading

A *S. flexneri rmlD* strain is unable to synthesize Oag due to a block in dTDP-rhamnose synthesis (a precursor of the Oag repeat unit) and has R-LPS (Van Den Bosch *et* al.,

Figure 4.3 Frequency of F-actin-tail formation by *S. flexneri* Δ*icsA* expressing $IcsA_i$ mutants.

Log-phase cultures of bacteria were added to semi-confluent monolayers of HeLa cells grown on glass coverslips. After centrifugation monolayers were incubated for 60 min to allow invasion, then 90 min in medium containing 40 μg/mL gentamycin. Monolayers were washed, and formalin fixed. bacteria were host cell nuclei were labelled with DAPI and F-actin comet tails were labelled with FITC-phalloidin. The coverslips were mounted on glass microscope slides and examined with an Olympus IX-70 microscope. The frequency of F-actin tail formation was determined by observing the percentage of infected HeLa cells (n=100) that had at least one F-actin tail. Data represents mean ± standard error. * represents (P <0.05); *** represents (P <0.001), as determined by Student's unpaired two-tailed *t*-test. Data are representative of 3 independent experiments.

Column A: *S. flexneri* Δ*icsA* $IcsA_{WT}$ (RMA2090)

Column B: *S. flexneri* Δ*icsA* $IcsA_{i56}$ (KMRM133)

Column C: *S. flexneri* Δ*icsA* $IcsA_{i193}$ (KMRM143)

Column D: *S. flexneri* Δ*icsA* $IcsA_{i288}$ (KMRM123)

Column E: *S. flexneri* Δ*icsA* $IcsA_{i312}$ (KMRM138)

Column F: *S. flexneri* Δ*icsA* $IcsA_{i502}$ (KMRM135)

Column G: *S. flexneri* Δ*icsA* $IcsA_{i598}$ (KMRM167)

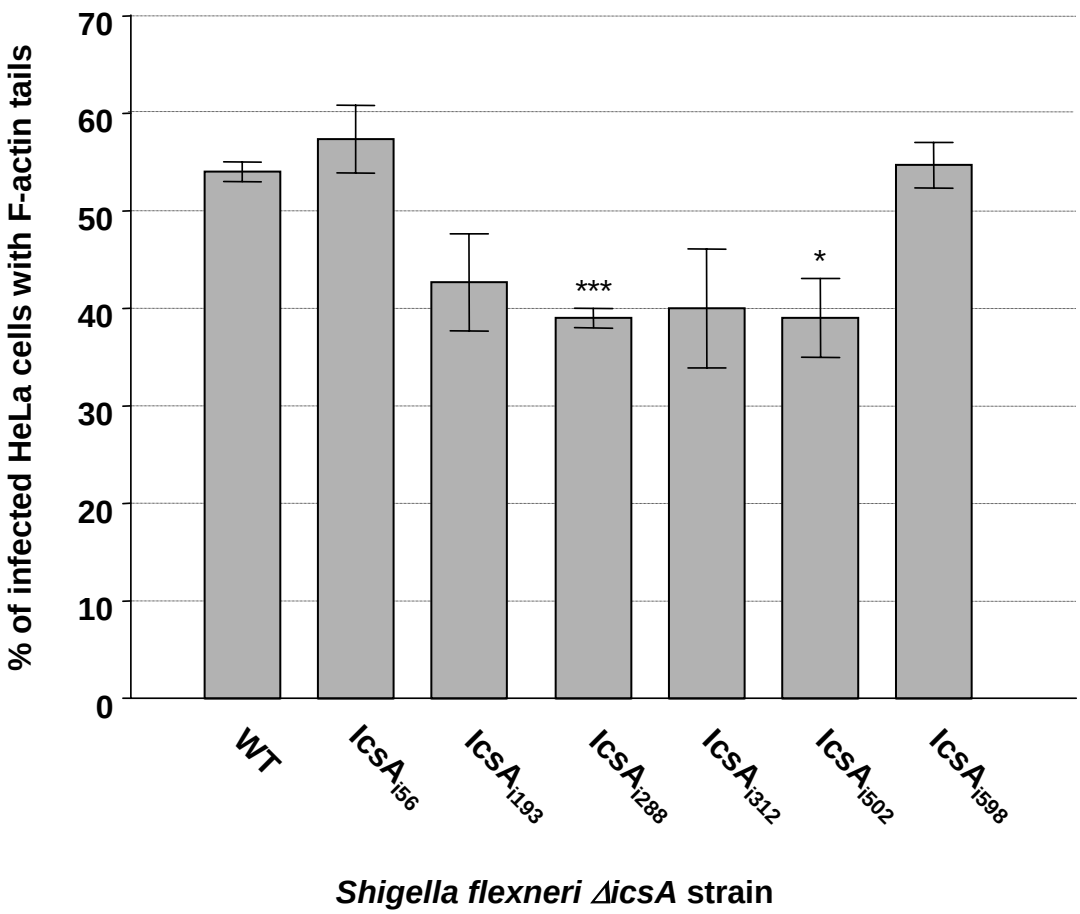
% of infected HeLa cells with F-actin tails
70
60
50
40
30
20
10
0
***
*
WT
IcsA i56
IcsA i193
IcsA i288
IcsA i312
IcsA i502
IcsA i598
Shigella flexneri ΔicsA strain

1997; Van Den Bosch and Morona, 2003). Studies in our laboratory have found that although *S. flexneri* Δ*icsA* Δ*rmlD* expressing $IcsA_{WT}$ from pIcsA (RMA2107; Table 2.1) produces F-actin comet tails of an altered morphology, it does so at a WT frequency and moves efficiently inside HeLa cells (Van Den Bosch and Morona, unpublished data). Interestingly, this strain also has an intercellular spread defect despite efficient F-actin comet tail formation. Although the basis of the intercellular spread defect of the R-LPS *S. flexneri* strain is still under investigation, increased recruitment of vinculin concomitant with thicker F-actin comet tails has been observed with this strain inside infected HeLa cells (Van Den Bosch and Morona, unpublished data). Hence the aim was to determine if *S. flexneri* Δ*icsA* Δ*rmlD* expressing $IcsA_{i193}$ or $IcsA_{i288}$ demonstrate this same phenotype.

4.3.1 Recruitment of endogenous vinculin by $IcsA_i$ mutants inside HeLa cells

HeLa cells were infected with *S. flexneri ΔicsA* expressing $IcsA_{i193}$, $IcsA_{i288}$ or $IcsA_{WT}$, and vinculin recruitment was visualised by staining with anti-vinculin antibody as described in Section 2.16.3. For *S. flexneri* Δ*icsA* $IcsA_{WT}$, vinculin was seen associated with the bacteria and throughout F-actin comet tails (Figure 4.4). For *S. flexneri* Δ*icsA* expressing either $IcsA_{i193}$ or $IcsA_{i288}$, although some intracellular bacteria exhibited WT vinculin recruitment others exhibited increased vinculin recruitment concomitant with thicker F-actin comet tails (Figure 4.4; Table 4.2).

4.3.2 Binding of vinculin by $IcsA_i$ mutants in *in vitro* pull-down assays with sheep brain extracts

As it was difficult to quantify vinculin recruitment by IF microscopy, and in order to obtain more quantitative data on vinculin recruitment, *S. flexneri* Δ*icsA* Δ*rmlD* expressing $IcsA_{WT}$, *S. flexneri* Δ*icsA* expressing $IcsA_{WT}$, $IcsA_{i193}$ or $IcsA_{i288}$ were used in pull-down

Figure 4.4 Vinculin recruitment by *S. flexneri* Δ*icsA* expressing $IcsA_{i193}$ or $IcsA_{i288}$

Log-phase cultures of bacteria were added to semi-confluent monolayers of HeLa cells grown on glass coverslips. After centrifugation monolayers were incubated for 60 min to allow invasion, then 90 min in medium containing 40 μg/mL gentamycin. Monolayers were washed, formalin fixed, permeabilised with 0.1% Triton X-100 in PBS, and blocked with 10% FCS in PBS. Bacteria were labelled with dapi (blue), vinculin was labelled with anti-vinculin and Alexa 594-conjugated donkey anti-mouse antibodies (red), and F-actin was labelled with FITC-phalloidin (green). The coverslips were mounted on glass microscope slides and examined with an Olympus IX-70 microscope with phase-contrast optics using 100x oil immersion objective. DAPI, Alexa 594, FITC-phalloidin and images were false colour merged using Metamorph (Version 6.3r7, Molecular devices). Arrows indicate F-actin tail formation. Strains were assessed in 3 independent experiments. Scale bars indicate 5 μm.

Panel A-E: *S. flexneri* Δ*icsA* $IcsA_{WT}$ (RMA2090)

Panel F-J: *S. flexneri* Δ*icsA* $IcsA_{i193}$ (KMRM143)

Panel K-O: *S. flexneri* Δ*icsA* $IcsA_{i288}$ (KMRM123)

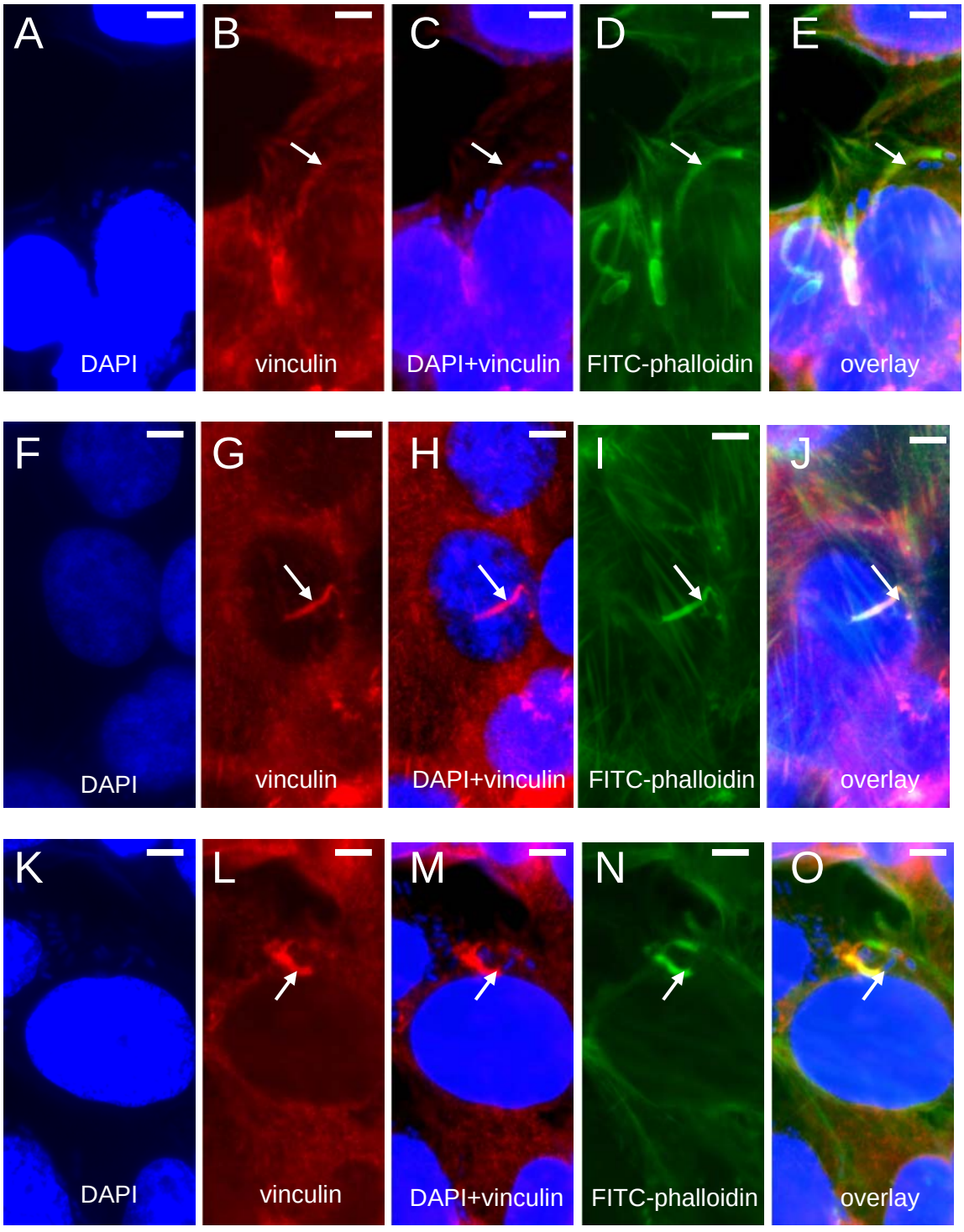
A
DAPI
B
vinculin
C
DAPI+vinculin
D
FITC-phalloidin
E
overlay
F
DAPI
G
vinculin
H
DAPI+vinculin
I
FITC-phalloidin
J
overlay
K
DAPI
L
vinculin
M
DAPI+vinculin
N
FITC-phalloidin
O
overlay

Table 4.2 -Vinculin recruitment by *S. flexneri ΔicsA* expressing $IcsA_{i193}$ or $IcsA_{i193}$

$IcsA_i$ mutant	vinculin recruitment[a]
$IcsA_{WT}$	+
$IcsA_{i193}$	+ and ++ [b]
$IcsA_{i288}$	+ and ++ [b]

[a] (++) Increased levels of vinculin associated with F-actin comet tails compared to $IcsA_{WT}$; (+) WT vinculin recruitment.

[b] Two populations of F-actin comet tails were observed: F-actin comet tails with WT vinculin recruitment; and F-actin comet tails with increased vinculin recruitment.

N.B. This data is based on qualitative observation of *S. flexneri* Δ*icsA* (RMA2041) expressing $IcsA_i$ mutants in infected HeLa cells.

experiments using sheep brain extract according to Section 2.17. These experiments involved incubating log-phase cultures of these strains with sheep brain extract (containing endogenous vinculin) under conditions that support actin polymerisation and F-actin comet tail formation. After a series of low stringency wash-steps, whole-cell lysates (Section 2.12.1) were prepared for SDS-PAGE and Western immunoblotting with anti-vinculin antibody (Sections 2.12.4 and Sections 2.12.6). Whilst vinculin was pulled-down with *S. flexneri* Δ*icsA* Δ*rmlD* $IcsA_{WT}$ (Figure 4.5, Lane 1) it could not be detected associated with *S. flexneri* Δ*icsA* expressing $IcsA_{WT}$, $IcsA_{i193}$ or $IcsA_{i288}$ (Figure 4.5, Lanes 2-4). This suggests that the phenotype of the R-LPS *S. flexneri* strain differs from the *S. flexneri* Δ*icsA* mutants expressing $IcsA_{i193}$ or $IcsA_{i288}$. As vinculin binding by *S. flexneri* Δ*icsA* expressing $IcsA_{WT}$, $IcsA_{i193}$ or $IcsA_{i288}$ (under the assay conditions) was below the level of detection, it was not possible to compare the relative levels of vinculin binding by these strains.

4.4 N-WASP Recruitment by $IcsA_i$ mutants inside HeLa cells

Since N-WASP is essential for *Shigella* F-actin comet tail formation and ABM, it was hypothesised that the inability (or reduced ability) of some of the $IcsA_i$ mutants to form F-actin comet tails and spread from cell-cell when expressed in *Shigella* was due to an inability or (reduced ability) to recruit N-WASP as a result of their linker-insertions. Correspondingly, strains expressing $IcsA_i$ mutants that were unable to form F-actin comet tails and spread intercellularly, and strains expressing $IcsA_i$ mutants that formed tails at a very low frequency and were unable to spread from cell-to-cell, were assessed for their ability to recruit N-WASP inside HeLa cells. Additionally, since the role of N-WASP in protrusion formation and intercellular spread (independent of its role in ABM) has not been investigated, strains expressing $IcsA_{i56}$, $IcsA_{i193}$ and $IcsA_{i288}$, $IcsA_{i312}$, $IcsA_{i502}$ $IcsA_{i595}$ and $IcsA_{i598}$ that readily formed F-actin comet tails but were defective in intercellular spread were also investigated. For these strains, it was hypothesised that although N-WASP recruitment and activation was

Figure 4.5 Analysis of vinculin binding by *S. flexneri* Δ*icsA* expressing $IcsA_{i193}$ or $IcsA_{i288}$ by *in vitro* pull-down assays.

S. flexneri strains to be examined were grown to log-phase in LB at 37°C and incubated with sheep brain extract at 37°C for 30 min under conditions to support F-actin comet tail formation. Bacteria were pelleted by centrifugation and after a series of low stringency wash-steps, whole-cell lysates were prepared for SDS-PAGE and Western immunoblotting analysis with anti-vinculin antibody. Samples represent the equivalent of 5×10^8 bacterial cells.

Lane 1: *S. flexneri* Δ*rmlD* Δ*icsA* $IcsA_{WT}$ (RMA2107)

Lane 2: *S. flexneri* Δ*icsA* $IcsA_{WT}$ (RMA2090)

Lane 3: *S. flexneri* Δ*icsA* $IcsA_{i193}$ (KMRM143)

Lane 4: *S. flexneri* Δ*icsA* $IcsA_{i288}$ (KMRM123)

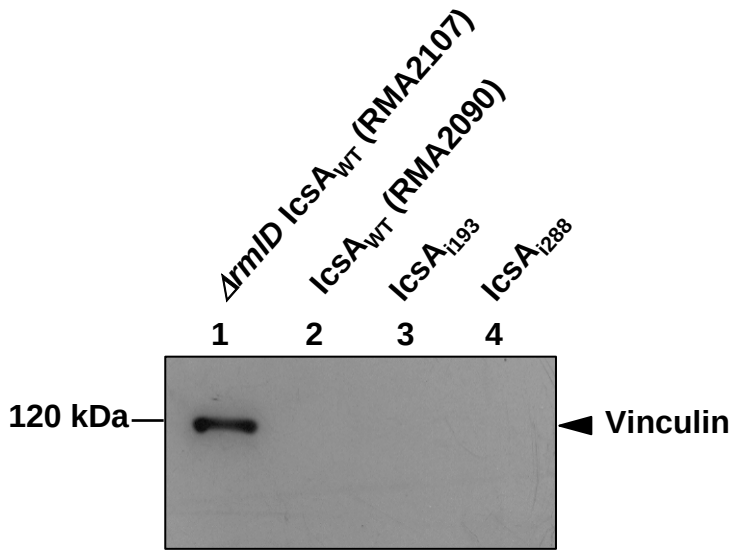
ΔrmlD IcsA$_{WT}$ (RMA2107)
IcsA$_{WT}$ (RMA2090)
IcsA$_{I193}$
IcsA$_{I288}$
1
2
3
4
120 kDa
Vinculin

sufficient to facilitate F-actin comet tail formation it might not be sufficient for intercellular spread (if indeed a role exists for N-WASP in this process). Accordingly, HeLa cells were infected with log-phase cultures of *S. flexneri* Δ*icsA* expressing different $IcsA_i$ proteins, and N-WASP recruitment was visualised by staining with anti-N-WASP antibody as described in Section 2.16.3.

Contrary to *S. flexneri* Δ*icsA* expressing $IcsA_{WT}$ that readily recruited N-WASP to intracellular bacteria in a polar fashion (Figure 4.6A-C), *S. flexneri* Δ*icsA* expressing $IcsA_{i185}$, $IcsA_{i219}$, $IcsA_{i226}$ $IcsA_{i230}$, $IcsA_{i244}$, $IcsA_{i248}$, $IcsA_{i268}$ and $IcsA_{i271}$, $IcsA_{i297}$, $IcsA_{i330a}$, $IcsA_{330b}$, $IcsA_{i342}$, $IcsA_{i346}$, $IcsA_{i381}$, $IcsA_{i532}$ and $IcsA_{i563}$ that were unable to form either F-actin comet tails (Table 4.1) or plaques were also unable to recruit N-WASP (Table 4.3). Additionally, N-WASP recruitment could not be detected for either *S. flexneri* Δ*icsA* $IcsA_{i228}$ that exhibited F-actin comet tail formation very rarely (Figure 4.1A; Table 4.3), or for *S. flexneri* Δ*icsA* $IcsA_{i346}$ that was unable to form F-actin comet tails but exhibited polar capping with F-actin (Figure 4.1C; Table 4.3).

S. flexneri Δ*icsA* expressing $IcsA_{i292}$ or $IcsA_{i633}$, which rarely exhibited F-actin comet tail formation (Table 4.1), were able to recruit N-WASP (Figure 4.6D-I; Table 4.3). *S. flexneri* Δ*icsA* expressing $IcsA_{i56}$, $IcsA_{i193}$, $IcsA_{i288}$, $IcsA_{i312}$, $IcsA_{i502}$ and $IcsA_{i595}$ that exhibited frequent F-actin comet tail formation (Table 4.1) but were unable to form plaques, were able to recruit N-WASP (Table 4.3).

Notably, $IcsA_i$ mutants were identified that were unable to recruit N-WASP despite possessing linker-insertions outside the proposed N-WASP binding region. This included mutants with linker-insertions within aa 330-381 ($IcsA_{i330a}$, $IcsA_{330b}$, $IcsA_{i342}$, $IcsA_{i346}$, $IcsA_{i381}$), a sub-region of the IcsB/Atg5 binding domain (aa 320-433); and mutants with

Figure 4.6 N-WASP recruitment by intracellular *S. flexneri* Δ*icsA* expressing $IcsA_{i292}$ or $IcsA_{i633}$.

Log-phase cultures of bacteria were added to semi-confluent monolayers of HeLa cells grown on glass coverslips. After centrifugation monolayers were incubated for 60 min to allow invasion, then 90 min in medium containing 40 µg/mL gentamycin. Monolayers were washed, formalin fixed, permeabilised with 0.1% Triton X-100 in PBS, and blocked with 10% FCS in PBS. Bacteria were labelled with DAPI (blue), and N-WASP was labelled with anti-N-WASP and Alex 594-conjugated donkey anti-rabbit antibodies (red). The coverslips were mounted on glass microscope slides and examined with an Olympus IX-70 microscope with phase-contrast optics using 100x oil immersion objective with a 1.5x enlarger. DAPI (**A**, **D**, **G**) and Alexa 594 (**B**, **E**, **H**) images were false colour merged (**C**, **F**, **I**) using Metamorph (Version 6.3r7, Molecular devices). Arrows indicate N-WASP recruitment. Strains were assessed in 3 independent experiments. Scale bars indicate 10 µm.

Panel A-C: *S. flexneri* Δ*icsA* $IcsA_{WT}$ (RMA2090)

Panel D-F: *S. flexneri* Δ*icsA* $IcsA_{i292}$ (KMRM104)

Panel G-I: *S. flexneri* Δ*icsA* $IcsA_{i633}$ (RMA109)

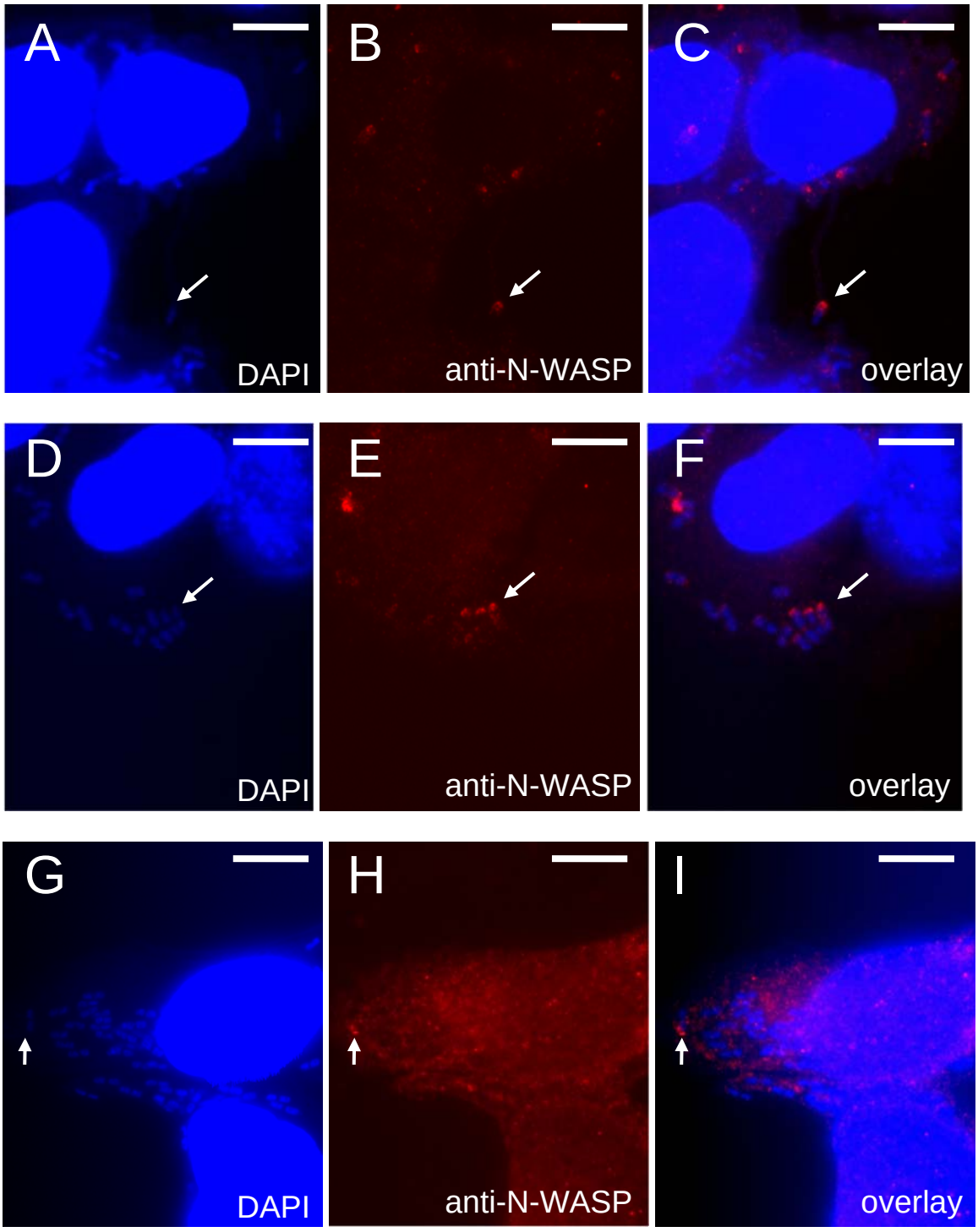
A
DAPI
B
anti-N-WASP
C
overlay
D
DAPI
E
anti-N-WASP
F
overlay
G
DAPI
H
anti-N-WASP
I
overlay

Table 4.3 – N-WASP recruitment by *S. flexneri* Δ*icsA* (RMA2041) expressing $IcsA_i$ mutants.

$IcsA_i$ mutant	N-WASP Recruitment[a]	$IcsA_i$ mutant	N-WASP Recruitment[a]
$IcsA_{WT}$	++	$IcsA_{i312}$	++
$IcsA_{i56}$	++	$IcsA_{i330a}$	-
$IcsA_{i185}$	-	$IcsA_{i330b}$	-
$IcsA_{i193}$	++	$IcsA_{i342}$	-
$IcsA_{i219}$	-	$IcsA_{i346}$	-
$IcsA_{i226}$	-	$IcsA_{i381}$	-
$IcsA_{i228}$	-	$IcsA_{i502}$	++
$IcsA_{i230}$	-	$IcsA_{i532}$	-
$IcsA_{i244}$	-	$IcsA_{i563}$	-
$IcsA_{i248}$	-	$IcsA_{i595}$	++
$IcsA_{i268}$	-	$IcsA_{i598}$	++
$IcsA_{i271}$	-	$IcsA_{i633}$	+
$IcsA_{i288}$	++	$IcsA_{i643}$	-
$IcsA_{i292}$	+	$IcsA_{i677}$	-
$IcsA_{i297}$	-	$IcsA_{i716}$	-

[a] ++,+,- indicate relative recruitment of N-WASP inside infected HeLa cells as determined by IF labelling of endogenous N-WASP.
(++) frequent recruitment; (+) recruitment observed rarely/feint detection; (-) not detected. N.B. This data is based on qualitative observation of *S. flexneri* Δ*icsA* (RMA2041) expressing $IcsA_i$ mutants in infected HeLa cells

.

linker-insertions within aa 502-730 (IcsA$_{i532}$, IcsA$_{i563}$, IcsA$_{i643}$, IcsA$_{i677}$, IcsA$_{i716}$), which includes polar localisation region #2 (a 507-620) and the putative auto-chaperone region (aa 634-735).

4.5 Effect of LPS-Oag on F-actin comet tail formation and N-WASP recruitment by *S. flexneri* expressing IcsA$_i$ mutants

Given that LPS Oag has previously been shown to mask IcsA function (Morona *et al*., 2003; Morona and Van Den Bosch, 2003b), it was of interest to determine if mutants that were unable to recruit N-WASP in a S-LPS background could do so in a R-LPS background, *S. flexneri* Δ*icsA* Δ*rmlD* (RMA2043). Furthermore, it was of interest to determine if expression of IcsA$_i$ mutants in this background would restore the ability of these IcsA$_i$ mutants to form F-actin comet tails. Hence, plasmids encoding the 16 IcsA$_i$ mutants listed in Table 4.4 were transformed into *S. flexneri* Δ*icsA* Δ*rmlD* strain (RMA2043) by electroporation (Section 2.10.4). For all these IcsA$_i$ mutant proteins, N-WASP recruitment could not be detected when these proteins were expressed in the S-LPS *S. flexneri ΔicsA* strain (RMA2041) within infected HeLa cells (Section 4.3).

4.5.1 F-actin tail formation by *S. flexneri* Δ*icsA* Δ*rmlD* expressing IcsA$_i$ mutants

HeLa cells were infected with log-phase cultures of the rough-LPS strains created in the previous section (Section 4.5) and analysed by IF microscopy according to Section 2.16.3. *S. flexneri* Δ*icsA* Δ*rmlD* strains expressing IcsA$_{i219,}$ IcsA$_{i244}$, IcsA$_{i248}$, IcsA$_{i268}$, IcsA$_{i271}$, IcsA$_{i297}$, IcsA$_{i330a}$, IcsA$_{i330b}$, IcsA$_{i342}$, IcsA$_{i346}$ and IcsA$_{i381}$ were unable to form F-actin comet tails (Table 4.4). Remarkably, R-LPS *S. flexneri* Δ*icsA* Δ*rmlD* strains expressing IcsA$_{i185}$, IcsA$_{i226}$, IcsA$_{i532}$ and IcsA$_{i563}$ that were unable to recruit N-WASP and form F-actin comet tails when expressed in S-LPS *S. flexneri* Δ*icsA* (RMA2041) strains, were able to form F-actin

Table 4.4 – Comparison of F-actin comet tail and N-WASP recruitment by S-LPS *S. flexneri ΔicsA* expressing $IcsA_i$ mutants and R-LPS *S. flexneri* Δ*icsA* Δ*rmlD* expressing $IcsA_i$ mutants

$IcsA_i$ mutant	*S. flexneri* Δ*icsA* S-LPS background[a]		*S. flexneri* Δ*icsA* Δ*rmlD* R-LPS background	
	F-actin tail formation[b]	N-WASP recruitment[c]	F-actin tail formation[b]	N-WASP recruitment[c]
$IcsA_{WT}$	++	++	++	++
$IcsA_{i185}$	-	-	+	+
$IcsA_{i219}$	-	-	-	-
$IcsA_{i226}$	-	-	+	+
$IcsA_{i228}$	+	-	+	+
$IcsA_{i244}$	-	-	-	-
$IcsA_{i248}$	-	-	-	-
$IcsA_{i268}$	-	-	-	-
$IcsA_{i271}$	-	-	-	+/-
$IcsA_{i297}$	-	-	-	-
$IcsA_{i330a}$	-	-	-	-
$IcsA_{i330b}$	-	-	-	-
$IcsA_{i342}$	-	-	-	-
$IcsA_{i346}$	-	-	-	-
$IcsA_{i381}$	-	-	-	-
$IcsA_{i532}$	-	-	+	+
$IcsA_{i563}$	-	-	+	+

[a] Data is from Tables 4.1 and 4.3.

[b] (++) frequent F-actin comet tail formation; (+) F-actin comet tail formation observed rarely; (-) not detected.

[c] (++) frequent N-WASP recruitment; (+) recruitment observed rarely; (+/-) feint detection; (-) not detected.

N.B. This data is based on qualitative observation of either *S. flexneri* Δ*icsA* (RMA2041) or *S. flexneri* Δ*icsA* Δ*rmlD* (RMA2043) expressing $IcsA_i$ mutants in infected HeLa cells.

comet tails (Table 4.4; Figure 4.7), albeit at a low frequency compared to *S. flexneri* Δ*icsA* Δ*rmlD* expressing $IcsA_{WT}$ (RMA2107) (Figure 4.7). For $IcsA_{i228}$, N-WASP recruitment could not be detected when this mutant was expressed in S-LPS *S. flexneri* Δ*icsA* (RMA2041) despite this strain occasionally forming F-actin comet tails (Table 4.4). However, when $IcsA_{i228}$ was expressed in the R-LPS strain *S. flexneri* Δ*icsA* Δ*rmlD*, F-actin comet tails formation occurred more frequently (albeit still at a low frequency compared to *S. flexneri* Δ*icsA* Δ*rmlD* expressing $IcsA_{WT}$) (Table 4.4).

4.5.2 N-WASP recruitment by *S. flexneri* Δ*icsA* Δ*rmlD* expressing $IcsA_i$ mutants

Many of the $IcsA_i$ mutants were still unable to induce F-actin comet tail formation when expressed in a R-LPS background and it was of interest to determine if these mutants exhibited any N-WASP recruitment. Additionally, it was necessary to verify that $IcsA_i$ proteins (identified in the previous section that were able to induce F-actin comet tail formation in a R-LPS background) were able to recruit N-WASP. Therefore, HeLa cells were infected with log-phase cultures of *S. flexneri* Δ*icsA* Δ*rmlD* expressing different $IcsA_i$ proteins. N-WASP recruitment was visualised by staining with anti-N-WASP antibody as described in Section 2.16.3.

S. flexneri Δ*icsA* Δ*rmlD* expressing $IcsA_{i185}$, $IcsA_{i226}$, $IcsA_{i228}$, $IcsA_{i532}$ or $IcsA_{i563}$ that were able to form F-actin comet tails were also able to recruit N-WASP (Figure 4.8; Table 4.4). Additionally, for *S. flexneri* Δ*icsA* Δ*rmlD* expressing $IcsA_{i271}$, N-WASP recruitment could be detected albeit faintly (Figure 4.8; Table 4.4). N-WASP recruitment could not be detected for the other strains that were investigated (Table 4.4).

In the previous chapter (Section 3.6), *in situ*, limited proteolysis with trypsin was performed on the twenty-two $IcsA_i$ mutants that were negative for plaque formation. The aim

Figure 4.7 F-actin comet tail formation by intracellular R-LPS *S. flexneri* Δ*icsA* Δ*rmlD* expressing IcsA$_i$ mutants

Log-phase cultures of bacteria were added to semi-confluent monolayers of HeLa cells grown on glass coverslips. After centrifugation monolayers were incubated for 60 min to allow invasion, then 90 min in medium containing 40 µg/mL gentamycin. Monolayers were washed, and formalin fixed. Bacteria were labelled with DAPI (blue) and F-actin was labelled with FITC-phalloidin (green). The coverslips were mounted on glass microscope slides and examined with an Olympus IX-70 microscope with phase-contrast optics using 100x oil immersion objective with a 1.5x enlarger. DAPI and FITC-phalloidin images were false colour merged using Metamorph (Version 6.3r7, Molecular devices). Arrows indicate F-actin tail formation. Strains were assessed in 3 independent experiments. Scale bars indicate 10 µm.

Panel A: *S. flexneri* Δ*icsA* Δ*rmlD* IcsA$_{WT}$ (RMA2107)

Panel B: *S. flexneri* Δ*icsA* Δ*rmlD* IcsA$_{i185}$ (KMRM149)

Panel C: *S. flexneri* Δ*icsA* Δ*rmlD* IcsA$_{i226}$ (KMRM145)

Panel D: *S. flexneri* Δ*icsA* Δ*rmlD* IcsA$_{i228}$ (KMRM148)

Panel E: *S. flexneri* Δ*icsA* Δ*rmlD* IcsA$_{i532}$ (KMRM157)

Panel F: *S. flexneri* Δ*icsA* Δ*rmlD* IcsA$_{i563}$ (KMRM280)

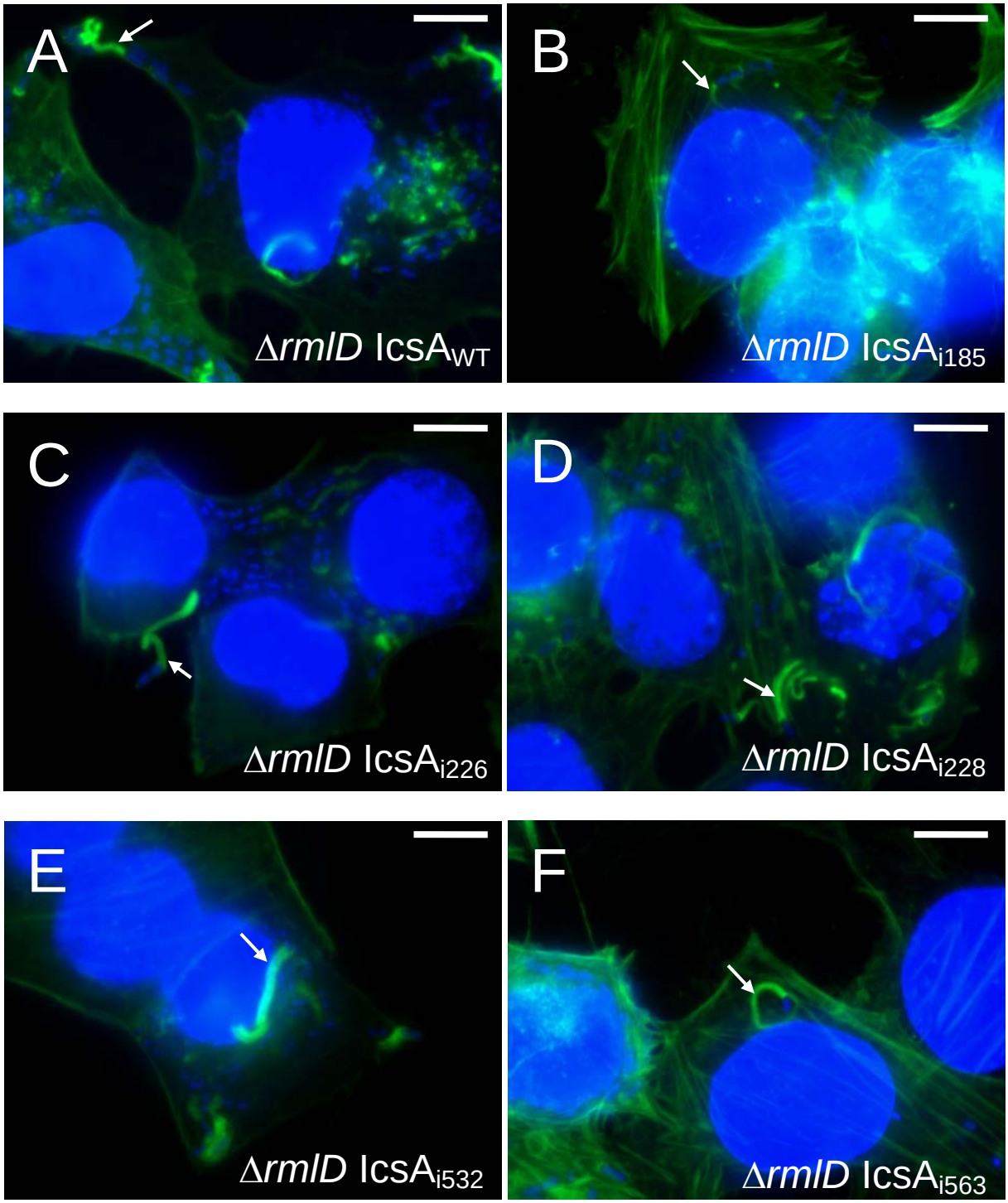
A
ΔrmlD IcsA$_{WT}$
B
ΔrmlD IcsA$_{i185}$
C
ΔrmlD IcsA$_{i226}$
D
ΔrmlD IcsA$_{i228}$
E
ΔrmlD IcsA$_{i532}$
F
ΔrmlD IcsA$_{i563}$

Figure 4.8 N-WASP recruitment by intracellular R-LPS *S. flexneri* Δ*icsA* Δ*rmlD* strains expressing $IcsA_i$ mutants.

Log-phase cultures of bacteria were added to semi-confluent monolayers of HeLa cells grown on glass coverslips. After centrifugation monolayers were incubated for 60 min to allow invasion, then 90 min in medium containing 40 µg/mL gentamycin. Monolayers were washed, formalin fixed, permeabilised with 0.1% Triton X-100 in PBS, and blocked with 10% FCS in PBS. Bacteria were labelled with DAPI (blue), and N-WASP was labelled with anti-N-WASP and Alex 594-conjugated donkey anti-rabbit antibodies (red). The coverslips were mounted on glass microscope slides and examined with an Olympus IX-70 microscope with phase-contrast optics using 100x oil immersion objective with a 1.5x enlarger. DAPI and Alexa 594 images were false colour merged using Metamorph (Version 6.3r7, Molecular devices). Arrows indicate N-WASP recruitment. Strains were assessed in 3 independent experiments. Scale bars indicate 10 µm.

Panel A: *S. flexneri* Δ*icsA* Δ*rmlD* $IcsA_{WT}$ (RMA2107)

Panel B: *S. flexneri* Δ*icsA* Δ*rmlD* $IcsA_{i185}$ (KMRM149)

Panel C: *S. flexneri* Δ*icsA* Δ*rmlD* $IcsA_{i226}$ (KMRM145)

Panel D: *S. flexneri* Δ*icsA* Δ*rmlD* $IcsA_{i228}$ (KMRM148)

Panel E: *S. flexneri* Δ*icsA* Δ*rmlD* $IcsA_{i271}$ (KMRM156)

Panel F: *S. flexneri* Δ*icsA* Δ*rmlD* $IcsA_{i532}$ (KMRM157)

Panel G: *S. flexneri* Δ*icsA* Δ*rmlD* $IcsA_{i563}$ (KMRM280)

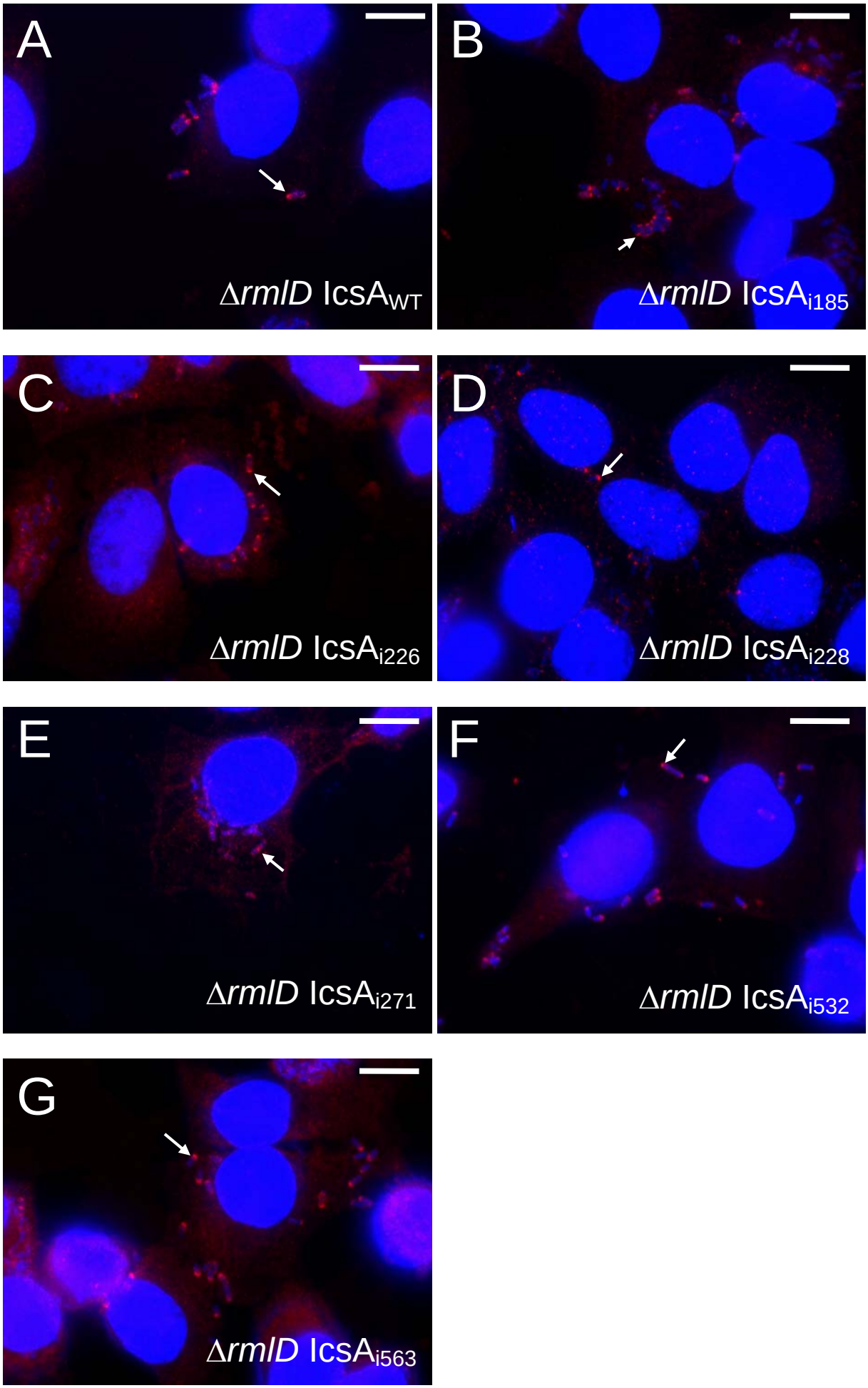
A
ΔrmlD IcsA$_{WT}$
B
ΔrmlD IcsA$_{i185}$
C
ΔrmlD IcsA$_{i226}$
D
ΔrmlD IcsA$_{i228}$
E
ΔrmlD IcsA$_{i271}$
F
ΔrmlD IcsA$_{i532}$
G
ΔrmlD IcsA$_{i563}$

of that experiment was to investigate if their lack of function was perhaps due to deleterious structural changes in the proteins resultant from their linker-insertions. Studies conducted in this chapter have examined the ability of these $IcsA_i$ mutants to interact with N-WASP and induce F-actin comet tail formation when expressed by either S-LPS *S. flexneri* Δ*icsA* or R-LPS *S. flexneri* Δ*icsA* Δ*rmlD* strains. Thirteen of the twenty-two $IcsA_i$ mutants analysed by limited proteolysis exhibited a WT proteolysis profile (Table 3.6). Eight of these thirteen mutants were unable to recruit N-WASP and form F-actin comet tails (Tables 4.1, 4.3 and 4.4), and the remaining five mutants exhibited a low level of activity. The other nine of the twenty-two $IcsA_i$ mutants analysed by limited proteolysis exhibited an altered proteolysis profile (Table 3.6). Six of these nine mutants were unable to recruit N-WASP and form F-actin comet tails and the remaining three mutants exhibited a low level of activity (Tables 4.1, 4.3 and 4.4). Notably, an altered proteolysis profile did not correlate with a complete lack of function. Overall, there was no clear correlation between the proteolysis profile and the activity of the mutant proteins.

4.5.3 F-actin tail formation and N-WASP recruitment by *S. flexneri* Δ*icsA* Δ*rmlD* expressing $IcsA_{\Delta 103\text{-}320}$, $IcsA_{\Delta 508\text{-}730}$ and $IcsA_{\Delta 103\text{-}507}$

The identification of $IcsA_i$ proteins that were able to recruit N-WASP and induce F-actin comet tails in a R-LPS background but not in the presence of S-LPS was of great interest. Based on this finding it was hypothesised that the IcsA deletion mutants reported by Suzuki *et al*. (1996, 1998, 2002) may also be subject to masking by Oag, perhaps to an even greater extent as these IcsA constructs possessed large deletions ranging in size from 188 aa to 404 aa. Suzuki *et al.*(1996) reported that $IcsA_{\Delta 103\text{-}320}$, $IcsA_{\Delta 508\text{-}730}$ and $IcsA_{\Delta 103\text{-}507}$ were unable to induce F-actin comet tail formation when expressed by a S-LPS *S. flexneri* Δ*icsA* strain, although $IcsA_{\Delta 508\text{-}730}$ did induce F-actin accumulation. This latter mutant was also reported to recruit N-WASP (Suzuki *et al*. 1998, 2002) whilst the others did not, although

data supporting these observations was not shown. Hence, plasmids obtained from Suzuki *et al.* encoding $IcsA_{\Delta 103\text{-}320}$ (pD10-*virG*1; Table 2.2), $IcsA_{\Delta 508\text{-}730}$ (pD10-*virG*3; Table 2.2) and $IcsA_{\Delta 103\text{-}507}$ (pD10-*virG*4; Table 2.2) were transformed were into the R-LPS strain *S. flexneri* Δ*icsA* Δ*rmlD* strain (RMA2043) by electroporation (Section 2.10.4). HeLa cells were infected with log-phase cultures of the resulting strains, and F-actin comet tail formation and N-WASP recruitment were visualised by staining with FITC-phalloidin and anti-N-WASP respectively (Section 2.16.3). As reported previously for when these proteins were expressed in a S-LPS background, none of the $IcsA_{\Delta}$ proteins were able induce F-actin tail formation when expressed in a R-LPS background (Figure 4.9). Additionally, Suzuki *et al.* (1996) reported that an S-LPS *S. flexneri* expressing $IcsA_{\Delta 508\text{-}730}$ (pD10-*virG*3) although unable to form F-actin comet tails was able to induce circumferential accumulation of F-actin Suzuki *et al*. (1996). A similar F-actin accumulation was observed when this IcsA construct was expressed in an R-LPS background (Figure 4.9). Suzuki *et al*. (1998) reported that S-LPS *S. flexneri* expressing $IcsA_{\Delta 508\text{-}730}$ was the only IcsA construct able to recruit N-WASP. However, all three constructs ($IcsA_{\Delta 103\text{-}320}$, $IcsA_{\Delta 508\text{-}730}$ and $IcsA_{\Delta 103\text{-}507}$) exhibited a low level of N-WASP recruitment when expressed in a R-LPS *S. flexneri* strain (Figure 4.10; Table 4.5).

4.6 Summary

In the previous chapter, 47 $IcsA_i$ mutants were created for structure-function studies (Section 3.2). Eighteen of these $IcsA_i$ mutants induced WT intercellular spreading when expressed in *S. flexneri* Δ*icsA* (Figure 4.11; Table 4.6). This chapter describes the characterisation of the intracellular behaviour of the remaining twenty-nine strains of *S. flexneri* expressing $IcsA_i$ mutants that demonstrated aberrant intercellular spreading. Nineteen of these twenty-nine strains were unable to either form F-actin comet tails or recruit N-WASP (Figure 4.11; Table 4.6). Remarkably, linker-insertions outside of the GRR region (within aa 330-381 and 532-563) were shown to disrupt N-WASP recruitment (Figure 4.11; Table 4.6).

Figure 4.9. F-actin comet tail formation by intracellular R-LPS *S. flexneri* Δ*icsA* Δ*rmlD* expressing $IcsA_{\Delta}$ mutants

Log-phase cultures of bacteria were added to semi-confluent monolayers of HeLa cells grown on glass coverslips. After centrifugation monolayers were incubated for 60 min to allow invasion, then 90 min in medium containing 40 µg/mL gentamycin. Monolayers were washed, and formalin fixed. Bacteria were labelled with DAPI (blue) and F-actin was labelled with FITC-phalloidin (green). The coverslips were mounted on glass microscope slides and examined with an Olympus IX-70 microscope with phase-contrast optics using 100x oil immersion objective with a 1.5x enlarger. DAPI and FITC-phalloidin images were false colour merged using Metamorph (Version 6.3r7, Molecular devices). Arrows indicate F-actin tail formation. Strains were assessed in 3 independent experiments. Scale bars indicate 10 µm.

Panel A: *S. flexneri* Δ*icsA* Δ*rmlD* $IcsA_{WT}$ (RMA2107)

Panel B: *S. flexneri* Δ*icsA* Δ*rmlD* $IcsA_{\Delta 103\text{-}320}$ (KMRM195)

Panel C: *S. flexneri* Δ*icsA* Δ*rmlD* $IcsA_{\Delta 507\text{-}730}$ (KMRM197)

Panel D: *S. flexneri* Δ*icsA* Δ*rmlD* $IcsA_{\Delta 103\text{-}507}$ (KMRM198)

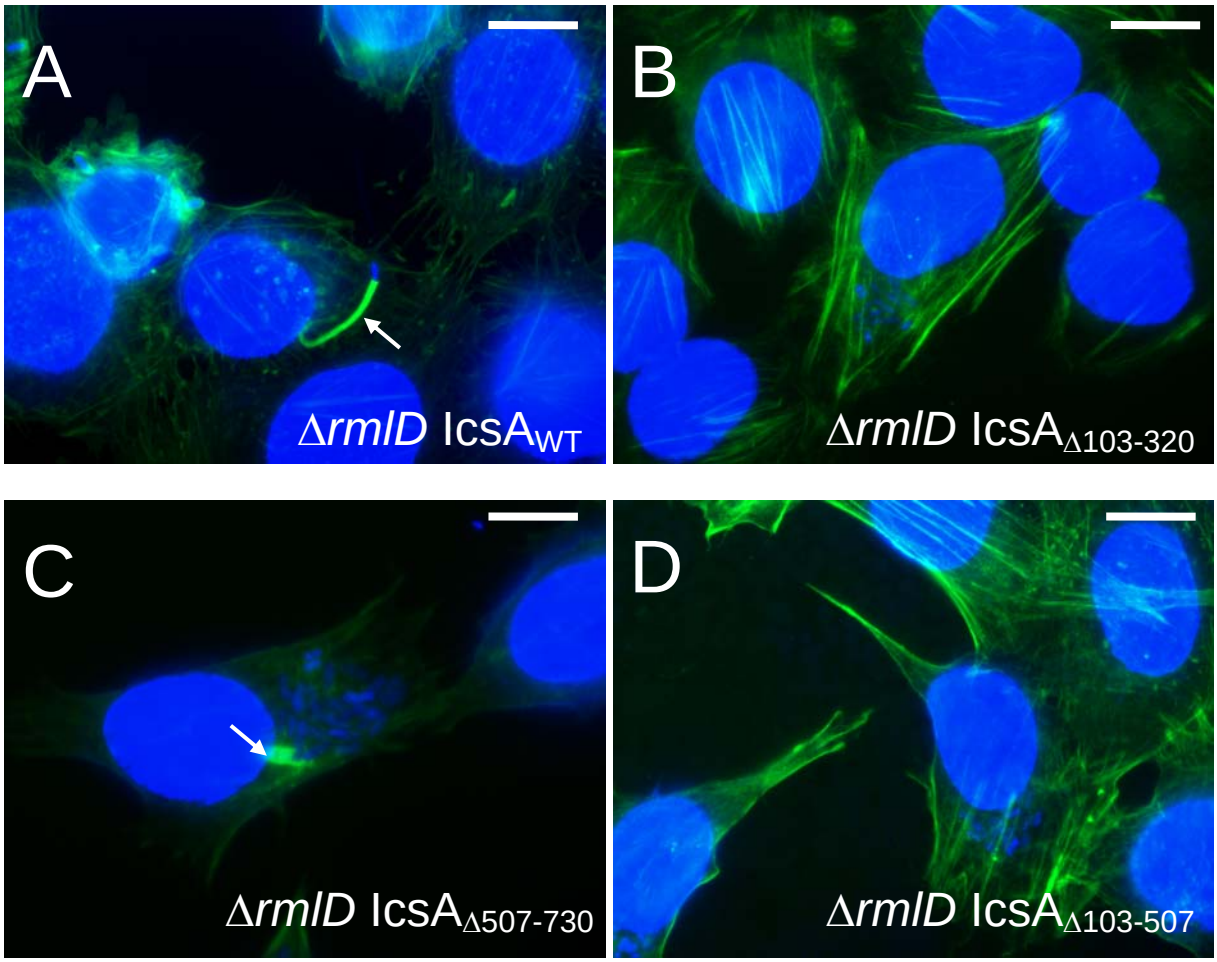
A
ΔrmlD IcsA$_{WT}$
B
ΔrmlD IcsA$_{Δ103-320}$
C
ΔrmlD IcsA$_{Δ507-730}$
D
ΔrmlD IcsA$_{Δ103-507}$

Figure 4.10 N-WASP recruitment by intracellular R-LPS *S. flexneri* Δ*icsA* Δ*rmlD* expressing $IcsA_{\Delta}$ mutants.

Log-phase cultures of bacteria were added to semi-confluent monolayers of HeLa cells grown on glass coverslips. After centrifugation monolayers were incubated for 60 min to allow invasion, then 90 min in medium containing 40 µg/mL gentamycin. Monolayers were washed, formalin fixed, permeabilised with 0.1% Triton X-100 in PBS, and blocked with 10% FCS in PBS. Bacteria were labelled with DAPI (blue), and N-WASP was labelled with anti-N-WASP and Alex 594-conjugated donkey anti-rabbit antibodies (red). The coverslips were mounted on glass microscope slides and examined with an Olympus IX-70 microscope with phase-contrast optics using 100x oil immersion objective. DAPI (**A**, **D**, **G**, **J**, **M**) and Alexa-594 (**B**, **E**, **H**, **K**, **N**) images were false colour merged (**C**, **F**, **H**, **L**, **O**) using Metamorph (Version 6.3r7, Molecular devices). Arrows indicate N-WASP recruitment. Strains were assessed in 3 independent experiments. Scale bars indicate 10 µm.

Panel A-C: *S. flexneri* Δ*icsA* Δ*rmlD* $IcsA_{WT}$ (RMA2107)

Panel D-F: *S. flexneri* Δ*icsA* Δ*rmlD* $IcsA_{\Delta 103\text{-}320}$ (KMRM195)

Panel G-I: *S. flexneri* Δ*icsA* Δ*rmlD* $IcsA_{\Delta 507\text{-}730}$ (KMRM197)

Panel J-L: *S. flexneri* Δ*icsA* Δ*rmlD* $IcsA_{\Delta 103\text{-}507}$ (KMRM198)

Panel M-O: *S. flexneri* Δ*icsA* Δ*rmlD* (RMA2043)

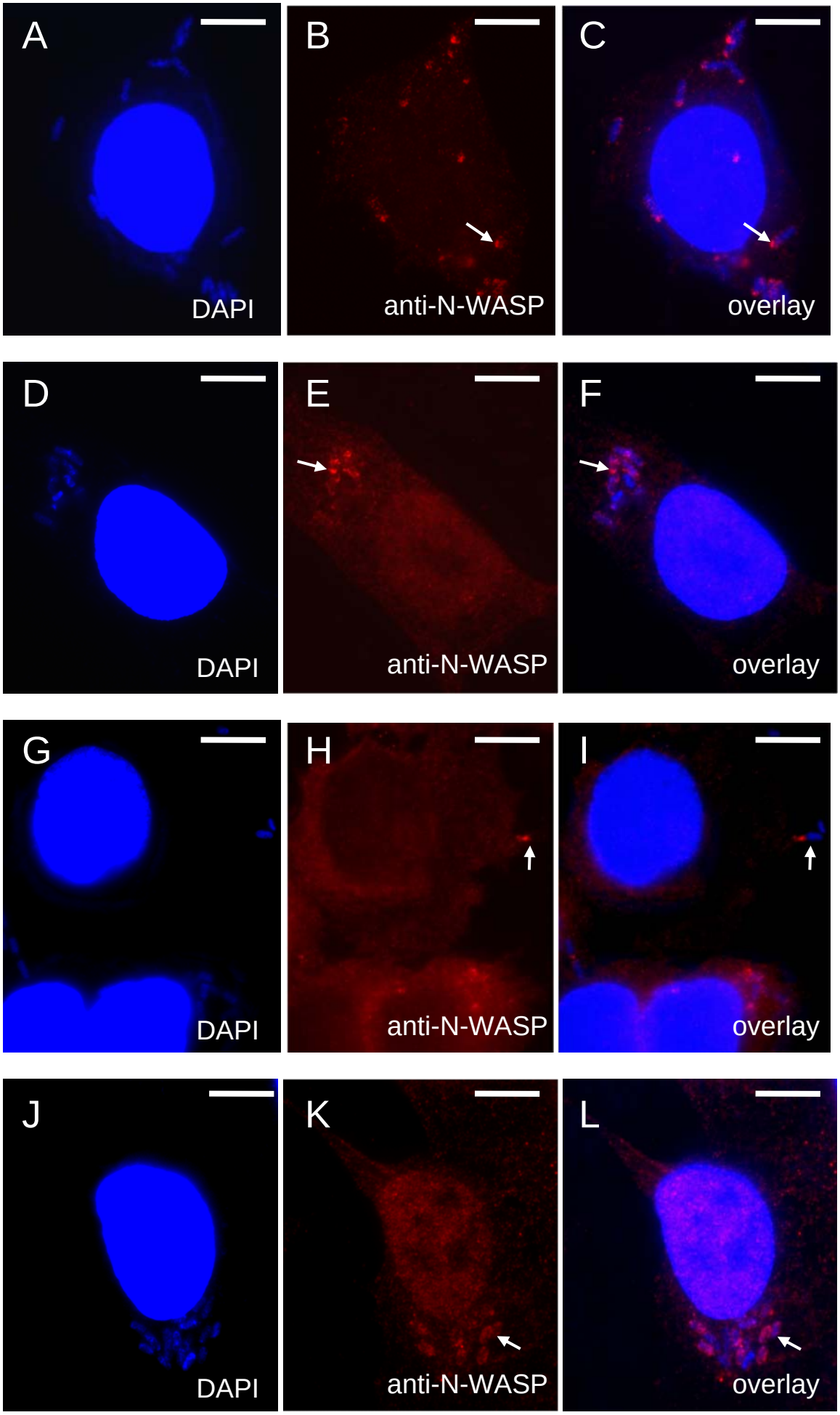

(**Figure 4.10 continued over page**)

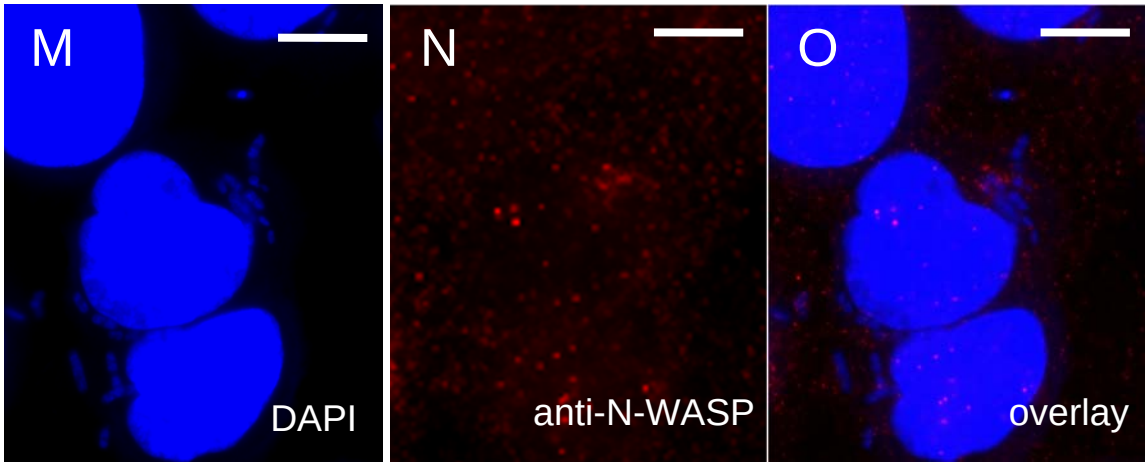

(**Figure 4.10 continued**)

Table 4.5 – F-actin comet tail and N-WASP recruitment by *S. flexneri* Δ*icsA* Δ*rmlD* expressing $IcsA_{\Delta}$ mutants

$IcsA_{\Delta}$ mutant	*S. flexneri* Δ*icsA* Δ*rmlD* background	
	F-actin tail formation[a]	**N-WASP recruitment**[a]
$IcsA_{WT}$	++	++
$IcsA_{\Delta 103\text{-}320}$	-	+/-
$IcsA_{\Delta 508\text{-}730}$	-	+/-
$IcsA_{\Delta 103\text{-}507}$	-	+/-

[a] (++) frequent F-actin comet tail formation or N-WASP recruitment; (+) low frequency F-actin comet tail formation or N-WASP recruitment; (+/-) feint detection; (-) not detected.

N.B. This data is based on qualitative observation of *S. flexneri* Δ*icsA* Δ*rmlD* (RMA2043) expressing IcsA deletion mutants in infected HeLa cells

Figure 4.11 Schematic locations of 5 amino acid insertions in 47 mutant $IcsA_i$ proteins and the resulting phenotypes.

The location of the linker-insertion for each of the 47 $IcsA_i$ mutants is indicated with a vertical line. (·····) indicates WT plaque formation; (– – –) indicates reduced plaque size, frequent F-actin tail formation and N-WASP recruitment; (– · –) indicates no plaques, infrequent F-actin tail formation and N-WASP recruitment; (———) indicates no plaques, no F-actin tail formation, and no N-WASP recruitment; (*****) indicates reduced IcsA production. Polar localisation region #1 (aa 1-104, orange); the GGR region (aa 140-307, green); the IcsB/Atg5 binding region (aa 320-433, red); polar localisation region #2 (aa 507-620, orange); and a putative auto-chaperone region (aa 634-735, white) are indicated. Novel N-WASP interacting regions (aa 330-381 and aa 508-730 identified in this study are also indicated.

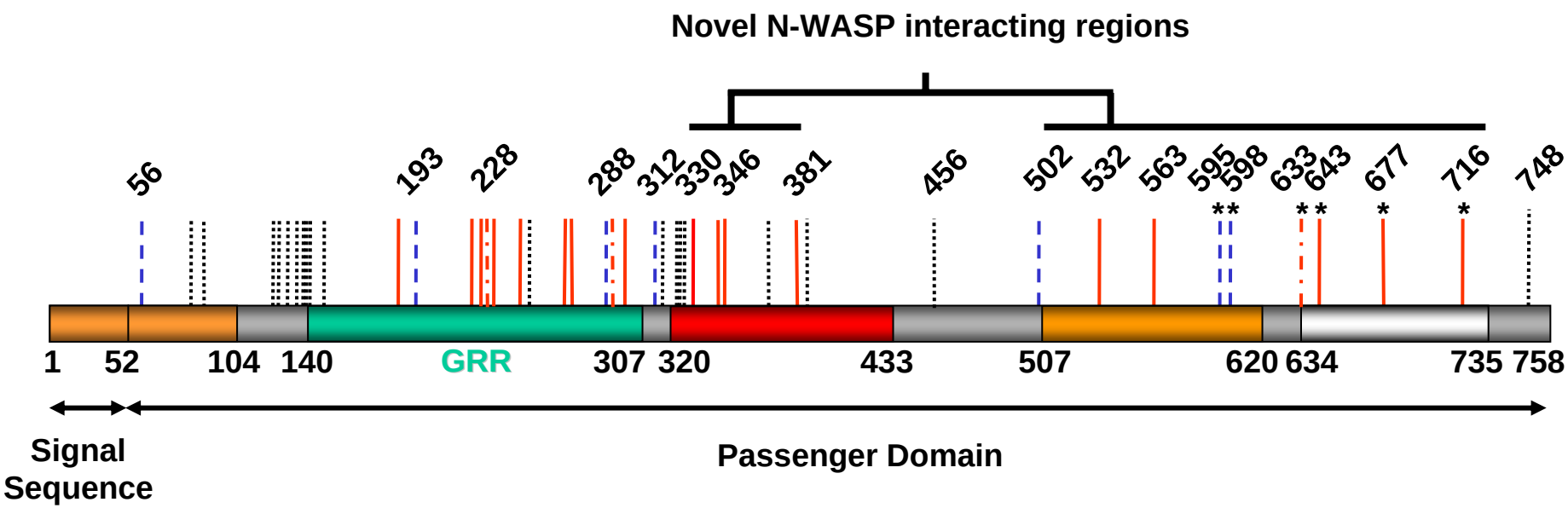
Novel N-WASP interacting regions
56
193
228
288
312
330
346
381
456
502
532
563
595
598
633
643
677
716
748
**
**
*
*
1
52
104
140
GRR
307
320
433
507
620
634
735
758
Signal Sequence
Passenger Domain

Table 4.6 – Summary of results for Chapters 3 and 4.

IcsA$_i$ mutant[a]	Phenotype of *S. flexneri* Δ*icsA* expressing IcsA$_i$				N-WASP interacting regions[f]	Additional Functional regions and features
	IcsA$_i$ production[b]	Plaque formation[c]	F-actin comet tails[d]	N-WASP recruitment[e]		
IcsA$_{i56}$	++++	+++	++	++		Polarity #1 (aa 1-104)
IcsA$_{i81}$	++++	++++	nt	nt		
IcsA$_{i87}$	++++	++++	nt	nt		
IcsA$_{i120}$	++++	++++	nt	nt		GRR#1 (aa 117-139)
IcsA$_{i122}$	++++	++++	nt	nt		
IcsA$_{i128}$	++++	++++	nt	nt		
IcsA$_{i132}$	++++	++++	nt	nt		
IcsA$_{i137}$	++++	++++	nt	nt		
IcsA$_{i138}$	++++	++++	nt	nt		
IcsA$_{i140}$	++++	++++	nt	nt		GRR #2 (aa 140-171)
IcsA$_{i148}$	++++	++++	nt	nt		
IcsA$_{i185}$	++++	-	-*	-**	N-WASP interacting region (aa 185-297)	GRR #3 (aa 172-205)
IcsA$_{i193}$	++++	+	++	++		
IcsA$_{i219}$	++++	-	-	-		GRR #4 (aa 206-239)
IcsA$_{i226}$	++++	-	-*	-**		
IcsA$_{i228}$	++++	-	+/-*	-**		
IcsA$_{i230}$	++++	-	-	-		
IcsA$_{i244}$	++++	-	-	-		GRR #5 (aa 240-273)
IcsA$_{i248}$	++++	-	-	-		
IcsA$_{i268}$	++++	-	-	-		
IcsA$_{i271}$	++++	-	-	-**		
IcsA$_{i288}$	++++	+	+	++		GRR #6 (aa 274-307)
IcsA$_{i292}$	++++	-	+/-	+		
IcsA$_{i297}$	++++	-	-	-		
IcsA$_{i312}$	++++	+	++	++		IcsB/Atg5 binding (aa 320-433)
IcsA$_{i314}$	++++	++++	nt	nt		
IcsA$_{i322}$	++++	++++	nt	nt		
IcsA$_{i324}$	++++	++++	nt	nt		
IcsA$_{i326}$	++++	++++	nt	nt		
IcsA$_{i330a}$	++++	-	-	-	N-WASP interacting region (aa 330-381)	
IcsA$_{i330b}$	++++	-	-	-		
IcsA$_{i342}$	++++	-	-	-		
IcsA$_{i346}$	++++	-	-	-		
IcsA$_{i369}$	++++	++++	nt	nt		
IcsA$_{i381}$	++++	-	-	-		
IcsA$_{i386}$	++++	++++	nt	nt		
IcsA$_{i456}$	++++	++++	nt	nt		
IcsA$_{i502}$	++++	+	+	++		
IcsA$_{i532}$	++++	-	-*	-**	N-WASP interacting region (aa 508-730)	Polarity #2 (aa 507-620)
IcsA$_{i563}$	++++	-	-*	-**		
IcsA$_{i595}$	+++	++	++	++		
IcsA$_{i598}$	++	++	++	++		
IcsA$_{i633}$	+	-	+/-	+		
IcsA$_{i643}$	+	-	-	-		Auto-chaperone (aa 634-735)
IcsA$_{i677}$	+	-	-	-		
IcsA$_{i716}$	++++	-	-	-		
IcsA$_{i748}$	++++	++++	nt	nt		

[a]IcsA$_i$ mutants with altered function are shaded grey; IcsA$_i$ mutants with WT function are unshaded. [b]Data from Chapter 3, Section 3.3. [c]Data from Chapter 3, Section 3.5. [d]Data from Chapter 4, Section 4.2. [e]Data from Chapter 4, Section 4.4. [f]Based on data from Sections 4.4 and 4.5. nt = not tested. F-actin comet tail formation (*) and/or N-WASP recruitment (**) in R-LPS *S. flexneri*.

Another significant finding of this chapter was the effect of LPS-Oag on N-WASP recruitment, with some $IcsA_i$ mutants ($IcsA_{i185}$, $IcsA_{i226}$, $IcsA_{i532}$ and $IcsA_{i563}$,) unable to recruit N-WASP when expressed by S-LPS strains of *S. flexneri*, but able to recruit N-WASP and form F-actin comet tails in a R-LPS background (Section 4.5; Table 4.6). Subsequently, IcsA deletion mutants of Suzuki *et al*. (1996) ($IcsA_{\Delta 103-320}$, $IcsA_{\Delta 508-730}$ and $IcsA_{\Delta 103-507}$) were also found to recruit N-WASP in a R-LPS background. Notably, two of these mutants ($IcsA_{\Delta 103-320}$, $IcsA_{\Delta 103-507}$) lack the proposed N-WASP binding region (aa 103-433). Therefore, these results indicate that other regions must interact with N-WASP (i.e. within aa 53-103 and aa 508-730).

Four $IcsA_i$ mutants ($IcsA_{i193,}$ $IcsA_{i288}$, $IcsA_{i312}$, $IcsA_{i502}$) exhibited marked reductions in intercellular spreading when expressed by *S. flexneri* Δ*icsA* strains, despite frequent F-actin comet tail formation and N-WASP recruitment (Figure 4.11; Table 4.6; Section 4.2 and 4.4). The molecular basis of the severe intercellular spreading defect of these strains is unclear as this is a novel phenotype, and it warrants further investigation. However, for two of these strains, *S. flexneri* Δ*icsA* $IcsA_{i193}$ and *S. flexneri* Δ*icsA* $IcsA_{i288}$, heterogeneous F-actin comet tails were observed. One population had F-actin comet tails with WT morphology and the second population had thicker F-actin comet tails that were concomitant with increased vinculin recruitment (Section 4.3). A similar phenotype has also been observed for a R-LPS *S. flexneri* strain in our laboratory (Van Den Bosch and Morona, unpublished data).

Chapter Five

In silico structural modelling of the IcsA passenger domain

Chapter Five: *In silico* structural modelling of the IcsA passenger domain

5.1 Introduction

Currently, the structure of the IcsA protein is not known. However, the passenger domains of two ATs, *B. pertussis* P.69 Pertactin and *E. coli* Haemoglobin protease have been crystallised and both were found to form right-handed parallel β-helices (Emsley *et al*., 1996; Otto *et al*., 2005). From *in silico* analysis using the modelling programs BetaWrap and BetaWrapPro (McDonnell *et al*., 2006), it has been predicted that the majority of autotransporter passenger domains form this structure (Bradley *et al*., 2001; Junker *et al*., 2006). The general structure of a right-handed, parallel β-helix is represented in Figure 5.1 (http://betawrappro.csail.mit.edu/help.html). Each rung of the helix consists of three β-strands (β1, β2 and β3) connected by three turn regions (T1, T2 and T3). The lengths of turns T1 and T3 are variable, however turn T2 is almost always 2 residues long (Bradley *et al*., 2001; Jenkins and Pickersgill, 2001; Vretou *et al*., 2003). The strands from adjacent rungs stacked on top of each other in a parallel orientation. Usually, there are aliphatic residues or "an asparagine ladder" in T2 that facilitate the stacking of the rungs. In this chapter, various *in silico* analysis tools were employed to create a structural model for the IcsA passenger domain, and correlations made between these structure predictions and data from linker-mutagenesis and function studies (Chapters Three and Four).

Figure 5.1 The parallel right-handed β-helix

A – The structure of a right-handed, parallel β-helix

A diagram of the β-helix protein Pectate Lyase C (PDB ID: 1pcl) from *Erwinia chrysanthemi* (http://betawrappro.csail.mit.edu). Rungs of the right-handed β-helix consist of three β-strands connected by three turn regions. The strands from adjacent rungs stack on top of each other in a parallel orientation to form a parallel β-helix.

B – An individual rung of a β-helix

A diagram showing an individual rung of Pectate Lyase C (PDB ID: 1pcl) with three β-strands (β1, β2 and β3) connected by three turn regions (T1, T2 and T3) (http://betawrappro.csail.mit.edu/help.html).

A

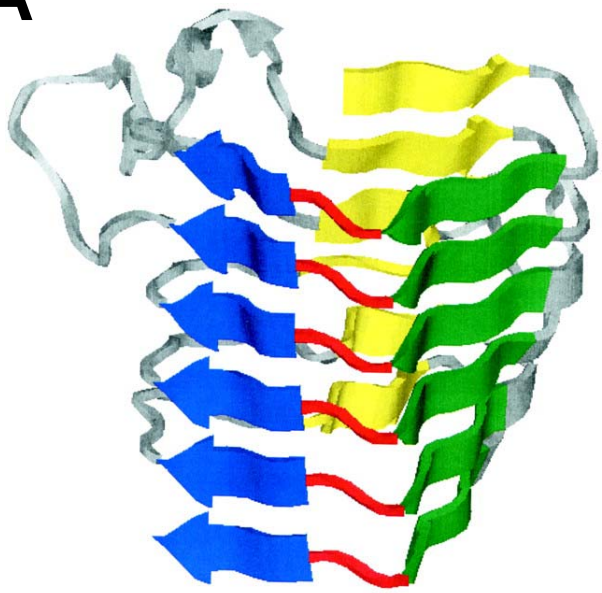

B

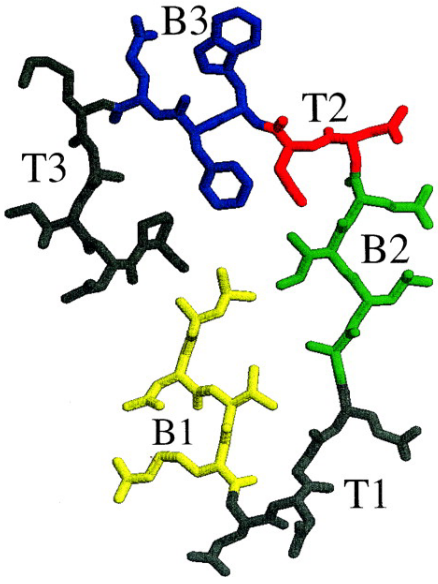

5.2 Secondary structure analysis

The coding sequence for the IcsA passenger domain (aa 53 – 758) was submitted to the PredictProtein server (http://www.predictprotein.org) and the PROF analysis program linked to this server was used to predict its secondary structure (Rost and Sander, 1993; Rost *et al*., 1996). The IcsA passenger was predicted to consist of alternating β-strands and loop regions with an overall composition of 58.5% β-strand, 41.5% loop regions, and devoid of α-helices (Figure 5.2). Such a secondary structure prediction is not unexpected given that the IcsA passenger domain, like that of the two crystallised ATs, is likely to form a β-helix structure.

5.3 BetawrapPro analysis

IcsA was analysed using BetawrapPro (http://betawrappro.csail.mit.edu; McDonnell *et al*., 2006). BetawrapPro predicts a packet of five rungs (one wrap/one β helix fold) and generates 10 possible overlapping wraps, in order of probability. The results of the BetawrapPro analysis predicted that the best wrap (*P* value: 0.0047) for the IcsA passenger domain (aa 53 – 758) was within residues 559 and 700 (Figure 5.3). Aside from identifying that a region within the IcsA passenger domain possesses a β-helical structure, the BetaWrapPro prediction yields only a very limited sequence-structure alignment. Six of the $IcsA_i$ mutants generated in Chapter Three possess linker-insertions in this region. $IcsA_{i563}$, $IcsA_{i598}$ and $IcsA_{i633}$ possess linker-insertions that corresponded to T1 of rung 1, 2 and 3 respectively, of the BetawrapPro model; $IcsA_{i595}$ and $IcsA_{i677}$ possess linker-insertions that corresponded to β1 of rung 2 and 5, respectively; and $IcsA_{i643}$ possesses a linker-insertion in β3 of rung 3. Of these mutants, $IcsA_{i595}$ (β1), $IcsA_{i598}$ (T1), $IcsA_{i633}$ (T1), $IcsA_{i643}$ (β3), $IcsA_{i677}$ (β1) demonstrated decreased production in *S. flexneri*. It is interesting to note that none of these mutants were predicted to have linker-insertions within T2 of the helix, which is

Figure 5.2 Prediction of the secondary structure of the IcsA passenger domain

A – PROF secondary structure prediction.

Results from the PROF analysis program (Rost and Sander, 1993; Rost *et al*., 1996) predicting the secondary structure of the IcsA passenger domain. The top line indicates the number of the first amino acid in each line and the last amino acid of protein sequence. The second line (AA) shows the submitted amino sequence that corresponds to the IcsA passenger domain (aa 53-758; GenBank accession # AAA26547). The third line (PROF sec) represents the predicted secondary structure for the residue above where E = extended (strand) (red), H = Helix (blue) and L = loop (green). The fourth line (Rel sec) represents the confidence of the secondary prediction (0=low to 9=high) and bottom line (Sub sec) indicates the secondary structure of residues where the confidence of the secondary prediction was >5.

B – PROF Summary of secondary structure composition.

A summary of the results from the PROF analysis program (Rost and Sander, 1993; Rost *et al*., 1996) showing the overall secondary structure composition of the IcsA passenger domain.

A

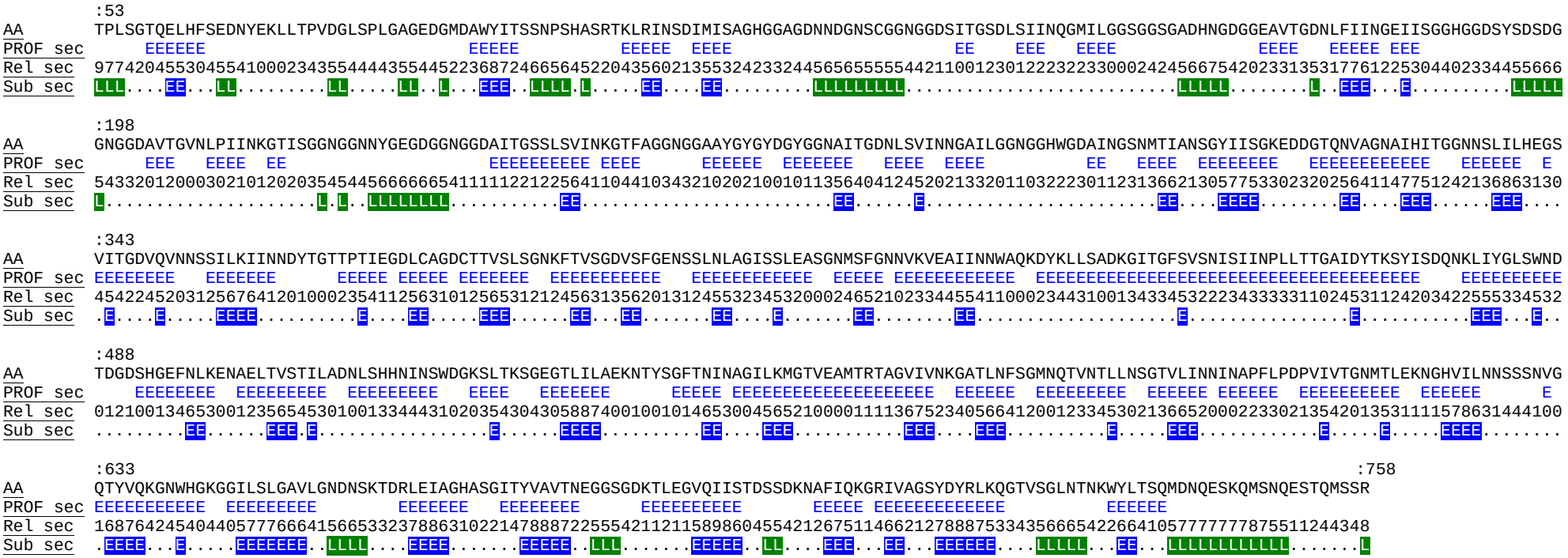

B

Secondary structure type	H (helix)	E (strand)	L (loop)
% in IcsA (aa 53-758)	0	58.50	41.50

Figure 5.3 BetawrapPro analysis of the IcsA passenger domain

BetawrapPro analysis (http://betawrappro.csail.mit.edu) predicted that the best β-helix fold (P-value: 0.0047) for the IcsA passenger domain (aa 53 – 758) was within residues 559 and 700. Each line represents one rung of the helix and consists of three β-strands (β1, β2 and β3) connected by three turn regions (T1, T2 and T3). The positions of linker-insertions within this region that were generated in Chapter 3, are shown in bold and underlined (see text for details).


β1 T1 β2 T2 β3 T3
RUNG 1 559 VEAMTR.....TAGVIVNKGATLNFSGMNQTVNTLLNSGT 593
RUNG 2 594 VLINNINAP..FLPDPVIVTGNMTLEK.....NGH 621
RUNG 3 622 VILNNSSS...NVGQTYVQKGNWHGKGGI.....LSLGA 652
RUNG 4 653 VLGNDNS.....KTDRLEIAGHASGI.....TY 675
RUNG 5 676 VAVTNEGGSGDKTLEGVQIISTDSS..... 700

regarded as non-permissive to epitope insertion and would be likely to disrupt the overall stability of structure (Jenkins and Pickersgill, 2001; Vretou *et al*., 2003).

5.4 PHYRE structure prediction

The PHYRE automatic fold recognition program (http://www.sbg.bio.ic.ac.uk/phyre) was used to predict the tertiary structure of the IcsA passenger domain and a model was displayed using PyMOL (http://pymol.sourceforge.net, DeLano Scientific). The protein was threaded on *B. pertussis* P.69 Pertactin (PDB# 1DAB). Region aa 301-737 of IcsA was predicted (E-value = 6.7×10^{-12}) to form a right-handed β-helix (Figure 5.4). Twenty-two of the $IcsA_i$ mutants generated in Chapter 3 possessed linker-insertions in this region (aa 301-737), 15 of which were shown to affect IcsA function (Table 4.6). Of these 15 linker-insertions, 10 were located in loop regions ($IcsA_{i330a}$, $IcsA_{i330b}$, $IcsA_{i342}$, $IcsA_{i346}$, $IcsA_{i381}$, $IcsA_{i502}$, $IcsA_{i532}$, $IcsA_{i563}$, $IcsA_{i633}$ and $IcsA_{i643}$) and 5 were located in β-strands ($IcsA_{i312}$, $IcsA_{i595}$, $IcsA_{i598}$, $IcsA_{i677}$ and $IcsA_{i716}$). Seven linker-insertions within aa 301-737 did not affect function (Table 4.6); one of these was located in a β-strand ($IcsA_{i369}$) and the remaining 6 were located in loop regions ($IcsA_{i314}$, $IcsA_{i322}$, $IcsA_{i324}$, $IcsA_{i326}$, $IcsA_{i386}$ and $IcsA_{i456}$). Interestingly, the PHYRE structure prediction correlated well to the BetawrapPro model. The PHYRE structure prediction program, a threading program, relies on homology of the queried protein to proteins of known structure. The alignment created by the PHYRE program to thread IcsA onto the Pertactin structure exhibited only 11% identity between the two proteins over the modelled region. Hence, this program was only able to model approximately half of the IcsA passenger domain.

Figure 5.4 PHYRE structure prediction of the IcsA passenger domain

The PHYRE automatic fold recognition program (http://www.sbg.bio.ic.ac.uk/phyre) was used to predict the structure of the IcsA passenger domain (aa 53-758) and a model was created using PyMOL (http://pymol.sourceforge.net, DeLano Scientific). The region aa 301-737 of IcsA was predicted (E-value = 6.7e-12) to form a right-handed β-helix. Twenty-two of the $IcsA_i$ mutants generated in Chapter 3 possessed linker-insertions in this region. The location of insertions in this region that prevented plaque formation are shown in red, the location of insertions that reduced plaque size are shown in blue and the location of insertions that had no effect on the function of IcsA are shown in green. The location of insertions that affected IcsA production are shown in magenta. **A** and **B** are alternate 180 degree views.

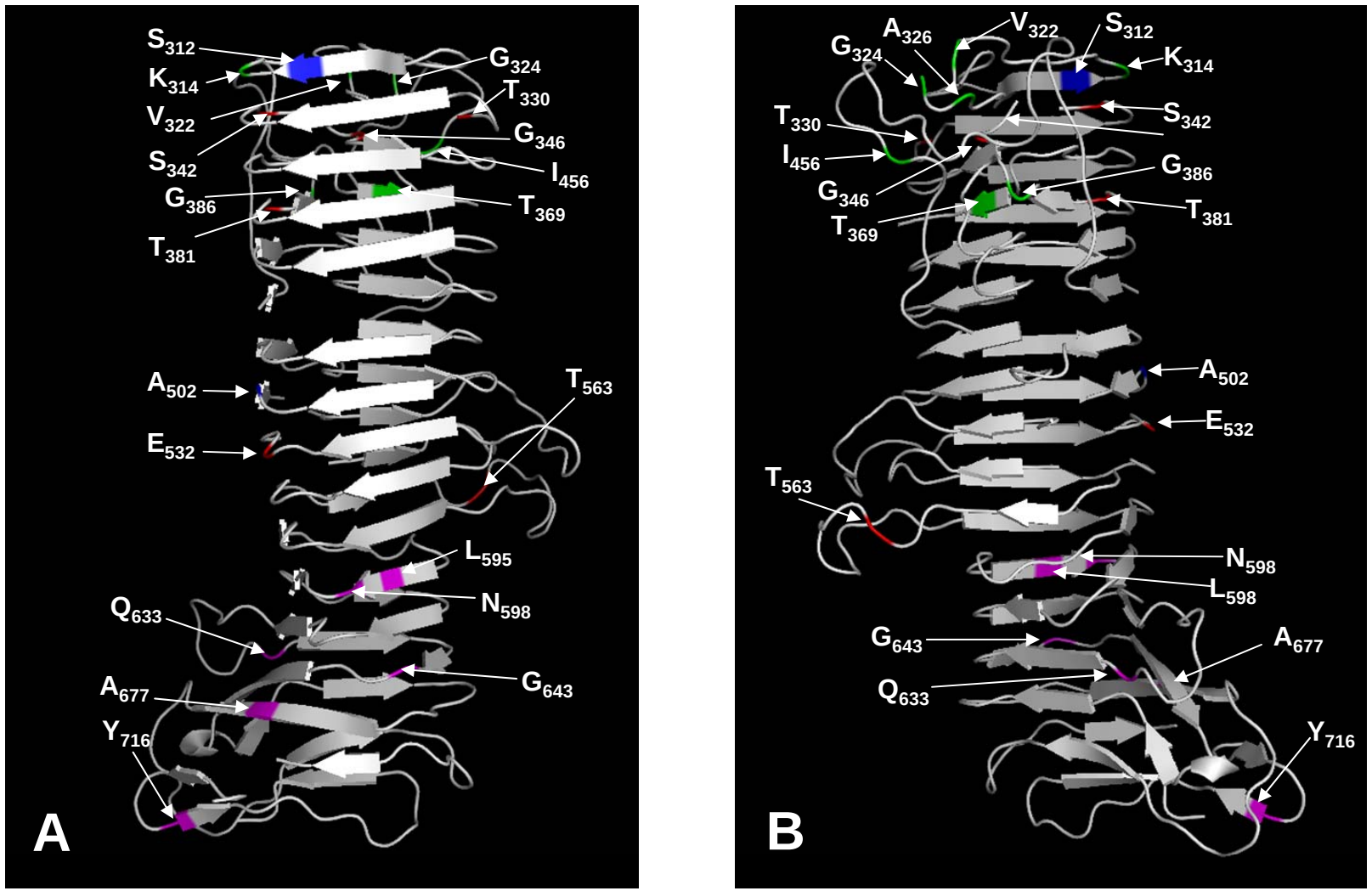
S312
K314
V322
S342
G386
T381
G324
T330
G346
I456
T369
A502
E532
T563
L595
N598
Q633
A677
Y716
G643
A
A326
V322
S312
G324
K314
T330
S342
I456
G386
G346
T381
T369
A502
E532
T563
N598
L598
G643
A677
Q633
Y716
B

5.5 Robetta structure prediction

In order create a more complete model of the IcsA passenger domain, including regions that lack sequence identity to other proteins of known structure, the IcsA passenger domain was submitted to the Robetta server (http://robetta.bakerlab.org), which incorporates both comparative modelling and the Rosetta *ab initio* structure prediction method. A model was displayed using PyMOL (http://pymol.sourceforge.net, DeLano Scientific) (Figure 5.5). The Robetta program, consistent with the PHYRE and BetawrapPro programs predicted that the IcsA passenger domain forms a right-handed β-helix, although the sequence–structure alignment created by Robetta did not correlate to the sequence-structure alignments created by PHYRE and BetawrapPro, with the predicted secondary structure varying greatly between these models. The distance from the N-terminus to the C-terminus of the IcsA passenger domain was calculated to be 136.52 Å using the measure function of the PyMOL program (Figure 5.5A), making the predicted length of the IcsA passenger domain shorter than the 210 Å (21 nm) VL-type Oag chains that extend from the surface of *S. flexneri* (West *et al*., 2005).

Interestingly, the Robetta model predicts extended loop regions protruding from the β-helix backbone within each of the polar localisation regions, the GRR region and the IcsB/Atg5 binding region (Figure 5.5). Additionally, the Robetta program predicted two α-helices within the IcsA passenger domain, protruding from loop regions within the β-helix backbone at aa 260-270 (“YGYGYDGTGGN”) and aa 549-558 (“INAGILKMGT”) (Figure 5.6). These α-helices were not identified by the PROF secondary structure prediction or PHYRE threading programs (Figures 5.2 and 5.4). The first α-helix (aa 260-270) was predicted to lie within the GRR #5, and a linker-insertion at aa 268 within the predicted helix completely abolished IcsA function in N-WASP recruitment (Figure 5.6B; Table 4.6). The second α-helix (aa 549-558) was located within polar localisation region #2. Notably, linker-insertions either upstream (at aa 532) or immediately downstream (at aa 563) of this α-helix

Figure 5.5 Reported functional regions represented on the Robetta structural model of the IcsA passenger domain

The Robetta server (http://robetta.bakerlab.org) was used to predict the structure of the IcsA passenger domain and a model was displayed using PyMOL (http://pymol.sourceforge.net, DeLano Scientific). Previously identified functional regions reported in the literature are shown. Regions responsible for polar targeting of IcsA are coloured orange: polar localisation region #1 (aa 1-104) **[1]**; and polar localisation region #2 (aa 507-620) **[4]**. A glycine-rich repeat region (GRR; aa 140-307) that interacts with the host protein N-WASP is coloured green **[2]**. The *Shigella* IcsB protein, and the host autophagy protein Atg5 binding region is coloured red **[3]**. The putative auto-chaperone domain of IcsA (aa 634-735) is coloured aqua **[5]** and IcsP cleavage site between aa 758-759 is coloured dark blue **[6]**. **A** and **B** are alternate 180 degree views. The distance from the N-terminal residue to the C-terminal residue of the IcsA passenger domain (indicated by the dotted line) was calculated (using PyMOL) to be 136.52 Å.

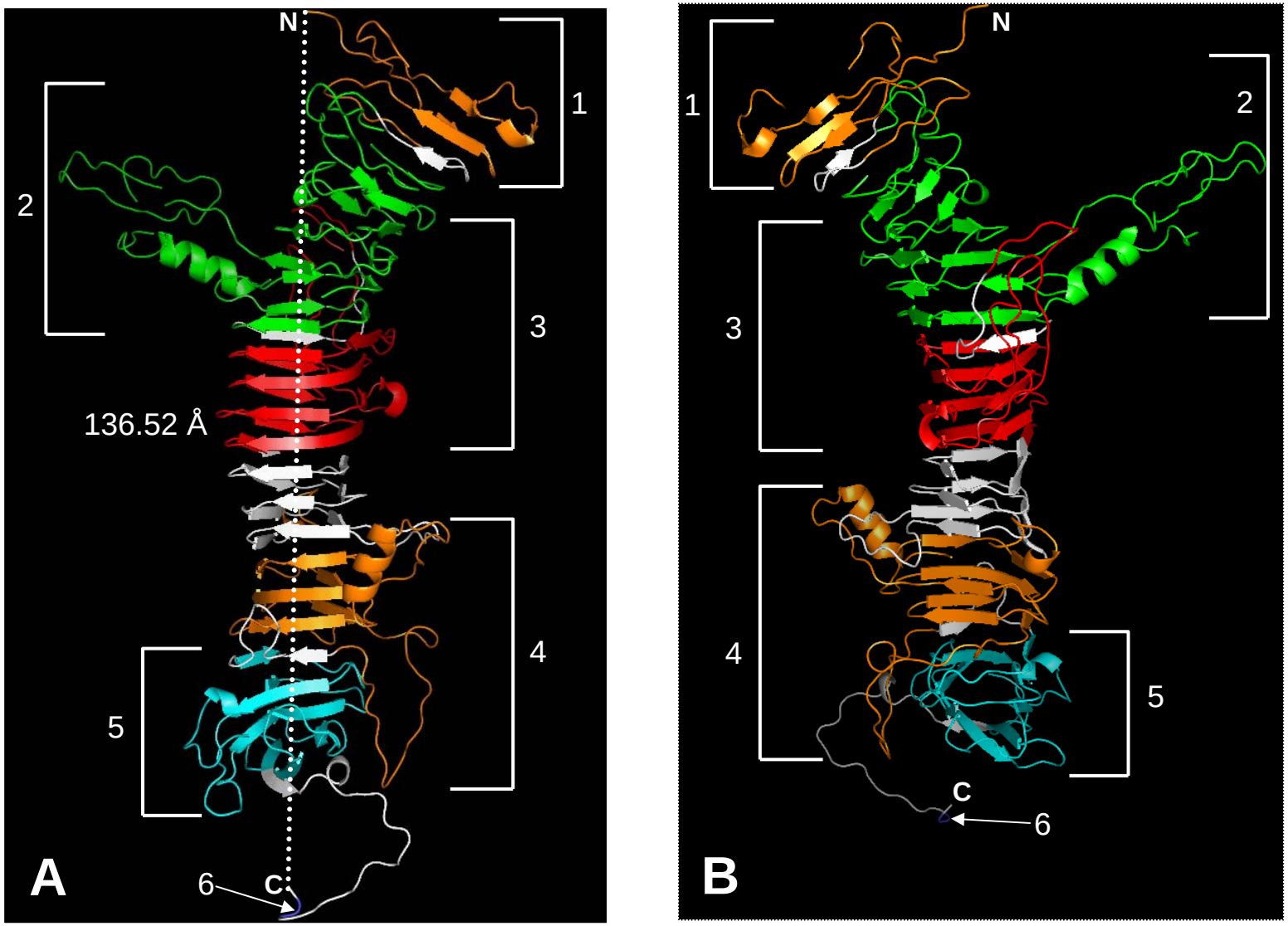
N
1
2
3
136.52 Å
4
5
6
C
A
N
1
2
3
4
5
C
6
B

Figure 5.6 Predicted α-helices and cysteine residues of the IcsA passenger domain Robetta model

The Robetta server (http://robetta.bakerlab.org) was used to predict the structure of the IcsA passenger domain (aa 53-758) and a model was created using PyMOL (http://pymol.sourceforge.net, DeLano Scientific). This diagram shows the overall structure predicted by the Robetta program (**A**) with two predicted α-helices (**B and D**) and two cysteines (C_{275} and C_{279}) (**C**) predicted to be located in close proximity also labeled. The first α-helix is located at aa 260-270 and a linker-insertion at aa 268 within the predicted helix was found to disrupt IcsA function (**B**). The second α-helix is located at aa 549-558; linker-insertions either upstream (at aa 532) or immediately downstream (at aa 563) of this α-helix disrupted polar targeting of IcsA and N-WASP binding by IcsA (**D**).

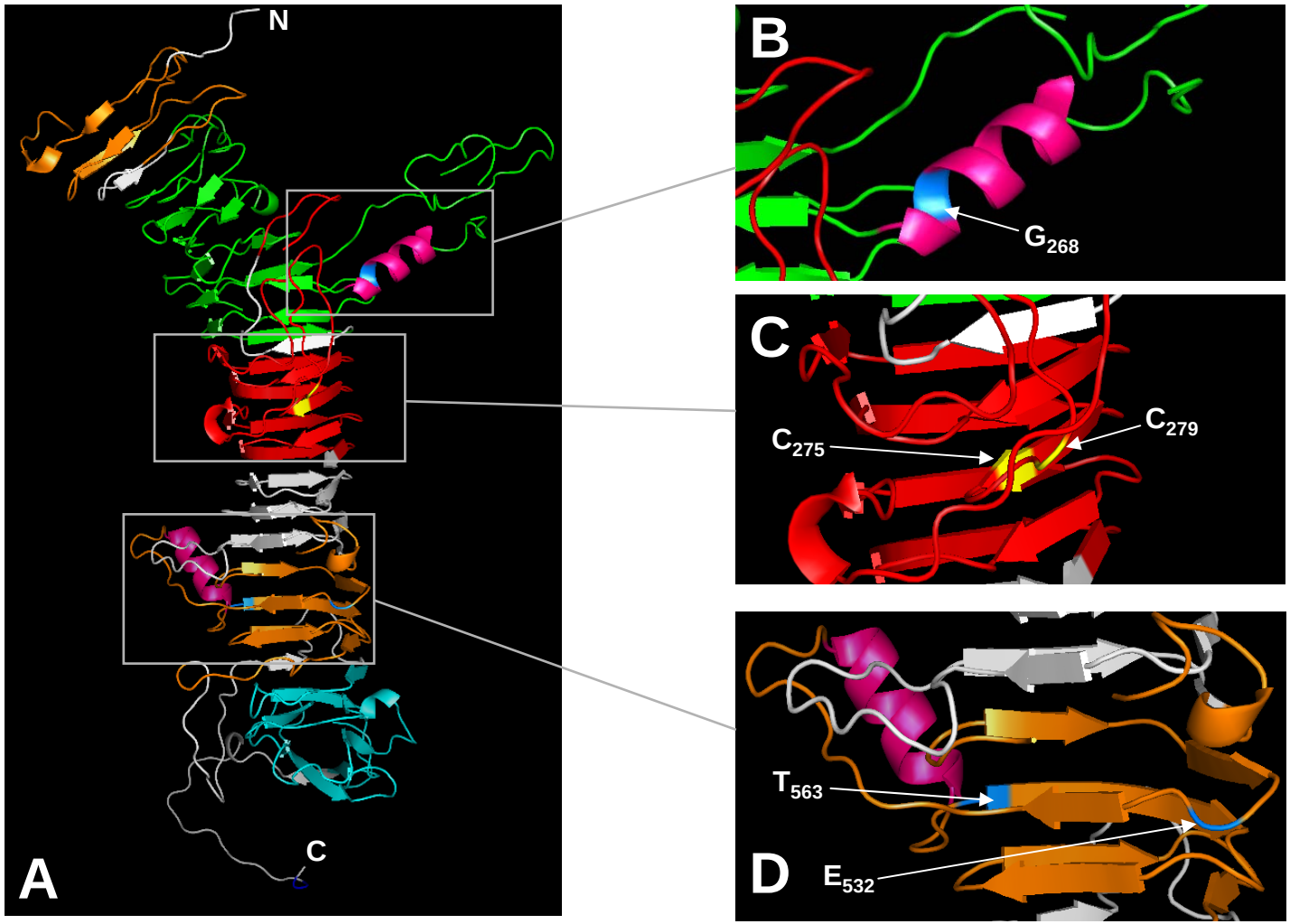
N
C
A
B
G268
C
C275
C279
D
T563
E532

disrupted polar targeting of IcsA, and also affected N-WASP binding (Figure 5.6D; Table 4.6).

Another feature of the Robetta model is that two cysteines (C_{275} and C_{279}) within the passenger domain are predicted to be located in close proximity (Figure 5.6B). This was of interest as IcsA has been shown to form at least one disulphide bond in the periplasm where it is thought to exist in a partially folded state prior to its translocation across outer-membrane (Brandon *et al*., 2001). However, analysis of the IcsA passenger domain with DISULFIND, a disulphide bonding state and cysteine connectivity prediction server (Ceroni *et al.*, 2006), suggested that the probability of disulphide bond formation between C_{275} and C_{279} was low (Figure 5.7).

In Chapter Three, 29 of the linker-insertions were shown to affect IcsA function. Of these linker-insertions, 21 were located in predicted loop regions of the Robetta model ($IcsA_{i185}$, $IcsA_{i193}$, $IcsA_{i219}$, $IcsA_{i226}$, $IcsA_{i228}$, $IcsA_{i230}$, $IcsA_{i244}$, $IcsA_{i248}$, $IcsA_{i271}$, $IcsA_{i288}$, $IcsA_{i312}$, $IcsA_{i330a}$, $IcsA_{i330b}$, $IcsA_{i346}$, $IcsA_{i381}$, $IcsA_{i532}$, $IcsA_{i595}$, $IcsA_{i598}$, $IcsA_{i643}$, $IcsA_{i677}$ and $IcsA_{i716}$), 7 were located in β-strands ($IcsA_{i56}$, $IcsA_{i292}$, $IcsA_{i297}$, $IcsA_{i342}$, $IcsA_{i502}$, $IcsA_{i563}$ and $IcsA_{i633}$) and one was located in an α-helix ($IcsA_{i268}$) (Figure 5.8; Table 5.1). Of the 18 linker-insertions within the passenger domain that had not affect on function, 2 of these were located in a β-strands ($IcsA_{i87}$ and $IcsA_{i369}$) and the remaining 16 were located in loop regions ($IcsA_{i81}$, $IcsA_{i120}$, $IcsA_{i122}$, $IcsA_{i128}$, $IcsA_{i132}$, $IcsA_{i137}$, $IcsA_{i138}$, $IcsA_{i140}$, $IcsA_{i148}$, $IcsA_{i314}$, $IcsA_{i322}$, $IcsA_{i324}$, $IcsA_{i326}$, $IcsA_{i386}$, $IcsA_{i456}$ and $IcsA_{i748}$) (Figure 5.9; Table 5.1).

Overall, this suggests there is no clear correlation between the phenotypes of the $IcsA_i$ mutants and the nature of the linker-insertion site predicted by the Robetta program. However, the Robetta model did predict that 37 of the 47 linker-insertions were located within loop regions (Table 5.1).

Figure 5.7 Prediction of disulphide bond formation between cysteine residues of the IcsA passenger domain.

Results from DISULFIND: Disulfide Bonding State and Cysteine Connectivity Prediction Server (Ceroni *et al.*, 2006) analysis of the IcsA passenger domain. The top line (AA) shows the submitted amino sequence that corresponds to the IcsA passenger domain (aa 53-758) with cysteine residues shaded yellow. The second line (DB_state) represents the predicted disulfide bonding state for the residue above where 1 = disulfide bonded and 0 = not disulfide bonded). The bottom line (DB_conf) represents the confidence of the disulfide bonding state prediction (0=low to 9=high).

```
AA    53 TPLSGTQELHFSEDNYEKLLTPVDGLSPLGAGEDGMDAWYITSSNPSHASRTKLRINSDIMISAGHGGAGDNNDGNSCG
DB_state                                                                            0
DB_conf                                                                             0


AA   132 GNGGDSITGSDLSIINQGMILGGSGGSGADHNGDGGEAVTGDNLFIINGEIISGGHGGDSYSDSDGGNGGDAVTGVNLP
DB_state
DB_conf


AA   211 IINKGTISGGNGGNNYGEGDGGNGGDAITGSSLSVINKGTFAGGNGGAAYGYGYDGYGGNAITGDNLSVINNGAILGGN
DB_state
DB_conf


AA   290 GGHWGDAINGSNMTIANSGYIISGKEDDGTQNVAGNAIHITGGNNSLILHEGSVITGDVQVNNSSILKIINNDYTGTTP
DB_state
DB_conf
               +---+
               |   |
AA   369 TIEGDLCAGDCTTVSLSGNKFTVSGDVSFGENSSLNLAGISSLEASGNMSFGNNVKVEAIINNWAQKDYKLLSADKGIT
DB_state       1   1
DB_conf        0   0


AA   448 GFSVSNISIINPLLTTGAIDYTKSYISDQNKLIYGLSWNDTDGDSHGEFNLKENAELTVSTILADNLSHHNINSWDGKS
DB_state
DB_conf

AA   527 LTKSGEGTLILAEKNTYSGFTNINAGILKMGTVEAMTRTAGVIVNKGATLNFSGMNQTVNTLLNSGTVLINNINAPFLP
DB_state
DB_conf


AA   606 DPVIVTGNMTLEKNGHVILNNSSSNVGQTYVQKGNWHGKGGILSLGAVLGNDNSKTDRLEIAGHASGITYVAVTNEGGS
DB_state
DB_conf


AA   685 GDKTLEGVQIISTDSSDKNAFIQKGRIVAGSYDYRLKQGTVSGLNTNKWYLTSQMDNQESKQMSNQESTQMSSR
DB_state
DB_conf
```

Figure 5.8 Robetta model of the IcsA passenger domain and linker-insertion sites that disrupted IcsA function.

The Robetta server (http://robetta.bakerlab.org) was used to predict the structure of the IcsA passenger domain and a model was created using PyMOL (http://pymol.sourceforge.net, DeLano Scientific). Twenty-nine of the $IcsA_i$ mutants generated in Chapter three were found have altered function. The location of linker-insertions that prevented plaque formation are shown in red, the location of insertions that reduced plaque size are shown in blue and the location of insertions that affected IcsA production are shown in magenta. **A** and **B** are alternate 180 degree views.

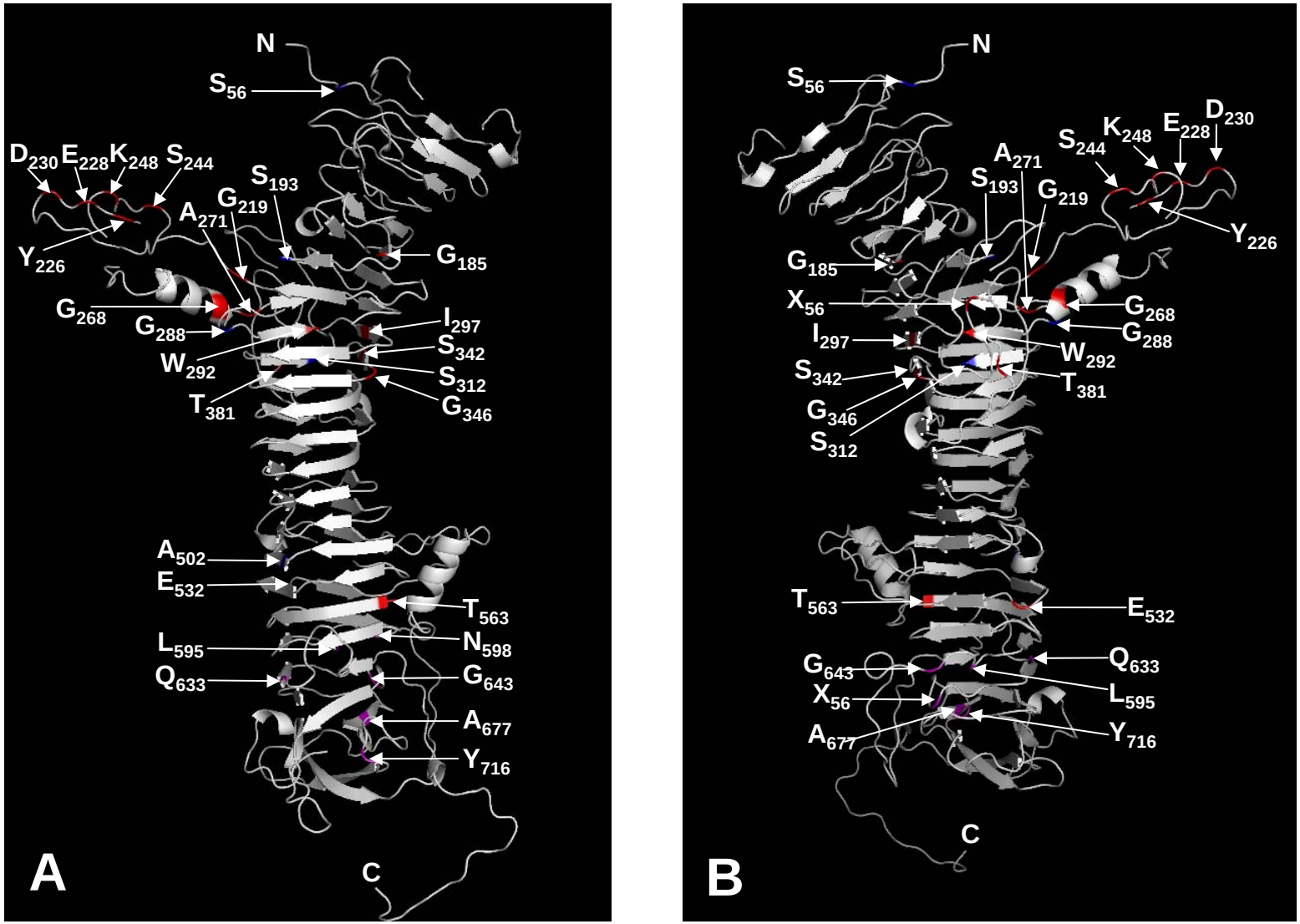
N
S56
D230 E228 K248 S244
S193
G219
A271
Y226
G185
G268
G288
I297
W292
S342
S312
T381
G346
A502
E532
T563
L595
N598
Q633
G643
A677
Y716
C
A
N
S56
D230
E228
K248
S244
A271
S193
G219
Y226
G185
X56
G268
G288
I297
W292
S342
T381
G346
S312
T563
E532
G643
Q633
X56
L595
A677
Y716
C
B

Table 5.1 – Comparison of Robetta structural model and linker-mutagenesis studies

IcsA$_i$ mutant[a]	Structural location of linker-insertion on Robetta model	Phenotype of *S. flexneri* Δ*icsA* expressing IcsA$_i$				N-WASP interacting regions[f]	Additional functional regions and features
		IcsA$_i$ production[b]	Plaque formation[c]	F-actin comet tails[d]	N-WASP recruitment[e]		
IcsA$_{i56}$	Beta strand	++++	+++	++	++		Polarity #1 (aa 1-104)
IcsA$_{i81}$	Loop region	++++	++++	nt	nt		
IcsA$_{i87}$	Beta strand	++++	++++	nt	nt		
IcsA$_{i120}$	Loop region	++++	++++	nt	nt		GRR#1 (aa 117-139)
IcsA$_{i122}$	Loop region	++++	++++	nt	nt		
IcsA$_{i128}$	Loop region	++++	++++	nt	nt		
IcsA$_{i132}$	Loop region	++++	++++	nt	nt		
IcsA$_{i137}$	Loop region	++++	++++	nt	nt		
IcsA$_{i138}$	Loop region	++++	++++	nt	nt		
IcsA$_{i140}$	Loop region	++++	++++	nt	nt		GRR #2 (aa 140-171)
IcsA$_{i148}$	Loop region	++++	++++	nt	nt		
IcsA$_{i185}$	Loop region	++++	-	-*	-**	N-WASP interacting region (aa 185-297)	GRR #3 (aa 172-205)
IcsA$_{i193}$	Loop region	++++	+	++	++		
IcsA$_{i219}$	Loop region	++++	-	-	-		GRR #4 (aa 206-239)
IcsA$_{i226}$	Loop region	++++	-	-*	-**		
IcsA$_{i228}$	Loop region	++++	-	+/-*	-**		
IcsA$_{i230}$	Loop region	++++	-	-	-		
IcsA$_{i244}$	Loop region	++++	-	-	-		GRR #5 (aa 240-273)
IcsA$_{i248}$	Loop region	++++	-	-	-		
IcsA$_{i268}$	Alpha Helix	++++	-	-	-		
IcsA$_{i271}$	Loop region	++++	-	-	-**		
IcsA$_{i288}$	Loop region	++++	+	+	++		GRR #6 (aa 274-307)
IcsA$_{i292}$	Beta strand	++++	-	+/-	+		
IcsA$_{i297}$	Beta strand	++++	-	-	-		
IcsA$_{i312}$	Loop region	++++	+	++	++		IcsB/ Atg5 binding (aa 320-433)
IcsA$_{i314}$	Loop region	++++	++++	nt	nt		
IcsA$_{i322}$	Loop region	++++	++++	nt	nt		
IcsA$_{i324}$	Loop region	++++	++++	nt	nt		
IcsA$_{i326}$	Loop region	++++	++++	nt	nt		
IcsA$_{i330a}$	Loop region	++++	-	-	-	N-WASP interacting region (aa 330-381)	
IcsA$_{i330b}$	Loop region	++++	-	-	-		
IcsA$_{i342}$	Beta strand	++++	-	-	-		
IcsA$_{i346}$	Loop region	++++	-	-	-		
IcsA$_{i369}$	Beta strand	++++	++++	nt	nt		
IcsA$_{i381}$	Loop region	++++	-	-	-		
IcsA$_{i386}$	Loop region	++++	++++	nt	nt		
IcsA$_{i456}$	Loop region	++++	++++	nt	nt		
IcsA$_{i502}$	Beta strand	++++	+	+	++		
IcsA$_{i532}$	Loop region	++++	-	-*	-**	N-WASP interacting region (aa 508-730)	Polarity #2 (aa 507-620)
IcsA$_{i563}$	Beta strand	++++	-	-*	-**		
IcsA$_{i595}$	Loop region	+++	++	++	++		
IcsA$_{i598}$	Loop region	++	++	++	++		
IcsA$_{i633}$	Beta strand	+	-	+/-	+		
IcsA$_{i643}$	Loop region	+	-	-	-		Auto-chaperone (aa 634-735)
IcsA$_{i677}$	Loop region	+	-	-	-		
IcsA$_{i716}$	Loop region	++++	-	-	-		
IcsA$_{i748}$	Loop region	++++	++++	nt	nt		

[a]IcsA$_i$ mutants with altered function are shaded grey; IcsA$_i$ mutants with WT function are unshaded. [b]Data from Chapter 3, Section 3.3. [c]Data from Chapter 3, Section 3.5. [d]Data from Chapter 4, Section 4.2. [e]Data from Chapter 4, Section 4.4. [f]Based on data from Sections 4.4 and 4.5. nt = not tested. F-actin comet tail formation (*) and/or N-WASP recruitment (**) in R-LPS *S. flexneri*.

Figure 5.9 Robetta model of the IcsA passenger domain and linker-insertion sites that had no effect on IcsA function.

The Robetta server (http://robetta.bakerlab.org) was used to predict the structure of the IcsA passenger domain and a model was created using PyMOL (http://pymol.sourceforge.net, DeLano Scientific). Eighteen of the $IcsA_i$ mutants generated in Chapter three were found to have WT function. The locations of the linker-insertions in these mutants are shown in green. **A** and **B** are alternate 180 degree views.

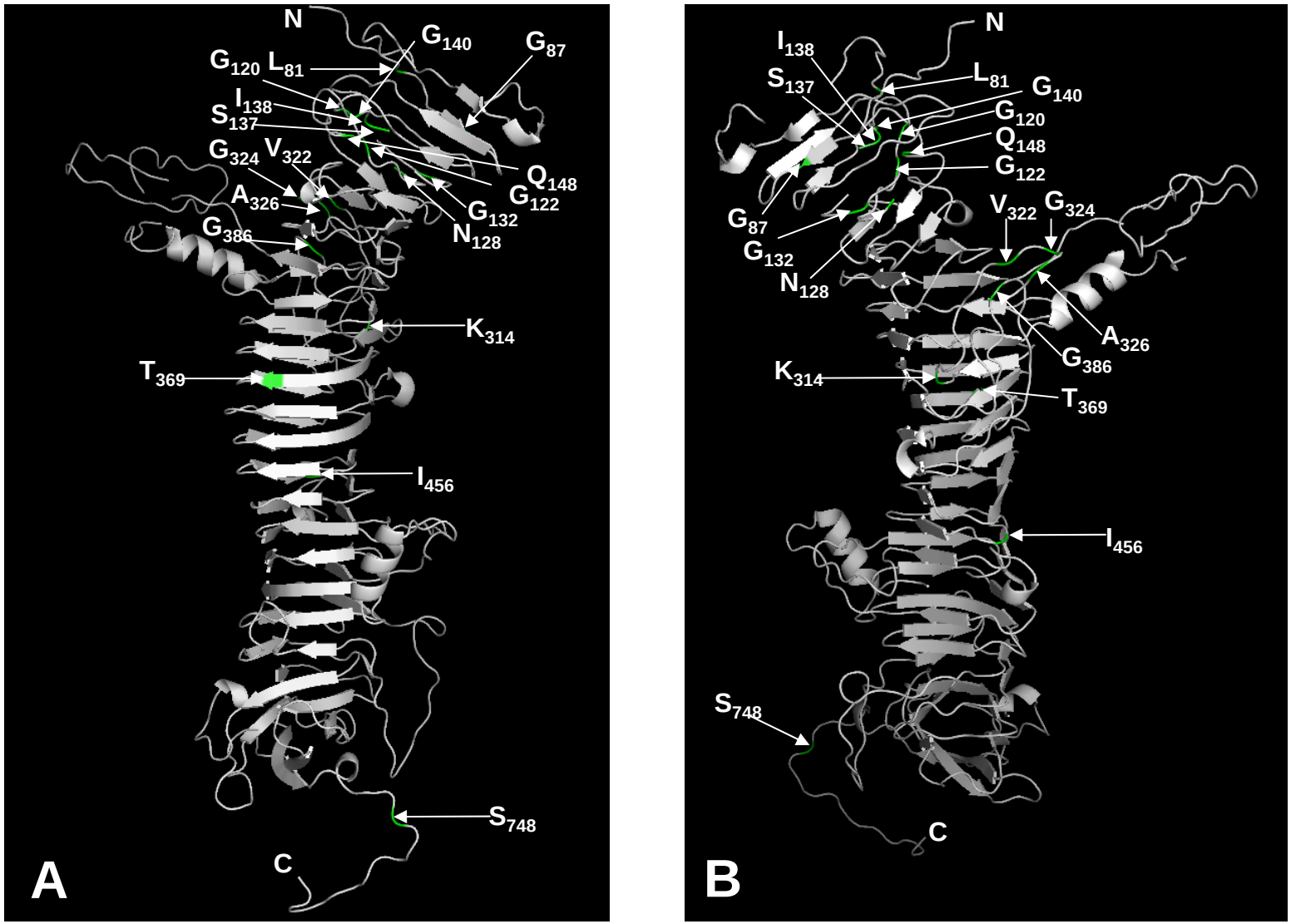
N
G140
G87
G120
L81
I138
S137
G324
V322
Q148
A326
G122
G132
G386
N128
K314
T369
I456
S748
C
A
N
I138
L81
S137
G140
G120
Q148
G122
G87
V322
G324
G132
N128
A326
G386
K314
T369
I456
S748
C
B

5.6 Summary: IcsA structure-function

The IcsA passenger domain was independently predicted to form a right-handed parallel β-helix structure by three different *in silico* analysis programs (BetawrapPro, PHYRE, and Robetta). This was validated by a predicted secondary structure profile consistent with this 3-D structure (~60 % β-strand and ~40% loop regions). However, the Robetta program predicted two α-helices protruding from loop regions within the β-helix backbone at aa 260-270 and aa 549-558 (Section 5.5; Figure 5.6) The first α-helix (aa 260-270) was located in GRR #5, within the proposed N-WASP binding region, and was predicted to protrude from the β-helix backbone to form a cleft with GRR regions 1-4. A role of this α-helical loop in N-WASP binding correlates with the finding that a linker-insertion at aa 268 within this predicted helix, completely abolished this function of the IcsA protein (Table 5.1). The second α-helix (aa 549-558) was predicted within polar localisation region #2 and may represent a polar targeting structural motif as linker-insertions either upstream (at aa 532) or immediately downstream (at aa 563) of this disrupted polar targeting of IcsA (Table 5.1). The Robetta model predicted extended loop regions protruding from the β-helix backbone within each of the polar localisation regions, the GRR region and also the IcsB/Atg5 binding region. These loop regions could possibly be responsible for mediating the interaction of these regions of IcsA with their respective ligands. In the absence of any 3-D structural data for IcsA this model provides a useful tool for guiding future studies investigating IcsA interactions with N-WASP, vinculin, Atg5 and IcsB.

Interestingly, the majority of the linker-insertions were predicted to be located within loop regions by the Robetta model. This would suggest that loop regions may be preferred regions for insertion of 5 aa linkers, and may reflect compatibility with IcsA production and export, and hence bacterial viability.

Chapter Six

Investigation of IcsA oligomerisation

Chapter Six: Investigation of IcsA oligomerisation

6.1 Introduction

One of the proposed models for export of AT proteins across the OM is the oligomeric model, in which translocation of the passenger domain proceeds through a central pore formed by an oligomer of translocation domains (Veiga *et al*., 2002). The model was proposed after the observation that the translocation domain of the IgA protease AT protein forms oligomeric structures in the OM (Veiga *et al*., 2002). However, endeavours to show oligomerisation of *N. meningitidis* NalP and *E. coli* AIDA-I have been unsuccessful (Oomen *et al*., 2004; Muller *et al*., 2005). It is not known if IcsA is able to oligomerise, as no experiments investigating this have been reported. Hence the aim of this chapter was to investigate this possibility.

6.2 *In situ* cross-linking

In order to determine if IcsA forms an oligomer in the outer-membrane, *in situ* chemical cross-linking was performed with formaldehyde and Dithio-bis (succinimidylpropionate) (DSP) according to Sections 2.15.1 and 2.15.2, respectively. Briefly, intact log-phase bacteria were treated with chemical cross-linking agents then whole-cell lysates were subjected to SDS-PAGE and Western immunoblotting with an anti-IcsA antibody (Sections 2.12.4 and 2.12.6). *S. flexneri* Δ*icsA* $IcsA_{WT}$ (RMA2090; Table 2.1) was used for these experiments as it expresses IcsA from a multicopy plasmid and has a higher levels of IcsA than the WT strain 2457T. A high molecular weight band with an apparent molecular size greater than 190 kDa was observed on one occasion following treatment of

bacteria with formaldehyde but this was not reproducible in three subsequent experimental attempts (Figure 6.1A). Treatment with the cross-linking agent DSP, however, consistently lead to the presence of two high molecular weight (HMW) bands, both greater than 460 kDa (as determined by comparison with protein standards) (Figure 6.1B). Concurrent with the appearance of these HMW bands, a reduction in the 120 kDa band that corresponds to the monomeric form of IcsA was observed. The formation of similar HMW oligomers was also observed with an R-LPS strain *S. flexneri* Δ*icsA* Δ*rmlD* $IcsA_{WT}$ (RMA2107), indicating oligomerisation was independent of LPS-Oag (Figure 6.1B, Lanes 3 and 4). This oligomer formation was reversed by the addition of β-mercaptoethanol, which hydrolyses the disulphide bond formed by the cross-linker (Figure 6.1B, Lanes 2 and 4).

6.3 Negative dominance of $IcsA_i$ mutants

Assuming that IcsA forms oligomeric structures in the OM, it is possible that some $IcsA_i$ mutants when co-expressed with $IcsA_{WT}$ might exert a negative dominant effect, disrupting either IcsA export or function in ABM and intercellular spread. Hence, to enable co-expression studies, $IcsA_{WT}$ was cloned into the plasmid pBBRMCS2 (Kovach *et al*., 1995; Table 2.3), a cloning vector compatible with the pBR322-based plasmids created in Chapter Three that encode $IcsA_i$ mutants. This was achieved by digesting pIcsA (Table 2.3) with *EcoR*I and *Sal*I, and then ligating the *EcoR*I-*Sal*I fragment encoding *icsA* into the multiple cloning site of similarly digested pBBRMCS2. The ligated construct was then transformed into *E. coli* DH5α (Table 2.1) and transformants selected on the basis of Km^R Ap^S and blue/white selection (Section 2.3.2). The plasmid pBBRMCS2-*icsA* (pKMRM252) confirmed by restriction enzyme digestion, was then isolated from DH5α and electroporated into *S. flexneri* Δ*icsA* (RMA2041) to create KMRM254. The expression of IcsA from this construct was confirmed by the ability of this strain to form plaques on HeLa cell monolayers (Section 2.16.2) (Figure 6.2A).

Figure 6.1 Chemical cross-linking of IcsA in *S. flexneri* S-LPS and R-LPS strains.

Log-phase cultures of *S. flexneri* strains were treated with either 0.5% (w/v) formaldehyde (**A**) or 0.2 mM Dithio-bis (succinimidylpropionate) (DSP) (**B**), and whole-cell lysates were electrophoresed on a 7.5% SDS-PAGE and analysed by Western immunoblotting with anti-IcsA polyclonal antibody. Formaldehyde (0.5%) treated (+) and untreated (–) samples are indicated at the bottom of the figure, and these samples were either heated at 60°C for 10 min or at 100°C for 5 min prior to loading. DSP treated (+) and untreated (–) samples are indicated at the bottom of the figure, and all these sample were heated at 60°C for 10 min prior to loading. Samples represent $4x10^8$ cells.

A - Lanes 1-4: *S. flexneri* Δ*icsA* $IcsA_{WT}$ (RMA2090)

B - Lanes 1-2: *S. flexneri* Δ*icsA* $IcsA_{WT}$ (RMA2090)

Lanes 3-4: *S. flexneri* Δ*rmlD* Δ*icsA* $IcsA_{WT}$ (RMA2107)

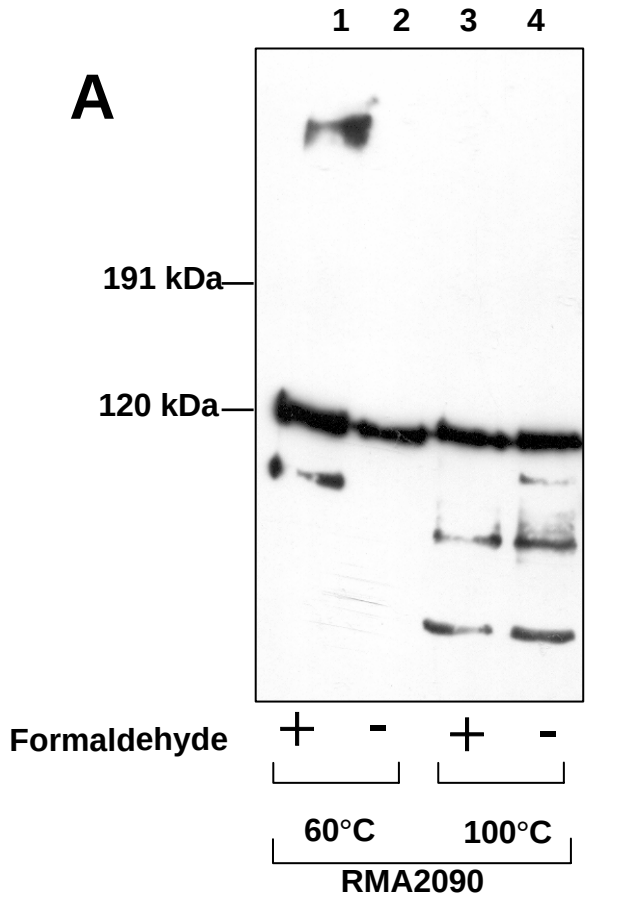
A
1 2 3 4
191 kDa
120 kDa
Formaldehyde
+ - + -
60°C
100°C
RMA2090

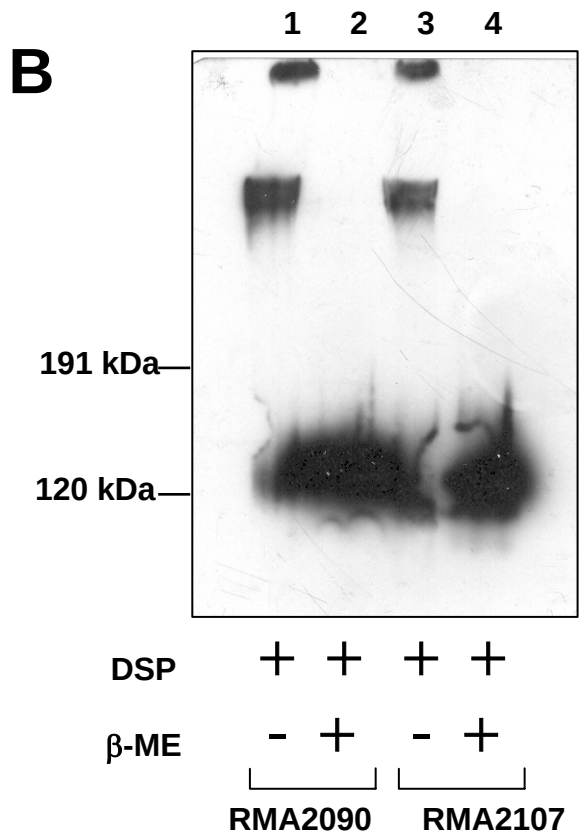
B
1 2 3 4
191 kDa
120 kDa
DSP
+ + + +
β-ME
- + - +
RMA2090
RMA2107

Figure 6.2 Plaque formation by *S. flexneri* Δ*icsA* co-expressing $IcsA_{WT}$ and $IcsA_i$ mutants.

S. flexneri strains to be examined were grown to log-phase in LB at 37°C. Bacteria were diluted and added to confluent HeLa cell monolayers. At 90 min post-infection an overlay of medium containing gentamycin and 0.5% (w/v) agarose was added. A second overlay, additionally containing 0.1% (w/v) Neutral Red solution was added at 24 h post-infection and plaque formation observed 6-8 h later. Arrows indicate plaque formation.

Panel A: *S. flexneri*Δ*icsA* $IcsA_{WT}$ (KMRM254)

Panel B: *S. flexneri*Δ*icsA* $IcsA_{WT}$ $IcsA_{WT}$ (KMRM255)

Panel C: *S. flexneri*Δ*icsA* $IcsA_{WT}$ $IcsA_{i193}$ (KMRM261)

Panel D: *S. flexneri*Δ*icsA* $IcsA_{WT}$ $IcsA_{i228}$ (KMRM260)

Panel E: *S. flexneri*Δ*icsA* $IcsA_{WT}$ $IcsA_{i248}$ (KMRM259)

Panel F: *S. flexneri*Δ*icsA* $IcsA_{WT}$ $IcsA_{i288}$ (KMRM263)

Panel G: *S. flexneri*Δ*icsA* $IcsA_{WT}$ $IcsA_{i502}$ (KMRM264)

Panel H: *S. flexneri*Δ*icsA* $IcsA_{WT}$ $IcsA_{i532}$ (KMRM257)

Panel I: *S. flexneri*Δ*icsA* $IcsA_{WT}$ $IcsA_{i563}$ (KMRM256)

Panel J: *S. flexneri*Δ*icsA* $IcsA_{WT}$ $IcsA_{i677}$ (KMRM258)

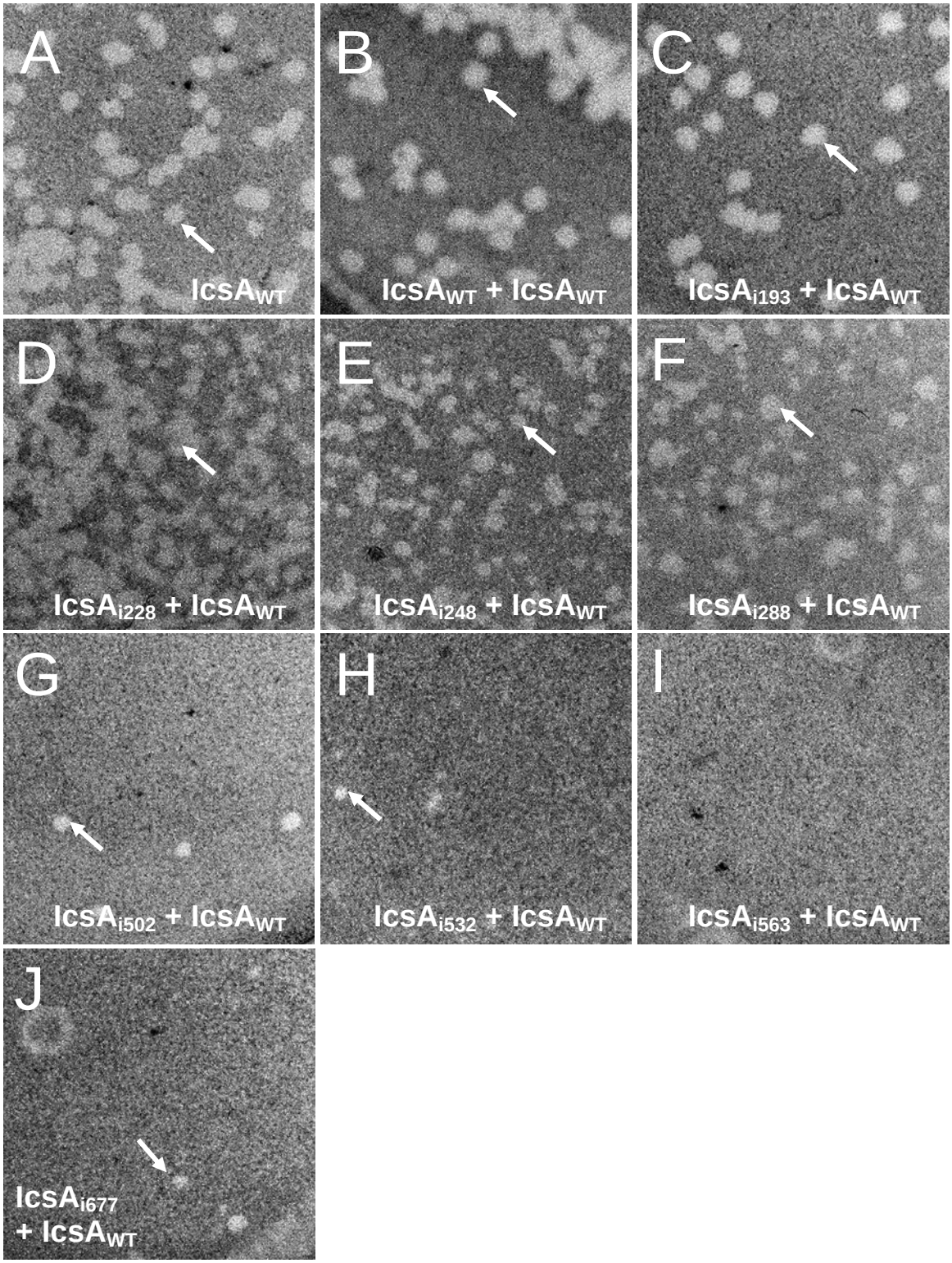
A
IcsA$_{WT}$
B
IcsA$_{WT}$ + IcsA$_{WT}$
C
IcsA$_{i193}$ + IcsA$_{WT}$
D
IcsA$_{i228}$ + IcsA$_{WT}$
E
IcsA$_{i248}$ + IcsA$_{WT}$
F
IcsA$_{i288}$ + IcsA$_{WT}$
G
IcsA$_{i502}$ + IcsA$_{WT}$
H
IcsA$_{i532}$ + IcsA$_{WT}$
I
IcsA$_{i563}$ + IcsA$_{WT}$
J
IcsA$_{i677}$
+ IcsA$_{WT}$

The plasmid pBBRMCS2-*icsA* (pKMRM252) was then transformed into the strain *S. flexneri* Δ*icsA* [pIcsA] (RMA2090; Table 2.1), which already expresses $IcsA_{WT}$ from pIcsA (Table 2.3). The resultant strain, KMRM255 (Table 2.2), was used as a control for subsequent experiments. pBBRMCS2-*icsA* (pKMRM252) was also transformed into 8 different *S. flexneri* Δ*icsA* $IcsA_i$ strains expressing either $IcsA_{i193}$ (pKMRM43), $IcsA_{i228}$ (pKMRM32), $IcsA_{i248}$ (pKMRM19), $IcsA_{i288}$ (pKMRM23), $IcsA_{i502}$ (pKMRM35), $IcsA_{i532}$ (pKMRM16), $IcsA_{i563}$ (pKMRM11), or $IcsA_{i677}$ (pKMRM34). These strains were chosen randomly from the twenty-nine strains from Chapter three (Section 3.5) that demonstrated defective plaque formation. The effect of co-expression of $IcsA_i$ mutants with $IcsA_{WT}$ on intercellular spreading and F-actin comet tail formation was then investigated.

6.3.1 Effect on Intercellular spread

To determine the effect of co-expression of $IcsA_i$ mutants with $IcsA_{WT}$ on intercellular spreading, the capacity of each strain (created in Section 6.3) to form plaques on HeLa cell monolayers was assessed (Section 2.16.2) (Figure 6.2). A summary of the results is shown in Table 6.1. *S. flexneri* Δ*icsA* co-expressing $IcsA_{i193}$ and $IcsA_{iWT}$ formed plaques that were comparable to the control strain, KMRM255 (harbouring two plasmids, both encoding $IcsA_{WT}$) (Figure 6.2B and C). *S. flexneri* Δ*icsA* co-expressing either $IcsA_{i228}$, $IcsA_{i248}$ or $IcsA_{i288}$ with $IcsA_{WT}$ formed heterogeneous sized plaques that were slightly smaller than the control strain (Figure 6.2 D-F). *S. flexneri* Δ*icsA* co-expressing either $IcsA_{i502}$, $IcsA_{i532}$ or $IcsA_{i677}$ with $IcsA_{WT}$ exhibited an approximately 50-100-fold reduction in the number of plaques and these plaques were also markedly smaller than the control strain (Figure 6.2 G, H, J). Plaques could not be detected for *S. flexneri* Δ*icsA* co-expressing $IcsA_{i563}$ with $IcsA_{WT}$. Hence, several of the $IcsA_i$ mutants exhibited a negative dominant effect on IcsA function in intercellular spreading.

Table 6.1 - Effect of co-expression of $IcsA_{WT}$ with $IcsA_i$ mutants on Intercellular spreading and F-actin comet tail formation by *S. flexneri*

KMRM Collection Number[a]	IcsA proteins	Plaque formation[b]	F-actin tail formation[c]
254	$IcsA_{WT}$	++	++
255	$IcsA_{WT}$ + $IcsA_{WT}$	++	++
261	$IcsA_{i193}$ + $IcsA_{WT}$	++	++
260	$IcsA_{i228}$ + $IcsA_{WT}$	+	++
259	$IcsA_{i248}$ + $IcsA_{WT}$	+	++
263	$IcsA_{i288}$ + $IcsA_{WT}$	+	++
264	$IcsA_{i502}$ + $IcsA_{WT}$	+/-	++
257	$IcsA_{i532}$ + $IcsA_{WT}$	+/-	+*
256	$IcsA_{i563}$ + $IcsA_{WT}$	-	++
258	$IcsA_{i677}$ + $IcsA_{WT}$	+/-	++

[a] Strain ID; *S. flexneri* Δ*icsA* (pBBRMCS2-*icsA*) strain harbouring the corresponding $IcsA_i$ mutant on a pBR322-derived plasmid.

[b] (++), (+/-), (-) indicate relative plaque sizes and frequency on HeLa cell monolayers. (++) plaque size produced by or comparable to *S. flexneri* Δ*icsA* pBBRMCS2-*icsA* (KMRM254); (+) smaller heterogeneous plaque sizes; (+/-) few, small plaques only; (-) plaque formation not detected.

[c] (++), (+) indicate relative frequency of F-actin tail formation as determined by IF microscopy. (*) F-actin comet tails had an altered morphology.

Data is based on qualitative observation of plaque formation for three independent experiments.

6.3.2 Effect on F-actin comet tail formation

To investigate whether the defects in plaque formation exhibited by strains co-expressing $IcsA_i$ proteins and $IcsA_{WT}$ (Section 6.3.1) were due to an inability to form F-actin comet tails, IF microscopy was used to assess F-actin comet tail formation inside host cells. HeLa cells were infected with log-phase cultures of *S. flexneri* Δ*icsA* co-expressing $IcsA_{WT}$ with different $IcsA_i$ proteins, and F-actin comet tail formation was visualised by staining with FITC-phalloidin, as described in Section 2.16.3. A summary of the phenotypes for each strain is shown in (Table 6.1). *S. flexneri* Δ*icsA* strains co-expressing $IcsA_{i193}$, $IcsA_{i228}$, $IcsA_{i248}$, $IcsA_{i288}$, $IcsA_{i502}$, $IcsA_{i563}$, or $IcsA_{i677,}$ with $IcsA_{WT}$, were all able to readily form F-actin comet tails (Figure 6.3). Interestingly, *S. flexneri* Δ*icsA* co-expressing $IcsA_{i532}$ and $IcsA_{WT}$ formed F-actin tails at a low frequency and these displayed an altered morphology (Figure 6.3 F) compared to *S. flexneri* Δ*icsA* co-expressing $IcsA_{WT}$ and $IcsA_{WT}$ (Figure 6.3 B). These results do not rule out a small effect on F-actin comet tail formation being sufficient to drastically reduce plaque formation efficiency. *S. flexneri icsA* mutants were identified in Chapter Three and Four that demonstrated marked reductions in plaque formation (Section 3.5), despite only slight reductions in the frequency of F-actin comet tail formation (Section 4.2).

6.4 Effect of co-expression of epitope-tagged $IcsA_{i87::FLAG}$ with $IcsA_{i563}$ and $IcsA_{i677}$ mutants

It was hypothesised that there may be an effect on expression, production, or export of $IcsA_{WT}$ when it is co-expressed with $IcsA_i$ mutants in *S. flexneri*. In order to be able to differentiate between the IcsA molecules, an epitope-tagged form of IcsA with WT function was created.

Figure 6.3 F-actin tail formation by *S. flexneri* Δ*icsA* co-expressing $IcsA_{WT}$ and $IcsA_i$ mutants.

Log-phase cultures of bacteria were added to semi-confluent monolayers of HeLa cells grown on glass coverslips. After centrifugation monolayers were incubated for 60 min to allow invasion, then 90 min in medium containing 40 µg/mL gentamycin. Monolayers were washed, formalin fixed, permeabilised with 0.1% Triton X-100 in PBS, and blocked with 10% FCS in PBS. Bacteria were labelled with anti-LPS antibody and Alexa 594-conjugated donkey anti-rabbit (red) and F-actin was labelled with FITC-phalloidin (green). The coverslips were mounted on glass microscope slides and examined with an Olympus IX-70 microscope with phase-contrast optics using 100x oil immersion objective with a 1.5x enlarger. Alexa 594 and FITC-phalloidin, images were false colour merged using Metamorph (Version 6.3r7, Molecular devices). Arrows indicate F-actin tail formation. Strains were assessed in 3 independent experiments. Scale bars indicate 10 µm.

Panel A: *S. flexneri*Δ*icsA* $IcsA_{WT}$ $IcsA_{WT}$ (KMRM255)

Panel B: *S. flexneri*Δ*icsA* $IcsA_{WT}$ $IcsA_{i228}$ (KMRM260)

Panel C: *S. flexneri*Δ*icsA* $IcsA_{WT}$ $IcsA_{i248}$ (KMRM259)

Panel D: *S. flexneri*Δ*icsA* $IcsA_{WT}$ $IcsA_{i288}$ (KMRM263)

Panel E: *S. flexneri*Δ*icsA* $IcsA_{WT}$ $IcsA_{i502}$ (KMRM264)

Panel F: *S. flexneri*Δ*icsA* $IcsA_{WT}$ $IcsA_{i532}$ (KMRM257)

Panel G: *S. flexneri*Δ*icsA* $IcsA_{WT}$ $IcsA_{i563}$ (KMRM256)

Panel H: *S. flexneri*Δ*icsA* $IcsA_{WT}$ $IcsA_{i677}$ (KMRM258)

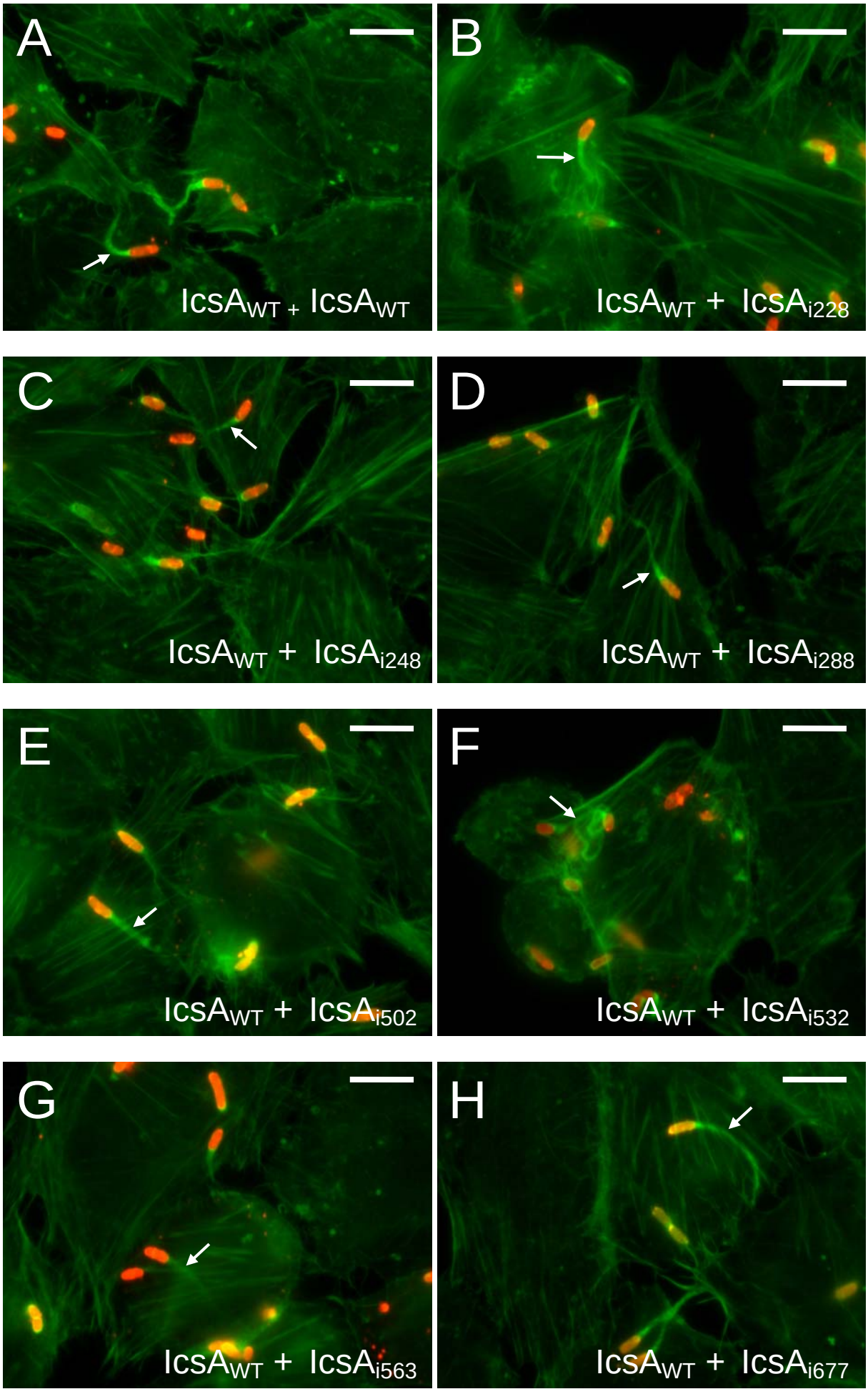
A
IcsA$_{WT}$ + IcsA$_{WT}$
B
IcsA$_{WT}$ + IcsA$_{i228}$
C
IcsA$_{WT}$ + IcsA$_{i248}$
D
IcsA$_{WT}$ + IcsA$_{i288}$
E
IcsA$_{WT}$ + IcsA$_{i502}$
F
IcsA$_{WT}$ + IcsA$_{i532}$
G
IcsA$_{WT}$ + IcsA$_{i563}$
H
IcsA$_{WT}$ + IcsA$_{i677}$

6.4.1 Epitope tagging of IcsA$_{i87}$

Sites permissive for epitope were identified in Chapter Three. Mutant IcsA$_{i87}$ when expressed in *S. flexneri* was found to be comparable to IcsA$_{WT}$ with respect to levels of production, polar localisation on the surface of bacteria and function as determined by the plaque assay. Therefore, mutant IcsA$_{i87}$ was chosen as a target for epitope insertion. A synthetic FLAG epitope (DYKDDDDK) was inserted into pKMRM1, the plasmid encoding IcsA$_{i87}$, as described in Sections 2.9.1-2.9.4. Briefly, complementary oligonucleotides encoding the FLAG epitope (IcsA_FLAG_R1 and IcsA_FLAG_R1; Table 2.4) were annealed together and resultant dsDNA with the appropriate 5' overhang was ligated into the unique *Not*I site within the linker-insertion region of pKMRM1. This construct was confirmed by DNA sequencing using primer 2156 IcsAF (Table 2.4) (Section 2.6.5). This construct pKMRM1::FLAG (pKMRM250) was sub-cloned (as for Section 6.3) into pBBRMCS2 and the resultant pBBRMCS2-IcsA$_{i87::FLAG}$ (pKMRM270) was transformed into *S. flexneri* Δ*icsA* (RMA2041) to produce *S. flexneri* Δ*icsA* IcsA$_{i87::FLAG}$ (KMRM273). Expression of the epitope tagged construct in *S. flexneri* was confirmed by Western immunoblotting of whole-cell lysates (Sections 2.12.1, 2.12.4 & 2.12.6) (used as a control in Figure 6.6, Lane 1), and indirect IF of whole bacteria (Sections 2.12.7) with anti-FLAG M2 antibody (Section 2.1.1) (Figure 6.4). The IcsA$_{i87::FLAG}$ protein was detected on the surface of *S. flexneri* and was distributed in a polar fashion. Additionally, *S. flexneri* Δ*icsA* IcsA$_{i87::FLAG}$ (KMRM273) was able to spread intercellularly, as demonstrated by plaque formation on HeLa cell monolayers (Section 2.16.2) (Figure 6.5A). The latter result indicated that IcsA$_{i87::FLAG}$ was fully functional.

6.4.2 Co-expression of IcsA$_{i87::FLAG}$ with IcsA$_{i563}$ and IcsA$_{i677}$ mutants

As IcsA$_{i563}$ and IcsA$_{i677}$ exerted a clear negative dominant effect on IcsA$_{WT}$ function in intercellular spreading (Table 6.1), these two mutant proteins were chosen for further co-expression studies in subsequent Sections. The apparent negative dominance of IcsA$_{i677}$ was

Figure 6.4 Expression of $IcsA_{i87::FLAG}$ on the surface of *S. flexneri* Δ*icsA*.

S. flexneri strains to be examined were grown to log-phase in LB at 37°C. Bacteria were formalin fixed and centrifuged onto poly-L-lysine-coated coverslips. Bacteria were incubated with anti-FLAG M2 monoclonal antibody and incubated with Alexa 488-conjugated donkey anti-mouse antibody (green). The coverslips were mounted on glass microscope slides and examined with an Olympus IX-70 microscope with phase-contrast optics using a 100 x oil immersion, objective with a 1.5 x enlarger. Phase-contrast (**A** and **D**) and Alexa-488 (**B** and **E**) images were false colour merged using Metamorph (**C** and **F**). Scale bars indicate 10 μm.

Panel A-C: *S. flexneri* Δ*icsA* $IcsA_{i87::FLAG}$ (KMRM273)

Panel D-E: *S. flexneri* Δ*icsA* $IcsA_{WT}$ (RMA2090)

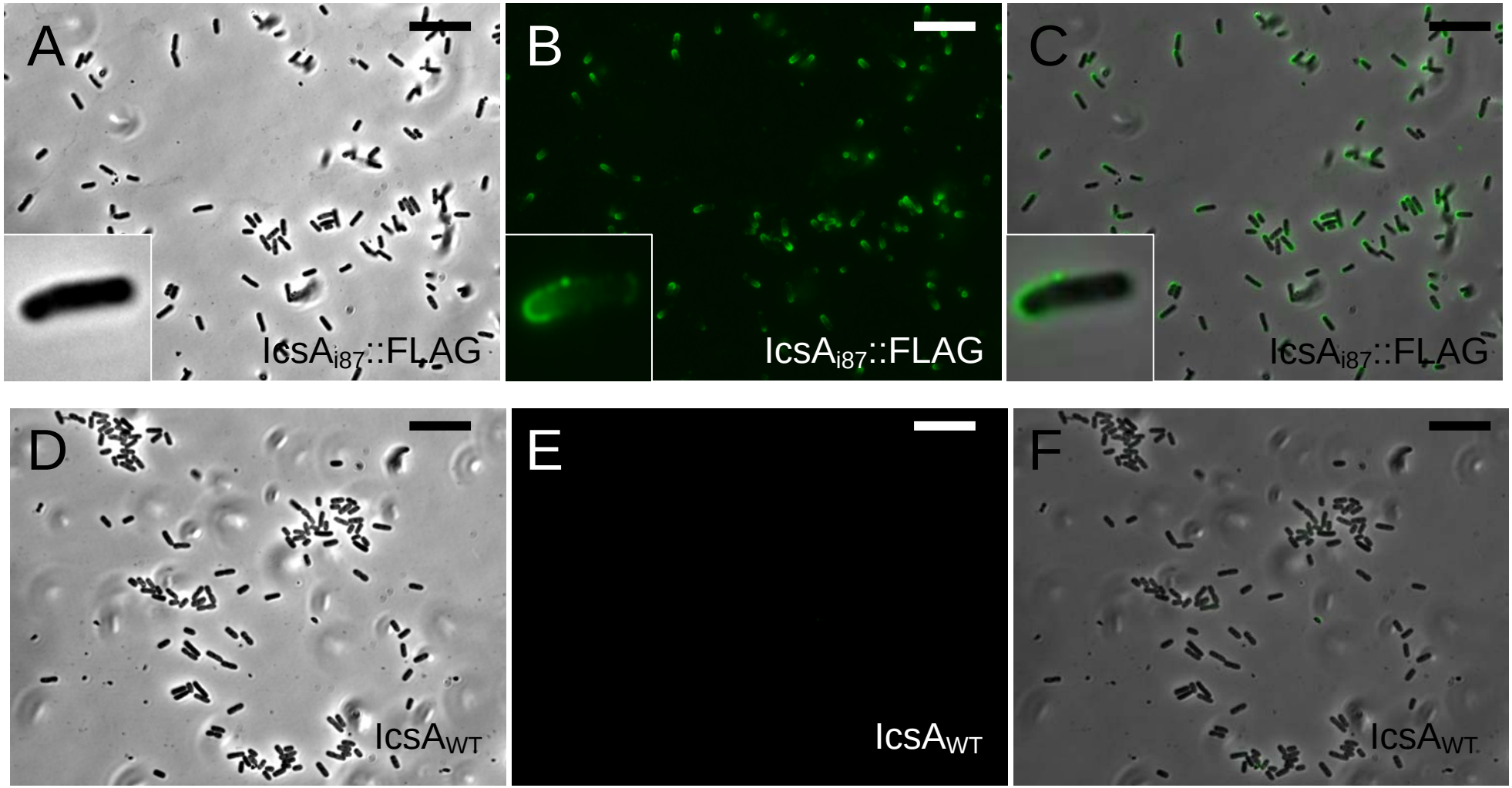
A
IcsA$_{i87}$::FLAG
B
IcsA$_{i87}$::FLAG
C
IcsA$_{i87}$::FLAG
D
IcsA$_{WT}$
E
IcsA$_{WT}$
F
IcsA$_{WT}$

Figure 6.5 Plaque formation by *S. flexneri* Δ*icsA* co-expressing IcsA$_{i87::FLAG}$ and IcsA$_{i}$ mutants.

S. flexneri strains to be examined were grown to log-phase in LB at 37°C. Bacteria were diluted and added to confluent HeLa cell monolayers. At 90 min post-infection an overlay of medium containing gentamycin and 0.5% (w/v) agarose was added. A second overlay, additionally containing 0.1% (w/v) Neutral Red solution was added at 24 h post-infection and plaque formation observed 6-8 h later. Arrows indicate plaque formation.

Panel A: *S. flexneri*Δ*icsA* IcsA$_{i87::FLAG}$ (KMRM273)

Panel B: *S. flexneri*Δ*icsA* IcsA$_{i87::FLAG}$ IcsA$_{WT}$ (KMRM275)

Panel C: *S. flexneri*Δ*icsA* IcsA$_{i87::FLAG}$ IcsA$_{i563}$ (KMRM276)

Panel D: *S. flexneri*Δ*icsA* IcsA$_{i87::FLAG}$ IcsA$_{i677}$ (KMRM277)

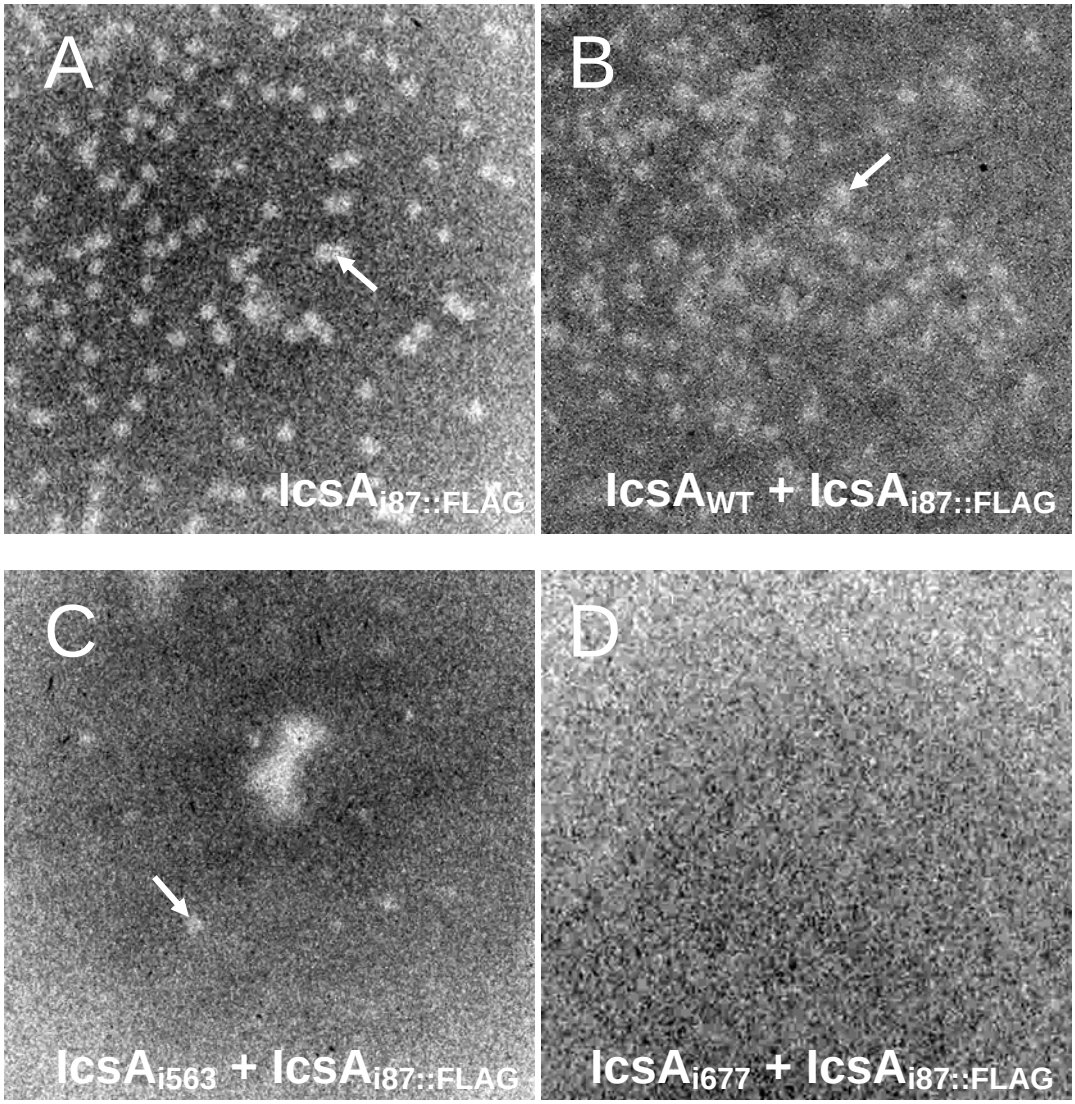
A
IcsA$_{i87::FLAG}$
B
IcsA$_{WT}$ + IcsA$_{i87::FLAG}$
C
IcsA$_{i563}$ + IcsA$_{i87::FLAG}$
D
IcsA$_{i677}$ + IcsA$_{i87::FLAG}$

particularly interesting as this mutant protein possesses a linker-insertion within the putative auto-chaperone region of IcsA (aa 643-735), was produced at very low levels in *S. flexneri* (Section 3.3), and could not be detected on the surface of bacteria (Section 3.4). Hence, the plasmid encoding $IcsA_{i87::FLAG}$ (pKMRM270; Table 2.3) was electroporated into *S. flexneri* Δ*icsA* expressing $IcsA_{i532}$ (KMRM111; Table 2.2) and *S. flexneri* Δ*icsA* expressing $IcsA_{i677}$ (KMRM134; Table 2.2) to produce KMRM276 and KMRM277, respectively. For comparison, pKMRM270 was also electroporated into *S. flexneri* Δ*icsA* expressing $IcsA_{WT}$ (RMA2090), to produce *S. flexneri* Δ*icsA* expressing both $IcsA_{WT}$ and $IcsA_{i87::FLAG}$ (KMRM275).

6.4.3 Effect on intercellular spread

Firstly, the aim was to confirm that the same negative dominant effect on plaque formation is observed when $IcsA_{i532}$ and $IcsA_{i677}$ are co-expressed with $IcsA_{i87::FLAG}$ in *S. flexneri*, to that which was observed when these $IcsA_i$ mutants were co-expressed with $IcsA_{WT}$ in Section 6.3.1 Therefore, the ability of *S. flexneri* Δ*icsA* expressing $IcsA_{i563}$ and $IcsA_{i87::FLAG}$ (KMRM276), *S. flexneri* Δ*icsA* expressing $IcsA_{i677}$ and $IcsA_{i87::FLAG}$ (KMRM277), and *S. flexneri* Δ*icsA* expressing $IcsA_{WT}$ and $IcsA_{i87::FLAG}$ (KMRM275) to form plaques on HeLa cell monolayers was examined (Section 2.16.2). The co-expression of either $IcsA_{i563}$ or $IcsA_{i677}$ with $IcsA_{i87::FLAG}$ produced a negative dominant effect. KMRM276 exhibited both a marked reduction in plaque size and an approximately 50-100-fold reduction in the number of plaques compared to the control strain (Figure 6.5C). Notably, KMRM277 was unable to form detectable plaques (Figure 6.5D) (Table 6.2). This was in contrast to *S. flexneri* Δ*icsA* expressing $IcsA_{WT}$ and $IcsA_{i87::FLAG}$ (KMRM275), which readily formed plaques (Figure 6.5B) that were only slightly smaller than *S. flexneri* Δ*icsA* expressing $IcsA_{i87::FLAG}$ alone (KMRM273; Figure 6.5A).

Table 6.2 - Effect of co-expression of $IcsA_i$ mutants on $IcsA_{i87::FLAG}$ function in plaque formation on HeLa cell monolayers, and production and surface expression in *S. flexneri*

KMRM Collection Number[a]	IcsA proteins	Plaque formation[b]	$IcsA_{i87::FLAG}$ production[c]	$IcsA_{i87::FLAG}$ surface expression[d]
273	$IcsA_{i87::FLAG}$	+++	+	+
275	$IcsA_{iWT+}$ $IcsA_{i87::FLAG}$	++	+	+
276	$IcsA_{i563+}$ $IcsA_{i87::FLAG}$	+/-	+	+
277	$IcsA_{i1677+}$ $IcsA_{i87::FLAG}$	-	+	+
RMA2041	-	-	-	-

[a] Strain ID; *S. flexneri* Δ*icsA* strain harbouring the corresponding IcsA proteins on a multi-copy number plasmid(s).

[b] (+++), (++), (+), (+/-) ,(-) indicate relative plaque sizes and frequency on HeLa cell monolayers. (+++) plaque size produced by *S. flexneri* Δ*icsA* $IcsA_{i87::FLAG}$ (KMRM273); (++) slight reduction in plaque size compared to KMRM273; (+) marked reduction in plaque size; (+/-) marked reduction in plaque size and 50-100-fold reduction in number of plaques; (-) plaque formation not detected.

[c] (+) and (-) indicate relative levels of production of $IcsA_{i87::FLAG}$ as determined by Western immunoblotting with anti-FLAG M2 antibody. (+) production comparable to KMRM273; (-) production not detected.

[d] (+)and (-) indicate relative levels of $IcsA_{i87::FLAG}$ expression on the surface of bacteria as determined by indirect immunofluorescence with anti-FLAG M2 antibody. (+) surface expression comparable to KMRM273. (-) surface expression not detected.

Data is based on qualitative observation for three independent experiments.

6.4.4 Detection of $IcsA_{i87::FLAG}$ co-expressed with $IcsA_{i532}$ and $IcsA_{i677}$ mutants by Western immunoblotting

In order to examine the effect on $IcsA_{i87::FLAG}$ protein production arising from the co-expression of $IcsA_i$ mutants, SDS-PAGE and Western immunoblotting with anti-FLAG M2 antibody was performed on whole cell lysates of log-phase cultures of the strains used above in Section 6.4.1 (Sections 2.12.1, 2.12.4, 2.12.6). Production of $IcsA_{i87::FLAG}$ when co-expressed with $IcsA_{WT}$ in *S. flexneri* Δ*icsA* was comparable to production of $IcsA_{i87::FLAG}$ when expressed alone (Figure 6.6, Lanes 1 and 6). Co-expression of $IcsA_{i563}$ with $IcsA_{i87::FLAG}$ in *S. flexneri* Δ*icsA* resulted in a slight reduction in $IcsA_{i87::FLAG}$ production (Figure 6.6, Lane 4) compared to *S. flexneri* Δ*icsA* $IcsA_{WT}$ $IcsA_{i87::FLAG}$ (Figure 6.6, Lane 6). Co-expression of $IcsA_{i677}$ with $IcsA_{i87::FLAG}$ in *S. flexneri* Δ*icsA* resulted in $IcsA_{i87::FLAG}$ production that was comparable to *S. flexneri* Δ*icsA* $IcsA_{WT}$ $IcsA_{i87::FLAG}$ (Figure 6.6, Lane 5); this was in spite of the fact that plaque formation could not be detected for *S. flexneri* Δ*icsA* $IcsA_{677}$ $IcsA_{i87::FLAG}$ whilst *S. flexneri* Δ*icsA* $IcsA_{WT}$ $IcsA_{i87::FLAG}$ readily formed plaques (Figure 6.5; Table 6.2).

Additionally, Western immunoblotting of $IcsA_{i87::FLAG}$ expressed from pKMRM1::FLAG (pKMRM250) (Figure 6.6, Lane 3) indicated that it was comparable to production of this same protein expressed from pBBRMCS2-$IcsA_{i87::FLAG}$ (pKMRM270) (Figure 6.6, Lane 1). This confirms the suitability of the plasmids for use in co-expression studies.

6.4.5 Detection of $IcsA_{i87}$::FLAG when co-expressed with $IcsA_{i563}$ and $IcsA_{i677}$ on the surface of *S. flexneri*

Next, the aim was to elucidate if co-expression of $IcsA_i$ mutants had an effect on the expression, and/or the localisation of the $IcsA_{i87::FLAG}$ protein on the surface of bacteria. Hence, log-phase cultures of *S. flexneri* Δ*icsA* co-expressing $IcsA_{i87::FLAG}$ and $IcsA_{WT}$

Figure 6.6 Western blot analysis of $IcsA_{i87::FLAG}$ production.

S. flexneri strains to be examined were grown to log-phase in LB at 37°C. Whole-cell lysates were prepared, and electrophoresed on a 7.5% SDS-PAGE gel, and subjected to Western blot analysis with anti-FLAG M2 monoclonal antibody. The ~116 kDa band corresponds to full-length $IcsA_{i87::FLAG}$ and the ~95 kDa band corresponds to the cleaved form (i.e. $IcsA_{i87::FLAG}'$). Samples represent the equivalent of 1 x 10^8 cells.

Lane 1: *S. flexneri* Δ*icsA* $IcsA_{i87::FLAG}$[a] (KMRM273)

Lane 2: *S. flexneri* Δ*icsA* $IcsA_{WT}$ (RMA2090)

Lane 3: *S. flexneri* Δ*icsA* $IcsA_{i87::FLAG}$[b] (KMRM268)

Lane 4: *S. flexneri* Δ*icsA* $IcsA_{i87::FLAG}$[a] $IcsA_{i563}$ (KMRM276)

Lane 5: *S. flexneri* Δ*icsA* $IcsA_{i87::FLAG}$[a] $IcsA_{i677}$ (KMRM277)

Lane 6: *S. flexneri* Δ*icsA* $IcsA_{i87::FLAG}$[a] $IcsA_{WT}$ (KMRM275)

[a] $IcsA_{i87::FLAG}$ expressed from pBBRMCS2-$IcsA_{i87::FLAG}$ (pKMRM270).

[b] $IcsA_{i87::FLAG}$ expressed from pKMRM1::FLAG (pKMRM250).

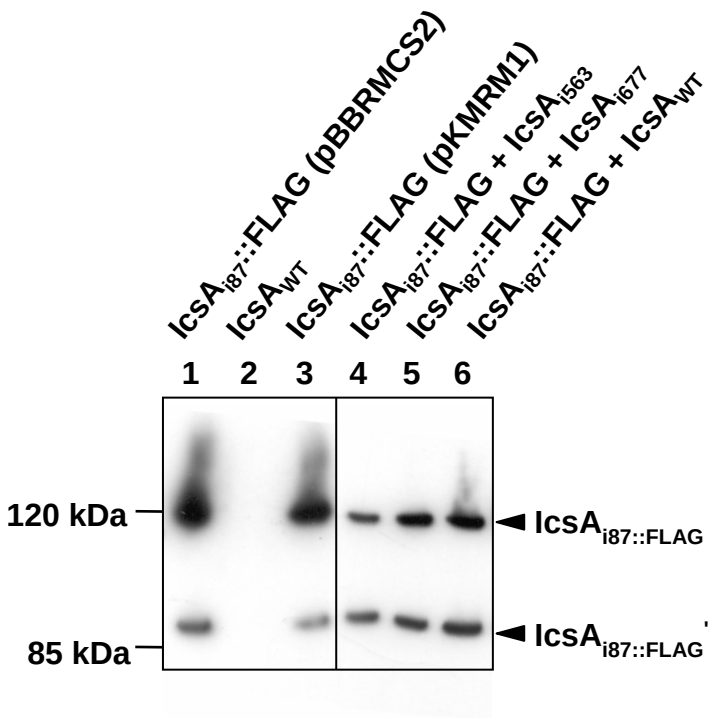
IcsA$_{i87}$::FLAG (pBBRMCS2)
IcsA$_{WT}$
IcsA$_{i87}$::FLAG (pKMRM1)
IcsA$_{i87}$::FLAG + IcsA$_{i563}$
IcsA$_{i87}$::FLAG + IcsA$_{i677}$
IcsA$_{i87}$::FLAG + IcsA$_{WT}$
1 2 3 4 5 6
120 kDa
85 kDa
IcsA$_{i87::FLAG}$
IcsA$_{i87::FLAG}$'

(KMRM275), *S. flexneri* Δ*icsA* co-expressing $IcsA_{i87::FLAG}$ and $IcsA_{i563}$ (KMRM276), *S. flexneri* Δ*icsA* co-expressing $IcsA_{i87::FLAG}$ and $IcsA_{i677}$ (KMRM277) and a negative control strain of *S. flexneri* Δ*icsA* expressing $IcsA_{WT}$ (RMA2090) were formalin fixed and analysed by immunofluorescence (IF) microscopy with anti-FLAG M2 (Section 2.12.7). Although a slight difference in $IcsA_{i87::FLAG}$ production between and KMRM275 and KMRM276 was detected by Western immunoblotting (Section 6.4.4; Figure 6.6), for both of these strains, as well as KMRM277, the $IcsA_{i87::FLAG}$ protein could be readily detected on the surface of each *S. flexneri* strain producing $IcsA_{i87::FLAG}$ (Figure 6.7) (Table 6.2).

6.7 Summary

In this Chapter, the hypothesis that IcsA is able to oligomerise was investigated using chemical cross-linking and examining potential negative dominance effects of co-expressing mutant $IcsA_i$ proteins with $IcsA_{WT}$. Two high molecular weight complexes containing IcsA were detected upon treatment of *S. flexneri* with the chemical cross-linker DSP (Figure 6.1B). This is the first time this has been reported for IcsA. Although this data suggests that IcsA forms oligomeric structures the fact that these complexes may comprise a heterogeneous population of proteins can not be excluded. Additional biochemical evidence of an IcsA-IcsA interaction and experiments such as pull-downs and co-immunoprecipitation are required. However, several $IcsA_i$ mutants ($IcsA_{i228}$, $IcsA_{i248}$, $IcsA_{i288}$, $IcsA_{i502}$, $IcsA_{i532}$, $IcsA_{i563}$ and $IcsA_{i677}$) had an apparent negative dominant effect on $IcsA_{WT}$ function in intercellular spreading when these proteins were co-expressed in *S. flexneri* (Figure 6.2) This demonstrates that an IcsA-IcsA protein interaction is occurring. Two of these mutants ($IcsA_{i563}$ and $IcsA_{i677}$) were found to exert a negative dominant effect on $IcsA_{WT}$/ $IcsA_{i87::FLAG}$ that was independent of any effect on $IcsA_{WT}$ production, export and polar localisation (Figure 6.6 and 6.7; Table 6.2). These results suggest that these $IcsA_i$ mutants directly inhibit function of $IcsA_{WT}$ in ABM. $IcsA_{i563}$ possesses a linker-insertion within polar localisation region #2 (aa

Figure 6.7 Expression IcsA$_{i87::FLAG}$ on the surface of *S. flexneri* strains.

S. flexneri strains to be examined were grown to log-phase in LB at 37°C. Bacteria were formalin fixed and centrifuged onto poly-L-lysine-coated coverslips. Bacteria were incubated with anti-FLAG M2 monoclonal antibody and incubated with Alexa 488-conjugated donkey anti-mouse secondary antibody. The coverslips were mounted on glass microscope slides and examined with an Olympus IX-70 microscope with phase-contrast optics using a 100 x oil immersion, objective with a 1.5 x enlarger. Phase-contrast (**A, D, G**, **J**) and Alexa 488 (**B, E, H**, **K**) images were false colour merged using Metamorph (Version 6.3r7, Molecular devices) (**C, F, I, L**). Scale bars indicate 5 μm.

Panel A-C: *S. flexneri* Δ*icsA* IcsA$_{i87::FLAG}$ IcsA$_{WT}$ (KMRM275)

Panel D-F: *S. flexneri* Δ*icsA* IcsA$_{i87::FLAG}$ IcsA$_{i563}$ (KMRM276)

Panel G-I: *S. flexneri* Δ*icsA* IcsA$_{i87::FLAG}$ IcsA$_{i677}$ (KMRM277)

Panel J-L: *S. flexneri* Δ*icsA* IcsA$_{WT}$ (RMA2090)

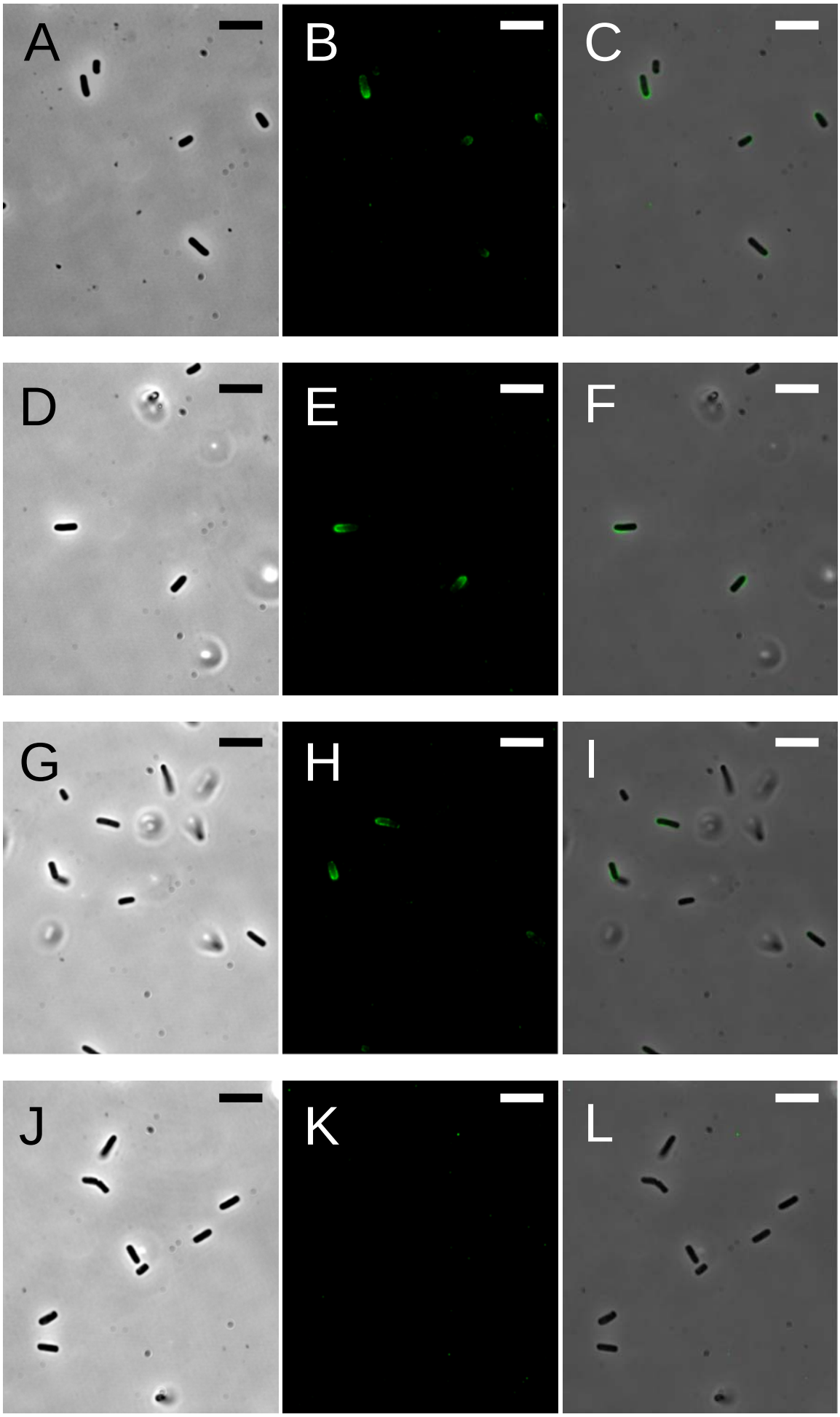
A
B
C
D
E
F
G
H
I
J
K
L

507-620), and in addition to having a localisation defect it is unable to interact with N-WASP when expressed in *S. flexneri* Δ*icsA*. Since co-expression of $IcsA_{i563}$ did not affect localisation of $IcsA_{WT}$ / $IcsA_{i87::FLAG}$, this would suggest the negative dominant effect is related to the latter phenotype. $IcsA_{i677}$ possesses a linker-insertion within a putative auto-chaperone region (aa 634-735), is produced at very low levels by *S. flexneri*, and cannot be detected on the surface of bacteria. As co-expression of $IcsA_{i677}$ did not affect production of $IcsA_{WT}$/$IcsA_{i87::FLAG}$ the molecular basis of the negative dominant effect of this mutant is unclear. However, for other AT proteins (SSP, BrkA and Pet) expression of a native auto-chaperone region alone in *trans* can compensate mutants of these proteins lacking this region (Ohnishi *et al*., 1994; Oliver *et al*., 2003; Dutta *et al*., 2003). Perhaps the mutated auto-chaperone region of $IcsA_{i677}$ exerts a direct affect on folding of $IcsA_{WT}$/$IcsA_{i87::FLAG.}$

Chapter Seven

Investigation of LPS distribution in *Escherichia coli* bacteria

Chapter Seven: Investigation of LPS distribution in *Escherichia coli* bacteria

7.1 Introduction

The lipopolysaccharide (LPS) molecules on the surface of *Shigella* are non-uniform, and have variable O-antigen (Oag) chain lengths. Usually, most of the LPS molecules have Oag chain lengths clustered around a modal value (Goldman and Hunt, 1990). *S. flexneri* serotype 2a has LPS with two modal chain lengths: an S-type (12-17 Oag repeat units), that is dependent on the chromosomally encoded Wzz_{SF}, and a VL-type (>90 Oag repeat units) determined by the virulence plasmid-encoded Wzz_{pHS-2} (Hong and Payne, 1997).

Recent studies involving *S. flexneri* strains showed that newly synthesised IcsA can be detected on lateral regions as well as the old pole, and that its detection with antibodies on lateral regions was masked by Oag chains (Morona *et al*., 2003; Morona and Van Den Bosch, 2003b). The observation that IcsA is readily detected at the poles in WT *S. flexneri* and is not masked by the presence of VL-type LPS Oag may be explained by two hypotheses. Firstly, the IcsA protein is more concentrated at the bacteria cell poles. In support of this hypothesis, immunogold labelling of a R-LPS *S. flexneri rmlD* mutant, where Oag is not present to mask IcsA, has shown that IcsA is still detected more readily at the poles than the lateral regions (Van Den Bosch *et al*., 1997). However a second hypothesis, not yet investigated, is that the LPS profile may be different at the poles compared to the lateral regions of the bacterium, with either a higher ratio of S-type S-LPS to VL-type S-LPS, or R-LPS to S-LPS molecules. Whether or not the distribution of R-LPS and S-LPS, and S-LPS with different Oag modal lengths is uniform over the entire surface of the bacterium is not known. Current models for

the interaction between LPS Oag and IcsA (and hence the role of LPS in ABM) are based on the assumption that there is a uniform distribution of the different LPS populations on the surface of *S. flexneri*. Therefore, it was of interest to determine if the LPS profile on the surface of *S. flexneri* is the same at the old pole as it is at the lateral regions of the bacterium.

To obtain LPS representation of the old cell pole, minicells were investigated. Minicell mutants have a mutation that results in incorrect placement of the division septum, such that septation occurs close to the old cell pole to form spherical, anucleate minicells. Interestingly, a minicell-producing mutant of *S. flexneri* has been shown to form plaques and F-actin comet tails, suggesting that such a mutation has no significant affects on virulence and ABM (Gemski and Griffin *et al*., 1980). The LPS profile of minicells derived from S-LPS bacteria has not been reported before. The aims of this chapter were to prepare minicells derived from the old cell pole of *S. flexneri* and *E. coli* K-12 (producing LPS with *S. flexneri* Oag), and examine their LPS profiles.

7.2 Construction of a minicell mutant

7.2.1 Construction of a suicide vector encoding a disrupted *minD* gene

Allelic-exchange mutagenesis was undertaken to create minicell-producing mutants of *S. flexneri* 2457T (Table 2.1) by replacing the chromosomally encoded *minD* with a disrupted copy. To accomplish this, a suicide vector encoding a disrupted copy of *minD* was created. A flow diagram outlining the creation of this construct is shown in Figure 7.1.

PCR (Section 2.7.2) was performed using primers minF and minR (Table 2.4) to amplify the *min* locus from *S. flexneri* 2457T chromosomal DNA isolated according to Section 2.5.1 (Figure 7.1 – [1]). The 2064 bp amplified DNA comprised the *minCDE* coding region as well as 98 bp upstream and 164 bp downstream. As disruption of *minD* leads to a

Figure 7.1 Construction of pCACTUS-*minD::*Km^R (pKMRM180a).

[1] The *minCDE* coding region from *S. flexneri* 2457T was PCR amplified using primers minF and minR. **[2]** The kanamycin-resistance (Km^R) cartridge was PCR amplified from pKD4 DNA with primers P1_*Pac*I and P2_*Pac*I (Table 2.4) to incorporate *Pac*I restriction sites at either end of the amplified fragment. **[3]** Both PCR fragments were, ligated into pGEMT-Easy (Promega) to yield pGEMT-*minCDE* (pKMRM96) and pGEMT-Km$^R{}_{PacI}$ (pKMRM99). **[4]** pGEMT-*minCDE* (pKMRM96) and pGEMT-Km$^R{}_{PacI}$ (pKMRM99) were digested with *Pac*I and the Km^R cartridge was ligated into the *Pac*I linearised pGEMT-*minCDE* (pKMRM96). **[5]** The *minCDE*::Km^R fragment was PCR amplified from pGEMT-*minCDE*::Km^R with primers minF_*BamH*I and minR_*BamH*I to incorporate *BamH*I restriction sites at either end of the amplified fragment. **[6]** This fragment was ligated into the BamHI site of the suicide vector, pCACTUS to yield the pCACTUS-*minCDE*::Km^R construct (pKMRM180a).

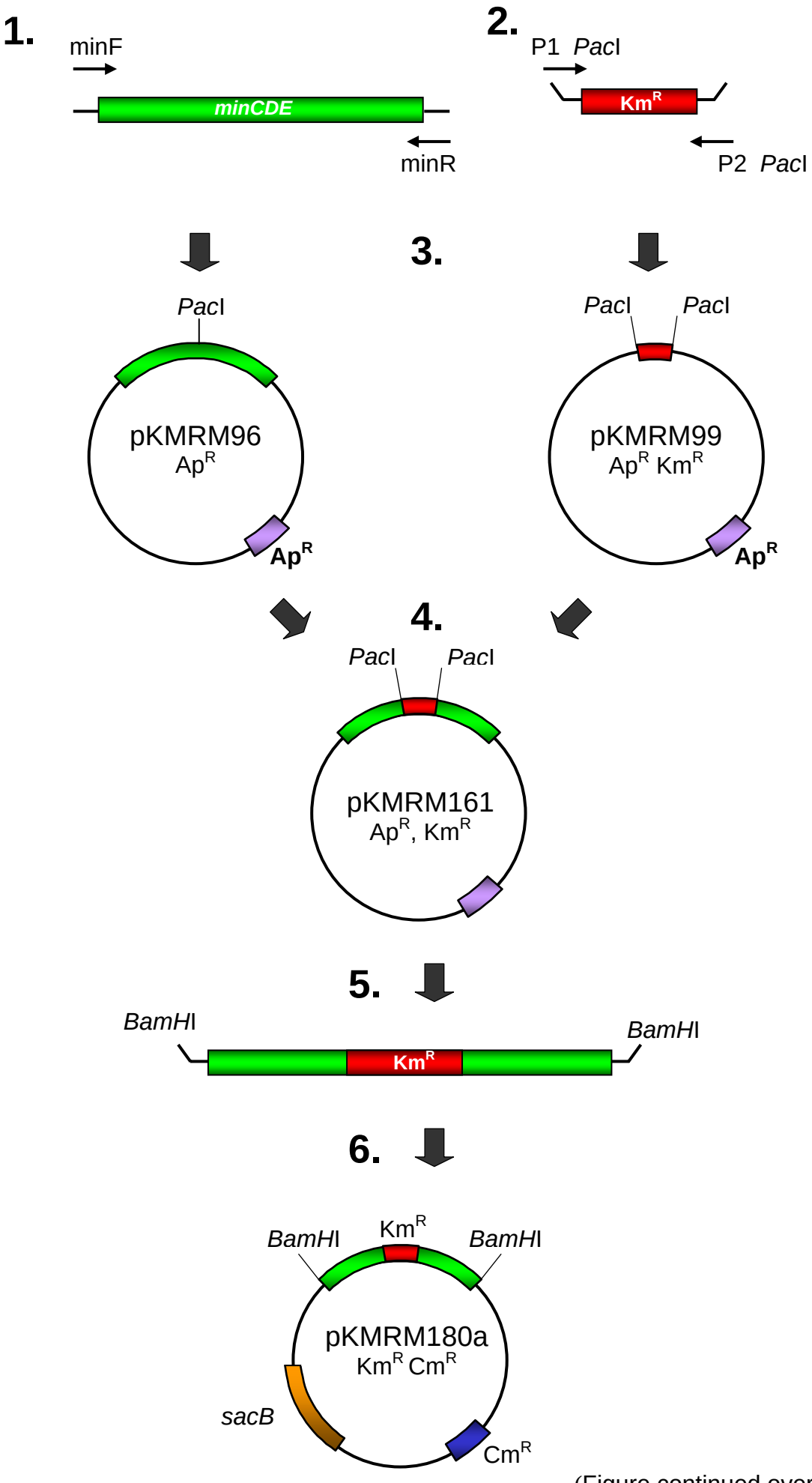

(Figure continued over page)

Figure 7.1 (Cont'd) Construction of pCACTUS-*minD::*Km^R (pKMRM180a).

[7] Allelic-exchange mutagenesis was undertaken using this construct itself and additionally this construct was used as a PCR template **[8]** for Lambda Red recombinase mediated mutagenesis **[9]**.

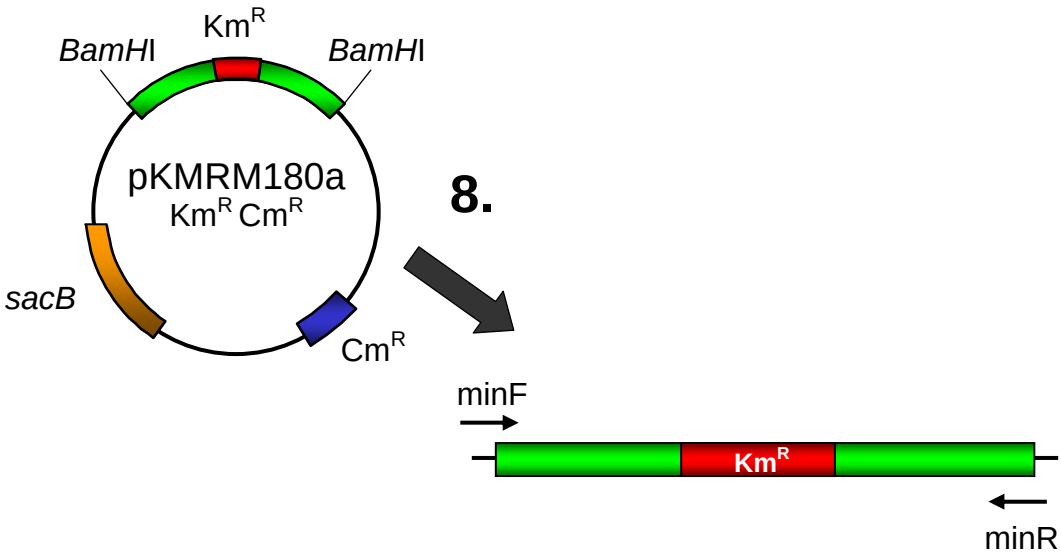

7.

9.

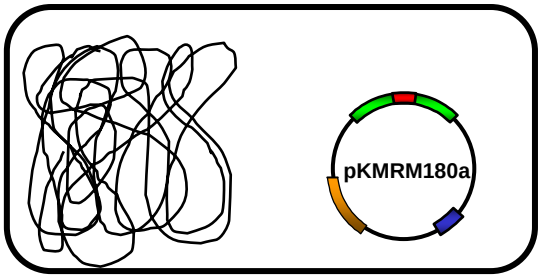

***S. flexneri* 2457T**
and
***E. coli* UT5600**

Allelic-exchange mutagenesis using pCACTUS-based system

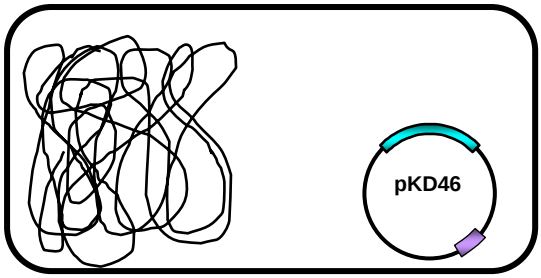

***S. flexneri* 2457T**
and
***E. coli* UT5600**

Allelic-exchange mutagenesis using λ Red phage mutagenesis system

minicell phenotype (de Boer *et al*., 1989), a native *Pac*I restriction site within the coding region of *minD* was chosen as a target site for insertion of an antibiotic resistance cartridge to inactivate the gene. A 1493 bp fragment, comprising a kanamycin-resistance (Km^R) cartridge and flanking FRT (FLP recognition target) sites, was amplified by PCR (Section 2.7.2) from pKD4 plasmid DNA (Table 2.3; Section 2.5.2) (Figure 7.1 – [2]). To facilitate cloning of the Km^R cartridge, PCR was performed using primers P1_*Pac*I and P2_*Pac*I (Table 2.4) to incorporate *Pac*I restriction sites at either end of the amplified fragment. Both PCR fragments were purified (Section 2.8.2), ligated into pGEMT-Easy (Promega; Table 2.3; Section 2.9.4) and transformed into chemically competent *E. coli* DH5α (Sections 2.10.1 and 2.10.2) (Figure 7.1 – [3]). After screening transformants on the basis of blue/white selection (Section 2.3.2) and Ap^R for DH5α [pGEMT-*minCDE*] (KMRM96), and Ap^R and Km^R for DH5α [pGEMT-Km^R_{PacI}] (KMRM99), plasmids pKMRM96 and pKMRM99 with the expected inserts were obtained (Section 2.5.2).

Subsequently, plasmids pGEMT-*minCDE* (pKMRM96) and pGEMT-Km^R_{PacI} (pKMRM99) were digested with *Pac*I (Section 2.6.2). The digested fragment comprising the Km^R cartridge was purified by gel extraction (Section 2.8.1), ligated into the *Pac*I linearised pGEMT-*minCDE* (pKMRM96) and transformed into *E. coli* DH5α as before. Ap^R and Km^R transformants were screened by PCR with primers minF and minR, and plasmid DNA was prepared from a transformant that yielded an amplicon of approximately 3549 bp, corresponding to the *minCDE*::Km^R fragment (Figure 7.1 – [4]).

The *minCDE*::Km^R fragment was PCR amplified from pGEMT-*minCDE*::Km^R (pKMRM161) with primers minF_*Bam*HI and minR_*Bam*HI (Table 2.4) to incorporate *Bam*HI restriction sites at either end of the amplified fragment (Figure 7.1 – [5]). This 3565 bp fragment was digested with *Bam*HI and ligated into similarly digested, suicide vector, pCACTUS (Table 2.3) (Figure 7.1 – [6]). The ligated DNA was transformed into DH5α and

plasmid DNA was isolated from Cm^R, Km^R and Ap^S transformants. The pCACTUS-*minCDE*::Km^R construct (pKMRM180a) was confirmed by PCR with primers minF and minR, and by restriction digestion with *Bam*HI (Section 2.6.2).

Having created the above mutagenesis construct, allelic-exchange mutagenesis was undertaken using the construct itself (Section 7.2.2) (Figure 7.1 – [7]), and by using this construct as a PCR template for λ Red recombinase mediated mutagenesis (Section 7.2.3) (Figure 7.1 – [8] and [9]).

7.2.2 Allelic-exchange mutagenesis with pCACTUS-*minD::*Km^R

The mutagenesis construct (pKMRM180a) created in Section 6.2.1 was electroporated into *S. flexneri* 2a WT strain 2457T (Sections 2.10.3 and 2.10.4) and allelic-exchange mutagenesis was performed as described in Chapter Two (Section 2.11.1). Repeated attempts at mutagenesis of *S. flexneri* 2457T were unsuccessful, yielding only single cross-over events or no colonies following plating on selective medium.

As attempts to construct a minicell-producing mutant in *S. flexneri* with the pCACTUS mutagenesis construct (pKMRM180a) were unsuccessful, mutagenesis of *E. coli* K-12 was attempted. *E. coli* K-12 is used routinely in genetic studies on *Shigella* (Goldberg and Theriot, 1995; Monack and Theriot, 2001; Charles *et al.*, 2001; Janakiraman and Goldberg, 2004; Nilsen *et al.*, 2005) and is highly amenable to genetic manipulation. There is >99% sequence identity between the *min* locus of *S. flexneri 2a* strain 2457T and *E. coli* K-12 strain MG1655 (data not shown). Hence, the mutagenesis construct created in Section 6.2.1 was electroporated into *E. coli* Δ*ompT* (UT5600; Table 2.1) (Sections 2.10.3 and 2.10.4), and mutagenesis was conducted as before (Section 2.11.1). However, this was also unsuccessful.

7.2.3 Allelic-exchange mutagenesis with λ Red phage recombinase

As attempts at mutagenesis with the pCACTUS construct were unsuccessful, the plasmid pCACTUS-*minD*::Km^R (pKMRM180a) was used as a PCR template with primers minF and minR (Table 2.4) in an attempt to construct a chromosomal *minD* mutation using the λ Red phage recombinase mutagenesis system (Datsenko and Wanner, 2000). *S. flexneri* 2457T and *E. coli* Δ*ompT* (UT5600) were transformed with pKD46 (Table 2.3) to produce KMRM79 and KMRM78 respectively, and mutagenesis was performed as described in Chapter Two (Section 2.11.2). Once again repeated attempts at mutagenesis of *S. flexneri* 2457T were unsuccessful. However, the initial attempt at mutagenesis of *E. coli* Δ*ompT* (UT5600) was successful, yielding approximately 1000 putative mutants. Isolated colonies were screened for Ap^S and Cm^S to ensure the pKD46 plasmid and the pCACTUS-*minCDE*::Km^R (pKMRM180a) PCR template were not present. The chromosomal mutation was confirmed by PCR analysis of an isolated colony (Sections 2.5.4 and 2.7.2) with primers minF and minR, which produced an amplicon of approximately 3549 bp corresponding to *minCDE*::Km^R (Figure 7.2, Lane 4), This was in contrast to the 2064 bp amplicon seen upon PCR analysis of the UT5600 parent strain.

In order to create an unmarked minicell mutant, the plasmid pCP20 (Table 2.3) was electroporated into the strain isolated above, UT5600 *minD*::Km^R (KMRM183; Table 2.2). pCP20 encodes an FLP recombinase. Thermal induction of this recombinase, as detailed in Section 2.11.2, results in FLP-mediated excision of the Km^R cartridge (via its flanking FRT sites), leaving an 85 bp "scar" (Datsenko and Wanner, 2000). The resultant strain UT5600 *minD*::85nt (KMRM186; Table 2.2) was confirmed by PCR analysis (Figure 7.2, Lane 3).

Having generated a marked minicell mutant UT5600 *minD*::Km^R (KMRM183), it was thus possible to try and transduce this mutation into *S. flexneri* 2457T using P1 phage

Figure 7.2 PCR confirmation of mutagenesis of the *min* locus.

The chromosomal mutation of *minD* was confirmed by PCR analysis of an isolated colony of *E. coli* UT5600 *minD*::Km^R (KMRM183) with primers minF and minR, which resulted in an amplicon of approximately the expected 3549 bp corresponding to *minCDE*::Km^R (**Lane 4**). This was in contrast to the 2064 bp amplicon seen upon PCR analysis of the parent strain UT5600 (**Lane 2**). FLP-mediated excision of the Km^R cartridge to create the strain UT5600 *minD*::85nt (KMRM186) was confirmed by the presence of a 2149 bp amlicon (**Lane 3**). Amplicon sizes were estimated by comparison to the SPP1/*Eco*RI DNA marker (**Lane 1**).

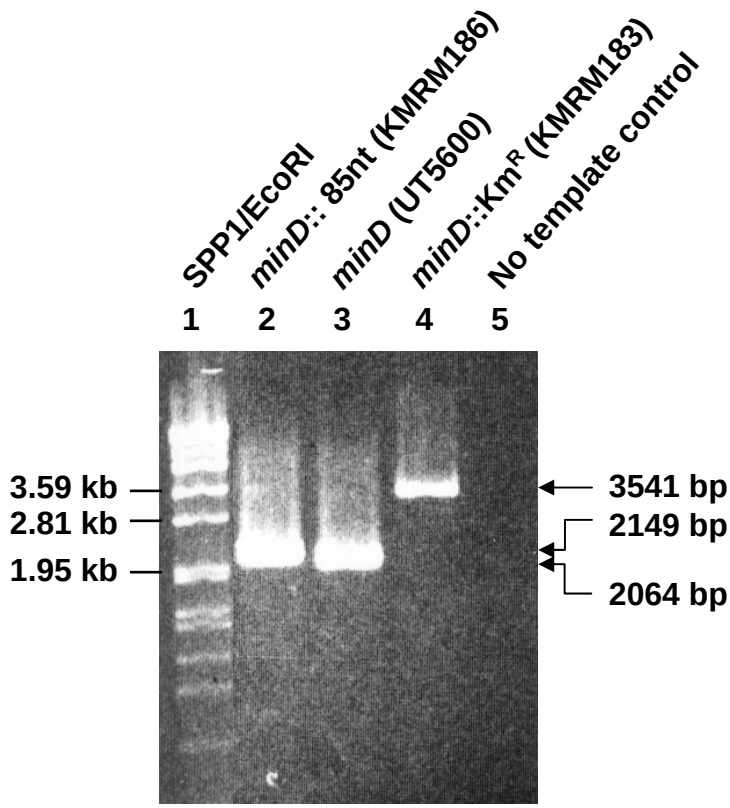
SPP1/EcoRI
minD:: 85nt (KMRM186)
minD (UT5600)
minD::KmR (KMRM183)
No template control
1
2
3
4
5
3.59 kb
2.81 kb
1.95 kb
3541 bp
2149 bp
2064 bp

(Sections 2.11.3.1 and 2.11.3.2.). However, despite repeated attempts with independent phage stocks, no transductants were obtained.

7.3 Phase-contrast microscopy of *E. coli* minicell mutants

Phase-contrast microscopy was used to directly observe the production of minicells by *E. coli* strains UT5600 *minD*::Km^R (KMRM183), UT5600 *minD*::85nt (KMRM186) and their parent strain UT5600 grown to log-phase in LB broth at 37°C (Sections 2.13.1 and 2.17). Whilst *E. coli* UT5600 formed uniform rod-shaped cells approximately 3 μm in length (Figure 7.3A), both UT5600 *minD*::Km^R (KMRM183) and UT5600 *minD*::85nt (KMRM186) had a minicell phenotype as they formed small spherical minicells, and some filamentation was also observed (Figure 7.3, B and C). This confirmed the minicell phenotype.

7.4 Construction of smooth LPS minicell-producing mutant of *E. coli* K-12 expressing IcsA

To determine the distribution of different LPS populations in *E. coli* K-12 it was necessary to genetically manipulate the minicell mutant created in Section 6.2, UT5600 *minD*::85nt (KMRM186), to enable it to produce S-LPS. The parent strain used to construct the *E. coli* K-12 minicell strain possesses only R-LPS most likely due to an IS5 insertion within the *rfb* locus (which encodes genes required for Oag biosynthesis), a mutation commonly found in *E. coli* K-12 strains (Liu and Reeves, 1994). Hence, to obtain Oag expression, strains were complemented with pRMA154, a Km^R plasmid that encodes Oag biosynthesis genes from *S. flexneri* (Morona *et al.*, 1994; Table 2.3). Plasmid pIcsA (Table 2.3), which confers Ap^R (and encodes IcsA), was initially transformed into UT5600 *minD*::85nt (KMRM186) to produce UT5600 *minD*::85nt [pIcsA] (KMRM187). Immunofluorescence microscopy of UT5600 *minD*::85nt [pIcsA] (KMRM187) as well as its parent strain UT5600 carrying pIcsA (KMRM87) was performed. The results confirmed that

Figure 7.3 Phase-contrast microscopy of *E. coli* minicell mutants.

E. coli strains UT5600 *minD*::Km^R (KMRM183) (**B**), UT5600 *minD*::85nt (KMRM186) (**C**) and their parent strain UT5600 (**A**) were grown to log-phase in LB at 37°C, formalin fixed and centrifuged onto poly-L-lysine-coated coverslips. The coverslips were mounted on glass microscope slides and examined with an Olympus IX-70 microscope with phase-contrast optics using a 100× oil immersion objective and a 1.5× enlarger. Arrows indicate minicells and arrow heads indicate whole cells. Scale bars indicate 10 μm.

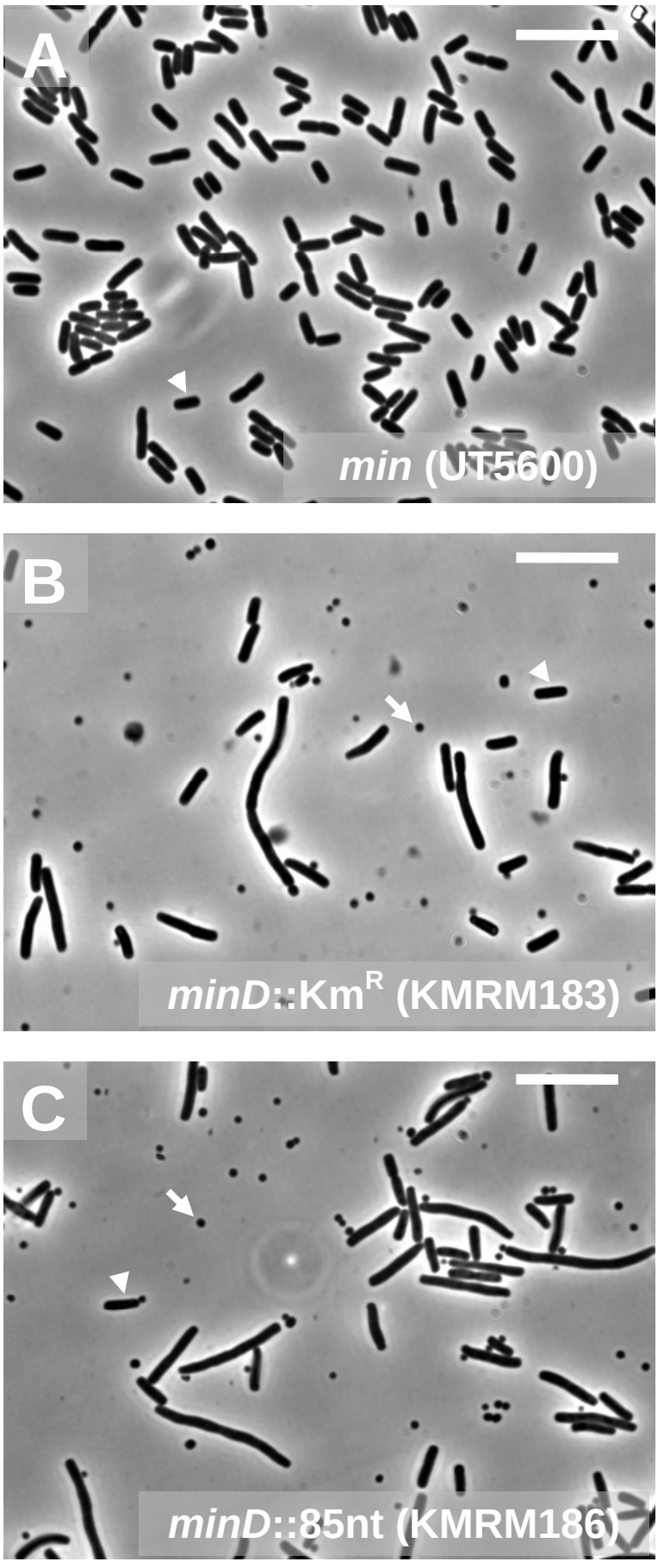
A
min (UT5600)
B
minD::KmR (KMRM183)
C
minD::85nt (KMRM186)

(as expected) IcsA polarity was maintained in these strains, and for the minicell-producing mutant KMRM187, IcsA was present on the surface of minicells (Figure 7.4)

KMRM187 was conjugated with RMA160 (Table 2.1) and RMA156 (Table 2.1) to introduce pRMA154 and pJRD215 (an empty control vector), respectively. LPS was prepared from the resulting strains, UT5600 *minD*::85nt [pIcsA] [pRMA154] (KMRM191) and UT5600 *minD*::85nt [pIcsA] [pJRD215] (KMRM189), as described in Section 2.14.1. LPS analysis by SDS page and silver-staining (Section 2.14.2) confirmed that pRMA154 was able to confer S-LPS phenotype with a modal length of 12-20 repeat units (Figure 7.5, Lanes 7 and 8). The *E. coli* strain UT5600 contains a deletion of the chromosomal region *ompT- fepC* that contains the *fepE* gene (Elish *et al*., 1988; Grodberg and Dunn, 1988; Sugimura and Higashi, 1988). Accordingly, this strain had a single modal length conferred by the *E. coli* K-12 wzz_{EC} gene (Batchelor *et al*., 1991).

7.5 Analysis of LPS of minicell-producing mutants of *E. coli* expressing IcsA

In order to determine if the LPS profile of minicells corresponds that of the whole cells, minicells and whole cells were purified from UT5600 *minD*::85nt [pIcsA] [pRMA154] (KMRM191) and UT5600 *minD*::85nt [pIcsA] [pJRD215] (KMRM189) using density sucrose gradient centrifugation, as described in Section 2.13.2. Analysis of the purified fractions using phase-contrast microscopy indicated that minicells and whole cells were purified to a high level of purity (>99% of cells) using this method (Figure 7.6). LPS was prepared independently from purified minicells and whole cells (Section 2.14.1), obtained from both stationary-phase and log-phase cultures. As IcsA polarity is reinforced at cell division (Goldberg *et al.*, 1994), it was also of interest to see if there was a difference in the LPS profiles at these phases of growth. Analysis by SDS-PAGE and silver-staining (Section

Figure 7.4 Detection of IcsA on the surface of a minicell-producing mutant of *E. coli* expressing IcsA by immunofluorescence microscopy.

The *E. coli* strain UT5600 [pIcsA] (KMRM87) (**A-C**) and its isogenic minicell-producing derivative UT5600 *minD*::85nt [pIcsA] (KMRM187) (**D-F**) and were grown to log-phase in LB at 37°C. Bacteria were formalin fixed and centrifuged onto poly-L-lysine-coated coverslips. Bacteria were incubated with a rabbit poly-clonal anti-IcsA antiserum and incubated with Alexa 488-conjugated donkey anti-rabbit secondary antibodies. The coverslips were mounted on glass microscope slides and examined with an Olympus IX-70 microscope with phase-contrast optics using a 100× oil immersion objective with a 1.5x enlarger. Phase-contrast images (**A, D**) and fluorescence images (**B, E**) were false colour merged (**C, F**) using Metamorph (Version 6.3r7, Molecular devices). Arrows indicate minicells and arrow heads indicate whole cells. Scale bars indicate 5 μm.

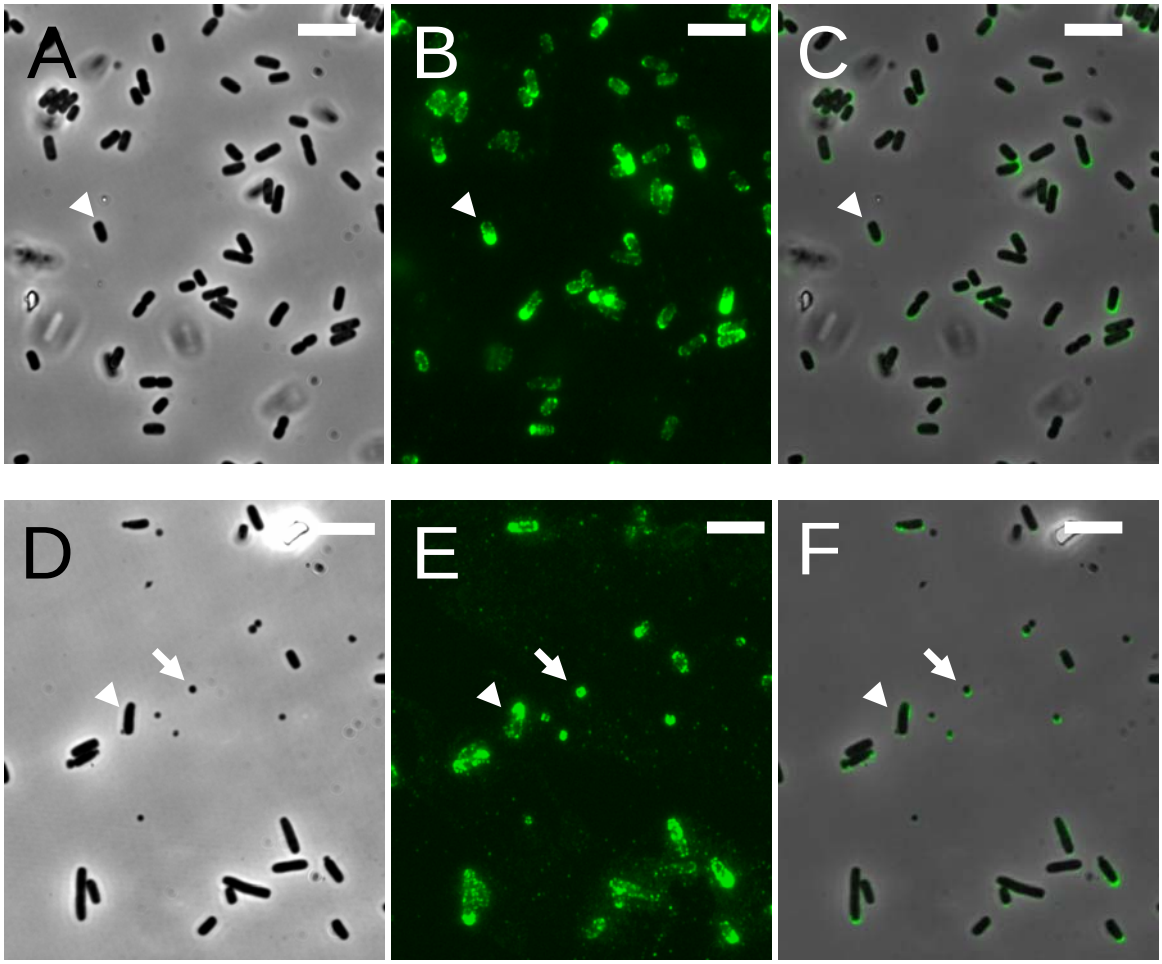
A
B
C
D
E
F

Figure 7.5 Silver-stained SDS-PAGE analysis of LPS from *E. coli* minicells and whole cells

Minicell-producing mutants of *E. coli* were grown to log-phase or stationary phase in LB and minicells and whole cells were fractionated by density sucrose gradient centrifugation. LPS was prepared from 4 x 10^8 minicells and 10^8 whole cells from either the smooth-LPS (S-LPS) strain UT5600 *minD*::85nt [pIcsA] [pRMA154] (KMRM191) or the rough LPS (R-LPS) strain UT5600 *minD*::85nt [pIcsA] [pJRD215] (KMRM189) were electrophoresed on a 15% polyacrylamide gel and silver-stained. Numbers (n) left of the figure indicate the number of Oag repeats in corresponding LPS bands.

Log-phase
Lane 1: minicell fraction, UT5600 *minD*::85nt [pIcsA] [pRMA154] (KMRM191) – S-LPS.
Lane 2: whole cell fraction, UT5600 *minD*::85nt [pIcsA][pRMA154] (KMRM191) – S-LPS.

Stationary-phase
Lane 3: minicell fraction, UT5600 *minD*::85nt [pIcsA] [pRMA154] (KMRM191) – S-LPS.
Lane 4: whole cell fraction, UT5600 *minD*::85nt [pIcsA] [pRMA154] (KMRM191) – S-LPS.
Lane 5: minicell fraction, UT5600 *minD*::85nt [pIcsA] [pJRD215] (KMRM189) – R-LPS.
Lane 6: whole cell fraction, UT5600 *minD*::85nt [pIcsA] [pJRD215] (KMRM189) – R-LPS.

Lane 7: non-fractionated UT5600 *minD*::85nt [pIcsA] [pRMA154] (KMRM191) – S-LPS.
Lane 8: non-fractionated UT5600 *minD*::85nt [pIcsA] [pJRD215] (KMRM189) – R-LPS.

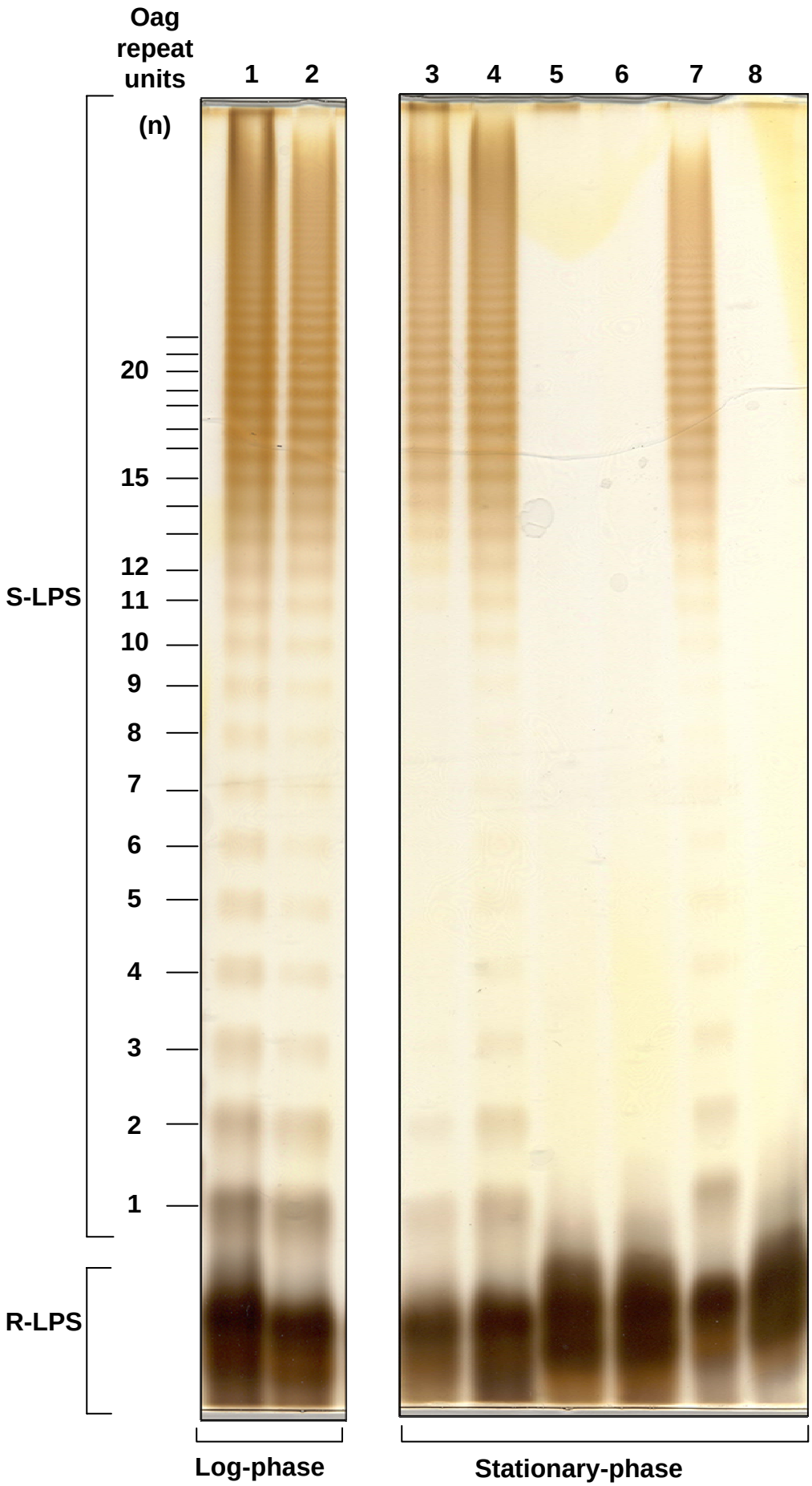
Oag repeat units (n)
1
2
3
4
5
6
7
8
20
15
12
11
10
9
8
7
6
5
4
3
2
1
S-LPS
R-LPS
Log-phase
Stationary-phase

Figure 7.6 Phase-contrast microscopy of minicell and whole cell fractions obtained by sucrose density gradient centrifugation.

Minicell-producing mutants of *E. coli*, KMRM189a (**A and B**) and KMRM191 (**C and D**) were grown to log-phase or stationary-phase in LB broth and minicells and whole cells were fractionated by sucrose density gradient centrifugation. Samples of the minicell fractions (**A and C**) and whole cell fractions (**B and D**) of each strain were formalin fixed and centrifuged onto poly-L-lysine-coated coverslips. The coverslips were mounted on glass microscope slides and examined with an Olympus IX-70 microscope with phase-contrast optics using a 100× oil immersion, objective. Scale bars indicate 10 μm.

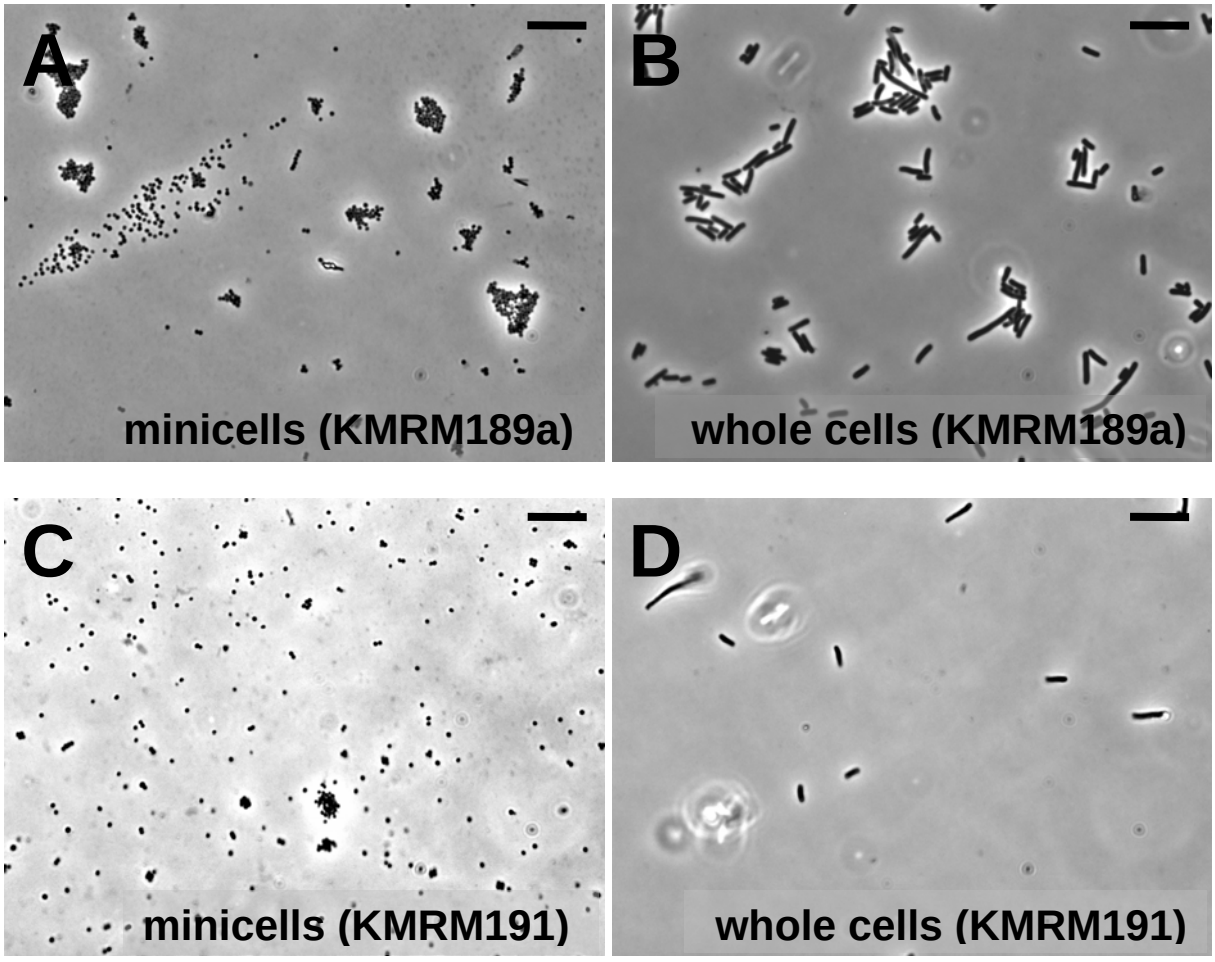
A
minicells (KMRM189a)
B
whole cells (KMRM189a)
C
minicells (KMRM191)
D
whole cells (KMRM191)

2.14.2) showed no difference between the LPS profiles of minicells and whole cells with comparable levels of S-LPS with a modal length of 12-20 repeat units for from either log-phase or stationary phase cultures (Figure 7.5, Lanes 1-6).

7.6 Summary

The LPS analysis of a minicell mutant has not been reported before. This chapter compared the LPS profiles and the relative distribution of R-LPS and S-LPS populations in whole cells and minicells of *E. coli*. No obvious difference was observed for LPS profiles of minicells and whole cells, suggesting the different LPS populations are uniformly distributed on the polar and lateral regions of the bacterium. This is the first time that S-LPS of minicells has been directly investigated. Work in this chapter did not address the distribution of the VL-type and the S-type LPS-Oag populations of *S. flexneri* since a *min* mutant of *S. flexneri* could not be made. Interestingly, a *S. flexneri* wzz_{SF} mutant which produces the VL-type S-LPS, but lacks the S-type modal length, is avirulent and unable to form either F-actin comet tails or plaques, due to masking of IcsA by LPS-Oag. Clearly, if these LPS populations with VL-type Oag chains were largely restricted to the lateral surface, then masking should not occur over the polar regions where IcsA is predominantly expressed, and this mutant should have had little defect in ABM. Therefore, it is more likely that VL-type and S-type LPS is uniformly distributed over the surface of bacteria. Indeed, the results of this chapter support the hypotheses that LPS populations are distributed uniformly, that IcsA polarity occurs as a direct result of targeted protein export to the poles, and that increased detection of the IcsA at the pole is not a result of a decreased number of S-LPS molecules in this region.

Chapter Eight

Discussion

Chapter Eight: Discussion

8.1 Overview: IcsA structure and function

The IcsA (VirG) protein of *S. flexneri* is a polarly localised, OM protein that is essential for virulence (Lett *et al*., 1989; Bernardini *et al.*, 1989; Goldberg *et al.*, 1993; Goldberg, 2001; Suzuki and Sasakawa, 2001). Within host cells, IcsA activates the host actin regulatory protein, N-WASP, which in turn recruits the Arp2/3 complex that nucleates host actin to form F-actin (Suzuki *et al*., 1998, Suzuki *et al*., 2002; Suzuki and Sasakawa, 2001). The resultant F-actin comet tails initiate bacterial ABM and intercellular spread. The N-terminal, surface-exposed region of IcsA, the passenger domain (aa 53-758), is responsible for IcsA activity in ABM. Specifically, a GRR region (103-433) has been shown to be sufficient for N-WASP binding *in vitro* (Suzuki *et al*., 1998, Suzuki *et al*., 2002), although aa 53-508 are required for actin polymerisation *in vitro* (Goldberg, 2001). Previous IcsA structure and function studies have relied predominantly on large deletions of IcsA regions. Such approaches may have resulted in the removal of multiple functional domains, complicating the interpretation of the phenotypes of the *icsA* mutants in those studies. The need for a more comprehensive study of IcsA structure-function remained. Hence, pentapeptide linker-insertion mutagenesis of IcsA was undertaken and 47 $IcsA_i$ mutants were created for structure-function studies. Furthermore, previous studies have provided evidence of masking of IcsA function by LPS-Oag (Morona *et al*., 2003; Morona and Van Den Bosch, 2003b). Consequently, in addition to evaluating the ability of various $IcsA_i$ mutants to interact with N-WASP, the aim was to also investigate the influence of LPS-Oag on IcsA:N-WASP interactions.

Investigating the state of IcsA in the OM environment was also important to our understanding of how IcsA interacts with host proteins such as N-WASP, as well as LPS molecules. The influence of LPS on IcsA localisation and function (Morona *et al*., 2003) suggested that it was important to firstly investigate whether IcsA exists as an oligomer in the OM, similar to the *Neisseria* IgA protease (an AT protein) (Veiga *et al*., 2002), and secondly to determine the profile of the LPS populations located at the old-cell pole where IcsA is predominantly localised.

As the tertiary structure of IcsA has not yet been determined, various *in silico* analysis tools were used to create structural models for IcsA, and an attempt was made to correlate data obtained from the mutagenesis studies to these models.

8.2 Production of $IcsA_i$ mutants and identification of an auto-chaperone region (aa 595-716)

Of the 47 $IcsA_i$ mutants that were created, six ($IcsA_{i595}$, $IcsA_{i598}$, $IcsA_{i633}$, $IcsA_{i643}$, $IcsA_{i677}$ and $IcsA_{i716}$) demonstrated aberrant production when expressed in *S. flexneri* (Section 3.3; Figure 3.3A). These $IcsA_i$ mutants showed reductions in both cell-associated and secreted forms; in some cases, the secreted proteins were below detectable levels in culture supernatants (Section 3.3; Figure 3.3B). However, production of three of these mutants ($IcsA_{i595}$, $IcsA_{i598}$ and $IcsA_{i633}$) was restored to WT levels when they were expressed in the *E. coli* UT5600 [Δ*ompP* Δ*ompT*] (Section 3.3; Figure 3.3C). This was consistent with the hypothesis that these may be sensitive to degradation by endogenous OM proteases present in WT *S. flexneri* but absent in UT5600. Interestingly, production of three other mutants ($IcsA_{i643}$, $IcsA_{i677}$ and $IcsA_{i716}$) was still greatly reduced in *E. coli* UT5600, suggesting they may be sensitive to degradation by periplasmic proteases (e.g. DegP Skp, and SurA). Indeed DegP has been implicated in IcsA export (Purdy *et al*., 2002).

Oliver *et al.* (2003) have recently described a putative intra-molecular chaperone region of the passenger domain, conserved between several AT proteins including IcsA (aa 634-735). In *B. pertussis* AT protein, BrkA, deletion of this auto-chaperone region (aa 601-692) made the protein susceptible to degradation by OM proteases and trypsin. Similarly, this has also been shown for homologous regions within two other autotransporter proteins, SSP and Pet (Ohnishi *et al*., 1994; Dutta *et al.*, 2003). Our data supports the hypothesis that this region of IcsA functions as an auto-chaperone conferring stability to the passenger domain during translocation across the OM. It is not clear why the $IcsA_{\Delta 507\text{-}730}$ deletion construct of Suzuki *et al.* (1996) did not exhibit a similar sensitivity to OM proteases as it was reported to be expressed at WT levels in *S. flexneri.*

8.3 Refinement of the IcsA polar targeting region

Two regions of the passenger domain (aa 1-104 and aa 507-620) have been attributed to polar localisation of IcsA (Suzuki *et al*., 1996; Charles *et al*., 2001). In the course of the studies conducted in this thesis, two $IcsA_i$ mutants, $IcsA_{i532}$ and $IcsA_{i563}$ were isolated that had altered IcsA localisation on the surface of *S. flexneri* (Section 3.4; Figure 3.6). Both of these mutants possessed linker-insertions within polar localisation region #2 (aa 507-620). Interestingly, the Robetta model of IcsA structure predicted an α-helix protruding from a loop region within the β-helix backbone at aa 549-558, which is located between these to insertions (Section 5.5; Figure 5.6). A similar α-helix is present within the C-terminal region of HbP crystal structure (Figure 1.9B; Otto *et al*., 2005). It is not known if HbP is polarly targeted but several other ATs (*S. flexneri* SepA, *E. coli* AIDA-I, *B. pertussis* BrkA, and *N. meningitidis* NalP) have recently been reported to be polarly targeted (Jain *et al*., 2006). Regions homologous to the IcsA polar localisation regions have not been identified within these AT proteins, however the absence of any clear sequence similarity might not be so unexpected if the targeting mechanism is mediated by a structural motif. Of the three mutants ($IcsA_{i56}$, $IcsA_{i81}$, $IcsA_{i87}$) that possessed linker-insertions within polar localisation region # 1 (aa 1-

104), all were distributed polarly on the surface of *S. flexneri*, comparable to $IcsA_{WT}$ (Section 3.4; Figure 3.7). These data indicate that region #2 is the predominant targeting region and that region #1 is not able to compensate for mutational alterations in region #2.

The identification of two mutants $IcsA_{i532}$ and $IcsA_{i563}$ in which polar targeting was disrupted has enabled us to refine the region involved in polar targeting to aa 532-563, and it is hypothesised that an α helix with this region (aa 549-558) is involved in mediating this polar targeting.

8.4 IcsA-mediated N-WASP activation and initiation of ABM

IcsA aa 103-433 have been shown to be adequate for N-WASP binding, as established by *in vitro* pull-down assays (Suzuki *et al.,* 1998; 2002), and IcsA aa 53-508 are sufficient to induce actin polymerisation during *in vitro* assays (Goldberg, 2001). Therefore, it has been suggested that the residues involved in N-WASP activation are within this region (Suzuki et *al.,* 1996; Suzuki and Sasakawa, 2001; Goldberg, 2001). A prominent feature of this region is a series of glycine-rich repeats (Section 1.2.3; Figure 1.5; Goldberg *et al.*, 1993), and as deletion of part of this region (aa 104-226) has been reported to abolish F-actin tail formation (Suzuki *et al*., 1996), the GRR region has long been thought to be largely responsible for mediating the IcsA:N-WASP interaction.

In Chapter Three, twenty-two of the *S. flexneri* strains expressing $IcsA_i$ mutants were unable to form plaques on tissue culture monolayers, and a further seven demonstrated intermediate phenotypes, exhibiting varying degrees of intercellular spreading defects (Section 3.5; Table 3.5). Further characterisation of the intercellular behaviour of these twenty-nine strains (Sections 4.2 and 4.4) indicated that nineteen of these strains, in addition to being unable to spread from cell-to-cell, were unable to form either F-actin comet tails or recruit N-WASP (Tables 4.1 and 4.3). Nine of these $IcsA_i$ mutants possessed linker-insertions

within the GRR region, however, the remaining ten $IcsA_i$ mutants possessed linker-insertions that were located within either a small sub-region of the IcsB binding region (aa 346-381), or a region containing both the polar localisation region and the putative auto-chaperone region (aa 502-730). These potentially constitute novel functional regions involved in N-WASP binding and activation. Nonetheless, previous work in our laboratory has provided evidence of masking of IcsA function by LPS-Oag (Morona *et al*., 2003; Morona and Van Den Bosch, 2003b), and it was hypothesised that the inability of some of these $IcsA_i$ mutants to interact with N-WASP may be an indirect consequence of masking by LPS-Oag. Thus before concluding that these novel regions were involved in N-WASP recruitment, the ability of these $IcsA_i$ mutants to interact with N-WASP when expressed by R-LPS *S. flexneri* strains (which possess LPS molecules lacking Oag) was also investigated.

8.4.1 Effect of Oag on N-WASP-IcsA interaction

Perhaps one of the most remarkable findings from the work conducted in this thesis was that the interaction between N-WASP and IcsA inside host cells was influenced by the presence of LPS-Oag. Mutants $IcsA_{i185}$, $IcsA_{i226}$, $IcsA_{i532}$ and $IcsA_{i563}$, were unable to recruit N-WASP and induce F-actin comet tails when expressed in S-LPS *S. flexneri* Δ*icsA* strains. The mutants were, however, able to recruit N-WASP and form F-actin tails in a R-LPS *S. flexneri* Δ*icsA* Δ*rmlD* background (albeit at a lower frequency compared to *S. flexneri* Δ*icsA* Δ*rmlD* expressing $IcsA_{WT}$) (Section 4.5.1-2; Figures 4.7 and 4.8). Hence, mutations of IcsA that abolish N-WASP recruitment may not necessarily be the direct result of mutation/deletion of the entire N-WASP binding region of IcsA. The result highlighted a potential short-coming of the work of Suzuki *et al.* (1996, 1998, 2002), which only examined IcsA mutants in a S-LPS background. Consequently, three of the IcsA mutants of Suzuki *et al*. (1996) ($IcsA_{\Delta 103-320}$, $IcsA_{\Delta 103-507}$, and $IcsA_{\Delta 507-730}$), although unable to recruit N-WASP when expressed by S-LPS *S. flexneri* Δ*icsA* (RMA2041), were able to recruit N-WASP when expressed by R-LPS *S. flexneri* Δ*icsA* Δ*rmlD* (RMA2043) (Section 4.5.3; Figure 4.10).

Two models could account for the inability of IcsA mutants to interact with N-WASP in the presence of LPS-Oag. In the first model, multiple regions of IcsA interact with N-WASP, and in some mutant IcsA proteins at least one of these N-WASP binding regions is disrupted. The remaining N-WASP binding region(s) is(are) masked by LPS-Oag. In the second model, the defect in N-WASP recruitment is not the result of direct mutation of N-WASP binding regions. Instead, an alteration in conformation or length of the IcsA protein occurs as a result its mutation (i.e. linker-insertion or deletion) such that the mutant protein becomes masked by LPS-Oag. Hence, N-WASP is unable to interact with the IcsA mutants due to steric hindrance by LPS-Oag. For example, the $IcsA_{\Delta}$ mutant proteins constructed by Suzuki *et al.* (1996; 1998; 2002) all possess deletions of at least 188 aa, which significantly truncate the protein. The truncated proteins may be less prominent on the surface of bacteria, and are consequently more prone to masking by LPS-Oag.

Investigation of $IcsA_i$ mutants and $IcsA_{\Delta}$ mutants in a R-LPS background has enabled regions involved in N-WASP recruitment and activation to be more clearly identified. This has made possible the identification of two novel functional regions (aa 330-381 and aa 502-730) (Figure 4.11). The role of these regions in N-WASP recruitment and activation (based on examination of $IcsA_i$ and $IcsA_{\Delta}$ mutants in both S-LPS and R-LPS backgrounds) is discussed below.

8.4.2 Role of the GRR region of IcsA in N-WASP interaction

The minimal region of IcsA required for N-WASP interaction has been defined to aa 103-433 by *in vitro* pull-down (Suzuki *et al*., 1998). Therefore it was not surprising that most of the linker-insertions within this region disrupted IcsA function in N-WASP recruitment and ABM. Fifteen $IcsA_i$ mutants had linker-insertions within the "GRR" region (aa 140-307) and nine of these mutant proteins ($IcsA_{i185}$, $IcsA_{i219}$, $IcsA_{i226}$, $IcsA_{i230}$, $IcsA_{i244}$, $IcsA_{i248}$, $IcsA_{i268}$, $IcsA_{i271}$ and $IcsA_{i297}$) were to unable induce N-WASP recruitment and F-actin comet tail

formation when expressed by *S. flexneri* in infected cells (Sections 4.2 and 4.4; Tables 4.1 and 4.3). According to the IcsA Robetta model, the majority of the linker-insertions within these nine $IcsA_i$ mutants are predicted to be located within an extended loop region protruding from the β-helix backbone that forms a putative binding cleft with the remaining N-terminal region (Figure 5.8; Table 5.1). Interestingly, two of these mutants ($IcsA_{i185}$, $IcsA_{i226}$) were able to recruit N-WASP and form F-actin comet tails when expressed by a R-LPS *S. flexneri* strain, albeit at a reduced level compared to $IcsA_{WT}$ (Section 4.5.1-2; Figures 4.7 and 4.8).

Although deletion of aa 104-226 (within the GRR) has been reported to abolish F-actin comet tail formation (Suzuki *et al*., 1996) this has not been correlated with N-WASP recruitment in either S-LPS or R-LPS backgrounds. Data from this thesis confirms the involvement of the region (aa 104-226) identified by Suzuki *et al*. (1996) in N-WASP recruitment, with linker-insertions within aa 185-226 affecting N-WASP recruitment and ABM. Furthermore, an additional region of the GRR region (aa 230-297) has also been shown to be involved in N-WASP recruitment and activation. However, as a R-LPS *S. flexneri* strain expressing $IcsA_{\Delta 103\text{-}320}$ demonstrated a low level of N-WASP recruitment (Section 4.5.3; Figure 4.10), this is consistent with linker mutagenesis data showing that regions outside of the GRR are also involved in N-WASP recruitment/activation.

8.4.3 Role of aa 330-381 of IcsA (within the IcsB binding region) in N-WASP interaction

Ten $IcsA_i$ mutants had linker-insertions within region aa 320-433 and five of these mutants ($IcsA_{i330a}$, $IcsA_{330b}$, $IcsA_{i342}$, $IcsA_{i346}$ and $IcsA_{i381}$) when expressed by *S. flexneri* were unable to form either plaques, F-actin comet tails, or recruit N-WASP (Sections 4.2 and 4.4; Tables 4.1 and 4.3). According to the Robetta model, the linker-insertions within 4 out of 5 of these $IcsA_i$ mutants ($IcsA_{i330a}$, $IcsA_{330b}$, $IcsA_{i346}$ and $IcsA_{i381}$) were predicted to be located within loop regions in the β-helix backbone (Figure 5.8; Table 5.1). These mutants all possess

linker-insertions within a region of IcsA (aa 320-433) that interacts with the *Shigella* IcsB protein and a host autophagy protein, Atg5 (Ogawa *et al*., 2003; Ogawa *et al*., 2005). In the cytosol, IcsB prevents binding of Atg5 to this region of IcsA through competitive inhibition thereby preventing initiation of degradation of the bacteria via the autophagy pathway (Ogawa *et al.*, 2005). It is important to note that these *icsA*$_i$ mutants differ from the *icsB* mutants from previous studies (Ogawa *et al*., 2003; Ogawa *et al*., 2005), which were also unable to form plaques in tissue culture monolayers but were able to form F-actin tails and exhibit actin-based motility at a similar frequency to the WT at early time-points (Ogawa *et al*., 2005).

Investigation of a R-LPS *S. flexneri* strain expressing IcsA$_{\Delta 103\text{-}507}$ demonstrated a low level of N-WASP recruitment (Section 4.5.3; Figure 4.10). As this deletion mutation removes both the GRR region and the IcsB regions, this suggested that an additional region(s) was(were) involved in N-WASP recruitment/activation.

8.4.4 Role of aa 508-730 of IcsA in N-WASP interaction

The combination of our mutagenesis approach and our investigation of the effect of LPS-Oag has enabled us to separate the phenotypic properties associated with region aa 508-730. The results demonstrate that region aa 508-730 has a role in N-WASP activation and F-actin comet tail formation that is independent of its role in IcsA localisation. Deletion of the region incorporating amino acids 508-730 of IcsA has previously shown to affect F-actin comet tail formation. However, the IcsA$_{\Delta 508\text{-}730}$ mutant also displayed aberrant localisation on the surface of bacteria complicating the interpretation of this mutant's phenotype (Suzuki *et al*., 1996). Indeed, the authors of that paper suggested that the defect in F-actin comet tail formation resulted from non-polar localisation of IcsA.

Data from this thesis has demonstrated that mutants $IcsA_{i532}$ and $IcsA_{i563}$ are non-polarly expressed on the surface of *S. flexneri*, and are unable to induce F-actin comet tail formation in S-LPS strains (like $IcsA_{\Delta 507-730}$) (Sections 4.2; Tables 4.1) However, F-actin comet tail formation was restored, albeit at a low frequency, when these mutants were expressed in a R-LPS strain (Section 4.5.1; Figure 4.7). The same was not observed for $IcsA_{\Delta 508-730}$ which was unable to induce F-actin comet tail formation in R-LPS strains (Section 4.5.3; Figure 4.9). This indicates an additional defect occurs as a result of deleting this region that is independent of the effect on IcsA polarity. With respect to the data suggesting that aa 53-508 of IcsA is sufficient for N-WASP activation (Goldberg, 2001), this model is based on *in vitro* data and it may be that inside cells, in the presence of host regulatory proteins, this region is sufficient of N-WASP recruitment but not its activation. This is also consistent with the observation that a R-LPS strain expressing $IcsA_{\Delta 508-730}$ was able to recruit N-WASP inside HeLa cells but unable to initiate F-actin comet tail formation, and only a low level of F-actin accumulation around the bacteria was observed (Section 4.5.3; Figure 4.9-10).

As discussed earlier (Section 8.2), a putative auto-chaperone region (aa 634-735) has also been identified within this region (aa 508-730). However, it is not possible to determine the contribution of this region to N-WASP recruitment and activation due to the production defect exhibited by $IcsA_i$ mutants with mutations in this region. The decreased ability ($IcsA_{i595}$, $IcsA_{i598}$, $IcsA_{i633}$) and inability ($IcsA_{i643}$, $IcsA_{i677}$, $IcsA_{i716}$) of $IcsA_i$ mutants to recruit N-WASP, form F-actin comet tails and spread intercellularly when expressed by *S. flexneri* is likely to be caused by their low level of production.

8.4.5 Multiple regions of IcsA (the GRR region, aa 330-381 and 508-730) are required to activate N-WASP via interactions with its WH1 and GBD/CRIB domains

It was particularly interesting that the presented results suggest regions outside of the GRR of IcsA are also important for N-WASP recruitment and F-actin comet tail formation, and as introduced earlier (Section 8.4.1), a model was proposed to reconcile this data in which multiple regions of IcsA are required for recruitment and activation of N-WASP. This model is supported by demonstration that the WH1 domain (aa 34-138) and the CRIB/GTPase (aa 203-222) domains of N-WASP are independently recruited to *S. flexneri*, inside N-WASP-deficient cell lines or HeLa cells (Lommel *et al.*, 2001; Moreau *et al*., 2000). Although N-WASP constructs lacking the WH1 domain were still capable of supporting *Shigella* ABM in N-WASP (-/-) cells, the bacteria exhibited shorter F-actin comet tails (Lommel *et al.*, 2001). The impact of these shorter F-actin comet tails on ABM and intercellular spread was not investigated in these studies and hence the authors could not comment on the significance of the WH1-IcsA interaction. The regions of IcsA responsible for the interactions with each of the N-WASP domains have not been determined before. Pull-down studies have demonstrated that the aa 53-506 region of the IcsA passenger domain interacts with the WH1, GBD, PH and IQ regions of N-WASP (Suzuki *et al*., 2002).

More specifically, it was hypothesised that the failure of some $IcsA_i$ mutants to activate N-WASP was due to a failure to interact with either of these domains (WH1 or CRIB). Whilst $IcsA_i$ mutants were unable to interact with one of these domains, they would still be able to interact with the other. Indeed, to test this hypothesis we acquired WH1-GFP (aa 1-148 of rat N-WASP) and CRIB-GFP (aa 148-273 of rat N-WASP) fusion proteins encoded on eukaryotic expression vectors from Professor Micheal Way (Moreau *et al*., 2000). Recruitment of ectopically expressed WH1-GFP and CRIB-GFP to *S. flexneri* Δ*icsA* expressing either $IcsA_{i185}$, $IcsA_{i219}$ $IcsA_{i226}$, $IcsA_{i330b}$, $IcsA_{i346}$, $IcsA_{i532}$ or $IcsA_{i563}$ in infected

HeLa cells was investigated. These strains were chosen as they were unable to form F-actin comet tails, and recruitment of N-WASP could not be detected (Tables 4.1 and 4.3). This work has since been completed in our laboratory by Luisa Van Den Bosch using CV-1 cells, which were found to be more readily transfected with the eukaryotic expression vectors and supported efficient ABM and intercellular spread of *S. flexneri*. All seven of these strains were found to recruit the CRIB region of N-WASP but not the WH1 region, thereby supporting our hypothesis (Van Den Bosch, May and Morona, unpublished data). Additionally, these findings highlight the potential importance of the WH1:IcsA interaction in N-WASP activation, ABM, and intercellular spreading, as all seven $IcsA_i$ mutants exhibit cell-cell spreading defects (Section 3.5, Table 3.5).

However, these experiments were conducted using S-LPS strains. In keeping with the proposed models (Section 8.4.1), it is possible that the WH1 binding region in these $IcsA_i$ mutants may not have been mutated directly but may be masked by LPS-Oag. Therefore, it would be important to conduct similar experiments using R-LPS isogenic strains. Additionally, the identification of $IcsA_i$ mutants that interact with the WH1 region but not the CRIB region would help to elucidate the respective binding domains within IcsA for each of these N-WASP domains.

8.4.6 Role of host accessory proteins

Since IcsA has been shown to bind both the WH1 and GBD/CRIB regulatory regions of N-WASP, it is perhaps not surprising that host ligands of these regions (e.g. WIP and Cdc42) are not essential for IcsA mediated activation of N-WASP (Egile *et* al., 1999; Loisel *et al*., 1999, Moreau *et al.*, 2000; Zettl and Way, 2002; Shibata *et al.*, 2002). It may be that IcsA has evolved to circumvent the need for accessory activators of N-WASP by interacting with multiple domains of N-WASP. It is now understood that IcsA activation of N-WASP occurs independent of Cdc42 (Egile *et* al., 1999; Loisel *et al*., 1999; Shibata *et al.*, 2002)

Instead, IcsA mimics Cdc42 activity by binding to the GBD/CRIB region in order to induce its active conformation. It would also be of interest to investigate whether the newly identified Toca-1 protein (Ho *et al*., 2004) is required for *Shigella* ABM, or if IcsA is able to mimic the function of this protein by binding to the WH1 region of N-WASP.

8.5 Intercellular spreading defect of $IcsA_i$ mutants with proficient F-actin comet tail formation and ABM

The ability to form F-actin comet tails correlated to N-WASP recruitment irrespective of plaque formation. This was expected: N-WASP has been shown to be essential for IcsA-mediated F-actin comet tail formation. However, this thesis describes the first *icsA* mutants that have proficient F-actin comet tail formation but are defective in intercellular spread. For *S. flexneri ΔicsA* strains expressing $IcsA_{i193}$ and $IcsA_{i312}$, the frequency of tail formation was statistically equivalent to *S. flexneri ΔicsA* expressing $IcsA_{WT}$ (Section 4.2; Figure 4.3), despite the fact that these strains exhibited a dramatic reduction in intercellular spreading (Section 3.5; Table 3.5). The molecular basis of this defect is currently under investigation, but these findings highlight the need for intercellular spreading to be directly assessed when determining the relative contribution of various host and bacterial factors to the process of ABM. One hypothesis is that IcsA is involved in the process of protrusion formation and intercellular spread. This is based on the observation that 85% of bacteria in protrusions are actively dividing (Prevost *et al*., 1992), which may place IcsA at the tip of protrusion. In this way, IcsA may act to recruit host factors required for protrusion formation and intercellular spread, in addition to its role in ABM.

8.6 Oligomerisation of IcsA and AT proteins.

The mechanism(s) of export of AT proteins onto the bacterial surface is(are) not completely understood. One of the models for AT translocation across the OM is the

oligomeric model, whereby translocation of the passenger domain proceeds through a central pore formed by an oligomer of translocation domains (Veiga *et al*., 2002) (Figure 1.6C). This is based on the observation that translocation domain of the *N. gonorrhoeae* IgA protease formed oligomeric structures (Veiga *et al.* 2002). It was this observation that was the basis for the investigation of IcsA oligomerisation in Chapter Four.

8.6.1 IcsA oligomerisation and its role in IcsA biogenesis and function

As demonstrated for the IgA protease, the presence of high molecular weight complexes containing IcsA was detected by Western immunoblotting following treatment of *S. flexneri* chemical cross-linker with DSP (Section 6.2; Figure 6.1). Specifically, two high molecular weight complexes (> 460 kDa) were detected. Due to their very high molecular weights, the exact size of the complexes formed could not be determined, but they could be hexamers similar to those formed by IgA protease. However, it is also possible that that these complexes contain additional proteins other than IcsA. The DSP cross-linker is able to penetrate the cell-membrane and either of these two complexes that were detected may include export components. For example, if the Omp85 model of AT protein export is correct (or relevant for IcsA), the IcsA complexes may include components of the Omp85 pore, which includes four currently identified components Omp85, YfgL, YfiO, and NlpB (Wu *et al*., 2005). Further characterisation of these complexes by combining DSP cross-linking with co-immunoprecipitation and mass-spectrometric analysis will enable these hypotheses to be tested.

Nevertheless, while the presence of other proteins in these complexes can not be excluded, the negative dominance exerted by $IcsA_i$ mutants ($IcsA_{i228}$, $IcsA_{i248}$, $IcsA_{i288}$, $IcsA_{i502}$, $IcsA_{i532}$, $IcsA_{i563}$ and $IcsA_{i677}$) on $IcsA_{WT}$ and $IcsA_{i87::FLAG}$ provides evidence of an IcsA:IcsA interaction (Section 6.3). The molecular basis for the negative dominance of these mutants was unclear, however, for $IcsA_{i563}$ and $IcsA_{i677}$ this effect was not due to effects on

either protein production or export onto the surface of the bacteria (Section 6.4.4-5; Figures 6.6 and 6.7)

A hypothesis to explain the negative dominance phenotype of $IcsA_i$ mutants is that the role of oligomerisation is independent of protein export and is required for protein functionality. For example, oligomeric IcsA may be the form of IcsA that interacts with N-WASP. Another hypothesis is that oligomerisation may act to increase local concentration of IcsA (thereby excluding LPS molecules) and in the process, overcoming potential masking of IcsA function by LPS-Oag. This might explain why the N-WASP recruitment defect of certain $IcsA_i$ mutants ($IcsA_{i185}$, $IcsA_{i226}$, $IcsA_{i532}$ and $IcsA_{i563}$) is LPS-Oag dependent. Examination of the oligomerisation potential of these mutants would enable this hypothesis to be tested.

It has been suggested that if AT translocation does indeed proceed through an oligomeric pore that the putative auto-chaperone regions identified in several ATs (including SSP, Pet, BrkA and IcsA) may play a role in stabilising this pore. Moreover, mutation of this region may abolish pore formation, preventing translocation of the passenger domains, resulting in degradation by periplasmic proteases (Dutta *et al.*, 2003). $IcsA_{i677}$ possesses a linker-insertion within the putative auto-chaperone region of IcsA and may be sensitive to degradation by periplasmic proteases (Section 3.3; Figure 3.3). However, preliminary data shows that oligomerisation of $IcsA_{i677}$ can still be detected (albeit faintly) following DSP cross-linking and Western immunoblotting (May, unpublished observations) so this hypothesis would appear unlikely. Similar experiments with other mutants of this region ($IcsA_{i633}$, $IcsA_{i643}$, $IcsA_{i716}$ and $IcsA_{\Delta 507\text{-}730}$) have not yet been conducted and investigation of the oligomerisation potential of these mutants will enable this hypothesis to be tested more comprehensively.

8.6.2 Oligomerisation of other AT proteins

Attempts to show oligomerisation of ATs other than IgA protease and IcsA have proven unsuccessful. The main discrepancy between the study involving IgA protease (Veiga *et al*., 2002) and other studies (Oomen *et al*., 2004; Muller *et al*., 2005) was the protein purification protocols used. Veiga *et al*. (2002) used the detergent Zwittergent 3-14 (Calbiochem, #693017) to solubilise the oligomeric structures from the OM, whereas the others studies have used Triton X-100 (Oomen *et al*., 2004; Muller *et al*., 2005). The latter detergent, in addition to extracting AT proteins from the OM, may also disrupt any complexes they had formed. Consequently, this might explain why Muller *et al*. (2005) were unable to detect oligomerisation of the AT AIDA-I by either electron microscopy or gel filtration of the purified protein. Additionally, in this study DSP cross-linked samples were heated at 100 °C prior to SDS/PAGE and Western immunoblotting, which may have also disrupted the oligomers. Skillman *et al.* (2005) reported that the purified EspP AT was also monomeric, even when Zwittergent 3-14 was used to extract the protein from the OM. These authors have reconciled their data with that of Veiga *et al.* (2002) by suggesting that there are two classes of AT, monomeric and oligomeric (Skillman *et al.*, 2005). The other evidence in support of a monomeric export model was the crystal structure of the NalP translocation domain in which the α helical linker region of the translocation domain (located between the passenger domain and the β-barrel pore) was positioned inside of the β-barrel pore (Figure 1.7; Oomen *et al*., 2004). However, as the NalP translocation domain was denatured during the purification procedure and refolded *in vitro*, the crystal structure may not represent the protein's native structure in the OM.

Although oligomerisation has not been shown for any other native AT proteins (other than IgA protease and IcsA), it has been demonstrated for hybrid proteins comprising protein fusions to AT translocation domains. Jose *et al*. (2002) demonstrated that the bovine adrenodoxin (Adx) protein fused to the AIDA-I translocation domain was able to dimerise on

the surface of *E. coli.* Similar data has been obtained using the partner leucine zippers of the eukaryotic transcriptional factors, Fos and Jun, fused to translocation domains of IgA protease (Veiga *et al.*, 2003). In both cases, the heterologous passenger domains that were used were chosen as they are only functional upon dimerisation. Therefore proper function of these proteins could be used as an indicator for dimerisation. However, as dimerisation of these proteins normally occurs independent of the AT translocation domains to which they were fused, these experiments do not provide evidence that ATs themselves oligomerise, only that such behaviour is possible and may be mediated via the passenger domains (note that the study by Veiga *et al*. (2002) involving the IgA protease examined oligomerisation of the translocation domain alone).

8.7 *In silico* analysis predicts a β-helical IcsA passenger domain

8.7.1 Predicted structural features of the IcsA passenger domain

Three independent structure prediction programs (BetawrapPro, PHYRE and Robetta) predicted that the IcsA passenger domain forms a right-handed parallel β-helix (Sections 5.3-5.5). Interestingly, the IcsA Robetta model (Figure 5.5) appears remarkably like the recently solved crystal structure of the AT, Haemoglobin protease (Hbp) (Figure 1.9B; Otto *et al.*, 2005). Robetta utilises threading and *ab initio* algorithms and it is possible that the Robetta program has threaded IcsA on the Hbp structure (the output of the program is very limited and does not feature these details). However, this may not be the case since the Robetta model differed to the PHYRE model which relies on a threading algorithm alone.

The Robetta model also predicts two cysteines (C_{275} and C_{279}) in close proximity (Figure 5.6), but analysis of the IcsA passenger domain with the DISULFIND, a disulphide bonding state and cysteine connectivity prediction server (Ceroni *et al.*, 2006) suggested the probability of disulphide bond formation between C_{275} and C_{279} was low (Figure 5.7). This is probably due to the short distance between the two amino acid residues. A paucity of cysteine

residues in AT proteins has been noted, and difficulties exporting heterologous passenger domains containing cysteines have been demonstrated (Klauser *et al*., 1990; Jose *et al*., 1995; Henderson *et al*., 2004). Therefore, the role of the cysteine residues in IcsA biogenesis and function are unclear. The IcsA passenger domain has been shown to be folded during secretion, and although it can form at least one intramolecular disulfide bond, this folding does not require disulfide bond formation (Brandon and Goldberg, 2001). This study by Brandon and Goldberg involved use of reducing agents and a *dsbA* mutant lacking the periplasmic disulfide bond-forming enzyme DsbA. It would be of interest to mutate the cysteine residues within IcsA in order to examine the role they play in IcsA biogenesis and/or function.

8.7.2 Interaction between the IcsA passenger domain and LPS-Oag

The finding that IcsA passenger domain has a β-helical structure and the apparent effect of LPS Oag in IcsA function is interesting due to the fact that many such proteins have been reported to interact with oligosaccharides (Steinbacher *et al*., 1996 Jenkins and Pickersgill, 2001; Freiberg *et al*., 2003; Henderson *et al*., 2004) (Section 1.3.4). The P22 phage tail spike protein has a well-characterised interaction with LPS-Oag (Steinbacher *et al*., 1996). Based on X-ray crystallography data the Oag binding site for TSP has been shown to be located in the central part of the β-helix (Steinbacher *et al*., 1996). It is not known if IcsA interacts similarly with LPS-Oag. An interaction between IcsA and Oag is consistent with the proposal that in ABM, LPS-Oag is responsible for maintaining unipolar IcsA localisation to ensure efficient ABM and intercellular spread (Sandlin *et al.*, 1995; Robbins *et al*., 2001). This model is based on the observation that R-LPS strains display altered IcsA localisation with IcsA detected on the lateral regions as well as the poles. It has been suggested that LPS Oag reinforces IcsA polarisation by reduction of OM fluidity, thereby preventing diffusion of IcsA away from the pole towards lateral regions of the bacterium (Sandlin *et al.*, 1995; Robbins *et al*., 2001). However, it might be that LPS-Oag at the poles interacts with IcsA

thereby immobilising it. Consistent with this model is the recent data of Ghosh and Young (2005) in which they found a sub-population of LPS are embedded in stable domains at the poles. As IcsA function is not dependent on the actual chemical composition of the Oag repeat unit (Sandlin *et al*., 1996), it is unlikely that the interaction of IcsA with LPS-Oag is a specific interaction like that of TSP with Oag, but instead a weak interaction. Oligomerisation of IcsA may also play a role in limiting its diffusion in the OM. However, as the results of this thesis indicate that oligomerisation is independent of LPS-Oag (Section 6.2; Figure 6.1), this would not account for the phenotype of R-LPS *S. flexneri* strains. Other hypotheses to account for the distribution of IcsA in R-LPS strains are presented in Chapter One (Section 1.7.2).

8.8 Conclusions

The structure-function study of the IcsA protein conducted in this thesis has lead to a refinement of the second polar targeting region (aa 507-620) of IcsA to aa 532-563, and has identified several novel functional regions within the IcsA passenger domain. This includes a putative auto-chaperone region (aa 595- 716) and two further N-WASP interacting regions (aa 330-381 and 508-730), in addition to the GRR region, which was identified previously as the N-WASP binding region. As well as identifying novel N-WASP interacting regions, LPS-Oag has been shown to have a dramatic affect on the interaction of N-WASP with IcsA. Furthermore, oligomerisation of IcsA was also demonstrated for the first time, although the role this plays in either IcsA biogenesis or its function in N-WASP activation and ABM is unclear.

It is apparent that IcsA has evolved to activate N-WASP in the presence of host regulatory proteins that maintain the inactive conformation of N-WASP, and it has also evolved to function in the presence of LPS-Oag on the bacterial surface. The determination of the structure of IcsA and IcsA in complex with N-WASP (with and without LPS-Oag), would clearly assist our understanding of the activation process.

It is not foreseeable when a tertiary structure of IcsA will be resolved. Multi-domain proteins such as IcsA (and N-WASP) are often difficult to crystalise and are too large for NMR structure determination (Kim *et al*., 2004). In the meantime, the Robetta model created in Chapter Five is currently being used as guide for ongoing work in our laboratory.

References

Adler, B., Sasakawa, C., Tobe, T., Makino, S., Komatsu, K. and Yoshikawa, M. (1989) A dual transcriptional activation system for the 230 kb plasmid genes coding for virulence-associated antigens of *Shigella flexneri*. *Mol Microbiol*. **3**: 627-635.

Allaoui, A., Mounier, J., Prevost, M.C., Sansonetti, P.J. and Parsot, C. (1992) *icsB*: a *Shigella flexneri* virulence gene necessary for the lysis of protrusions during intercellular spread. *Mol. Microbiol.* **6**: 1605-1616.

Ally, S., Sauer, N.J., Loureiro, J.J., Snapper, S.B., Gertler, F.B. and Goldberg, M.B. (2004) *Shigella* interactions with the actin cytoskeleton in the absence of Ena/VASP family proteins. *Cellular Microbiology*. **6**: 355-366.

Achtman, M., Manning, P.A., Edelbluth, C., Herrlich, P. (1979) Export without proteolytic processing of inner and outer membrane proteins encoded by F sex factor tra cistrons in *Escherichia coli* minicells. *Proc. Natl. Acad. Sci.* **76**: 4837-41.

Batchelor, R.A., Haraguchi, G.E., Hull, R.A., Hull, S.I. (1991) Regulation by a novel protein of the bimodal distribution of lipopolysaccharide in the outer membrane of *Escherichia coli*. *J Bacteriol.* **173**: 5699–5704.

Bernardini, M.L., Mounier, J., d'Hauteville, H., Coquis-Rondon, M. and Sansonetti, P.J. (1989) Identification of *icsA*, a plasmid locus of *Shigella flexneri* that governs bacterial intra- and intercellular spread through interaction with F-actin. *Proc. Natl. Acad. Sci. U.S.A.* **86**: 3867-3871.

Blocker, A., Gounon, P., Larquet, E., Niebuhr, K., Cabiaux, V., Parsot, C. and Sansonetti, P. (1999) The tripartite type III secretion of *Shigella flexneri* inserts IpaB and IpaC into host membranes. *J. Cell Biol*. **147**:683-93.

Brandon, L.D. and Goldberg, M.B. (2001) Periplasmic transit and disulfide bond formation of the autotransported *Shigella* Protein IcsA. *J. Bacteriol.* **183**: 951-958.

Brandon, L.D., Goehring, N., Janakiraman, A., Yan, A.W., Wu, T., Beckwith, J. and Goldberg, M.B. (2003) IcsA, a polarly localized autotransporter with an atypical signal peptide, uses the Sec apparatus for secretion, although the Sec apparatus is circumferentially distributed. *Mol. Microbiol*. **50**: 45-60.

Bulieris, P.V., Behrens, S., Holst, O. and Kleinschmidt, J.H. (2003) Folding and insertion of the outer membrane protein OmpA is assisted by the chaperone Skp and by lipopolysaccharide. *J Biol Chem*. **278**: 9092-9099.

Burton, E.A., Oliver, T.N. and Pendergast, A.M. (2005) Abl kinases regulate actin comet tail elongation via an N-WASP-dependent pathway. *Mol. Cell. Biol.* **25**: 8834-8843.

Carlier, M.F., Le Clainche, C., Wiesner, S. and Pantaloni, D. (2003a) Actin-based motility: from molecules to movement. *Bioessays*. **25**: 336-345.

Carlier, M.F., Nioche, P., Broutin-L'Hermite, I., Boujemaa, R., Le Clainche, C., Egile, C., Garbay, C., Ducruix, A., Sansonetti, P.J. and Pantaloni, D. (2000) GRB2 links signalling to actin assembly by enhancing interaction of neural Wiskott-Aldrich syndrome protein (N-WASP) with actin-related protein (ARP2/3) complex. *J. Biol. Chem*. **275**: 21946-21952.

Ceroni, A., Passerini, A., Vullo, A., Frasconi, P. (2006) DISULFIND: a disulfide bonding state and cysteine connectivity prediction server. *Nucleic Acids Res.* **34**:177-81.

Chakraborty, T., Ebel, F., Domann, E., Niebuhr, K., Gerstel, B., Pistor, S., Temm-Grove, C.J., Jockusch, B.M., Reinhard, M., Walter, U. and Wehland, J. (1995) A focal adhesion factor directly linking intracellularly motile *Listeria monocytogenes* and *Listeria ivanovii* to the actin-based cytoskeleton of mammalian cells. *EMBO J.* **14**: 1314-1321.

Charles, M., Magdalena, J., Theriot, J.A. and Goldberg, M.B. (1999) Functional Analysis of a Rickettsial OmpA Homology Domain of *Shigella flexneri* IcsA. *J. Bacteriol.* **181**: 869-878.

Charles, M., Perez, M., Kobil, J.H. and Goldberg, M.B. (2001) Polar targeting of *Shigella* virulence factor IcsA in *Enterobacteriacae* and *Vibrio*. *Proc. Natl. Acad. Sci. U.S.A.* **98**: 9871-9876.

Datsenko, K.A. and Wanner, B.L. (2000) One-step inactivation of chromosomal genes in *Escherichia coli* K-12 using PCR products. *Proc. Natl. Acad. Sci. U.S.A.* **97**: 6640-6645.

David, V., Gouin, E., Troys, M.V., Grogan, A., Segal, A.W., Ampe, C. and Cossart, P. (1998) Identification of cofilin, coronin, Rac and capZ in actin tails using a *Listeria* affinity approach. *J. Cell. Sci*. **111**: 2877-2884.

Davison, J., Heusterspreute, M., Chevalier, N., Ha-Thi, V. and Brunel, F. (1987) Vectors with restriction site banks. V. pJRD215, a wide-host-range cosmid vector with multiple cloning sites. *Gene*. **51**: 275-280.

de Boer, P.A., Crossley, R.E. and Rothfield, L.I. (1989) A division inhibitor and a topological specificity factor coded for by the minicell locus determine proper placement of the division septum in *E. coli*. *Cell*. **56**: 641-649.

Desvaux, M., Parham, N.J. and Henderson, I.R. (2004) The autotransporter secretion system. *Res. Microbiol.* **155**: 53-60.

d'Hauteville, H. and Sansonetti, P.J. (1992) Phosphorylation of IcsA by cAMP-dependent protein kinase and its effect on intercellular spread of *Shigella flexneri*. *Mol. Microbiol.* **6**: 833-841.

d'Hauteville, H., Dufourcq Lagelouse, R., Nato, F. and Sansonetti, P.J. (1996) Lack of cleavage of IcsA in *Shigella flexneri* causes aberrant movement and allows demonstration of a cross-reactive eukaryotic protein. *Infect. Immun.* **64**: 511-517.

Dorman, C.J. and Porter, M.E. (1998) The *Shigella* virulence gene regulatory cascade: a paradigm of bacterial gene control mechanisms. *Mol. Microbiol.* **29**:677-684.

Dutta, P.R., Sui, B.Q. and Nataro, J.P. (2003) Structure-function analysis of the enteroaggregative *Escherichia coli* plasmid-encoded toxin autotransporter using scanning linker mutagenesis. *J. Biol. Chem.* **278**: 39912-39920.

Egile, C., d'Hauteville, H., Parsot, C. and Sansonetti, P.J. (1997) SopA, the outer membrane protease responsible for polar localisation of IcsA in *Shigella flexneri*. *Mol. Microbiol*. **23**: 1063-1073.

Egile, C., Loisel, T.P., Laurent, V., Li, R., Pantaloni, D., Sansonetti, P.J. and Carlier, M.-F. (1999) Activation of the Cdc42 effector N-WASP by the *Shigella flexneri* IcsA protein promotes actin nucleation by Arp2/3 complex and bacterial actin-based motility. *J. Cell Biol.* **146**: 1319-1332.

Elish, M.E., Pierce, J.R. and Earhart, C.F. (1988) Biochemical analysis of spontaneous *fepA* mutants of *Escherichia coli. J. Gen. Microbiol*. **134**: 1355-1364.

Emsley, P., Charles, I.G., Fairweather, N.F. and Isaacs, N.W. (1996) Structure of *Bordetella pertussis* virulence factor P.69 pertactin. *Nature.* **381**: 90-92.

Enninga, J., Mounier, J., Sansonetti, P., Tran Van Nhieu, G. (2005) Secretion of type III effectors into host cells in real time. *Nat. Methods*. **2**: 959-65.

Esue, O., Cordero, M., Wirtz, D. and Tseng, Y. (2005) The assembly of MreB, a prokaryotic homolog of actin. *J. Biol. Chem.* **280**: 2628-2635.

Fekkes, P. and Driessen, A.J. (1999) Protein targeting to the bacterial cytoplasmic membrane. *Microbiol. Mol. Biol. Rev.* **63**: 161-173.

Fernandez, R.C. and Weiss, A.A. (1994) Cloning and sequencing of a *Bordetella pertussis* serum resistance locus. *Infect. Immun.* **62**: 4727-4738.

Figge, R.M., Divakaruni, A.V. and Gober, J.W. (2004) MreB, the cell shape-determining bacterial actin homologue, co-ordinates cell wall morphogenesis in *Caulobacter crescentus*. *Molecular Microbiology*. **51**: 1321-1332.

Freiberg, A., Morona, R., Van den Bosch, L., Jung, C., Behlke, J., Carlin, N., Seckler, R. and Baxa, U. (2003) The tailspike protein of Shigella phage Sf6. A structural homolog of Salmonella phage P22 tailspike protein without sequence similarity in the β-helix domain. *J. Biol. Chem.* **278**: 1542-1548.

Frischknecht, F., Cudmore, S., Moreau, V., Reckmann, I., Rottger, S., Way, M. (1999) Tyrosine phosphorylation is required for actin-based motility of vaccinia but not *Listeria* or *Shigella*. *Curr. Biol.* **9**:89-92.

Fukuda, I., Suzuki, T., Munakata, H., Hayashi, N., Katayama, E., Yoshikawa, M. and Sasakawa, C. (1995) Cleavage of *Shigella* surface protein VirG occurs at a specific site, but the secretion is not essential for intracellular spreading. *J. Bacteriol.* **177**: 1719-1726.

Fukuoka, M., Miki, H. and Takenawa, T. (1997) Identification of N-WASP homologs in human and rat brain. *Gene* **196**:43-48.

Galler, A., Garcia Arguinzonis, M., Baumgartner, W., Kuhn, M., Smolenski, A., Simm, A. and Reinhard, M. (2005) VASP-dependent regulation of actin cytoskeleton rigidity, cell adhesion, and detachment. *Histochemistry and Cell Biology*: 1-18.

Gertler, F.B., Niebuhr, K., Reinhard, M., Wehland, J. and Soriano, P. (1996) Mena, a relative of VASP and Drosophila Enabled, is implicated in the control of microfilament dynamics. *Cell.* **87**: 227-239.

Gemski, P., Griffin, D.E. (1980) Isolation and characterization of minicell-producing mutants of *Shigella* spp. *Infect Immun.* **30**: 297-302.

Ghosh, A.S. and Young, K.D. (2005) Helical disposition of proteins and lipopolysaccharide in the outer membrane of *Escherichia coli. J. Bacteriol.* **187**: 1913-1922.

Girardin, S.E., Tournebize, R., Mavris, M., Page, A., Li, X., Stark, G.R., Bertin, J., DiStefano, P.S., Yaniv, M., Sansonetti, P.J. and Philpott, D.J. (2001) CARD4/Nod1 mediates NF-κB and JNK activation by invasive *Shigella flexneri. EMBO Rep.* **2**: 736–742.

Goldberg, M.B., Barzu, O., Parsot, C. and Sansonetti, P.J. (1993) Unipolar localisation and ATPase activity of IcsA, a *Shigella flexneri* protein involved in intracellular movement. *J Bacteriol*. **175**: 2189-2196.

Goldberg, M.B., Theriot, J. and Sansonetti, P.J (1994) Regulation of surface presentation of IcsA, a *Shigella* protein essential to intracellular movement and spread, is growth phase dependent. *Infect Immun*. **62**: 5664-5668.

Goldberg, M.B. and Theriot, J.A. (1995) *Shigella flexneri* surface protein IcsA is sufficient to direct actin-based motility. *Proc Natl Acad Sci U S A*. **92**: 6572-6576.

Goldberg, M.B. (1997) *Shigella* actin-based motility in the absence of vinculin. *Cell. Motil. Cytoskeleton.* **37**:44-53.

Goldberg, M.B. (2001) Actin-based motility of intracellular microbial pathogens. *Microbiol. Mol. Biol. Rev.* **65**: 595-626.

Goldman, R.C. and Hunt, F. (1990) Mechanism of O-antigen distribution in lipopolysaccharide. *J. Bacteriol.* **172**: 5352-9.

Gouin, E., Gantelet, H., Egile, C., Lasa, I., Ohayon, H., Villiers, V., Gounon, P., Sansonetti, P.J., Cossart, P. (1999) A comparative study of the actin-based motilities of the pathogenic bacteria *Listeria monocytogenes*, *Shigella flexneri* and *Rickettsia conorii*. *J Cell Sci*. **112**: 1697-1708.

Grodberg, J. and Dunn, J. (1988) *ompT* encodes the *Escherichia coli* outer membrane protease that cleaves T7 RNA polymerase during purification. *J. Bacteriol.* **170**: 1245-1253.

Gumbiner, B.M. (1996) Cell adhesion: the molecular basis of tissue architecture and morphogenesis. *Cell*. **84**:345-57

Henderson, I.R., Navarro-Garcia, F. and Nataro, J.P. (1998) The great escape: structure and function of the autotransporter proteins. *Trends Microbiol*. **6**: 370-378.

Henderson, I.R. and Nataro, J.P. (2001) Virulence Functions of Autotransporter Proteins. *Infect. Immun.* **69**: 1231-1243.

Henderson, I.R., Navarro-Garcia, F., Desvaux, M., Fernandez, R.C. and Ala'Aldeen, D. (2004) Type V Protein Secretion Pathway: the Autotransporter Story. *Microbiol. Mol. Biol. Rev.* **68**: 692-744.

Higgins, D., Thompson, J., Gibson, T., Thompson J. D., Higgins D. G., Gibson T. J. (1994). CLUSTAL W: improving the sensitivity of progressive multiple sequence alignment through sequence weighting,position-specific gap penalties and weight matrix choice. *Nucleic Acids Res.* **22**: 4673-4680.

Hitchcock, P.J. and Brown, T.M. (1983) Morphological heterogeneity among *Salmonella* lipopolysaccharide chemotypes in silver-stained polyacrylamide gels. *J Bacteriol* **154**:269-277.

Ho, H.Y., Rohatgi, R., Ma, L. and Kirschner, M.W. (2001) CR16 forms a complex with N-WASP in brain and is a novel member of a conserved proline-rich actin-binding protein family. *Proc. Natl. Acad. Sci. U.S.A.* **98**: 11306-11311.

Ho, H.Y., Rohatgi, R., Lebensohn, A.M., Le Ma, Li J., Gygi, S.P. and Kirschner, M.W. (2004) Toca-1 mediates Cdc42-dependent actin nucleation by activating the N-WASP-WIP complex. *Cell.* **118**: 203-216.

Hong, M. and Payne, S.M. (1997) Effect of mutations in *Shigella flexneri* chromosomal and plasmid-encoded lipopolysaccharide genes on invasion and serum resistance. *Mol Microbiol*. **24**: 779-791.

Insall, R.H. and Machesky, L.M. (2004) Regulation of WASP: PIP2 Pipped by Toca-1? *Cell.* **118**: 140-141.

Jacob-Dubuisson, F., Fernandez, R. and Coutte, L. (2004) Protein secretion through autotransporter and two-partner pathways. *Biochimica et Biophysica Acta (BBA) - Molecular Cell Research*. **1694**: 235-257.

Jain, S., van Ulsen, P., Benz, I., Schmidt, M.A., Fernandez, R., Tommassen, J. and Goldberg, M.B. (2006) Polar Localisation of the Autotransporter family of large bacterial virulence Proteins. *J. Bacteriol.* **188**: 4841-4850.

Janakiraman, A. and Goldberg, M.B. (2004) Evidence for polar positional information independent of cell division and nucleoid occlusion. *Proc Natl Acad Sci U S A*. **8**: 8.

Jenkins, J. and Pickersgill, R. (2001) The architecture of parallel beta-helices and related folds. *Prog. Biophys. Mol. Biol.* **77**: 111-175.

Jennison, A.V. and Verma, N.K. (2004) Shigella flexneri infection: pathogenesis and vaccine development. *FEMS Microbiology Reviews*. **28**: 43-58.

Jin, Q., Yuan, Z., Xu, J., Wang, Y., Shen, Y., Lu, W., Wang, J., Liu, H., Yang, J., Yang, F., Zhang, X., Zhang, J., Yang, G., Wu, H., Qu, D., Dong, J., Sun, L., Xue, Y., Zhao, A., Gao, Y., Zhu, J., Kan, B., Ding, K., Chen, S., Cheng, H., Yao, Z., He, B., Chen, R., Ma, D., Qiang, B., Wen, Y., Hou, Y. and Yu, J. (2002) Genome sequence of *Shigella flexneri* 2a: insights

into pathogenicity through comparison with genomes of *Escherichia coli* K12 and O157. *Nucleic Acids Res.* **30**: 4432–4441.

Johnson, R.P. and Craig, S.W. (1994) An intramolecular association between the head and tail domains of vinculin modulates talin binding. *J. Biol. Chem.* **269**: 12611-1219.

Johnson, R.P. and Craig, S.W. (1995) F-actin binding site masked by the intramolecular association of vinculin head and tail domains. *Nature.* **373**: 261-264.

Jose, J., F. Jahnig, F. and Meyer, T. F. (1995) Common structural features of IgA1 protease-like outer membrane protein autotransporters. *Mol. Microbiol.* **18:**378-380.

Jose, J., Kramer, J., Klauser, T., Pohlner, J. and Meyer, T.F. (1996) Absence of periplasmic DsbA oxidoreductase facilitates export of cysteine-containing passenger proteins to the *Escherichia coli* cell surface via the IgA beta autotransporter pathway. *Gene* **178**:107–110.

Jose, J., Bernhardt, R., Hannemann, F. (2002) Cellular surface display of dimeric Adx and whole cell P450-mediated steroid synthesis on *E. coli. J Biotechnol.* **95**: 257-68.

Junker, M., Schuster, C.C., McDonnell, A.V., Sorg, K.A., Finn, M.C., Berger, B. and Clark, P.L. (2006) Pertactin β-helix folding mechanism suggests common themes for the secretion and folding of autotransporter proteins. *Proc. Natl. Acad. Sci. U S A.* **103**: 4918-4923.

Kadurugamuwa, J.L., Rohde, M., Wehland, J. and Timmis, K.N. (1991) Intercellular spread of *Shigella flexneri* through a monolayer mediated by membranous protrusions and associated with reorganization of the cytoskeletal protein vinculin. *Infect Immun*. **59**: 3463-3471.

Kim, A.S., Kakalis, L.T., Abdul-Manan, N., Liu, G.A., Rosen, M.K. (2000) Autoinhibition and activation mechanisms of the Wiskott-Aldrich syndrome protein. *Nature.* **404**: 151-158.

Kim, D.E., Chivian, D. and Baker, D. (2004) Protein structure prediction and analysis using the Robetta server. *Nucleic Acids Res*. **32**: W526–W531.

Klauser, T., Pohlner, J., Meyer, T. F. (1990) Extracellular transport of cholera toxin B subunit using *Neisseria* IgA protease beta-domain: conformation-dependent outer membrane translocation. *EMBO*. **9**:1991–1999.

Kocks, C., Marchand, J., Gouin, E., d'Hauteville, H., PJ, S., Carlier, M.-F. and Cossart, P. (1995) The unrelated surface proteins ActA of *Listeria monocytogenes* and IcsA of *Shigella flexneri* are sufficient to confer actin-based motility on *Listeria innocua* and *Escherichia coli* respectively. *Mol. Microbiol.* **18**: 413-423.

Kotloff, K.L., Noriega, F., Losonsky, G.A., Sztein, M.B., Wasserman, S.S., Nataro, J.P. and Levine, M.M. (1996) Safety, immunogenicity, and transmissibility in humans of CVD 1203, a live oral *Shigella flexneri* 2a vaccine candidate attenuated by deletions in *aroA* and *virG*. *Infect. Immun.* **64**:4542-4548.

Kotloff, K., Winickoff, J., Ivanoff, B., Clemens, J., Swerdlow, D., Sansonetti, P., Adak, G.K., Levine, M.M. (1999) Global burden of Shigella infections: implications for vaccine development and implementation of control strategies. *Bull. World. Health Organ.* **77**: 651-666.

Kotloff, K.L., Taylor, D.N., Sztein, M.B., Wasserman, S.S., Losonsky, G.A., Nataro, J.P., Venkatesan, M., Hartman, A., Picking, W.D., Katz, D.E., Campbell, J.D., Levine, M.M. and T.L. Hale, T.L. (2002) Phase I evaluation of Δ*virG Shigella sonnei* live, attenuated, oral vaccine strain WRSS1 in healthy adults. *Infect Immun.* **70**: 2016-2021.

Kovach, M.E., Elzer, P.H., Hill, D.S., Robertson, G.T., Farris, M.A., Roop, R.M. 2nd, Peterson, K.M. (1995) Four new derivatives of the broad-host-range cloning vector pBBR1MCS, carrying different antibiotic-resistance cassettes. *Gene*. **166**: 175-6.

LaBrec, E.H., Schneider, H., Magnani, T.J. and Formal, S.B. (1964) Epithelial cell penetration as an essential step in the pathogenesis of bacillary dysentery. *J. Bacteriol.* **88**: 1503-1518.

Lai, E.M., Nair, U., Phadke, N.D., Maddock, J.R. (2004) Proteomic screening and identification of differentially distributed membrane proteins in *Escherichia coli*. *Mol. Microbiol.* **52**: 1029-44.

Laine, R.O., Zeile, W., Kang, F., Purich, D.L. and Southwick, F.S. (1997) Vinculin proteolysis unmasks an ActA homolog for actin-based *Shigella* motility. *J. Cell Biol.* **138**: 1255-1264.

Lan, R. and Reeves, P.R. (2002) Escherichia coli in disguise: molecular origins of Shigella. *Microbes Infect*. **4**: 1125-1132.

Lett, M.C., Sasakawa, C., Okada, N., Sakai, T., Makino, S., Yamada, M., *et al.* (1989) *virG*, a plasmid-coded virulence gene of *Shigella flexneri*: identification of the VirG protein and determination of the complete coding sequence. *J Bacteriol*. **171**: 353-359.

Liu, D. and Reeves, P.R.(1994) *Escherichia coli* K12 regains its O antigen. *Microbiology*. **140:** 49-57.

Loisel, T.P., Boujemaa, R., Pantaloni, D. and Carlier, M.-F. (1999) Reconstitution of actin-based motility of *Listeria* and *Shigella* using pure proteins. *Nature*. **401**: 613-616.

Lommel, S., Benesch, S., Rottner, K., Franz, T., Wehland, J. and Kuhn, R. (2001) Actin pedestal formation by enteropathogenic *Escherichia coli* and intracellular motility of *Shigella flexneri* are abolished in N-WASP-defective cells. *EMBO Rep.* **2**: 850-857.

Lucchini, S., Liu, H., Jin, Q., Hinton, J.C.D. and Yu, J. (2005) Transcriptional Adaptation of *Shigella flexneri* during infection of macrophages and epithelial cells: insights into the strategies of a cytosolic bacterial pathogen. *Infect. Immun.* **73**: 88-102.

Ma, L., Cantley, L.C., Janmey, P.A. and Kirschner, M.W. (1998a) Co-requirement of specific phosphoinositides and small GTP-binding protein Cdc42 in inducing actin assembly in Xenopus egg extracts. *J. Cell Biol.* 140:1125–1136.

Ma, L., Rohatgi, R. and Kirschner, M.W. (1998b) The Arp2/3 complex mediates actin polymerization induced by the small GTP-binding protein Cdc42. *Proc. Natl. Acad. Sci. U.S.A.* **95**: 15362-15367.

Macpherson, D.F., Morona, R., Beger, D.W., Cheah, K.C. and Manning, P.A. (1991) Genetic analysis of the *rfb* region of *Shigella flexneri* encoding the Y serotype O-antigen specificity. *Mol. Microbiol.* **5**:1491-1499.

Magdalena, J. and Goldberg, M. (2002) Quantification of *Shigella* IcsA required for bacterial actin polymerization. *Cell Motility and the Cytoskeleton*. **51**: 187-196.

Makino, S., Sasakawa, C., Kamata, K., Kurata, T. and Yoshikawa, M. (1986) A genetic determinant required for continuous reinfection of adjacent cells on large plasmid in *S. flexneri* 2a. *Cell*. **46**: 551-555.

Martinez-Quiles, N., Rohatgi, R., Anton, I.M., Medina, M., Saville, S.P., Miki, H., Yamaguchi, H., Takenawa, T., Hartwig, J.H., Geha, R.S., Ramesh, N. (2001) WIP regulates N-WASP-mediated actin polymerization and filopodium formation. *Nat Cell Biol.* **3**: 484-91.

Maurer, J., Jose, J. and Meyer, T.F. (1997) Autodisplay: one-component system for efficient surface display and release of soluble recombinant proteins from *Escherichia coli*. *J. Bacteriol.* **179**: 794-804.

McDonnell, A.V., Menke, M., Palmer, N., King, J., Cowen, L., Berger, B. (2006) Prediction and comparative modeling of sequences directing β-sheet proteins by profile wrapping. *Proteins: Structure, Function, and Bioinformatics*. **63**: 976-985.

Miller, J.H. (1992) Assay for β-galactosidase. In Experiments in molecular genetics. New York: Cold Spring Harbour Laboratory Press, pp. 352-355

Miki, H., Miura, K. and Takenawa, T. (1996). N-WASP, a novel actin-depolymerizing protein, regulates the cortical cytoskeletal rearrangement in a PIP2-dependent manner downstream of tyrosine kinases. *EMBO J.* **15**: 5326-5335.

Miki, H. and Takenawa, T. (2003) Regulation of actin dynamics by WASP family proteins. *J. Biochem. (Tokyo)* **134**: 309-313.

Mimuro, H., Suzuki, T., Suetsugu, S., Miki, H., Takenawa, T. and Sasakawa, C. (2000) Profilin is required for sustaining efficient intra- and intercellular spreading of *Shigella flexneri*. *J. Biol. Chem.* **275**: 28893-28901.

Monack, D.M. and Theriot, J.A. (2001) Actin-based motility is sufficient for bacterial membrane protrusion formation and host cell uptake. *Cellular Microbiology*. **3**: 633-647.

Moreau, V., Frischknecht, F., Reckmann, I., Vincentelli, R., Rabut, G., Stewart, D. and Way, M. (2000) A complex of N-WASP and WIP integrates signalling cascades that lead to actin polymerization. *Nat Cell Biol*. **2**: 441-448.

Morona, R., Mavris, M., Fallarino, A. and Manning, P.A. (1994) Characterization of the *rfc* region of *Shigella flexneri*. *J. Bacteriol.* **176**: 733-747.

Morona, R., Van Den Bosch, L. and Manning, P.A. (1995) Molecular, genetic, and topological characterization of O-antigen chain length regulation in *Shigella flexneri*. *J. Bacteriol.* **177**: 1059-1068.

Morona, R., Daniels, C. and Van Den Bosch, L. (2003) Genetic modulation of *Shigella flexneri* 2a lipopolysaccharide O antigen modal chain length reveals that it has been optimized for virulence. *Microbiology*. **149**: 925-939.

Morona, R. and Van Den Bosch, L. (2003a) Multicopy *icsA* is able to suppress the virulence defect caused by the wzz_{SF} mutation in *Shigella flexneri*. *FEMS Microbiology Letters*. **221**: 213-219.

Morona, R. and Van Den Bosch, L. (2003b) Lipopolysaccharide O antigen chains mask IcsA (VirG) in *Shigella flexneri. FEMS Microbiology Letters*. **221**: 173-180.

Mounier, J., Vasselon, T., Hellio, R., Lesourd, M. and Sansonetti, P.J. (1992) *Shigella flexneri* enters human colonic Caco-2 epithelial cells through the basolateral pole. *Infect. Immun.* **60**: 237-248.

Mounier, J., Laurent, V., Hall, A., Fort, P., Carlier, M., Sansonetti, P. and Egile, C. (1999) Rho family GTPases control entry of *Shigella flexneri* into epithelial cells but not intracellular motility. *J Cell Sci*. **112**: 2069-2080.

Muller, D., Benz, I., Tapadar, D., Buddenborg, C., Greune, L. and Schmidt, M.A. (2005) Arrangement of the translocator of the autotransporter adhesin involved in diffuse adherence on the bacterial surface. *Infect. Immun.* **73**:3851-3859.

Murayama, S.Y., Sakai, T., Makino, S., Kurata, T., Sasakawa, C. and Yoshikawa, M. (1986) The use of mice in the Sereny test as a virulence assay of *shigellae* and enteroinvasive *Escherichia coli*. *Infect Immun*. **51**: 696-698.

Murray, A. W. (1991) Cell cycle extracts. *Methods Cell Biol.* **36**: 581-605.

Murray, G.L. (2004). The role of *wzz* genes in Salmonella typhimurium virulence. Department of Microbiology and Immunology, University of Adelaide, South Australia. Ph.D. thesis.

Nakata, N., Sasakawa, C., Okada, N., Tobe, T., Fukuda, I., Suzuki, T., *et al.* (1992) Identification and characterization of *virK*, a virulence-associated large plasmid gene essential for interceullular spreading of *Shigella flexneri*. *Molecular Microbiology*. **6**: 2387-2395.

Nakata, N., Tobe, T., Fukuda, I., Suzuki, T., Komatsu, K., Yoshikawa, M. and Sasakawa, C. (1993) The absence of a surface protease, OmpT, determines the intercellular spreading ability of *Shigella*: the relationship between the *ompT* and *kcpA* loci. *Molecular Microbiology*. **9**: 459-468.

Nilsen, T., Yan, A.W., Gale, G. and Goldberg, M.B. (2005) Presence of multiple sites containing polar material in spherical *Escherichia coli* cells that lack MreB. *J. Bacteriol.* **187**: 6187-6196.

Niyogi, S.K. (2005) Shigellosis. *J Microbiol*. **43**: 133-143.

Oaks, E.V., Wingfield, M.E. and Formal, S.B. (1985) Plaque formation by virulent *Shigella flexneri. Infect Immun*. **48**: 124-129.

Ogawa, H., Nakamura, A. and Nakaya., R. (1968) Cinemicrographic study of tissue cell cultures infected with *Shigella flexneri*. *Jpn. J. Med. Sci. Biol.* **21**:259-273

Ogawa, M., Suzuki, T., Tatsuno, I., Abe, H. and Sasakawa, C. (2003) IcsB, secreted via the type III secretion system, is chaperoned by IpgA and required at the post-invasion stage of *Shigella* pathogenicity. *Molecular Microbiology*. **48**: 913-931.

Ogawa, M., Yoshimori, T., Suzuki, T., Sagara, H., Mizushima, N. and Sasakawa, C. (2005) Escape of intracellular *Shigella* from autophagy. *Science*. **307**: 727-731.

Ogawa, M. and Sasakawa, C. (2006) Intracellular survival of Shigella. *Cellular Microbiology*. **8**: 177-184.

Ohnishi, Y., Nishiyama, M., Horinouchi, S. and Beppu, T. (1994) Involvement of the COOH-terminal pro-sequence of *Serratia marcescens* serine protease in the folding of the mature enzyme. *J. Biol. Chem.* **269**: 32800-32806.

Okada, N., Sasakawa, C., Tobe, T., Yamada, M., Nagai, S., Talukder, K.A., Komatsu, K., Kanegasaki, S., Yoshikawa, M. (1991) Virulence-associated chromosomal loci of *Shigella flexneri* identified by random Tn5 insertion mutagenesis. *Mol Microbiol*. **5**: 187-195.

Oliver, D.C., Huang, G., Nodel, E., Pleasance, S. and Fernandez, R.C. (2003) A conserved region within the *Bordetella pertussis* autotransporter BrkA is necessary for folding of its passenger domain. *Mol Microbiol*. **47**: 1367-1383.

Oomen, C., van Ulsen, P., Van Gelder, P., Feijen, M., Tommassen, J. and Gros, P. (2004) Structure of the translocator domain of a bacterial autotransporter. *EMBO J*. **23**: 1257-1266.

Otto, B.R., Sijbrandi, R., Luirink, J., Oudega, B., Heddle, J.G., Mizutani, K., Park, S.Y., Tame, J.R. (2005) Crystal structure of Hemoglobin Protease, a heme binding autotransporter protein from pathogenic *Escherichia coli*. *J. Biol. Chem.* **280**: 17339-17345.

Pallen, M.J., Chaudhuri, R.R. and Henderson, I.R. (2003) Genomic analysis of secretion systems. *Curr. Opin. Microbiol.* **6**: 519-527.

Pantaloni, D., Clainche, C.L. and Carlier, M.-F. (2001) Mechanism of Actin-Based Motility. *Science*. **292**: 1502-1506.

Peterson, J.H., Szabady, R.L. and Bernstein, H.D. (2006) An unusual signal peptide extension inhibits the binding of bacterial presecretory proteins to the signal recognition particle, trigger factor, and the SecYEG complex. *J. Biol. Chem.* **281**:9038-9048.

Philpott, D.J., Yamaoka, S., Israel, A. and Sansonetti, P.J. (2000) Invasive *Shigella flexneri* activates NF-kappa B through a lipopolysaccharide-dependent innate intracellular response and leads to IL-8 expression in epithelial cells. *J Immunol*. **165**: 903-914.

Perdomo, J.J., Gounon, P. and Sansonetti, P.J. (1994) Polymorphonuclear leukocyte transmigration promotes invasion of colonic epithelial monolayer by *Shigella flexneri*. *J. Clin. Invest.* **93**: 633-643.

Pohlner, J., Halter, R. and Meyer, T.F. (1987) *Neisseria gonorrhoeae* IgA protease. Secretion and implications for pathogenesis. *Antonie Van Leeuwenhoek.* **53**: 479-484.

Prevost, M.C., Lesourd, M., Arpin, M., Vernel, F., Mounier, J., Hellio, R. and Sansonetti, P.J. (1992) Unipolar reorganization of F-actin layer at bacterial division and bundling of actin filaments by plastin correlate with movement of *Shigella flexneri* within HeLa cells. *Infect. Immun.* **60**: 4088-4099.

Purdy, G.E., Hong, M. and Payne, S.M. (2002) *Shigella flexneri* DegP facilitates IcsA surface expression and is required for efficient intercellular spread. *Infect. Immun.* **70**: 6355-6364.

Qi, H.-Y., Hyndman, J.B. and Bernstein, H.D. (2002) DnaK promotes the selective export of outer membrane protein precursors in SecA-deficient *Escherichia coli*. *J. Biol. Chem.* **277**: 51077-51083.

Ratcliff, S.W., Luh, J., Ganesan, A.T., Behrens, B., Thompson, R., Montenegro, M.A., Morelli, G., Trautner, T.A. (1979) The genome of Bacillus subtilis phage SPP1: the arrangement of restriction endonuclease generated fragments. *Mol. Gen. Genet.* **168**:165-72.

Rathman, M., Jouirhi, N., Allaoui, A., Sansonetti, P., Parsot, C. and Tran Van Nhieu, G. (2000a) The development of a FACS-based strategy for the isolation of *Shigella flexneri* mutants that are deficient in intercellular spread. *Mol Microbiol*. **35**: 974-990.

Rathman, M., de Lanerolle, P., Ohayon, H., Gounon, P., Sansonetti, P. (2000b) Myosin light chain kinase plays an essential role in *S. flexneri* dissemination.. *J Cell Sci.* **113**:3375-86.

Robbins, J.R., Monack, D., McCallum, S.J., Vegas, A., Pham, E., Goldberg, M.B. and Theriot, J.A. (2001) The making of a gradient: IcsA (VirG) polarity in *Shigella flexneri. Molecular Microbiology*. **41**: 861-872.

Rohatgi, T., Ma, L., Miki, H., Lopez, M., Kirchhausen, T., Takenawa, T. and Kirschner, M.W. (1999) The interaction between N-WASP and the Arp2/3 complex links Cdc42-dependent signals to actin assembly. *Cell* 97: 221–231

Rohatgi, R., Ho, H.Y. and Kirschner, M.W. (2000) Mechanism of N-WASP activation by CDC42 and phosphatidylinositol 4, 5-bisphosphate. *J. Cell. Biol.* **150**: 1299-1310.

Rost, B. and Sander, C. (1993) Prediction of protein secondary structure at better than 70% accuracy. *J. Mol. Biol.* **232**: 584-599.

Rost, B., Fariselli, P. and Casadio, R. (1996) Topology prediction for helical transmembrane proteins at 86% accuracy. *Prot. Science*. **7**: 1704-1718.

Russell, R.A. (2005) Investigation of the glycine rich repeat region of *Shigella flexneri* IcsA. Department of Microbiology and Immunology, University of Adelaide, South Australia. Honours thesis.

Sakaguchi, T., Kohler, H., Gu, X., McCormick, B.A. and Reinecker, H.C. (2002) *Shigella flexneri* regulates tight junction-associated proteins in human intestinal epithelial cells. *Cell Microbiol.* **4**: 367-381.

Sandlin, R.C., Lampel, K., Keasler, S., Goldberg, M.B., Stolzer, A. and Maurelli, A.T. (1995) Avirulence of rough mutants of *Shigella flexneri*: requirement of O antigen for correct unipolar localisation of IcsA in the bacterial outer membrane. *Infect. Immun.* **63**: 229-237.

Sandlin, R.C., Goldberg, M.B. and Maurelli, A.T. (1996) Effect of O side-chain length and composition on the virulence of Shigella flexneri 2a. *Mol. Microbiol*. **22**: 63-73.

Sansonetti, P.J., Kopecko, D.J., Formal, S.B. (1982) Involvement of a plasmid in the invasive ability of *Shigella flexneri*. *Infect. Immun.* **35**:852-860.

Sansonetti, P.J., Ryter, A., Clerc, P., Maurelli, A.T., Mounier, J. (1986) Multiplication of *Shigella flexneri* within HeLa cells: lysis of the phagocytic vacuole and plasmid-mediated contact hemolysis. *Infect. Immun*. **51**:461-9.

Sansonetti, P.J., Arondel, J., Fontaine, A., d'Hauteville, H. and Bernardini, M.L. (1991) *ompB* (osmo-regulation) and *icsA* (cell-to-cell spread) mutants of *Shigella flexneri*: vaccine candidates and probes to study the pathogenesis of shigellosis. *Vaccine*. **9**: 416-422.

Sansonetti, P.J., Mounier, J., Prevost, M.C. and Mege, R.M. (1994) Cadherin expression is required for the spread of *Shigella flexneri* between epithelial cells. *Cell*. **76**: 829-839.

Sansonetti, P.J., Tran Van Nhieu, G. and Egile, C. (1999) Rupture of the intestinal epithelial barrier and mucosal invasion by Shigella flexneri. *Clin Infect Dis*. **28**:466-75.

Sansonetti, P.J. and Phalipon, A. (1999) M cells as ports of entry for enteroinvasive pathogens: mechanisms of interaction, consequences for the disease process. *Semin Immunol*. **11**: 193-203.

Santapaola, D., Del Chierico, F., Petrucca, A., Uzzau, S., Casalino, M., Colonna, B., *et al* (2006) Apyrase, the product of the virulence plasmid-encoded *phoN2* (*apy*) gene of *Shigella flexneri*, is necessary for proper unipolar IcsA localisation and for efficient intercellular spread. *J. Bacteriol.* **188**: 1620-1627.

Schuch, R., Sandlin, R.C. and Maurelli, A.T. (1999) A system for identifying post-invasion functions of invasion genes: requirements for the Mxi-Spa type III secretion pathway of *Shigella flexneri* in intercellular dissemination. *Mol. Microbiol.* **34**: 675-689.

Sereny, B. (1957) Experimental keratoconjunctivitis shigellosa. *Acta Microbiol Acad Sci Hung*. **4**: 367-376.

Shere, K.D., Sallustio, S., Manessis, A., D'Aversa, T.G. and Goldberg, M.B. (1997) Disruption of IcsP, the major *Shigella* protease that cleaves IcsA, accelerates actin-based motility. *Molecular Microbiology*. **25**: 451-462.

Shibata, T., Takeshima, F., Chen, F., Alt, F.W. and Snapper, S.B. (2002) Cdc42 facilitates invasion but not the actin-based motility of *Shigella*. *Current Biology*. **12**: 341-345.

Skillman, K.M., Barnard, T.J., Peterson, J.H., Ghirlando, R. and Bernstein, H.D. (2005) Efficient secretion of a folded protein domain by a monomeric bacterial autotransporter. *Mol. Microbiol.* **58**: 945-958.

Skoudy, A., Nhieu, G.T., Mantis, N., Arpin, M., Mounier, J., Gounon, P., Sansonetti, P. (1999) A functional role for ezrin during *Shigella flexneri* entry into epithelial cells. *J. Cell Sci.* **112**: 2059-68.

Snapper, S.B., Takeshima, F., Anton, I., Liu, C.H., Thomas, S.M., Nguyen, D., Dudley, D., Fraser, H., Purich, D., Lopez-Ilasaca, M., Klein, C., Davidson, L., Bronson, R., Mulligan,

R.C., Southwick, F., Geha, R., Goldberg, M.B., Rosen, F.S., Hartwig, J.H., Alt, F.W. (2001) N-WASP deficiency reveals distinct pathways for cell surface projections and microbial actin-based motility. *Nat Cell Biol*. **3**: 897-904.

Southwick, F.S., Adamson, E.D., Purich, D.L. (2000) *Shigella* actin-based motility in the presence of truncated vinculin. *Cell. Motil. Cytoskeleton*. **45**:272-8.

Steinbacher, S., Baxa, U., Miller, S., Weintraub, A., Seckler, R. and Huber, R. (1996) Crystal structure of phage P22 tailspike protein complexed with *Salmonella* sp. O-antigen receptors. *Proc Natl Acad Sci U S A*. **93**: 10584-10588.

Steinhauer, J., Agha, R., Pham, T., Varga, A.W. and Goldberg, M.B. (1999) The unipolar *Shigella* surface protein IcsA is targeted directly to the bacterial old pole: IcsP cleavage of IcsA occurs over the entire bacterial surface. *Molecular Microbiology*. **32**: 367-377.

Suetsugu, S., Miki, H. and Takenawa, T. (2001) Identification of another actin-related protein (Arp) 2/3 complex binding site in neural Wiskott-Aldrich syndrome protein (N-WASP) that complements actin polymerization induced by the Arp2/3 complex activating (VCA) domain of N-WASP. *J. Biol. Chem.* **276**: 33175-33180.

Sugimura, K. and Higashi, N. (1988) A novel outer-membrane-associated protease in *Escherichia coli*. *J. Bacteriol.* **170**: 3650-3654.

Suzuki, T., Murai, T., Fukuda, I., Tobe, T., Yoshikawa, M. and Sasakawa, C. (1994) Identification and characterization of a chromosomal virulence gene, *vacJ*, required for intercellular spreading of *Shigella flexneri*. *Mol. Microbiol.* **11**: 31-41.

Suzuki, T., Lett, M.C. and Sasakawa, C. (1995) Extracellular transport of VirG protein in *Shigella*. *J Biol Chem*. **270**: 30874-30880.

Suzuki, T., Saga, S. and Sasakawa, C. (1996) Functional analysis of *Shigella* VirG domains essential for interaction with vinculin and actin-based motility. *J. Biol. Chem.* **271**: 21878-21885.

Suzuki, T., Miki, H., Takenawa, T. and Sasakawa, C. (1998) Neural Wiskott-Aldrich syndrome protein is implicated in the actin-based motility of *Shigella flexneri*. *Embo J*. **17**: 2767-2776.

Suzuki, T., Mimuro, H., Miki, H., Takenawa, T., Sasaki, T., Nakanishi, H., *et al.* (2000) Rho family GTPase Cdc42 is essential for the actin-based motility of *Shigella* in mammalian cells. *J. Exp. Med.* **191**: 1905-1920.

Suzuki, T. and Sasakawa, C. (2001) Molecular Basis of the Intracellular Spreading of Shigella. *Infect. Immun.* **69**: 5959-5966.

Suzuki, T., Mimuro, H., Suetsugu, S., Miki, H., Takenawa, T. and Sasakawa, C. (2002) Neural Wiskott-Aldrich syndrome protein (N-WASP) is the specific ligand for *Shigella* VirG among the WASP family and determines the host cell type allowing actin-based spreading. *Cellular Microbiology*. **4**: 223-233.

Szabady, R.L., Peterson, J.H., Skillman, K.M. and Bernstein, H.D. (2005) An unusual signal peptide facilitates late steps in the biogenesis of a bacterial autotransporter. *Proc Natl Acad Sci U S A*. **102**: 221-226.

Tatusova, T.A. and Madden, T.L. (1999) Blast 2 sequences - a new tool for comparing protein and nucleotide sequences. *FEMS Microbiol. Lett.* **174**:247-250.

Tilney, L.G. and Portnoy, D.A. (1989) Actin filaments and the growth, movement, and spread of the intracellular bacterial parasite, *Listeria monocytogenes*. *J. Cell. Biol.* **109**: 1597-1608.

Tran Van Nhieu, G., Clair, C., Bruzzone, R., Mesnil, M., Sansonetti, P. and Combettes, L. (2003) Connexin-dependent inter-cellular communication increases invasion and dissemination of *Shigella* in epithelial cells. *Nat Cell Biol*. **5**: 720-726.

Tran Van Nhieu, G., Enninga, J., Sansonetti, P. and Grompone, G. (2005) Tyrosine kinase signaling and type III effectors orchestrating Shigella invasion. *Current Opinion in Microbiology Host--microbe interactions: bacteria*. **8**: 16-20.

Tsai, C.M., Frasch, C.E. (1982) A sensitive silver stain for detecting lipopolysaccharides in polyacrylamide gels. *Anal. Biochem.* **119**: 115-9.

Uchiya, K., Tobe, T., Komatsu, K., Suzuki, T., Watarai, M., Fukuda, I., Yoshikawa, M., Sasakawa, C. (1995) Identification of a novel virulence gene, *virA*, on the large plasmid of *Shigella*, involved in invasion and intercellular spreading. *Molecular Microbiology*. **17**: 241-250.

Van Den Bosch, L., Manning, P.A. and Morona, R. (1997) Regulation of O-antigen chain length is required for *Shigella flexneri* virulence. *Mol. Microbiol.*. **23**: 765-775.

Van Den Bosch, L. and Morona, R. (2003) The actin-based motility defect of a *Shigella flexneri rmlD* rough LPS mutant is not due to loss of IcsA polarity. *Microbial Pathogenesis*. **35**: 11-18.

Veiga, E., Nikaido, H., de Lorenzo, V., Fernandez, L.A. (2002) Export of autotransported proteins proceeds through an oligomeric ring shaped by C-terminal domains. *EMBO J*. **21**: 2122-2131.

Veiga, E., de Lorenzo, V., Fernandez, L.A. (2003) Autotransporters as scaffolds for novel bacterial adhesins: surface properties of *Escherichia coli* cells displaying Jun/Fos dimerization domains. *J. Bacteriol*. **185**: 5585-90.

Veiga, E., de Lorenzo, V., Fernandez, L.A. (2004) Structural tolerance of bacterial autotransporters for folded passenger protein domains. *Mol. Microbiol.* **52**:1069-80.

Voulhoux, R., Bos, M., Geurtsen, J., Mols, M. and Tommassen, J. (2003) Role of a Highly Conserved Bacterial Protein in Outer Membrane Protein Assembly. *Science*. **299**: 262 - 265.

Vretou, E., Giannikopoulou, P., Longbottom, D., Psarrou, E. (2003) Antigenic organization of the N-terminal part of the polymorphic outer membrane proteins 90, 91A, and 91B of *Chlamydophila abortus*. *Infect Immun.* **71**: 3240-50.

West, N.P., Sansonetti, P., Mounier, J., Exley, R.M., Parsot, C., Guadagnini, S., Prevost, M.C., Prochnicka-Chalufour, A., Delepierre, M., Tanguy, M. and Tang, C.M. (2005) Optimization of virulence functions through glucosylation of Shigella LPS. *Science.* **307**: 1313-1317.

Winder, S.J. (2003) Structural insights into actin-binding, branching and bundling proteins. *Curr. Opin. Cell. Biol*. **15**: 14-22.

Wing, H.J., Yan, A.W., Goldman, S.R. and Goldberg, M.B. (2004) Regulation of IcsP, the Outer Membrane Protease of the Shigella Actin Tail Assembly Protein IcsA, by Virulence Plasmid Regulators VirF and VirB. *J. Bacteriol.* **186**: 699-705.

Wing, H.J., Goldman, S.R., Ally, S. and Goldberg, M.B. (2005) Modulation of an Outer Membrane Protease Contributes to the Virulence Defect of Shigella flexneri Strains Carrying a Mutation in the virK Locus. *Infect. Immun.* **73**: 1217-1220.

Wu, T., Malinverni, J., Ruiz, N., Kim, S., Silhavy, T. J. and Kahne, D. (2005) Identification of a multicomponent complex required for outer membrane biogenesis in *Escherichia coli*. *Cell*. **121**:235-245.

Yang, C., Huang, M., DeBiasio, J., Pring, M., Joyce, M., Miki, H., Takenawa, T., Zigmond, S.H. (2000) Profilin enhances Cdc42-induced nucleation of actin polymerization. *J. Cell Biol.* **150**:1001-1012.

Yarar, D., To, W., Abo, A., Welch, M.D. (1999) The Wiskott-Aldrich syndrome protein directs actin-based motility by stimulating actin nucleation with the Arp2/3 complex. *Curr. Biol.* **9**:555-8.

Yoshida, S., Katayama, E., Kuwae, A., Mimuro, H., Suzuki, T. and Sasakawa, C. (2002) *Shigella* deliver an effector protein to trigger host microtubule destabilization, which promotes Rac1 activity and efficient bacterial internalization. *Embo J*. **21**: 2923-2935.

Yoshida, S., Handa, Y., Suzuki, T., Ogawa, M., Suzuki, M., Tamai, A., Abe, A., Katayama, E., Sasakawa, C. (2006) Microtubule-severing activity of *Shigella* is pivotal for intercellular spreading. *Science*. **314**: 985-9.

Zettl, M. and Way, M. (2002) The WH1 and EVH1 domains of WASP and Ena/VASP family members bind distinct sequence motifs. *Curr Biol*. **12**: 1617-1622.

Zychlinsky, A., Prevost, M.C. and Sansonetti, P.J. (1992) Shigella flexneri induces apoptosis in infected macrophages. *Nature*. **358**: 167-169.

Zychlinsky, A., Thirumalai, K., Arondel, J., Cantey, J., Aliprantis, A. and Sansonetti, P. (1996) In vivo apoptosis in Shigella flexneri infections. *Infect. Immun.* **64**: 5357-5365.